306467332Y

Thesis Submitted for the Degree of
Doctor of Philosophy
at the University of Oxford

SPECTROSCOPIC STELLAR SURFACE GRAVITIES FROM METALLIC LINE PROFILES

R B Willis

BODLEIAN LIBRARY OXFORD
DEPOSITED
THESIS
17-7-98

Hertford College
Oxford

Hilary Term
1978

TABLE OF CONTENTS

CONTENTS

ABSTRACT

Page

CHAPTER 1 : STARS AND SURFACE GRAVITIES 1

1.1 Introduction 1
1.2 Definition of surface gravity 3
1.3 Surface gravities and stellar models 5
1.4 Direct methods 9
1.5 Photometric methods 14
1.6 Accuracy of mass determinations 17

CHAPTER 2 : STELLAR ATMOSPHERES AND STELLAR SPECTRA 19

2.1 Introduction 19
2.2 General theory 20
2.3 Calculation of model atmospheres 25
2.4 The treatment of absorption lines 32
2.5 Observable effects of gravitational acceleration on the atmosphere 42

CHAPTER 3 : METHODS USED TO DETERMINE SURFACE GRAVITIES 48

3.1 Spectroscopic classification schemes 48
3.2 Broad band photometry 49
3.3 Other measurements of the continuum 49
3.4 Intermediate and narrow band spectral classification 51
3.5 Spectral classification based on line strength 53
3.6 Precise and absolute measurements of spectroscopic gravities 56
3.7 Surface gravities derived from observations of binary stars 59
3.8 Conclusions 61

CHAPTER 4 : SURFACE GRAVITIES FROM METALLIC LINE PROFILES 63

4.1 Method 63
4.2 Oscillator strengths and abundance 69
4.3 Damping constants 71
4.4 Choice of lines 72
4.5 Observations and measurements 73

CHAPTER 5 : OSCILLATOR STRENGTHS OF NEUTRAL IRON 74

5.1 Introduction 74
5.2 The Oxford King furnace 78
5.3 Optical system and spectrophotometry 80
5.4 Choice of lines for furnace measurements 82
5.5 Experimental method 83
5.6 Reduction procedure 87
5.7 Oscillator strengths of lines measured in the furnace 89
5.8 Errors and uncertainties in the measurements 92
5.9 Comparison with other measurements 104

CHAPTER 6 : SOLAR SPECTRUM : FE I ABUNDANCE AND MICROTURBULENCE 111

6.1 Solar data 111
6.2 Calculation of equivalent widths 118
6.3 Determination of abundance and microturbulence 121
6.4 Significance of the microturbulence measurement 125
6.5 The solar iron abundance 128

CHAPTER 7 : SOLAR SPECTRUM : FE I DAMPING CONSTANTS 131

7.1 Introduction 131
7.2 Medium strong lines 132
7.3 The line FeI 5269 5A 133
7.4 Damping of strong lines 134
7.5 Calculated damping constants and other measurements 138

CHAPTER 8 : APPLICATION OF THE LABORATORY AND SOLAR MEASUREMENTS TO STELLAR SPECTRA 143

8.1 Introduction 143

8.2 Choice of stars 145

8.3 Effective temperature and model atmosphere for Arcturus 147

CHAPTER 9 : INTERPRETATION OF THE FE I SPECTRUM OF ARCTURUS 155

9.1 Spectroscopic data 155

9.2 Abundance and microturbulence determination 158

9.3 Determination of gravity 160

9.4 The surface gravity, Fe I abundance and microturbulence of Arcturus 168

CHAPTER 10 : MASS, LUMINOSITY AND RADIUS OF ARCTURUS 175

10.1 Values derived from this work 175

10.2 Comparison with other measurements 177

10.3 Discussion 179

CHAPTER 11 : SUMMARY AND CONCLUSIONS 182

APPENDIX I : COMPUTATION OF LINE PROFILES 188

APPENDIX II : UNITS AND SYMBOLS 197

REFERENCES 200

ACKNOWLEDGEMENTS

SPECTROSCOPIC STELLAR SURFACE GRAVITIES FROM METALLIC LINE PROFILES

by

Robin B Willis

Hertford College

A thesis submitted to the University of Oxford
for the Degree of Doctor of Philosophy
Hilary 1978

ABSTRACT

Accurate surface gravities are needed for studies of stellar atmospheres and to determine stellar masses. It is suggested that measurements of gravities for late type stars are usually subject to great uncertainties, especially as the results are sensitive to the assumed effective temperature. A method is therefore proposed using the damping wings of metal lines to measure the gravity; and weak lines from the same lower level as the strong line to determine the metal abundance.

Low excitation lines of FeI are used to demonstrate the method and new oscillator strengths are given for 51 transitions from the 0.00-0.12 and 0.86-0.99 eV levels. Using the furnace absorption technique the precision obtained is about 0.02 dex. Comparison with other authors' results shows systematic discrepancies between emission and absorption methods.

The oscillator strengths are used to interpret the observed line strengths and profiles in the solar spectrum. From 5 model atmospheres a microturbulence of 0.8 km/sec is found, and iron "abundances" of 7.5-7.7. Damping constants are found for strong and medium-strong lines and the values are close to the predictions of classical theories in contrast with the greater damping predicted by more recent calculations.

Using the measured oscillator strengths and damping constants the spectrum of Arcturus is used to derive an iron abundance of 6.99 and a microturbulence of 2.1 km/sec. The abundance is sensitive to the effective temperature, and 4400K is proposed from the observed flux distribution. The gravity determined from the profile of the line FeI 5269.5A is however insensitive to the adopted temperature and the measured value is log g = 1.45 $\pm$ 0.15 corresponding to a mass of 0.56 M(sun) for a radius of 23 R(sun). The gravity and mass are greater than the results of other methods which assume, and are sensitive to, lower effective temperatures.

It is concluded that metallic line profiles in the spectra of cool stars can yield precise gravities which are insensitive to the assumption of LTE or to the temperature in the atmosphere.

Figures & Tables

The tables and figures relevant to
each chapter are grouped together
at the end of the text of that chapter.

1 - STARS AND SURFACE GRAVITIES

1.1 Introduction

The gravitational acceleration at the surface of a star is one of the three principal factors which determine the physical characteristics of a stellar atmosphere. Broadly speaking the effective temperature, chemical composition and surface gravity decide the variation of pressure and temperature with depth in the atmosphere, the opacities, and all the many other detailed properties. An accurate knowledge of the surface gravity is therefore essential for almost all studies of stellar atmospheres.

Surface gravities derived from spectroscopic observations must rely to some extent on models of the stars' atmospheres and can therefore never be used as an absolute test of the theory of those models. Moreover in practice the spectrum is neither observed in its entirety nor reproduced exactly by the model. The gravity used in the work may then be wrong, in the sense that it is not the true value for the star, for two reasons. First, the observations may be reproduced by a combination of effective temperature, gravity and composition because an error in one parameter is offset by an error or errors in the others. Second, the theoretical basis may be wrong in such a way that an erroneous value of the gravity is necessary to give the observed spectrum.

Most of what is known about stars and stellar systems is derived from observation and analysis of the radiation emerging from the stellar atmosphere. Many of these results are sensitive to the value adopted for the surface gravity. Abundance determinations, for instance, are sometimes very sensitive to the surface gravity used in the analysis. Accurate gravities are therefore needed to yield precise abundances, which can then be used with confidence in studies of nucleosynthesis, stellar formation and evolution, etc.

Accurate values of the gravitational acceleration at the surface of a star also provide the measurements of masses which are essential for work on the structure and evolution of stars. The

only way to measure the mass of a star is by its gravitational attraction. If a binary system is observable the masses are related to the orbit by classical mechanics (ie Kepler's laws). Unfortunately the number of such systems which can be observed with sufficient accuracy is small. The mass can be derived however from the surface gravity, as will be shown in section 1.2. The determination of accurate surface gravities from observations of stellar spectra therefore assumes a wider significance.

1.2 Definition of surface gravity

In the context of stellar atmospheres the terms "surface gravitational acceleration", "surface gravity", "stellar gravity" or just "gravity" are synonymous and mean the gravitational force exerted on unit mass at the surface of the star. (The surface of a star cannot be defined precisely but refers to the region from which the observable radiation emerges.) By convention this force is expressed as an acceleration, so that surface gravities are usually measured in units of cm s^{-2} (CGS) or m s^{-2} (SI)*. "Spectroscopic gravity" means simply a gravity determined from observations of the stellar spectrum.

Two assumptions are usually made: that stars are spherical and symmetrical about their centres. Neither is true in general. Stars rotate and being fluid this leads to oblateness, with the equatorial diameter greater than the polar. For most stars the flattening at the poles is very small and sphericity a good approximation. But at high rotational velocities the simple assumption fails. Inhomogeneities (eg convection currents) also exist but the scale of such effects in relation to the overall dimensions of a star is likely to be small, so that symmetry is a very good approximation.

With these assumptions the force acting on an element of stellar material at a distance r from the centre of a star (figure 1.1) is directed towards the centre, and is determined solely by the mass M(r) included within radius r:

$$\rho(r)\ \delta A\ \delta r\ \frac{G\ M(r)}{r^2} \qquad (1.1)$$

The pressure P(r) gives a net force, again acting inwards:

$$P(r+\delta r)\,\delta A - P(r)\,\delta A = -\frac{dP(r)}{dr}\ \delta r \delta A \qquad (1.2)$$

Here dP(r)/dr is the total pressure gradient. The pressure of radiation acting on the element must also be included, and

---

* See Appendix II.

perhaps the effects of turbulent motions and magnetic fields as well. In general the total pressure is determined by:

$$P = P_{gas} + P_{radn.} + P_{turb.} + P_{magn.} \qquad (1.3)$$

Combining these two forces yields the equation of motion for the element, which may be written:

$$\frac{dP(r)}{dr} + \rho(r) \cdot \frac{GM(r)}{r^2} = -\rho(r) \frac{d^2r}{dt^2} \qquad (1.4)$$

Equation (1.4) is perfectly general and allows the stellar gravity at radius r to be defined as:

$$g(r) = \frac{GM(r)}{r^2} \qquad (1.5)$$

In nearly all stars the atmosphere is such a thin shell that the radius and included mass are essentially constant throughout, and are the overall mass and radius of the star, R & M respectively. This holds true even if the star pulsates, provided the amplitude of the pulsations is not too great, so that equation (1.4) becomes:

$$\frac{dP}{dr} + \rho g = -\rho \frac{d^2R}{dt^2} \qquad (1.6)$$

where g is the <u>surface gravity</u>:

$$g(R) = g = \frac{GM}{R^2} \qquad (1.7)$$

1.3 Surface gravities and stellar models

1.3.1 Stellar masses

If the radius of a star is known a measurement of its surface gravity allows the mass to be found, as equation (1.7) may be written:

$$M = \frac{gR^2}{G} \qquad (1.8)$$

This important result is by itself sufficient to justify efforts to measure g accurately. However its application is limited in practice by the difficulty of determining the radius R. Precise surface gravities can only give accurate masses if R is known with comparable precision. Thus the error in R can be taken to define the maximum acceptable error in the gravity g by deriving from equation (1.8)

$$(\Delta M/M)^2 = (\Delta g/g)^2 + 4(\Delta R/R)^2 \qquad (1.9)$$

and clearly the uncertainty in g will not be very significant if

$$\Delta g/g < \Delta R/R$$

The methods used to measure stellar radii are discussed below in order to give a quantitative estimate of the desired precision in g. It is helpful however first to define some of the terms used; and to consider briefly the context in which the measurements of gravity, radius and mass are used.

1.3.2 Structure and evolution of stars

Perhaps the ultimate test of stellar astrophysics is to relate the current observations of a star to its initial mass and chemical composition. Leaving aside rotation, magnetic fields and other perturbations and external effects (eg accretion) these initial properties should determine the characteristics at any time: the mass, luminosity and radius, and hence the effective

temperature and gravity and every detail of the observable spectrum.

The general principles can be described with the aid of an algorithm for the ideal procedure, (figure 1.2). The starting assumptions are a mass, M, and chemical composition $\underline{a}$, where $\underline{a}$ usually defines the relative abundance of each element with respect to hydrogen. A model of the internal structure of the star can then be calculated. From this model the radius and total rate of energy generation, which is also the total luminosity, L, may be predicted for time t_o. Changes in the structure and composition must then be computed to take account of the star's evolution and to yield the observable parameters (L,M,R, $\underline{a}$) (Iben, 1967, 1972, 1974).

This requires theories for energy generation and transport, equations of state, and the general physical conditions and processes within a star. Of course many approximations and assumptions may be made in order to construct the models but these are part of the theoretical basis being tested.

If a star is a member of a binary system it may be possible to determine the mass, luminosity and radius by direct methods (see section 3.7). Although some 70,000 such systems are known less than 100 have been observed with sufficient accuracy though the use of speckle interferometry (McCalister, 1977) is increasing the number. Moreover close binary pairs may be atypical; and the possibility of interaction by mass exchange, tidal effects and heating must be considered, not only now but throughout the formation and evolution of the stars. Stellar models must therefore be tested against isolated stars. It is not possible to determine the parameters (L,M,R) for such a star without using to some extent a model of the stellar atmosphere. The atmosphere is entirely determined by L,M,R and the chemical composition but can be represented more conveniently by (T_e, g, $\underline{a}$) where T_e is the effective temperature, defined by:

$$4\pi R^2 \sigma T_e^4 = L \qquad (1.10)$$

and σ is Stefan's constant. (It is essential that T_e be seen as nothing more than a useful parameter derived from the absolute properties R & L).

The final theoretical exercise in the idealised procedure is therefore to compute a model atmosphere for the star's values of (T_e, g, $\underline{a}$) and then to calculate the observable spectrum. If the observed spectrum differs from the theoretical an error must exist in one or more of the assumptions or theories. Fortunately the tests available are sometimes able to indicate broadly where the inconsistency has arisen. As the tests in figure (1.2) show, it may be possible to determine L and R independent of the model atmosphere. The observations needed for the full set of tests are unfortunately very difficult to obtain, and tend to suffer from large uncertainties.

1.3.3 Observations of stars

Observations may be made of the following:

a. The flux of radiation f_ν incident on the earth at frequency ν and hence also the integrated flux f defined by

$$f = \int_0^\infty f_\nu \, d\nu$$

b. The distance D of the star from the earth; trigonometric parallaxes are the principal source of accurate data.

c. The angular diameter θ ; that is, the apparent size of the star as seen from the earth.

Trigonometric parallaxes can only be measured for stars relatively close to the earth. The principal catalogues (eg Wolley et al, 1970; Hoffleit, 1964) list some 7,000 stars with parallaxes ranging from 0."76 (for Alpha Centauri) to about 0."005. The best results attain a positional accuracy of about 0."001 (Van Altena, 1974) and an absolute parallax with probable errors of about 0".005. But very few stars are near enough to allow such precision. There are only some 30-40 stars for which the distance is known to within 2 per cent; and about 700 within 20 pc and known to 10 per cent (Gliese, 1975).

Measurements of stellar angular diameters suffer from similar limitations and errors. The principal direct methods are interferometric: Michelson interferometry (Pease, 1921, 1931; Currie, 1974); amplitude interferometry (Hanbury Brown,1974;) and speckle interferometry (Labeyrie, 1970; Gezari et al., 1972; Bonneau et al., 1973). Lunar occultations have also been used to determine angular diameters (Nather et al., 1970; Barnes & Evans, 1976). These techniques are all limited to stars with relatively large apparent diameters, and even so the results are perhaps very uncertain. Individual measurements may be quoted with an accuracy of 2 per cent or better but the results from different methods frequently vary by 20 per cent or more and it is difficult to assess the relative merits of the techniques. Amplitude interferometry appears to be the most reliable of the interferometric methods (Blackwell and Shallis, 1977) but this method is not really suited to the cool late-type stars.

Angular diameters can also be determined from photometric measurements. These are not direct determinations however but must rely on model atmospheres for some part of the analysis. In an ideal procedure the use of model atmospheres introduces additional uncertainty in the derivation of L,M,R, and should therefore be avoided. Nevertheless some measure of the angular diameter is essential and necessity will force a return to photometric methods. (See section 1.5).

1.4 Direct Methods

1.4.1 Interpretation of the observations

a. flux measurements only

In principle the flux can be observed for any star, although there will be inevitable uncertainties due to absorption by the interstellar medium which may distort the shape of the flux curve. Ground-based observations must in addition be corrected to take account of absorption in the earth's atmosphere. This is important because the relative flux distribution must be used to derive a model atmosphere for the star. Typically the observed flux, both continuum and lines, is compared with the flux computed from theoretical models and hence parameters (T_e, g, $\underline{a}$) are obtained. Of course these values rely on the accuracy of the observations and the success of the theoretical models.

The chemical composition is thus determined. None of the other properties - mass, luminosity and radius - can be found however, as the very use of a model atmosphere implies that the flux distribution is a local property of the surface of the star and cannot be used to distinguish stars with different radii and luminosities; without the radius, the mass cannot be found. Notwithstanding this fact, values of effective temperature and gravity allow a test of stellar models. Equation (1.8) may be divided by equation (1.10) to show that

$$(M/L) = \frac{1}{4\pi\sigma G} (g/T_e^4) \qquad (1.11)$$

This functional relation between the mass-luminosity ratio, M/L, and the atmospheric parameters (T_e, g) can be the basis of comparisons between the predictions of stellar models and the observed properties of stars.

b. flux measurements and parallax

The addition of a parallax measurement to the flux provides three further possible derivations. First, the luminosity can be found without using a model atmosphere, since from

the inverse square law:

$$f = (L/4\pi D^2) \qquad (1.12)$$

In practice there must be some recourse to model atmospheres because the flux is not observable at all frequencies and the amount not observed must be estimated (the bolometric correction).

Secondly, the mass-luminosity ratio (equation 1.11) can be combined with this result to give the mass, although this result does depend on the model atmosphere:

$$M = \frac{1}{4\pi\sigma G} (g/T_e^4) L \qquad (1.13)$$

$$= (gfD^2/\sigma G T_e^4)$$

Thirdly, since values of M and g have been found, the radius follows by substituting equation (1.8) in equation (1.13):

$$R^2 = fD^2/\sigma T_e^4 \qquad (1.14)$$

c. flux measurements and angular diameter

Although in practice any star with a measureable angular diameter will also have a known parallax, it is worth considering what can be learnt from the flux and angular diameter alone. Perhaps the most important application, in principle at least, is the direct determination of effective temperatures independent of the model atmosphere. If the flux at the surface of the star is defined as F_ν and F corresponding to f_ν and f respectively, the flux, luminosity and effective temperature are all related:

$$F = \int_0^\infty f_\nu d\nu = \sigma T_e^4 \qquad (1.15)$$

$$L = 4\pi R^2 F \qquad (1.16)$$

Then

$$(f_\nu / F_\nu) = f / F = (R/D)^2 \qquad (1.17)$$

and by definition:

$$\theta = 2R/D = \sqrt{(f_\nu / F_\nu)} \qquad (1.18)$$

whence:

$$T_e = (2/\theta)^{\frac{1}{2}} (f/\sigma)^{\frac{1}{4}} \qquad (1.19)$$

d. flux measurements, parallax and angular diameter

Given these optimal measurements the properties of the star can be found with the minimum use of model atmospheres. The angular diameter and parallax yield the radius (equation 1.18); and the luminosity can be found from equation (1.12). The chemical composition and surface gravity must still be found from the spectrum but the model atmosphere is at least determined somewhat more precisely because the effective temperature can be derived from the direct observations (equation (1.19)).

1.4.2 Results from direct methods

Use of the direct methods outlined above at (d) is limited principally by a lack of absolute flux measurements and of accurate angular diameters. Michelson interferometry is restricted to stars with very large apparent sizes. Speckle interferometry appears to give accurate measurements of relatively small angular diameters (Gezari et al., 1972; Worden, 1976; Lynds et al., 1976; Blant et al., 1977). There are however some striking discrepancies between the results of

speckle and amplitude interferometry: for αHer the former gives 0."031 (Gezari et al., 1972) whereas Knapp et al., (1975) give 0."058 from Narrabri observations. In addition it may be difficult to interpret these observations in terms of a real stellar disk which is not uniformly bright (see chapter 8).

Under ideal conditions the mean error from observations of lunar occultations can be as low as 0."0005 (De Vegt, 1976) but this degree of precision is rarely approached. Measurements by a number of authors have been collated by Barnes & Evans (1976) who listed 27 stars, mainly of spectral type K or M and luminosity class III. The measured diameters ranged from 0."076 to 0."0025 with probable errors from about 2.5% at best to some 30% for the smaller values.

The principal results of the amplitude interferometry program at Narrabri observatory were summarised by Hanbury Brown et al. (1974). Measurements of 32 stars in the spectral range O5 to F8 have been corrected for limb darkening with the aid of detailed model atmosphere calculations; and for faint companions in the case of five stars. Hanbury Brown et al. were therefore able to present angular diameters for 32 stars, ranging from 0."066 to 0".00042. The precision claimed varied from $0."8 \times 10^{-3}$ in the worst case to $0."023 \times 10^{-3}$ in the best. Overall the average probable error was 6%.

Code et al. (1976) used these angular diameters to derive effective temperatures. In principle the method is that described at (c) above. The resulting values for T_e were quoted with uncertainties in the range 1.5% to 8%, according to the accuracy of the data since from (1.19):

$$(\Delta T_e/T_e) = \tfrac{1}{2}(\Delta\theta/\theta)^2 + \tfrac{1}{4}(\Delta f/f)^2 \qquad (1.20)$$

For 12 of the stars trigonometric parallaxes were used to derive the luminosity and radii (see d. above) thus completing the "model independent" part of figure 1.2. The precision of these results varied a good deal, reflecting the quality of the parallax measurements. But if the surface gravity were known exactly, the errors in R would have corresponded to uncertainties in the mass between 8% and 200%.

1.5 Photometric methods

Direct measurements of angular diameters are so few, and subject to such large uncertainties, that stellar radii must usually be derived from indirect methods. These are chiefly photometric and rely on the use of the observed flux distribution to deduce a model atmosphere.

The flux F is determined if T_e is fixed, eg by comparing the shape of observed and model flux curves. If the distance to the star is known fluxes F and f yield the radius (equation (1.17)). The total flux cannot be observed however because the ultra-violet and infra-red regions of the spectrum are absorbed by the earth's atmosphere or by the interstellar medium, and the bolometric correction needed to take account of the missing energy is itself uncertain. Model atmospheres are used to extrapolate the observable spectrum into the blue and red but the accuracy of these predictions cannot be assumed. There are corresponding uncertainties perhaps in the relation between the effective temperature of the star and the model atmosphere. The integrated flux defines the effective temperature of any particular model but there is no guarantee that the energy predicted in the extreme frequencies bears any real semblance to the true flux from the star, even though the model reproduces the observable spectrum.

In order to minimise such uncertainties more selective observations and analyses have been attempted. Wesselink (1969) used direct measurements of the angular diameters of 18 stars to calibrate the broad band colour index (B-V) against surface brightness. This is essentially an empirical relation between the observed fluxes and the values at the surface of the star, and avoids the use of model atmospheres. The calibration allowed Wesselink et al (1972) to derive angular diameters for some 2,300 stars. Linear diameters were also quoted but these rest on the assumption that total luminosity is also defined uniquely by the observable spectrum. This is a not uncommon

means of finding the distance to a star, and hence the linear diameter, since D follows from f and L (see equation (1.12)). But the luminosity cannot be found from the flux distribution alone. The angular diameters of Wesselink et al should therefore be used with trigonometric parallaxes where possible and the published linear diameters treated with caution.

Wesselink et al claim an accuracy of 8-12% for their angular diameters but the method is susceptible to unknown systematic errors. These arise chiefly from the use of an empirical surface brightness calibration which may not be valid for stars of different age, composition etc. These errors appear however to be largely eliminated if a similar method is applied using the Vand V-R magnitudes (Lacy, 1977).

Greater accuracy and certainty may be obtained by the detailed analysis of precisely defined observations, using model atmospheres. Thus equation (1.17) was the basis of the technique introduced by Gray (1967). Flux distributions were obtained from photometry and the model atmosphere determined by requiring the computed energy distribution to reproduce the observed. Although the effective temperature is available from the integrated flux predicted by the model it is not relevant to the determination of the radius which requires only the monochromatic absolute flux whereby the observed flux and a trigonometric parallax allow R to be found:

$$R = \text{const.}\ (1/\pi)\ \sqrt{(f_\nu / F_\nu)}$$

A total of 81 measurements using this method (Gray, 1967, 1968) cover stars in the range A3 to K2, mainly of luminosity class V, with uncertainties in R of about 7 to 13%. Although there may be unknown errors due to the model atmosphere calculations these results compare favourably with direct methods (see, for example, section 1.4.2. above).

A similar method was used by Blackwell and Shallis (1977) to determine the angular diameters of some 28 stars. Effective temperatures were found from observations of f_ν, essentially by comparing the ratio f_ν/f with the predictions of model atmospheres

$$(f_\nu / f) = (F_\nu / F) = \frac{F(\text{model})_\nu}{\sigma T_e^4} \qquad (1.21)$$

Once the effective temperature was fixed the flux F_ν could be computed and the angular diameter derived from equation (1.19). Uncertainties due to blanketing of the continuum and to interstellar extinction were minimised by using fluxes in the infra-red region. Moreover in this way the effect of uncertainties in the effective temperature or model were also largely eliminated: F_ν is insensitive to changes in the effective temperature or the detailed structure of the model for these wavelengths. Hence the derived angular diameter is insensitive to the effective temperature adopted for the calculation.

The accuracy claimed for these provisional measurements was of the order of 5% in θ corresponding perhaps to 5-10% in R according to the quality of the trigonometric parallaxes available. Comparison with the direct measurements from the Narrabri amplitude interferometer showed generally good agreement and more accurate infra-red fluxes would, it appears, allow even greater precision. This is especially promising because the method is well suited to cool stars which are not usually susceptible to amplitude interferometry.

1.6 Accuracy of mass determinations

In section 1.3.1 the accuracy of a mass determination from the surface gravity was shown to depend on the uncertainties in the gravity and in the radius, (equation (1.9)). The measurements of R described above allow quantitative estimates of the accuracy attainable. From equation (1.18) the probable error in R is derived:

$$(\Delta R/R)^2 = (\Delta D/D)^2 + (\Delta\theta/\theta)^2$$

so that (1.9) becomes:

$$(\Delta M/M)^2 = (\Delta g/g)^2 + 4\{ (\Delta D/D)^2 + (\Delta\theta/\theta)^2 \} \quad (1.22)$$

For a bright, relatively near-by star the probable error in the parallax may be as small as 2%. and the angular diameter could be known to within 5%. These correspond to a probable error in M of some 11% which would increase to some 15% for an uncertainty in g of 10% (0.04 dex).

More commonly however the probable errors in the parallax and angular diameter will be larger, corresponding to at least 10% in R (see above), and more probably at least 20%. The consequent uncertainty in the derived mass would be 40%. The equivalent error in the gravity (40% or 0.15 dex) would increase the probable error in the derived mass to nearly 60% (about 0.20 dex).

It follows that the accuracy of mass measurements will be significantly degraded if the acceleration due to gravity in the atmosphere is not known to better than 40% (0.15 dex). This may be taken to be the minimum aim for spectroscopic gravity determinations. In practice the probable error in g is usually much greater and stellar masses less certain in consequence.

Where the parallax and angular diameter are known well the mass determination will benefit from a surface gravity known to better than 10%. More precise measurements will however become limited by uncertainties in the helium abundance. This cannot be measured easily, and is especially difficult to establish for cool stars. It is therefore usual to adopt a "cosmic value" of 0.10 (with respect to H); and $\pm$0.02 uncertainty in this corresponds to some 6% in the derived gravity.

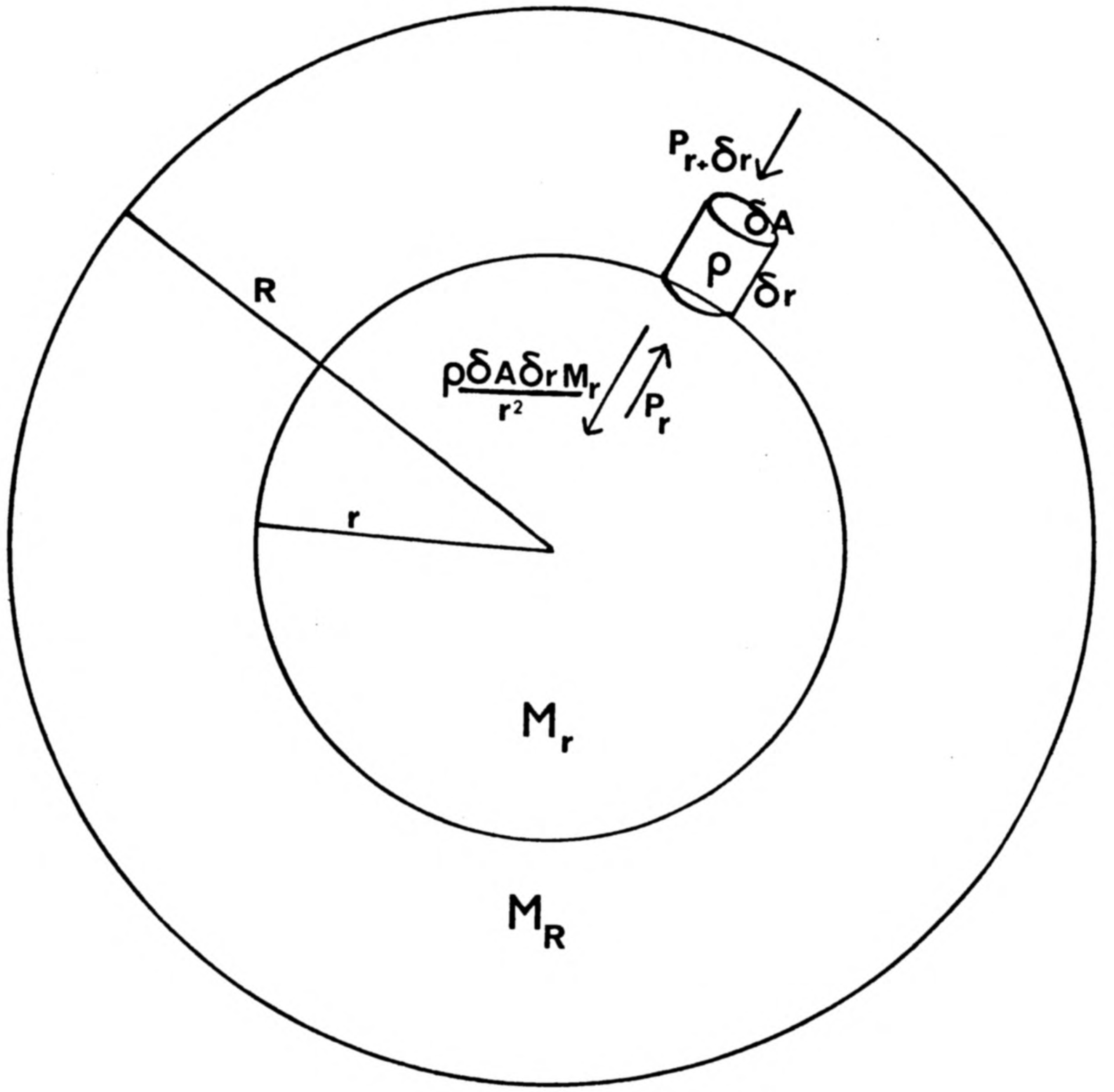
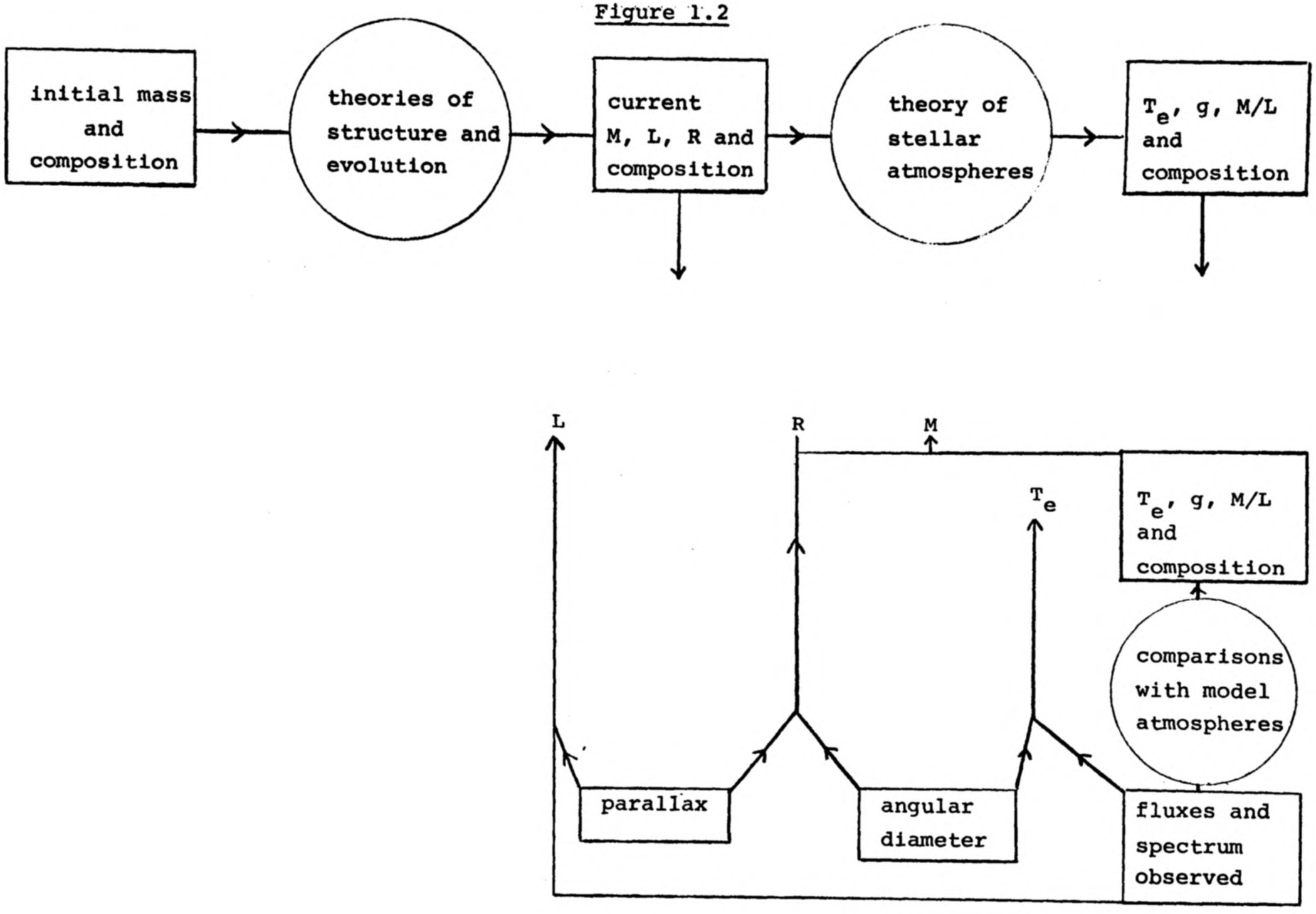

$P_{r+\delta r}$
δA
ρ
δr
R
$\frac{\rho \delta A \delta r M_r}{r^2}$
P_r
r
M_r
M_R

Figure 1·1

Figure 1.2


initial mass and composition
theories of structure and evolution
current M, L, R and composition
theory of stellar atmospheres
T_e, g, M/L and composition
L
R
M
T_e
T_e, g, M/L and composition
comparisons with model atmospheres
parallax
angular diameter
fluxes and spectrum observed

2. STELLAR ATMOSPHERES AND STELLAR SPECTRA

2.1 Introduction

In section 1.4.5 the optimal observations of a star were considered: parallax; fluxes; and an angular diameter determined from, say, interferometry. Yet even in such cases a model atmosphere is needed if only to provide the limb darkening data with which to interpret the measurement of the diameter. The theory of stellar atmospheres is therefore inescapable; and is used to deduce from observed spectral features properties such as the gravitational acceleration at the surface of a star. Quantitative models of the atmospheres of the sun and of other stars will be used herein to interpret observations of both the continuous spectrum and of absorption lines. A comprehensive account of the conditions determining the emergent radiation from a star would however be otiose. This chapter therefore summarises very briefly some of the more important relations between the properties of an atmosphere and the emergent spectrum. It assumes results which are derived in any of the standard texts (eg Unsold (1955); Aller (1963); Mihalas (1970)), and which are given here in order to:

a. emphasise that while the effective temperature largely determines the overall shape and appearance of the spectrum, the surface gravity decides the pressure in the atmosphere and hence affects all conditions in the atmosphere as a whole;

b. indicate the observable differences in the emergent spectrum which theory predicts would arise from differences in the acceleration due to gravity at the surface of the star;

c. outline the theory of the formation of absorption lines which will be used in later chapters.

2.2 General Theory

2.2.1 The nature of stellar atmospheres

The term stellar atmosphere is usually taken to mean the part of the star emitting the observed radiation. There are however no precise limits: the corona of the sun for instance extends far beyond the disk normally observed. It is also possible (though highly improbable) for a photon to escape from the interior of a star. Visible radiation however originates almost entirely in a comparatively thin shell - in the case of the sun some hundreds of kilometers in thickness. This region is the photosphere; and most models of stellar atmospheres are models of the star's photosphere.

As the thickness of the atmosphere is usually very small compared with the radius of curvature, it may be treated locally as a plane. This greatly simplifies the problems of analysis and computation. Other assumptions which are generally valid, at least in the first approximation, are as follows:

a. The atmosphere is homogeneous except in the normal (ie radial) direction;
b. the atmosphere is in hydrostatic equilibrium;
c. the atmosphere is in a steady state;
d. the atmosphere is in energy equilibrium (ie no energy is generated in the atmosphere, merely transported through it)

With these assumptions, properties of the atmosphere are functions of only the depth in the atmosphere. Thus the specific intensity depends only on the depth and the polar angle (see figure 2.1)

$$dE_\nu = I_\nu(z,\theta)\, dA \cos\theta\, d\nu\, d\omega\, dt \qquad (2.1)$$

and the flux, defined as the net rate of energy flow across unit area, will be normal to the atmosphere and depend only on the depth:

$$F_\nu(z) = (1/\pi) \int I_\nu(z,\theta) \cos\theta \, d\omega$$

$$= 2 \int_{-1}^{1} I_\nu(z,\mu) \, d\mu \qquad (2.2)$$

where $\mu = \cos\Theta$

2.2.2 Absorption and emission

The processes of absorption, emission and scattering may be represented macroscopically by considering an element in the atmosphere (figure 2.2). For an incident intensity I_ν the energy removed from the beam is

$$dE_\nu = k_\nu I_\nu d\omega d\nu dt \rho dA ds \qquad (2.3)$$

where k_ν is the extinction coefficient at frequency ν
In general k_ν will comprise true absorption and scattering

$$k_\nu = \kappa_\nu + \sigma_\nu \qquad (2.4)$$

Similarly the emission coefficient j_ν is defined by the energy replaced:

$$dE_\nu = j_\nu d\omega d\nu dt \rho dA ds \qquad (2.5)$$

2.2.3 Equation of transfer

In a steady state the energy change in a beam passing through the element is emission less extinction:

$$dI_\nu d\nu d\omega dA dt = j_\nu d\nu d\omega dt dA ds - k_\nu I_\nu \rho dA ds d\nu d\omega dt \quad (2.6)$$

or

$$(\mu/\rho)\cdot(dI_\nu/dz) = j_\nu - k_\nu I_\nu$$

since $dz = \mu ds$ in a plane-parallel atmosphere.

This equation may be further simplified by defining:

a. the optical depth τ_ν by $d\tau_\nu = -\rho k_\nu dz$ (2.7)

b. the source function S by $S_\nu = j_\nu/k_\nu$ (2.8)

so that equation (2.6) becomes:

$$\mu(dI_\nu/d\tau_\nu) = I_\nu - S_\nu \quad (2.9)$$

2.2.4 Radiative transfer and local thermodynamic equilibrium

A formal solution of equation (2.9) follows by integrating to give

$$I_\nu(\tau_\nu,\mu) = I_\nu(\tau_0,\mu)\exp-(\tau_0-\tau_2) + \int_{\tau_2}^{\tau} S(t)\exp-(t-\tau_2)/\mu \, dt/\mu$$

In the great majority of atmospheres two boundary conditions also exist: first, no radiation is incident on the atmosphere; second, the atmosphere is essentially infinite (in terms of optical depth). Then the intensity is just

$$I_\nu(\tau_\nu,\mu) = \int_{\tau_\nu}^{\infty} S_\nu(t)\exp(-(t-\tau)/\mu)\,dt/\mu \qquad (2.10)$$

and it can be shown similarly that

$$F_\nu(\tau_\nu) = -2\int_0^{\infty} S_\nu(t)\cdot E_2|t-\tau_\nu|\,dt \qquad (2.11)$$

The source function S represents the interaction of the radiation field with the atmosphere. Many atomic processes may be involved: bound-bound, bound-free, and free-bound transitions; collisional ionisation, excitation and de-excitation; recombination; scattering. As these may be neither isotropic nor coherent the calculation of the source function invariably involves approximations. The extent of these largely determines the complexity of a model atmosphere calculation.

The source function becomes particularly simple if it is assumed that:

a. there is only pure absorption;

b. the ionisation and excitation at any point in the atmosphere are determined by the Saha and Boltzmann equations;

c. the intensity of radiation is given by Planck's law.

These assumptions constitute the classical concept of local

thermodynamic equilibrium (LTE) where all properties of the radiation field and the plasma are defined by a unique local temperature. Moreover the Kirchhoff-Planck law applies so that

$$j_\nu = k_\nu B_\nu(T) \tag{2.12}$$

and the source function is the Planck function, allowing equation (2.6) to be written:

$$(dI_\nu/d\tau_\nu) = I_\nu - B_\nu\{T(\tau_\nu)\} \tag{2.13}$$

with

$$I_\nu(0,\mu) = \int_0^\infty B_\nu(t)\exp(-t/\mu)\ dt/\mu \tag{2.14}$$

$$F_\nu(0) = 2 \int_0^\infty B_\nu(t)\ E_2(t)\ dt \tag{2.15}$$

2.3 Calculation of model atmospheres

2.3.1 Defining the problem

The aim is to derive a model atmosphere which is internally consistent; and which reproduces the observed spectrum. In the special case of the sun such models may be derived from the observed limb darkening (eg Elste,1967; Carbon and Gingerich, 1969). For other stars however the model must be computed, and the emergent radiation then found (using equation (2.15)). A model for assumed values of effective temperature, chemical composition and the acceleration due to gravity will not usually produce the desired spectrum, so the values must be adjusted to minimise any differences: this yields a model of the atmosphere of that particular star.

2.3.2 Constructing a model

The first step is to invoke the assumption of hydrostatic equilibrium to relate the pressure to the optical depth. As $dr = -dz$ equation (1.7) becomes:

$$(dP/dz) = -\rho g \qquad (2.16)$$

so with equation (2.7)

$$(dP/d\tau_\nu) = (g/k_\nu) \qquad (2.17)$$

Here p is the total pressure which, as indicated above, may include radiation, turbulence etc. The gas pressure may be found by defining an effective surface gravity: eg the radiation pressure may be included by writing:

$$(dP_g/d\tau_\nu) = g/k_\nu - (dP_R/d\tau_\nu)$$

$$= g_{eff}/k_\nu$$

An atmosphere may now be computed by integrating equation (2.17). In order to do this starting assumptions must be made about the variations of p_g and T with τ_ν. Then from p_g and T the equation of state (see next section) may be solved to give p_e, and hence the opacity and scattering.

The first calculation will not usually be in radiative equilibrium - let alone with the desired flux corresponding to the effective temperature. The integrated flux F must therefore be compared with the derived flux to change the temperature distribution; and to compute a new model.

Many additional stages are involved in the real computations. Convection must be considered. Line blanketing (see section 2.4.1. below) may also be introduced. Notwithstanding such important factors, it is clear from equation (2.17) that the surface gravity, other things being equal, determinesthe gas pressure in an atmosphere:

$$P_g(\tau_\nu) = \int_0^{\tau_\nu} (g/k_\nu)\, dt_\nu \qquad (2.18)$$

2.3.3. The equation of state

Gas pressure and temperature determine the electron pressure p_e and the extinction k_ν. This is not a simple relationship: in cool stars, for instance, molecule formation is important; and solutions of the detailed statistical equilibria may differ greatly from LTE. Nevertheless the assumption of LTE is valid

in many atmospheres. If LTE applies the Saha equation gives the degree of ionisation of every species:

$$N_j N_e / N_i = (2\pi mkT/h^2)^{3/2} \cdot (2U_j(T)/U_i(T)) \exp(-\chi_{ij}/kT) \quad (2.19)$$

where χ_{ij} is the ionisation potential, N_i, N_j the number densities of the successive states of ionisation and U(T) the partition functions. Taken together these equations determine p_e, p_g, and the opacity since they are constrained by three conditions: conservation of each element; charge conservation; and the gas law. The detailed relationships between p_e and p_g are sensitive to both temperature and chemical composition, eg because of the contribution of electrons by ionised metals or hydrogen. In most atmospheres however the qualitative behaviour is as follows:

a. where only a single ionisation stage is important, other things being equal:

$$P_e^2 \dot{\sim} X(T)\, P_g \quad (2.20)$$

b. for temperatures high enough to ionise hydrogen

$$2P_e \sim P_g \quad (2.21)$$

c. in (relatively) cool stars the abundance of metals (A) determines the electron density (because hydrogen is hardly ionised) and:

i. $p_e/p_g \sim A$ if the metals are ionised (2.22)

ii. $p_e/p_g \sim A^{2/3}$ if the metals are not ionised (2.23)

2.3.4. The extinction coefficient

The population and occupation numbers from the equation of state determine the opacity and scattering coefficients. Many elements and molecules contribute to the total extinction (see Appendix I). There are however two cases where a single opacity dominates.

At high temperatures (in early type stars - B, A, and early F) the opacity is due principally to hydrogen, and depends only on the density of neutral hydrogen

$$\kappa_\nu \sim X_1(T)\ N_H \tag{2.24}$$

As the hydrogen is mostly ionised:

$$N_H \sim N_{H^+}\ N_e$$

$$N_{H^+} \simeq N_e$$

$$\kappa_\nu \sim X_2(T)\ P_e^2 \tag{2.25}$$

also $$\rho \sim N_e m_H$$

$$P_e \sim 2P_g$$

so that with the equation of hydrostatic equilibrium

$$P_e \sim g^{\frac{1}{2}} \tag{2.26}$$

$$P_g \sim g^{\frac{1}{2}} \tag{2.27}$$

In contrast the opacity at visible frequencies in the atmospheres of cooler stars is dominated by the H^- ion:

$$\kappa_\nu \simeq \alpha_\nu(H^-)N_{H^-} \sim N_H N_e \tag{2.28}$$

$$\text{or} \quad \kappa_\nu \sim P_e \tag{2.29}$$

$$dP \sim (g/P_e)d\tau \tag{2.30}$$

As there is little hydrogen ionisation at these temperatures the concentration of hydrogen does not change. The electron pressure is however sensitive to the chemical composition and to temperature and pressure. Singly ionised metals are the principal source of electrons, and where the abundance of

metals relative to hydrogen is A, and the fraction ionised is X:

$$P_e \sim PAX \tag{2.31}$$

From the Saha equation $X \sim 1/P_e$ to give

$$P_e^2 \sim P \text{ for a given composition} \tag{2.32}$$

The equation of hydrostatic equilibrium then becomes:

$$dP \sim (g/P^{\frac{1}{2}})d\tau$$

$$P \sim g^{2/3} \tag{2.33}$$

$$P_e \sim g^{1/3} \tag{2.34}$$

2.3.5. Results of theoretical model calculations

Although the role of the acceleration due to gravity has been emphasised, the results of computations show that the temperature distribution $T(\tau)$ is, for a given effective temperature, independent of g to within a few percentage points (see, eg, the results of Carbon and Gingerich, 1969); it follows that the source function and emergent flux will also be determined principally by the effective temperature and this is borne out by the flux distributions predicted by the model atmospheres. This confirms the empirical result that a one-dimensional classification of stellar spectra by temperature can account for the more obvious variations; and arises because temperature determines, in the first instance, the ionisation, excitation etc in the atmosphere.

The pressure in the atmosphere does however depend on the surface gravity. As indicated above, g determines p_g (τ). The electron pressure is similarly related to the gravity, but varies far more with variations in the chemical composition, especially in cool stars. From equations (2.22) and (2.34) for instance changes in the chemical composition and in the surface gravity may be indistinguishable: eg a higher abundance of metals may mimic a higher gravity.

As T(τ) is essentially independent of g, any changes in the emergent spectrum arising from different gravities will occur because of changes in the relative opacities at different frequencies. Broadly speaking these effects are very small. In other words the ratio $k_\nu / \bar{k}$ is usually insensitive to p_e and p_g over the visible spectrum. This results from the dominance of either H or H^- in early and late type stars respectively. Where a single opacity determines the extinction coefficient, the frequency distribution will be unchanged. Such changes in the emergent spectrum as are predicted are due to the differential changes in opacity sources. In the blue and near ultraviolet for instance neutral and ionised metals may make an important contribution to the total extinction. The increased pressure at higher values of g will change the ionisation equilibria of these elements, and therefore the relative opacity. Similarly there is a sudden increase in the continuous absorption coefficient of neutral hydrogen shortwards of 3647A. This causes a discontinuity in the continuum spectrum - the Balmer discontinuity. At a given temperature the ratio of the hydrogen absorption on either side of 3647A is, broadly speaking, independent of pressure; whereas the contribution to the total opacity by, say, the H^- ion varies with pressure. This differential behaviour again leads to gravity sensitivity: the Balmer discontinuity is greater for lower gravities.

2.4 The Treatment of Absorption Lines

2.4.1 Line blanketing

The observed radiation from the sun and stars usually comprises a continuous spectrum, superimposed on which are discrete absorption and emission lines. These lines correspond to absorption and emission in the star's atmosphere between discrete atomic states. In principle such transitions could be included in the extinction coefficient used to construct a model; and the model would then predict the continuous spectrum and the lines. Practical difficulties prevent such a straightforward approach. Therefore the atmosphere usually gives only the continuous spectrum. But absorption by discrete lines cannot be ignored. The additional extinction by the lines - especially in the upper atmosphere - effectively blocks the radiative energy transfer. This increases the temperature in the lower regions: the "backwarming effect".

With fast modern computers it has become possible to make increasingly realistic approximations to the true extinction coefficient of lines plus continuous absorption and scattering. Such calculations involve either a selection of individual lines (eg Van Citters and Morton, 1970; Mihalas and Auer, 1970); or some statistically selected sample of transitions, and of line profiles (eg Carbon and Gingerich, 1969; Carbon, 1974; Kurucz, 1974; Bell et al, 1976). In late type stars the problem is particularly great: for example, the list used by Kurucz (1974) contains some 1 760 000 lines.

In early type stars the problems are less apparent. The spectrum shows relatively few lines, principally those of H and He. The lines are however more likely to be formed in non-LTE conditions. As the continuous opacity sources are also determined by the radiation field (through ionisation and excitation) model atmospheres for these stars are not easily computed. Techniques to deal with the non-LTE problems have therefore been developed. For example Mihalas and Auer (1970) and Auer and Mihalas (1969, 1970) presented models which

allow both lines and continuum to be formed in non-LTE conditions; and thereby reproduce the observed spectrum in a single computation. There is however little prospect of extending this technique to the more complex spectra of later type stars.

2.4.2 The absorption line spectrum

By convention an absorption line is described by the absorption depth a_ν relative to the flux in the continuum F_c :

$$a_\nu = 1 - F_\nu / F_c \qquad (2.35)$$

or, for the sun,

$$a_\nu(\mu) = 1 - I_\nu(0,\mu) / I_c(o,\mu) \qquad (2.36)$$

The shape of the observed line depends on many factors, including effects introduced by the instrument or by motions in the atmosphere. As these cannot easily be taken into the model it is often convenient to use the integrated line strength, expressed as an equivalent width:

$$W_\nu = \int_0^\infty a_\nu \, d\nu$$

or more commonly: $$W_\lambda = \int_0^\infty a_\lambda \, d\lambda \qquad (2.37)$$

An absorption line is formed because a transition introduces an additional extinction, at a frequency ν, in the atmosphere. Then the optical depth at that frequency is determined by the

sum of the extinction in the line and continuum:

$$d\tau_\nu = \frac{\kappa_\nu + \sigma_\nu + l_\nu}{\kappa_\nu + \sigma_\nu} d\tau_c$$

$$= (1 + l_\nu/k_c) d\tau_c \qquad (2.38)$$

where k_c is the extinction coefficient for the continuum in the region of the line. The analysis then proceeds in much the same way as for the continuum. There is of course the additional line opacity and the importance of this depends, as is apparent, on the ratio l/k. And as before there are simplifying assumptions. If it is assumed that the line is formed by pure absorption (ie no scattering) and in LTE, then

$$I_\nu(0,\mu) = \int_0^\infty B_\nu(\tau_\nu)\exp(-\tau_\nu/\mu)\ d\tau_\nu/\mu \qquad (2.39$$

and

$$F_\nu = 2\int_0^\infty B\ (\tau_\nu)\ E_2(\tau_\nu)\ d\tau_\nu \qquad (2.40)$$

More usually however the computation uses a reference optical depth scale, that for the continuum, so that the intensity,

for instance, is:

$$I_\nu(0,\mu) = \int_0^\infty B_\nu(\tau_0)\exp(-\tau_\nu/\mu)(1+l_\nu/k_0)d\tau_0/\mu$$

with $$d\tau_\nu = (1+l_\nu/k_0)d\tau_0$$

The variation of the line opacity with frequency determines the shape of the observed line. For this reason it is convenient to represent the opacity as

$$i_\nu = l_0\phi(\nu)$$

where $\phi(\nu)$ is a normalized profile function and l_0 the total line absorption coefficient. The profile function is considered in the next section and in Appendix I the calculation of l_0 is looked at more closely. It is sufficient therefore to note that the line absorption depends on the number of atoms in the ionization and excitation state corresponding to the transition; and on the strength of the transition. The former is determined (assuming LTE) by the Saha-Boltzmann equation and thus by the temperature, gas pressure and electron pressure in the atmosphere. The latter is ultimately a property of the particular transition and may be calculated from the wave-

functions for the two states. It is of course more usual to represent the processes by, for instance, the Einstein A and B coefficients: corresponding to absorption, spontaneous emission and stimulated emission. And in astrophysics - where the overwhelming majority of lines are observed in absorption - the oscillator strength formulation is generally adopted. The oscillator strength f_{ij} is a measure of the transition probability and allows the total line absorption to be written:

$$l_0 = (\pi e^2/mc)\, f_{ij}\, n_i (1 - g_i n_j / g_j n_i) \qquad (2.41)$$

where n_i, n_j are the numbers of atoms in the lower and upper states of the transition and the final factor is the correction for stimulated emission.

2.4.3 Line profile function

The profile function $\phi(\nu)$ reflects the physical conditions in the atmosphere. Neither the upper nor the lower level of a transition has a unique energy and their distribution is affected by interactions with perturbers in the atmosphere. In addition the absorbing atom will have a velocity with respect to the observer which introduces a Doppler shift of the profile.

These effects must be combined in order to find the profile function. Some of the computational methods are discussed in Appendix I. The main points however are as follows.

a. natural damping profile

The finite lifetime of an excited state corresponds to an uncertainty in its energy. Where a transition takes place

between two such states the line profile reflects the uncertainty in each level, and it may be shown that

$$l_\nu = \frac{\pi e^2}{mc} \cdot f_{ij} \cdot \frac{\Gamma/4\pi^2}{(\nu-\nu_0)^2 + (\Gamma/4\pi)^2} \qquad (2.42)$$

where:

$$\Gamma = \Gamma_i + \Gamma_j$$

$$\Gamma_i = \sum_{k<i} A_{ik}$$

$$\Gamma_j = \sum_{k<j} Ajk$$

Here Γ is the damping factor, by analogy with a classicial harmonic oscillator, and A_{jk} the Einstein coefficients.

b. collisional broadening

Four types of interaction are of astrophysical interest; and are characterised by the way the interaction varies with the separation of atom and pertruber. Under the classicial impact approximation for instance the interaction is described by a phase shift

$$\Delta\omega(t) = C_p/(\ r(t)\ )^p \qquad (2.43)$$

where:

i. p=2 for the linear Stark effect (hydrogenic atom + charged particle)

ii. p=3 for resonance broadening (atom A + atom A)

iii. p=4 for quadratic Stark effect (atom + charged particle)

iv. p=6 for van der Waals interaction (atom A + atom B)

In each case theory predicts a line shift (which is rarely of astrophysical importance) and a line profile of the same form as equation (2.42). Generally then:

$$\Gamma = \Gamma_{radn.} + \Gamma_{coll.}$$

where $\Gamma_{coll.} = \Gamma_6 + \Gamma_3 + (\Gamma_2 \text{ or } \Gamma_4)$

c. Doppler broadening and the Voigt function

If there is a Maxwellian velocity distribution (as under the LTE assumption) the probability distribution of the velocity component ξ along the line of sight is

$$dN/N = 1/\pi^{\frac{1}{2}} \cdot \exp(-\xi^2/\xi_0^2)\ d\xi/\xi_0 \qquad (2.44)$$

where $\xi_0^2 = 2kT/M$

(Turbulent motions with the same distribution may be included by writing

$$\xi_0^2 = 2kT/M + \xi_{turb}^2 \qquad (2.45)\ )$$

If the line is broadened solely by the Doppler effect then an observed frequency ν corresponds to a frequency $\nu(1 - \xi/c)$ in the rest frame of an atom with velocity ξ along the line of sight. Hence

$$l_\nu = \int_{-\infty}^{\infty} l_0(\nu - \nu\xi/c)\ W(\xi)\ d\xi$$

But $l(\nu - \nu\xi/c)$ is itself a Lorentz profile (equation (2.42)) so the general profile is a convolution of the two functions. This may be written, using equation (2.41), as

$$l_\nu = (\pi e^2/mc) \cdot f_{ij} \cdot H(a,v)/(\Delta\nu_D\ \pi^{\frac{1}{2}})$$

where H(a,v) is the Voigt function and:

$$\Delta\nu_D = \xi_0\nu_0/c$$

$$a = \Gamma/4\pi\Delta\nu_D$$

$$v = (\nu - \nu_0)/\Delta\nu_D$$

Qualitatively a is a measure of the relative importance of damping and Doppler broadening; and v a dimensionless measure of the distance from the line centre which gives the position on the profile in units of the Doppler width. The function H has a complex form but two extreme cases are important. First, when Doppler broadening dominates,

$$H(a,v) \sim \exp (-v^2)$$

and for points in the profile well outside the Doppler core (ie large values of v) damping is dominant and

$$H(a,v) \sim a/(\pi^{\frac{1}{2}} v^2)$$

2.4.4 Qualitative interpretation of line spectrum

Taking first the strength of the line (ie the equivalent width) the main factors are the oscillator strength and the number density of atoms in the lower state. The number density is determined by the abundance of the element and by the conditions in the atmosphere; and may therefore vary greatly.

The Saha-Boltzmann equation determines the relative occupation of a given level, which is therefore sensitive to temperature. If for instance the lower level is an excited state of a neutral

atom there may be very few absorbing atoms in a cool star. As the temperature increases in earlier type stars there will be greater excitation, and the line strength will increase. This continues until the ionisation outweighs the excitation and the line strength decreases again. The ionisation will also be sensitive to the electron pressure, and therefore to gravity and composition.

Turning to the profile, it is found that the equivalent width of a line is not a simple function of the number of absorbing atoms. In general there is a complex relation (the curve of growth) which depends on both the number of absorbing atoms and on the profile function. For very weak lines the equivalent width in a given atmosphere is proportional to the number of absorbing atoms; and increases linearly with eg abundance. As the line absorption continues to go up however the central part of the line has an absorption depth close to unity and the equivalent width changes little. Only when the wings of the line begin to contribute an appreciable amount does the equivalent width again increase.

2.5 Observable effects of gravitational acceleration on the atmosphere

2.5.1 The continuum; line blanketing

As indicated in section 2.3.5, the distribution of continuous opacity is often insensitive to gravity. However line blanketing may be sensitive to both p_e and p_g; as the gravity increases both p_e and p_g tend to increase and the strength of, eg, a neutral metal line increases because the degree of isonisation is reduced and because the collisional broadening is greater.

In late type stars with relatively cool atmospheres these effects are particularly discernible in the blue and ultraviolet spectrum. This region is crowded with absorption lines to such an extent that there is often no clear continuum. But even in early type stars there may be very broad lines which, though not individually observed, lead to the continuum being sensitive to pressure, and hence to gravity.

2.5.2 Hydrogen lines

The spectra of early type stars are dominated in the great majority of cases by broad, deep lines of hydrogen. Even in the spectra from cooler atmospheres these lines are often outstanding, so the theory of their formation merits special attention.

Hydrogen lines are also exceptional because the principal contribution to their profile comes from the linear Stark effect - due mainly to interactions with electrons. The line opacity in the wing of a H-line is therefore:

$$l_\nu \sim X_1(T) \cdot N_H \cdot \phi(\nu)$$

$$\sim X_1(T)\, P_g P_e$$

In an early type star most of the hydrogen is ionised and equation (2.25) above gave

$$\kappa_c \sim X_2(T)\ P_e^2$$

so that

$$l_\nu \sim X_3(T)\ P_e^3$$

and

$$l_\nu / \kappa_\nu \sim X_4(T)\ P_e \sim g^{\frac{1}{2}} \qquad (2.47)$$

In later type stars however the continuous opacity of the H^- ion gives:

$$l_\nu / \kappa_\nu \sim X(T)\ N_H \qquad (2.48)$$

As the degree of H-ionisation is small, the concentration of hydrogen will not change with pressure and the H-lines will not be sensitive to gravity.

2.5.3 Other absorption lines: ionisation equilibrium

Other absorption lines arise mainly from metals, and are affected by changes in the ionisation equilibrium, and in the profile function. These lines are rarely observed in the spectra of early type stars because the high temperatures ionise the metals; and because the lines are blurred by very high rotational velocities. Confining discussion therefore to cooler atmospheres, the continuous opacity will be largely H^- and the line opacity depends on the ionisation equilibrium. From equation (2.19)

$$N_0 = N_1 N_e \cdot \phi(T)$$

Three representative cases are then as follows.

i. where most of the element is ionised and the line is formed by the neutral atom:

$$N_0 \ll N_1 \text{ and } N_0 \sim P_e \quad \text{so that} \quad l_\nu / k_c \sim \text{const.} \quad (2.48)$$

and the line is insensitive to gravity.

ii. where most of the element is neutral and the line is formed by the neutral atom:

$$N_0 \gg N_1 \text{ and } N_0 \sim \text{const. so that}$$

$$l_\nu / k_\nu \sim 1/P_e$$

$$\sim g^{-1/3} \quad (2.49)$$

iii. where most of the element is neutral and the line is formed by the ion:

$$N_0 >> N_1 \text{ and } N_1 \sim 1/P_e \text{ so that}$$

$$l_\nu/k_\nu \sim 1/P_e^2$$

$$\sim g^{-2/3} \qquad (2.50)$$

2.5.4 Other absorption lines: broadening

Turning finally to the wings of a metal line, the effects of changes in the profile function must be added to the changes in the ionisation equilibrium. Van der Waals broadening arises principally from interactions with hydrogen atoms and tends to dominate the other components of the damping profile in cool stars. At the higher temperatures and electron pressures in early type stars the damping is more likely to be determined by the Stark effect.

In the latter case the absorption in the wing of a line is proportional to the electron pressure:

$$l_\nu \sim \Gamma_4$$

$$\sim X(T)\, P_e$$

These conditions are likely to exist in atmospheres where the element is mostly ionised; and where the continuous opacity is due to hydrogen. Therefore

$$l_\nu / k_c \sim X(T)(P_e/P_e^2)\cdot P_e$$

$$\sim \text{const.}$$

In contrast wherever Van der Waals damping is important the continuum opacity is likely to be due to the H^- ion.

$$l_\nu / k_c \sim \Gamma_6 / k_c$$

$$\sim P_g / P_e$$

Adding the effects of pressure changes on the ionisation equilibrium, as above, the overall sensitivity of the wing is as follows.

i. where most of the element is ionised and the line is formed by the neutral atom:

$$l_\nu / k_c \sim P_g \sim g^{2/3} \qquad (2.51)$$

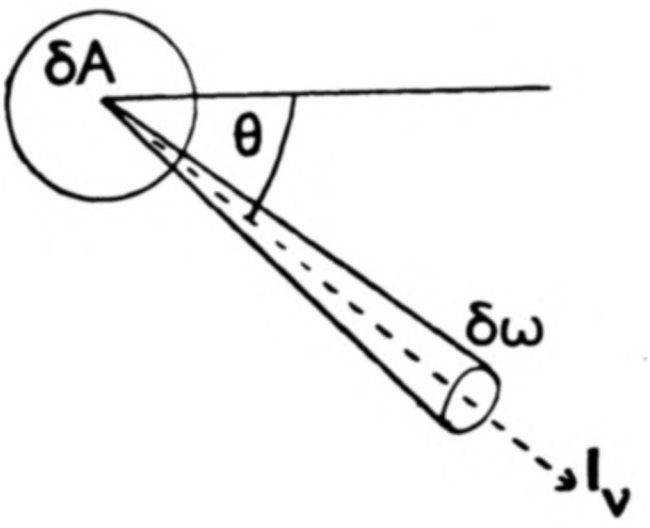
ii. where most of the element is neutral and the line is formed by the neutral atom:

$$l_\nu / k_c \sim P_g / P_e \sim g^{1/3} \qquad (2.52)$$

iii. where most of the element is neutral and the line is formed by the ion:

$$l_\nu / k_c \sim P_g / P_e^2 \sim \text{const.} \qquad (2.53)$$

Figure 2.1



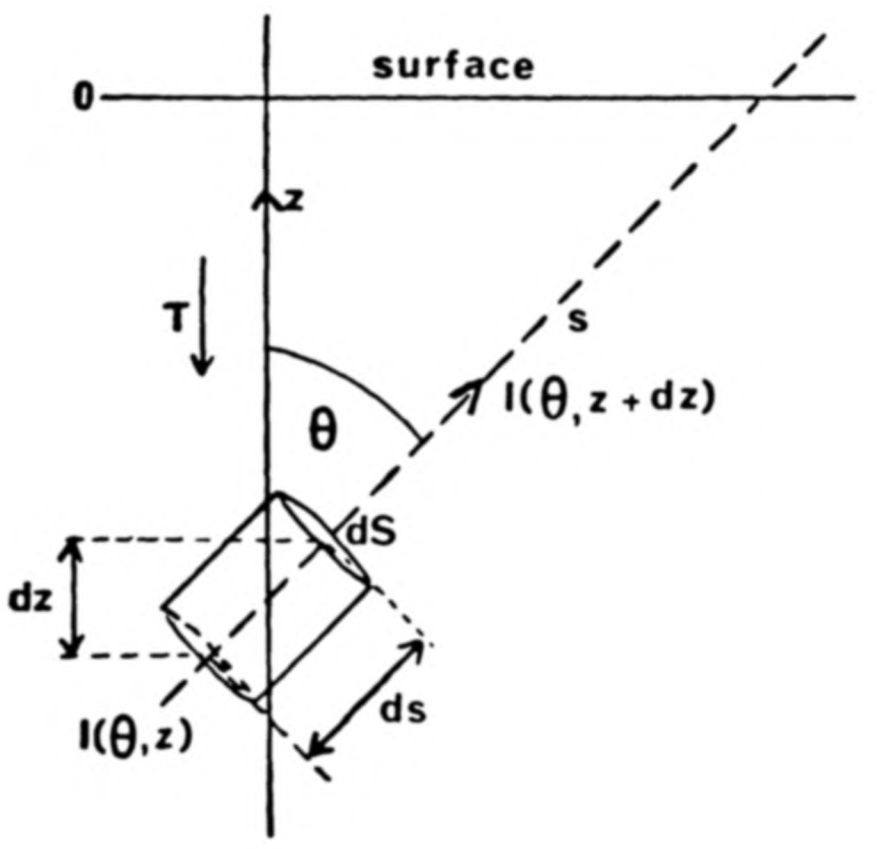


Figure 2.2

3. METHODS USED TO DETERMINE SURFACE GRAVITIES

3.1 Spectroscopic classifaction schemes

The relationships between a star's surface gravity and its spectrum are reflected in the very many multi-dimensional classifaction schemes for stellar spectra. Unfortunately the great majority of these schemes do not yield absolute surface gravities; many are wholly empirical; and very few achieve the desired precision. Furthermore these are usually measurements of the luminosity rather than the gravity, even though the gravity is the more fundamental parameter. Morgan (1937) emphasised the importance of g rather than L; and more recently Newell (1971, 1973) has discussed the advantages of a physical H-R diagram using (T_e,g) in place of (T_e , L).

Current measurements (Keenan, 1958; Stromgren, 1963, 1966; Schmidt-Kaler, 1965; Spite, 1966; Hauck and Westerlund, 1973; Fehrenbach and Westerlund, 1973) are still largely empirical, in so far as they rely on the calibration of spectroscopic parameters (albeit quantitative) against stars with known luminosities. It may then be difficult to interpret the scheme in terms of gravity because there may be no unique relationship between L and g.

As an empirical fact luminosity calibrations do usually work because the luminosity of a star usually is inversely related to its surface gravity. But this relies on a unique mass-luminosity ratio, an assumption known to be incorrect eg for different populations.

Although spectral classifaction does not yield precise gravities, such schemes do indicate:

a. the spectral features most sensitive to the pressure in the atmosphere;
b. methods of observation;
c. parameters defined to measure pressure-sensitive features;
d. the sensitivity of these criteria to other factors: eg temperature and chemical abundance.

For these reasons a number are considered below. But the many different schemes cannot be usefully reviewed here and only a very few illustrative examples are given of those considered when looking for a source of precisely measured gravities.

3.2 Broad-band photometry

Broad-band photometric systems generally use filters with effective widths of the order of 1000A and offer speed and accuracy even for faint objects. The most widely used is the UBV system (Johnson and Morgan 1953) but this covers only some 2000A of the spectrum, and the colours (U-B) and (B-V) allow only a coarse separation of giants and dwarfs.

Greater discrimination is possible if additional bands are used to extend the system to longer wavelengths. Among the more important systems are the bands UBVGRI (Stebbins and Whitford, 1964); RGU (Becker, 1948, 1954); and UBVRIJHKL (Johnson, 1965). Similar systems are readily defined, and calibrated. And the multiplicity of colours allows correction for the effects of interstellar reddening and chemical abundances.

Using model atmospheres theoretical colours can be computed to relate the classification to the parameters (T_e,g,$\underline{a}$). For example Parsons (1970, 1971ab) used the Stebbins and Kron (1956) 6 colour photometry and models for F and G giants but found that line blanketing, metal abundances and the poorly defined effective temperature made the derived gravity uncertain.

3.3 Other measurements of the continuum

With narrower bands the measurement of spectral features is more detailed, and the effects of gravity and temperature are more sharp. Effects of interstellar reddening are also reduced. Accordingly there are many photometric systems using intermediate bandwidths (about 200A) eg Walraven and Walraven (1960); Neff and Travis (1967); Crawford and Stromgren (1966); Borgman (1960); Golay (1963).

As far as discrete spectral features are concerned however, the only continuum feature which indicates gravity is the Balmer jump. Whatever sensitivity to gravity shown by photometric systems, in cool stars at least, arises from bands on either side of the jump. Photometric accuracy is essential though. In a late F type star, for instance,

$$dD_B/d \log g \sim 0.2$$

so that D_B must be measured to $0.^m02$ to fix log g within 0.1. Even so the gravity depends on knowing the metal abundance since typically:

$$dD_B/ dZ \sim 0.1$$

Finally the effective temperature must be taken into account and Breger and Kuhi (1970) find that an error of 0.01 in θ_e corresponds to 0.2 in log g.

Much the same problems arise even if the continuum is observed in greater detail, eg by a scanning spectrometer. Model atmospheres can then be used to compare the shape of the observed flux distribution (eg Stickland, 1971). Peytremann (1975) approached the same degree of sophistication with detailed syntheses of the seven-colour Geneva photometry. But in both cases blanketing corrections, the uncertain abundances, and the intrinsic sensitivity of the continuum to the effective temperature rather than the gravity made the results discouraging for the determination of precise surface gravities.

3.4 Intermediate and narrow band spectral classification

Spectral classifications also use narrow bands, defined by filters, by the exit slit of a spectrograph, or taken from photographic spectra. In this way measurements of individual features become practicable, including individual strong absorption lines. However different lines and spectral regions must be used for different types of star, according to age, chemical composition and temperature. The examples here are intended to do no more than illustrate the accuracy attainable; the range of application; and the limitations of the photometric methods.

3.4.1 Stromgren and Crawford uvby system

As an example of the intermediate band systems, the uvby magnitudes of Stromgren-Crawford (Stromgren, 1966) can be combined to give indices, corrected for reddening, as follows:

$$[c_1] = (u-v) - (v-b) - 0.2(b-y)$$

$$[m_1] = (v-b) - (b-y) + 0.18(b-y)$$

$$[u-b] = (u-b) - 1.84(b-y)$$

$[c_1]$ is a measure of the Balmer discontinuity; and $[m_1]$ of the continuum towards longer wavelengths. The resulting two-dimensional classification separates luminosity classes, but the detection of population differences is far from unambiguous and the system is more usually combined with the Crawford β index.

3.4.2 Crawford Hβ index

One of the most popular measures of hydrogen line strength is the β index (Crawford and Mander, 1966; Crawford, 1966). This is defined by two filters, with 30A and 150A widths, centred on the Hβ line at 4860A. In this way the strength of the line is measured against the local continuum.

Absolute magnitude calibrations of the index have been reviewed by Stromgren (1963, 1966), Petrie (1965) and Crawford (1973). Broadly speaking an accurate luminosity classification is possible for stars of spectral types B, A, and F. However the β index is more frequently used with the uvby system of Stromgren, Crawford and Barnes,(1970) to provide a three-dimensional classification corresponding to (Te,g,a).

Errors in β and in the other indices amount to uncertainties in log g of 0.2 to 0.3 for main sequence stars; for giants, where the effects of pressure are less, the error is greater. The same system also applies to later type stars because, although β becomes more sensitive to temperature than gravity, the Balmer discontinuity (the c_1 index) serves as an indicator of g.

The empirical calibration by Crawford (1966) indicates a high resolution by $[c_1]$ in terms of absolute magnitude, and hence in gravity. However Bell (1971, 1972) synthesised the photometric indices and found that the derived gravities were sensitive to blanketing and metal abundances. An extreme example, a K-dwarf, had

$$d \log g / d(u-b) \simeq 60$$

3.4.3 The Barbier and Chalonge method

The Barbier and Chalonge classification (Barbier and Chalonge 1939; Berger, 1962) uses the Balmer discontinuity and the pseudo-continuum formed by the closely packed hydrogen lines as the discontinuity is approached. Two parameters are defined: D_B and λ_1, the size and wavelength of the jump; and may be measured from photographic spectra or photometrically. These parameters are sufficient to define the effective temperature and gravity over the range O5-F7 with, for early type stars, accuracies of about 500° and 0.3 dex respectively.

A third parameter may also be added to take account of abundance effects. This is usually the gradient of the ultra-violet continuum (Chalonge and Divan, 1953).

3.5 Spectral classification based on line strength

The original spectral classes were based on visual estimates of line strengths, and more especially the ratios of line strengths although quantitative measurements followed rapidly (eg Hynek, 1935). These luminosity criteria are an empirically selected group of the lines which, as predicted by theory, show differential sensitivity to changes in the pressure in the atmosphere. Particular attention is drawn to the MKK system (Morgan, Keenan and Kellman, 1943) which provides luminosity classes for stars in any part of the spectral sequence, and largely subsumes the criteria of other authors (eg Adams et al, 1935; Young and Harper, 1924; Williams, 1936ab).

The MKK system depends on visual inspection of features in low or moderate dispersion spectra. Criteria are chosen to maximise the discrimination between different luminosities, but the chosen features are not necessarily ideal for quantitative work because:

a. the characteristic may be a blend of absorption lines which cannot easily be quantified; and
b. the MKK system cannot take into account any features of the continuous spectrum.

The majority of the line ratios in the MKK and other systems combine pairs of lines in order to remove the effects of differences in abundances; and moreover lines formed from different stages of ionisation. This confirms the results in section 2.5.3. The principle exceptions are the lines of hydrogen; and the very strong metal lines where broadening effects are important.

3.5.1 Hydrogen lines

The β index of Crawford has already been discussed but the Hβ and other Balmer lines are also used in many more classification schemes. In particular the H γ line has been calibrated against absolute magnitude both from photographic spectra and photometrically by many authors (eg Oke, 1957; Petrie, 1966; Kopylov, 1958; Furenlid, 1971). These calibrations are especially useful because they achieve useful accuracy which is largely independent of the spectral type of the star and insensitive to evolutionary changes. For example Klinglesmith (1971) combined Hγ with (B-V) colours to give an orthogonal pair of parameters over a wide range of temperature and gravity. It is however only possible to use the Balmer lines in this way for early type stars (spectral types B and A and F), as they are insensitive to log g for effective temperatures of about 7000K or less.

3.5.2 Strong metal lines

Both theory and the empirical evidence of visual classification schemes shows that strong metal lines will be sensitive to pressure because of broadening effects as well as changes in ionisation. These lines are particularly prominent in the spectra of cooler stars and, as hydrogen lines cannot be used as luminosity indicators, lines such as CaII H&K, CaI 4227A, NaI D, MgI 'b' and CN 4226A have been used in classification schemes. Examples are as follows:

(i) Spinrad and Taylor (1969) used flux ratios from narrow band photometry of both standard and program stars to define indices for 5 features:

CN band	4200A
CH band	4300A
CaI	4227A
MgI b	5175A
NaI D	5892A

These were then analysed in terms of gravity, microturbulence and metal abundance; the effective temperature was fixed from

broad-band photometry. The strong lines are of course sensitive to pressure and Spinrad and Taylor found that their combined observations allowed the gravity to be found independent of other parameters. However Gottlieb and Bell (1972) did not concur and suggested that abundance and gravity effects were not independent: the mutual uncertainty was about 0.3 dex.

(ii) A similar system was derived by Dickow et al (1970) using 6 indices:

g	The G-band peak
n	the CN band at 4226A
k	the break at 4000A
m	metallic line index
f	violet/green colour
u	uv/violet colour

Hansen and Kjaergaard (1971) attempted a calibration of this system against stars with known surface gravities but found the data from other methods of determining gravity were inadequate. They therefore used the internal correlations of the indices to find thatn and f gave the gravity with an internal consistency to within a factor three (about 0.5 dex.)

(iii) Griffin and Redman (1960) have developed a photo-electric technique which can be applied to virtually any strong spectral line and which has been used by many authors (see reviews by Redman (1966) and Whitney (1969)). For example Griffin (1961) found that the FeI triplet at 5250A was an excellent luminosity criterion, confirming the qualitative estimates of Thackeray (1949). Peat (1969) has explained this as a result of the relatively small pressure broadening of these lines; and of the changes in the iron ionisation equilibrium with pressure in late type stars.

(iv) Photometry of the Na I D lines (Griffin, 1961; Spinrad, 1962; Price, 1966) shows good separation of luminosity classes for spectral types later than about KO. The NaI infra-red

triplet is also a luminosity criterion (Sharpless, 1956; Whitford, 1966) for cooler stars, but only very sensitive in very cool stars (later than MO).

(v) The Mg I 'b' triplet has been investigated by many authors (eg Deeming, 1960; Price, 1966; Wood, 1969; Guinan and Harrison, 1975) and shows some sensitivity to luminosity below about G5 temperatures, but is only useful later than K5.

(vi) Many of the molecular bands in the spectrum are sensitive to pressure and hence to gravity. Examples are the MgH band (Wood, 1969); the CH G band (Griffin and Redman, 1960); and the CN bands near 4200A (McClure, 1970).

3.5.3 Wilson-Bappu method

As a final example of the importance of empirical schemes the Wilson-Bappu classification (Wilson and Bappu, 1957; Wilson, 1966) relies on a correlation between the width of the emission core of the CaII K line and the absolute magnitude of the star. Although the theoretical basis for this correlation is far from certain (Bappu and Silvaraman, 1971; Reiners, 1973; Ayres et al, 1975), the correlation is accurate, consistent and widely used.

3.6 Precise and absolute measurements of spectroscopic gravities

3.6.1 The hydrogen lines

The pressure sensitivity of the Balmer lines has been derived theoretically and demonstrated by their use in spectral classification schemes. It is therefore expected that they will be susceptible to more detailed analyses. This is indeed the case, and the early quantitative correlations with absolute magnitude have been developed to include model atmosphere computations: first in terms of the equivalent width of the line and then to take account of the line profile.

Balmer lines in early type stars can be observed with great accuracy but the derived surface gravities are liable to errors due to two areas of uncertainty in the theory of their formation. First, the pressure sensitivity arises principally from the wings of the lines, which are broadened by the linear Stark effect. This broadening is not amenable to calculation and successive approximations (Verwoij, 1936; Odgers, 1952; Kolb, 1957; Griem, 1960, 1962; Edmunds, Schulter and Wells, (ESW) 1967) have failed to produce a definitive solution. As a result of the difference between the Griem and ESW theories the absolute precision of the Balmer lines as gravity indicators is open to doubt. The second theoretical uncertainty is the model atmosphere. Both the continuum and the hydrogen lines are affected by deviations from LTE in the atmospheres of early type stars; and blanketing must also be taken account of if the model is to be reliable.

It is therefore particularly interesting that the full linearisation models of Mihalas (1972), using detailed non-LTE methods for both lines and continuum, and the Stark effect calculations of Smith et al (1971, 1973); Vidal et al (1973) reproduced Balmer line profiles within the observational error.

If the theoretical doubts are eliminated there will yet be residual errors arising from uncertainty in abundance and effective temperature. The existing applications of Balmer lines to spectroscopic gravity determinations (eg Klinglesmith, 1971; Strom and Peterson (1968), Peterson (1969); Olson (1968, 1969, 1975) suggest that the precision reached should be about 0.1 in log g.

3.6.2 Weak lines

The line ratios used in visual classification schemes find their counterpart in the use of the ionisation equilibrium to determine surface gravity from model atmospheres.

At its simplest this technique is a measure of the electron pressure where a line is formed and on this basis Pagel (1962)

investigated the behaviour of the MKK criteria. But the electron pressure varies through the atmosphere. The correct procedure therefore is to calculate the lines from a full, stratified model atmosphere. If the effective temperature is known from other observations, the gravity can then be adjusted until the observed strength of lines of the different ionisation stages of an element are reproduced - with, of course, a single abundance. There are however three sources of error which are not always recognised fully. First, the electron pressure depends very much on the metal abundances used to construct the model atmosphere. Higher abundances lead to higher values of p_e for a given gravity. If the star has a lower metallicity than allowed for in the model it will mimic a lower surface gravity. Second there are frequently uncertainties in the oscillator strengths used to compute the lines. Oscillator strengths of weak lines are not usually known precisely, and the lines must be weak if the effects of broadening are to be eliminated. Moreover there is a very real possibility of systematic errors between the oscillator strengths of different ionisations which will translate directly into a systematic error in the derived surface gravity. Third there is the possibility of non-LTE effects. For example Athay and Lites (1972) have predicted departures from LTE in the FeI - FeII equilibrium in the solar photosphere; and Smith (1974) has found evidence of similar departures in the atmosphere of supergiant stars.

Finally the effective temperature may not be known precisely; and is very often subject to very great uncertainties. As the ionisation equilibrium is very sensitive to temperature, gravity determinations by this method will have correspondingly large uncertainties. (See chapter 9).

As the internal error of these determinations is often as much as 0.2 dex, the true uncertainty taking account of abundances, oscillator strengths, non-LTE effects and uncertainty in the effective temperature must be very much greater. And the effects of oscillator strengths and non-LTE equilibria are likely to be systematic.

3.6.3 Strong metal lines

Strong metal lines such as Na I D and Mg I b have long been recognised as sensitive to pressure and correlations with absolute magnitude were soon established. As indicated above, such lines also feature in many quantitative spectral classifications. There are however relatively few examples of precise interpretations of the line profiles or strengths by means of model atmospheres. Cayrel de Strobel (1966, 1969) computed the equivalent widths of the NaI D and Mg I b lines for a grid of cool atmospheres and fitted profiles observed in late type stars. It was found that the equivalent width was too sensitive to microturbulence to determine log g at higher temperatures. Swamy (1966) also used the Na D lines to measure pressure; and Gray (1972) used photo-electric scans of the same lines to derive spectroscopic gravities for 14 late type stars. His analysis fixed g to within 20 per cent, and greater precision would be possible with more accurate observations. However, Gray also emphasised the additional uncertainty introduced by temperature. For a KOV star for instance, a change of 4 per cent in T_e changed the derived gravity by 340 per cent.

Other lines which are affected by pressure broadening and therefore suitable for gravity determinations include Ca I 4227A (Vardya and Bohm, 1965) and Ca II H&K (Lutz et al, 1973; Ayres et al 1975; Lutz and Kelker, 1975). All are subject to the temperature difficulties. Problems of oscillator strengths may be important; and the abundance must still be determined. Moreover the broadening of such lines involves damping constants which are not often known to better than a factor 3. Finally the possibility of non-LTE effects must again be borne in mind. For example Johnson et al (1973) found that the luminosity sensitivity of the OI multiplet at 7774A was mainly due to increases in the non-LTE effects as the gravity decreased.

3.7 Surface gravities derived from observations of binary stars

As binary stars are the only source of non-spectrographic surface gravities they are an important check on all other

methods. Visual binaries require a radius measurement to derive the gravity from the dynamical mass, so these results are not entirely independent of photometry and model atmospheres. Eclipsing binaries do however yield entirely independent masses and radii. There are unfortunately very few observable eclipsing binaries for stars later than G1. Cool stars must thus be compared with visual binaries only, where uncertain parallaxes limit the accuracy of the radius and hence the gravity.

Surface gravities of visual binaries have been derived by, for example, Gray (1967, 1969); Herbison-Evans et al (1971); Worth and Heinz (1974). Probable errors are usually less than 15 per cent, and this might be improved with the use of speckle or amplitude interferometry. Data from eclipsing systems are more plentiful and results and references are given in the review by Popper (1967); and by Popper (1974); Olson (1975); Batten (1973).

It is not easy to apply the usual spectral classifications to binaries, but a number of comparisons have been made between the dynamical surface gravities and the values derived spectroscopically. Most notable among these are the many attempts to establish which (if any) of the H-line broadening theories was correct. Examples are Olson (1968, 1975) and Popper (1970).

As an example of photometric schemes checked by binaries, the gravities of the Morgan-Neff system for A, F and G stars were compared by Neff (1969) with dynamic gravities from visual and eclipsing binaries. The conclusion was that the photometric gravities were systematically larger by about 0.3 dex. Notwithstanding explanations of this difference (eg poor model atmospheres) it is an indication of the failings mentioned above, and reinforces the conclusion that such methods are unsatisfactory where absolute surface gravities are wanted. Olson (1971) similarly used binaries to compare the uvby and gnkmf systems and (1974) to calibrate uby photometry.

3.8 Conclusions

The following conclusions may be drawn from the preceding discussion of representative schemes for determining surface gravity:

a. The hydrogen lines provide a satisfactory basis for the spectroscopic determination of gravities in early type stars. Model atmospheres for these stars appear to be adequate and the formation of the Balmer lines is understood - apart from the quantitative broadening function. Once the latter is resolved precise and absolute measurements will be possible with greater confidence. Furthermore the Balmer lines lend themselves to accurate photometry so that orthogonal (T_e, g) and (T_e, g,$\underline{a}$) spectral classifications are straightforward.

b. In stars of intermediate temperature it is more difficult to find a feature sensitive to gravity. However the Balmer discontinuity and lines may be combined to find the acceleration due to gravity.

c. For late type stars there are, broadly speaking, two possible approaches to the determination of precise, absolute gravities. The ionisation equilibrium of an element is intrinsically the most sensitive but suffers from uncertainties in oscillator strengths and in the statistical equilibrium between the two ionisation stages. Line profiles do not have these difficulties, but the broadening function is not usually known at all well and the abundance of the element must be found. In addition both are susceptible to errors in the effective temperature adopted, and the results from ionisation equilibria are particularly sensitive. Taking this into account, with the knowledge that effective temperatures are not easily defined for cool stars, it is doubtful whether any of the current measurements achieve an absolute accuracy better than 0.3 in log g.

There are of course many arbitrary or empirical schemes which derive surface gravities spectroscopically for cool stars, but the perceived need is for a method which:

i. is largely independent of effective temperature;

ii. does not rely on the validity of the LTE assumption;

iii. achieves an accuracy of 15 per cent in g.

4. SURFACE GRAVITIES FROM METALLIC LINE PROFILES

4.1 Method

The perceived need for more precise gravities for late type stars could be met by:

a. removing the uncertainties associated with the method of ionisation equilibrium of weak metal lines; or

b. improving the analysis of strong metal lines; or

c. finding an alternative pressure-sensitive feature.

(a) requires great improvements in the oscillator strengths; and moreover will in any case always be dependent on the model atmosphere; and on non-LTE effects which, at present, cannot be predicted with certainty. (c) is possible as there are empirical criteria, such as molecular bands, which might be used. However there are at present too many unknown factors eg oscillator strengths and the quantitative equation for molecular formation.

There is however considerable scope for improving the methods based on the pressure broadened wings of strong lines. As indicated above these are usually subject to considerable errors which arise from uncertainties in:

a. the effective temperature;

b. the abundance of the element;

c. the oscillator strength;

d. non-LTE effects.

Each of these affects the population of absorbing atoms or line opacity and, as the wing depends on this and the pressure

broadening, leads to the wrong gravity being derived. In addition the damping constants for the line are often poorly known, so that a further uncertainty is introduced into the computation of line profiles from model atmospheres.

The method used to eliminate or minimise these uncertainties can be given briefly in a simple form. Taking together equations (2.36), (2.38), and (2.40) (and dropping the frequency suffix for convenience):

$$a = \text{const} \int d\tau_c \{B(\tau)\exp(-\tau)(1+ 1/k_c) - B(\tau_c)\exp(-\tau_c)\}$$

If $1/k_c \ll 1$, as in the weak wing of a line:

$$a \simeq \text{const} \cdot 1/k_c$$

The absorption 1 depends on the profile function, which is essentially the damping profile if i. the line is strongly damped; and ii. the wing is looked at well outside the Doppler

core. In this way the wing of the line is insensitive to microturbulent velocities, which increase the Doppler width. Then from equations (2.39) and (2.42)

$$l \sim l_0 \Gamma$$

and

$$a \sim \text{const.} \cdot \Gamma \cdot f_{ij} n_i \qquad (4.1)$$

For the majority of strong lines in late type stars the damping is due principally to the interaction with neutral hydrogen and helium. Simple theory gives for this (see section 7.4 below)

$$\Gamma = \text{const.} \; C_6^{0.4} \; v^{0.6} \; N$$

where C_6 is a coefficient for the line, v the relative velocity of atom and perturber, and N the perturber density.

With the usual symbols:

$$V = \text{const} \left(T(1/m + 1/M) \right)^{\frac{1}{2}}$$

and since hydrogen generally dominates both the damping and the gas pressure in the atmospheres considered

$$N_H = P_g / kT$$

to give

$$a = \text{const } C_6^{0.4} n_i f_{ij} P_g T^{-0.7} \quad (4.3)$$

The absorption depth will thus be sensitive to changes in the pressure as the gravity changes. On the other hand the temperature structure is not changed greatly for different gravities, so the factor $T^{-0.7}$ will be of little importance. Furthermore even major uncertainties in the temperature in the atmosphere will matter little since, for example, a 10 per cent error in T corresponds to only 6 per cent in p_g.

In principle measurement of the absorption depth would, if the damping coefficient C_6 was known, determine p_g. However two other factors enter equation (4.3). First there is the oscillator strength. This can be measured; and, for strong

lines, with precision. Second the number of atoms n_i in the absorbing state must be found, using the Saha-Boltzmann equation, for the ionisation and excitation and the abundance of the element. n_i is therefore sensitive to the temperature and pressures in the atmosphere.

To avoid the uncertainties this introduces, n_i can be found from weak lines with the same lower level as the strong, damped line. For very weak lines:

$$W \sim \text{const } f'_{ij}\, n_i \qquad (4.4)$$

dividing (4.3) by (4.4)

$$a/W \sim \text{const } C_6^{0.4} \frac{f_{ij}}{f'_{ij}} P_g\, T^{-0.7} \qquad (4.5)$$

For real lines the cancellation of the effects of changes in n_i will not be so complete, but the ratio a/W will be very much less sensitive to temperature than would the absorption (a) alone. This is especially so if the lines are of similar wavelengths so that the continuum opacities are much the same and the same variations with depth occur. And the observations of the wing can be made where the absorption depth corresponds to the mean depth of the weak line, so the depths of formation

are very close. Furthermore the abundance derived from such very weak lines will, like the absorption in the wing of the strong line, be insensitive to any microturbulence.

Of course calculations will also have to take account of the variations with depth in the atmosphere which are ignored here. But the principle is clearly that the abundance should be determined in such a way that the combination of abundance and the Saha-Boltzmann equation gives the correct value of n_i.

4.2 Oscillator strengths and abundance

Oscillator strengths enter the method twice. First the oscillator strength of the strong line must be known. Secondly, there must be values for the lines used to derive the abundance. Weak lines must be used to find the abundance if the effects of damping and microturbulence on the line strengths are to be avoided (Blackwell et al, 1972a) and these typically have oscillator strengths some 5 orders of magnitude smaller than the strong lines. This presents very real difficulties because very few measured oscillator strengths are accurate over such ranges. Very often there is a systematic error according to line strength which would result in an erroneous abundance; and this error would be transmitted by the absorption computed for the wing of the line to the derived gravity.

Accurate oscillator strengths are however possible with the technique developed by Blackwell (see chapter 5) using the King furnace at Oxford. It was therefore decided that only these, and the few measurements of comparable accuracy, would be used.

It is again emphasised that, although any weak lines could be used to find the abundance, the result would then be liable to the errors introduced by errors in effective temperature: the wrong temperature structure means that the Saha-Boltzmann equation gives the wrong population.

Consider, for example, lines formed from an excited level of an ion. If the temperature used in the model atmosphere is too high the computations will predict more absorbing atoms than is in fact the case; and the derived abundance will be too low. But the same temperature effect will apply to the line absorption coefficient for the strong line. If the abundance derived from the weak lines is used to compute the absorption for a strong line from the same lower level the errors in the abundance and temperature will cancel each other. The position would be very

different if any weak lines were used indiscriminately, as they might then span a range of excitation potentials and be affected differently by the temperature distribution; and vary differentially with depth in the atmosphere.

Non-LTE effects are also largely eliminated by combining lines from the same lower level. Considerable deviations from LTE populations may exist, especially in the atmospheres of giant stars, but these are of little consequence when the abundance of that particular level is established.

4.3 Damping Constants

The damping constant (C_6) is needed to compute the profile. Laboratory measurements of these damping constants are however few and imprecise (see chapter 7).

Calculations of the interaction of hydrogen atoms and elements of astrophysical interest are also uncertain. Exact calculation of damping for the conditions prevailing in stellar atmospheres is not generally possible and the many approximate methods tend to predict only the qualitative behaviour of observed lines or, at best, are subject to very great uncertainties.

For these reasons the preferred source of damping constants was observations of the line profile in the solar spectrum. These solar profiles were combined with model atmospheres and abundances derived as indicated above to give an empirical damping coefficient. Of course this is not wholly satisfactory, since there may be errors due to the assumed model atmosphere. But it is felt to be the best method available at present; and the calculations of the NaI D lines by Blackwell et al (1972b) from the accurate theoretical damping coefficients of McNamara (1971) and Lewis et al (1971) suggest that models of the solar photosphere are sufficiently precise.

4.4 Choice of lines

The method chosen would be most precise for lines with high damping coefficients which exhibit extensive damping wings. Other things being equal, this suggests lines from high excitations. However the line must also be broad (as opposed to just highly damped) or the profile will be too dependent on macroturbulent velocities (Evans and Testerman, 1975). Finally section 2.5.4 showed that, other things being equal, the greatest sensitivity came from a neutral line of an element where the majority of atoms were ionised.

The choice was therefore constrained to strong lines, and the luminosity criteria used by others (section 3) were examined for candidates. A considerable number were however ruled out by the method to be used to determine the abundance. For example, NaI D and MgI b are broad lines with, in the late type stars, damping wings. But all are also formed from levels which do not give rise to other, weak lines which could be used to find the abundance.

Finally the lines had to be measurable in the Oxford King furnace. This restriction applied principally to the excitation potential, as lines of high excitation and small oscillator strength could not be studied.

Taking account of all these factors it was concluded that, for a preliminary study, lines should be chosen which originate from the ground state and 1 ev groups of neutral iron (FeI). In making this choice considerable weight was attached to the existence of accurate oscillator strengths (Blackwell et al, 1975) for some of the lines. But in the final chapter it will be seen that there are rather few other possible elements.

4.5 Observations and measurements

The first stages of the method were therefore:

a. measurement of oscillator strengths for the chosen lines;

b. observations and interpretation of weak solar lines to determine the abundance for the levels;

c. observations and interpretation of strong solar lines to determine the damping coefficients.

These are familiar problems and the aim was to reduce at each stage the possibility of systematic error, and to continue to emphasise the importance of absolute precision (cf Blackwell, 1974, 1976). Only in this way, it was felt, could the absolute surface gravity be found with the precision wanted.

5. OSCILLATOR STRENGTHS OF NEUTRAL IRON

5.1 Introduction

Oscillator strengths are of particular convenience in astrophysics where the problem of line formation usually consists of pure absorption from a lower level in equilibrium with the surrounding plasma and with the radiation field. They are however only one measure of the transition probability between two states. It is perhaps more familiar to look at this probability in terms of the Einstein coefficients or the lifetime which are related to the oscillator strength by the standard equations:

$$g_i f_{ij} = -g_j f_{ji} = \frac{mc^3}{8\pi^2 e^2 \nu^2} g_j A_{ji}$$

$$= \frac{mc}{4\pi e^2} g_i B_{ij} h\nu$$

and of course:

$$1/\tau_j = \sum_j A_{ji}$$

In principle therefore any measure of the line strength will, if the physical conditions which determine the number of atoms in the states are known, determine the oscillator strength. It is however difficult to establish these physical conditions precisely without taking great care over the source of the spectral line. And the line strength must be measured accurately. These two factors are, broadly speaking, the reasons for the very large uncertainties in most reported measurements of oscillator strengths.

The majority of results come from measurements of the emission lines formed in an arc or luminous shock tube. Many of the earlier values relied on free burning arcs (Corliss and Bozman, 1962; Allen and Asaad, 1957) but these have been superseded by the various forms of stabilized arc (eg Garz and Kock, 1969; Bridges and Kornblith, 1974). The aim of the more complex source is to increase the stability of the arc in both temperature and density during the time measurements are made. This is important because the source function and therefore the line strength is sensitive to both, and precise values for the plasma are needed to derive accurate oscillator strengths. Errors from the use of the wrong temperature and pressure can be very large (Takens, 1970; Wolnik and Berthel, 1973) but there is no simple or reliable way to determine these properties throughout the arc.

Emission lines are also observed from the discharge of a shock tube. Apart from the difficulties of measuring the line strength during the very short time of the discharge, it is again difficult to determine the population of absorbing atoms and hence the oscillator strength (Gilbert et al, 1974; Wolnik et al, 1970, 1971). There are also problems in allowing for the effects of collisional broadening at the very high pressures which are usual.

Both arc and shock tube measurements also suffer from the uncertainty of self-absorption. This arises because the hot, emitting plasma is generally observed through a relatively cool plasma at the edge of the source, where the temperature is least well determined. Part of the energy in the emission line may therefore be absorbed, and indeed stronger lines exhibit reversal.

As both arcs and shock tubes may also be subject to deviations from LTE it is not surprising that the results from such measurements are rarely quoted to better than a 10 per cent uncertainty in the oscillator strength; 25 per cent or more is more usual. Nevertheless emission methods, and arcs in particular, allow many lines to be measured simultaneously;

provide very high temperatures (c. 15 000K) for weak lines of high excitation; and account for the great majority of the reported values of oscillator strengths.

In complete contrast to the emission methods, the majority of absorption measurements are better suited to relatively strong lines of low excitations; and are able to examine perhaps no more than a few lines at one time. Absorption methods rely on the observation of a high temperature source through a column of absorbing atoms. This may be a shock tube if high excitations are required (eg Huber and Tobey, 1967) but is more commonly a simple furnace which vaporises the element which is being examined (King and King, 1935). The temperature needed for this is very much less than for emission; and is therefore more easily maintained at a constant value, and more precisely measured. The main difficulty then becomes the precise determination of the line strength. Even this is more simple for the absorption methods, because there is no self-absorption.

One variant of the absorption method actually eliminates the measurement of line strength, at least in the conventional sense. This uses the anomalous dispersion caused by the transition - eg to introduce a phase shift into one arm of an interferometer (Huber and Parkinson, 1972; Valters and Startsev, 1964) so that the fringes generated depend for their separation on the strength of the transition. The fringe separation can then be measured with non-linear detectors, photographically for instance, to find the oscillator strength.

As will be shown below, absorption methods are capable of giving results with an uncertainty of less than 5 per cent. But there are very few such measurements; and there is little prospect of applying the same techniques to lines from highly excited levels which, at the low temperatures used, are simply not populated to any measureable extent.

Similar accuracy, and similar or even greater restrictions, is associated with lifetime measurements. Direct measurements of

lifetimes are in principle very simple and give absolute oscillator strengths: the decay of an excited atom is determined by the lifetime and can be observed. Although straightforward applications of this have yielded oscillator strengths, the very short times present great difficulty. More usual therefore are the beam-foil techniques which rely on the very high speed of the atom, excited on passing through a thin foil, to translate the time of decay into a more tractable spatial decay. These and the more sophisticated techniques (eg see Corney, 1970; Whaling et al, 1969; Klose, 1971; Hilborn and de Zafra, 1973; Assousa and Smith, 1972) must however be corrected for the effects of cascading from higher levels which may also have been excited. In addition the measured lifetime gives an absolute oscillator strength only if the branching ratios of the various emission processes are known (eg from other, relative oscillator strengths).

Although there are other experimental methods, the final source of any great number of oscillator strengths are calculations of the wave functions. Calculations have been attempted for many atoms, assuming different coupling schemes and with different approximations to the wave function. For the more simple atoms pure LS coupling and Coulomb wave functions are reasonable approximations; and give oscillator strengths with some accuracy. For the more complex atoms however - and these include iron - the wave functions cannot be treated so precisely. Semi-empirical methods are however more successful (eg Ross, 1973; Kurucz, 1974; Kurucz and Peytreman, 1975) and, although they do not achieve the precision of experimental results, are useful additions for lines which cannot be observed.

5.2 The Oxford King furnace

The measurements for this work were made with the large King furnace developed at Oxford (Peach, 1966, 1969; Collins, 1970; Blackwell, 1974, 1975) and described by Collins (1970), Collins et al (1970), Blackwell and Collins (1972). Further information about the performance of the furnace is given by Shallis (1978) who also described the improvements to the system since these results were obtained.

A simplified view of the furnace is given in figure 5.1. A transformer supplies alternating current through the water-cooled bus bars to carbon blocks and hence to the furnace tube itself. In this way up to 200kW is generated in the 120 cm carbon tube which has a 5 cm internal diameter and is 2.5 cm thick. The temperature at full power would be in excess of 3000K but is controlled by reducing the applied voltage from the transformer.

A cooling jacket surrounds the furnace and allows the tube temperature to reach very high values without danger to the connections and soldered joints. The jacket also forms part of the vacuum chamber, evacuated by a rotary pump to less than a torr before being filled by an inert gas. Control of the pump and gas feed enabled any chosen pressure to be maintained within a torr or so.

At each end of the furnace are quartz windows for the light to pass through the furnace tube. At high temperatures iron from the tube diffuses along the furnace and is deposited on the cool windows. As the temperature of the tube is determined by means of a disappearing filament pyrometer, focussed on the normal faces of four blocks mounted within the tube, these deposits would change the correction which must in any case be applied for absorption by the windows (see below). The inert gas helps reduce the diffusion but to reduce deposits further the window used to measure the temperature is spaced some 150 cm from the end of the tube.

Although the temperature may be measured accurately at discrete points it is the distribution along the tube which is needed to determine the concentration of iron atoms, and the profile function for the lines formed in the column. It is therefore an advantage to have a uniform temperature which is well-defined by just four values. The Oxford furnace achieves this by means of carbon blocks spaced within the vacuum chamber so as to maintain an even distribution of energy. Collins et al (1970) and Blackwell et al (1975) report that the central 50 cms of the tube can be maintained at a uniform 2000^{o}K within the uncertainty of the measurement. 15 cm from each end of the tube the temperature is still 95 per cent of the central value. Outside the tube though the temperature falls off very sharply. This means that the length of the column of absorbing atoms is essentially the length of the tube; and that there is no uncertain region where the absorption can not be calculated.

5.3 Optical system and spectrophotometry

The optical system for the furnace had been developed over some years to use where possible mirror optics. This is seen in figure 5.2 which shows first the off-axis paraboloid giving a collimated beam from the xenon arc lamp. After passing through the furnace the spherical camera mirror forms an image of the arc on the entrance slit of the monochromator. In doing so the beam is incident on a half-silvered beam splitter which passes light to the second, identical spectrometer mounted directly above the first.

The spectrometers comprise first a Spectrosil prism in a Czerny-Turner mounting to isolate the selected spectral region on the entrance slit of the spectrometer-proper and thereby to prevent overlapping orders. The spectrometers are also a Czerny-Turner system but with a Bausch and Lomb grating ruled at 3160 cm^{-1} and 63^{o}. The focal length (9.5 metres) gives a dispersion at the exit slit of about 5 mm A^{-1} at 5100A in the tenth order. Finally a lens images the exit slits on the photocathode of the detector.* The quality of this optical system has been demonstrated by precise measurements of the profile of laser lines (Blackwell et al, 1971); and Blackwell et al (1967) discussed the low noise detection system which complements the optical system.

The detector system relies on the use of not one but two or more slits to provide a reference level for the detector and associated electronics. In the form of the apparatus used in this work, the exit slit assembly had two fixed slits of variable width on either side of a single slit which could be scanned across the spectrum by means of a stepping motor and gear chain. A rotating slotted drum behind the focussing lens then passed first light from the central slit only, then from the two fixed

---

*The lenses have now been replaced by off-axis paraboloids which image the exit slits on the cathode. The focus is thus independent of wavelength and the image does not move to different parts of the cathode which might have different responses. Efficiency in the blue and near ultraviolet is also improved.

slits only, to the detector. In use the slits were placed on the continuum and the fixed slits' width adjusted so that the same energy passed through them as through the central slit. Then, if the scanning slit crossed an absorption line, the energy would be measured by reference to the continuum level.

Low noise photomultipliers detected the chopped beam, and were cooled to about $-10^{\circ}C$ and operated below their nominal voltage in order to further reduce the dark current. The photocathode current was then amplified to give the input for a phase sensitive detector to measure the signal corresponding to the chopping frequency. Random fluctuations in the intensity of the lamp were therefore unimportant, but a systematic change would have reduced or increased the current, and thence the difference between the current from the line and continuum and the signal. To avoid this problem the control system maintained a constant mean photocathode current by regulating the EHT supply and hence the gain. If the current from the comparison slit illumination was C and from the scanning slit L, the mean current would have been $(C + L)/2$. But the gain automatically increased to give a mean current C. The signal detected by the phase locked amplifier was therefore

$$S = \frac{2C}{C + L} \cdot (C - L)$$

The system is then readily calibrated by blocking the light through the scanning slit, to give

$$S_o = 2C$$

so that the absorption depth of a line is derived from the measured signal S and calibration value S_o as:

$$d = \frac{2S}{S_o + S}$$

The remainder of the system comprised unexceptional analogue to digital convertors; integration of the measured signal; and facilities to record the signal on punched tape; to display the values; and to drive a simple chart recorder.

5.4 Choice of lines for furnace measurements

As indicated above, the lines for the gravity and abundance determination were to be strong and weak lines respectively from the same lower levels of the terms a^5D and a^5F of FeI. On astrophysical criteria (ie their strength in the solar and other spectra) suitable pairs were, for instance, 3886.28A (strong) and 5127.68A (weak); 3899.71A (strong) and 4445.5A (weak); 3895.7A (strong) and 4471.7A (weak); 3719.9A and 3859.9A (strong) and 5060.1A (weak) - all from the a^5D term. And 5269.9A (strong) and 6221.6A (weak) from a^5F. These lines were therefore an essential part of the program of oscillator strength measurements.

The selection of lines was however further influenced by the method of the measurements (see below) which required a series of lines without any large single difference in oscillator strength. In addition Blackwell et al (1975) had derived an absolute series of oscillator strengths for lines from the $a^5D_{0,1}$ levels which was to be used as a photometric scale for the further furnace measurements. It was thus necessary to link the new observations to those lines.

Finally the difficulty of determining the abundance from just one line (see chapters 6 and 9) was anticipated, and further weak lines were added to the program for the furnace, even though they were not from the same lower level as the strong lines. This amounted to measurements of all lines from the ground state term which could readily be observed in the furnace. For the excited group however the measurements were not expected to give more than preliminary results because, as will be discussed below, the application of the furnace technique to difference of more than about 0.1 eV would present special difficulties. The selection of excited lines was correspondingly less comprehensive, and was further restricted by practical limits on the furnace temperature (see section 5.7).

5.5 Experimental method

The method used to apply the Oxford furnace and spectrometers to the measurement of FeI oscillator strengths had been developed and improved over many years (Peach, 1969; Emerson, 1970; Collins, 1970; Collins et al, 1970; Blackwell and Collins, 1972; Blackwell et al, 1975, 1976; Blackwell, 1974, 1975). The experience of the many previous applications accounts in large part for the relative ease with which the results of this investigation were obtained. There were of course many difficulties. But these could be anticipated and their effects eliminated or minimised. In particular, the oscillator strengths reported by Blackwell et al (1975) from the Oxford furnace provided a calibration between the absolute oscillator strength of FeI lines from the 0.00 and 0.05 eV levels and the values of, for instance, Corliss and Warner (1964); and demonstrated the accuracy of the furnace technique. It was therefore possible to choose the furnace observations with foreknowledge, to a very good approximation, of the relative strengths of the lines. As will be shown this is desirable to ensure there is no great disparity in line strength. And more generally it was practicable to accept the previous results as prima facie evidence for the technique; and thus to devote greater effort to improving the reliability and precision of the detailed and numerous component measurements.

For observations of FeI a carbon furnace tube was first heated to about 1500K and evacuated, the pumping continuing for some hours while trace contaminants were vaporised and removed from the carbon. The tube was then cooled; and a carbon crucible containing iron filings inserted before raising the temperature to some 2700K under a pressure of about 300 torr of argon. In this way iron was vaporised and a high concentration of iron maintained in the tube for some hours. The inert gas ensured that the diffusion of iron vapour was not likely to contaminate the windows.

Although measurements could be made (and some were) with the crucible within the tube, it reduced the energy of the beam and thereby the signal to noise ratio. Measurements were usually made without the crucible, when the iron vapour pressure arises from the very large amounts of iron deposited on the carbon tube; and perhaps from iron carbide formed at the high furnace temperatures.

The theory underlying the furnace measurements is outlined in the next section, but very briefly rests on the relative strength of two absorption lines in the furnace spectrum. An initial step in the experimental method is therefore to choose the pairs of lines. As the photometry of the line is most accurate for lines of neither very small nor very large central depth, the lines in any single comparison should not be of greatly disparate strengths. Given the earlier data it was possible to predict pairs of lines which met this condition, and their relative strengths. The second step was therefore to increase the furnace temperature until the lines appeared in the spectrum measured by the two scanning slits of the two spectrometers; and to adjust the power supplied to the furnace until the desired central depths were reached. At the same time the vacuum pump and gas handling system were used to maintain a constant pressure of argon.

The gas pressure used depended on the temperature of the furnace. At low temperatures the Doppler broadening of the line is small, and damping effects would be important if the pressure were high. Pressure of 10 - 20 torr were therefore used at 1400-1600K. At higher temperatures however there is a larger Doppler width; and more need to prevent the diffusion of iron onto the windows, and to ensure LTE by collisional transitions. At temperatures of 2700K, for instance, up to 100 torr was accepted.

Once the lines were identified and the approximate strength established, the scanning system was set for the measurements. In the initial stages a coarse scan was employed, covering

perhaps 5 A in less than 200 steps. For the photometry proper however the scanning slit was set to traverse a very much smaller spectral range centred on the line. In the majority of the measurements this involved some 80 points separated by a constant distance, with the signal integrated for a second at each point. The line profile in each spectrometer was therefore sampled at 80 points separated by about 4 mA (according to the wavelength) and a pair of scans took something in excess of 80 seconds to complete.

With the spectrometers set on the centre of the lines the central depth was monitored until the furnace reached equilibrium Great importance was attached to ensuring that the temperature, pressure and accordingly the concentration of iron atoms did not change during the course of a set of observations. The furnace power and pressure were kept constant; and the temperature measured. But by far the more sensitive test of stability was the central depth of the lines which were being observed. No measurements were started until these were constant. And observations were rejected if the line strength did vary. The observations usually comprised a minimum of 25 scans of the line pair.

Before and after each set of scans the spectrometers' detector systems were calibrated to ensure that the light passing through the scanning slit, when positioned away from the line, was the same as that passing through the fixed, comparison slits. Similarly the detector system was calibrated by blocking the light through the scanning slit, equivalent to a 100 per cent absorption depth. The calibration signal S_o rarely changed by more than 0.2 per cent during the course of a set of scans, indicating the stability of the detector system.

The final step before starting the scans was to measure the temperature distribution in the furnace. Four small carbon blocks mounted on a carbon strip in the furnace gave accurate positions at the centre of the tube and 15, 30 and 45 cm from

the centre on which to focus the telescope of a Leeds and Northrup disappearing filament pyrometer. The temperatures were also measured at the end of the set of scans; and at least once during the course of the scans.

Following these preliminary measurements the lines were scanned automatically by the control system which traversed the slits; integrated and recorded the signal; and reversed the scanning motion at the end of each complete scan. The displayed signal and the chart recorder gave immediate measures of the line depth and of any change in line strength. But as already indicated, the measurements were not started until the furnace was stable. The only action necessary to maintain this equilibrium was to adjust the transformer voltage, which varied substantially due to fluctuations in the mains supply, and the gas pressure which tended to increase, presumably as a result of further outgassing from the tube.

As soon as the requisite number of scans was completed, and the temperature and spectrometer calibrations recorded, the furnace was cooled to less than 1000^{o}C. A further set of scans (usually 25) was then made with precisely the same spectrometer and detector configuration. The background illumination of the lamp was thereby measured to provide a correction to the equivalent width of the absorption lines (see below).

Finally the furnace was brought again to the working temperature and the same lines measured with the spectrometer-detectors reversed (ie the line which had been measured with the upper spectrometer was measured with the lower and vice versa). The background scans were also repeated with the alternative configuration.

5.6 Reduction procedure

The reduction of the measured profiles was carried out on the NOVA computer at the Department of Astrophysics, Oxford, using a variant of a BASIC program provided by Drs A D Petford and P A Ibbetson. Each stage of the operation was displayed so that any unusual features (eg punching errors or changes in the line strength) could be seen.

The first operation took each scan, applied the calibration (see section 5.3) to give the intensity relative to the "continuum", and fitted a straight line through the outermost points of the scan. This line defined the continuum against which the line strength was integrated to give an equivalent width: the dispersion - calculated from the grating position and calibration formula - and step size defined the wavelength scale. The same procedure was applied to the scans of the background lamp spectrum. Mean equivalent widths from these were then applied as corrections to each of the equivalent widths of the lines scanned on the respective spectrometers.

Next the program computed for each line the curve of growth for the particular furnace conditions. If the line was weak and the column of vapour uniform the equivalent width would be proportional to the oscillator strength. But the central depths of the lines were too great for this approximation; and the temperature varied along the length of the tube. The column of vapour was optically thin though so that the intensity in the line relative to the continuum could be written:

$$I_\nu / I_c = \exp(-L(\nu)) \doteqdot 1 - L(\nu)$$

where $$L(\nu) = \int_0^\infty dx\ n(x)\ l(\nu,x)$$

and $$W = \int_0^\infty d\nu \int dx\ n(x)\ l(\nu,x)$$

Here the equivalent width W is related to the density of absorbing atoms and the atomic absorption coefficient. As the pressure was always small thermal broadening dominates the profile function (see section 2.4) so that:

$$W = \int_0^\infty d\nu \int_0^\infty dx \; (\pi^{\frac{1}{2}} e^2/mc) \; f_{ij} \; N(x) \cdot$$

$$\exp(-\chi/kT(x)) \exp(-v^2)/\Delta\nu_D(x)$$

where N is the number density of FeI. Given the temperature distribution the values along the tube can be calculated. In this way absolute oscillator strengths might be found (King, 1942) but the number density is not easily established. Therefore the vapour density of iron at the local tube temperature was used (Nesmayanov, 1963) to determine the temperature variation along the tube of N, but not the absolute number. There was therefore an additional scaling factor F, and equivalent widths were computed for a range of values (F·f). From the set of observed equivalent widths, interpolation gave values of (F·f).

Repeating the process for the second line and set of equivalent widths, the same scaling factors give values (F·f'). Thus the relative oscillator strength is determined by taking the ratio. It is worth emphasising that the arbitrary measures (F·f) of the oscillator strength varied considerably within a set of scans, due to variations in the temperature and iron density. But the simultaneous measurements of the two lines meant that the ratio f/f' from pairs of equivalent widths was determined with much greater precision, as evident from the small standard deviations on the mean value.

Finally the same reduction procedure was applied to the measurements with the second spectrometer-line configuration.

5.7 Oscillator strengths of lines measured in furnace

Blackwell et al (1975) had measured 16 lines from the 0.00 and 0.05 levels of FeI and were able to display their 33 comparisons in a simple form, reproduced here as figure 5.3. As figure 5.4 shows, with the addition of the 84 line pairs measured for this work the same presentation would be impractical. The results from the furnace measurements are therefore given in table 5.1.

Columns 1 and 2 of table 5.1 give the wavelengths of the lines compared, with the line with the greater oscillator strength first. It should be noted that the measured lines from the a^5F term do not include the weak lines in the solar spectrum such as 6221.6A which has the same lower level as FeI 5269A. With a solar equivalent width of less than 10mA this would appear to be ideal for determining the abundance of iron. This and other weak lines identified in the furnace spectrum were, at the temperatures attainable, not of measureable strength. The limitation on the furnace temperature came from one of the carbon blocks which reached dangerous temperatures if the furnace much exceeded 2700K. High temperatures were needed to (i) increase the excitation of iron atoms to the a^5F term; and (ii) increase the vapour pressure and hence the number of absorbing atoms. For this reason a number of the measurements were made with such weak lines that only mean equivalent widths, from averaged scans, could sensibly be used. The relevant measured oscillator strengths are indicated in table 5.1 and should be considered only as very provisional values, more especially because it was later found that the localised heating of the carbon block was due to calcium carbonate deposited in the pipes carrying the cooling water. With this removed, the furnace is now regularly operated at temperatures in excess of 3000K.

Also indicated in table 5.1 are the comparisons where there was a large difference in excitation potentials of the two lines. As will be seen, this makes the measured oscillator strength less certain.

Columns 3-5 and 6-8 of table 5.1 give the number of scans, mean and standard deviation of the measured oscillator strength for the two spectrometer configurations respectively. The standard deviations are very small and would correspond to probable errors of less than 0.004 dex in the majority of cases. However the difference between the two measured values, listed in column 9, is much greater than the standard deviations would admit. The cause of these large differences will be discussed below, but it leads to a more substantial uncertainty in the mean value from the two configurations, given in column 10.

It is apparent from figure 5.4 that each point in the matrix of comparisons is overdetermined. The adopted values for the oscillator strength, relative to the line 3719A, could therefore be chosen to minimise, in a least squares sense, the differences between the measured relative oscillator strengths and the adopted values. Dr P G Craven provided an algorithm and computer code for this which assumed a probable error in each measurement proportional to $K(1 + (\log gf)^2)^{\frac{1}{2}}$. The form of this reflected the observed trend for greater standard deviations to be associated with greater relative oscillator strengths.

The oscillator strengths yielded by this algorithm are given in column 11 of table 5.1 with, in column 12, the residual defined by $(\log gf_{measured} - \log gf_{fitted})$. The value of K determined by the residuals was 0.0082 when the previous measurements of Blackwell et al (1975) were included. As shown in figure 5.5 the residuals lie, within expected limits, on a normal curve. The absence of any skewness or other features is consistent with the treatment of the measured values as real values plus random errors.

Residuals are discernibly larger for the lines from the a^5F level in table 5.1. There are two reasons for this. First the greater excitation introduces the possibility of errors in the furnace temperature having a significant effect on the value deduced from the equivalent widths. Secondly these lines were, as indicated, generally weaker than the ground state group of lines; and had correspondingly greater uncertainties in their widths.

The oscillator strengths were expressed relative to 3719A as there were absolute measurements which could be used to determine the absolute value of this line. Other lifetime measurements allowed absolute values for other FeI lines measured in the furnace, but the 3719A line was used because the z^5F^o upper level has a branching ratio of some 99 per cent for the transition to a^5D and about 1 per cent for the 5012A transition. The uncertain oscillator strength of the latter therefore introduced very little error into the oscillator strength of 3719A.

The absolute oscillator strengths derived from four different types of lifetime measurement are given in table 5.2, together with the absolute value found by Bell and Tubbs (1970) from atomic beam absorption. The mean value was adopted to give an absolute oscillator strength log gf =-0.43. The relative value found from the furnace measurements were then put on the same scale by:

$$\log gf = \log gf(3719A) + (\log gf - \log gf(3719A))_{furnace}$$

Table 5.3 gives the absolute values.

5.8 Errors and uncertainties in the measurements

The small residuals are evidence for the accuracy of the measurements but cannot rule out the possibility of systematic error. There is also the question of the difference between the values for the two configurations. Possible sources of error and uncertainty are therefore discussed briefly below.

a. furnace blends

It would not be possible to rule out contamination of the measured equivalent width by blending with another line. There were however no listed lines with the same wavelengths which might realistically be supposed to have any substantial strength in the furnace. Moreover the lines were, in general, measured at more than one temperature and with different tubes in the furnace. It would therefore be likely that the blend's contribution to the total equivalent width would vary differentially, and show up as an inconsistent value with large residuals. But there might be some small contribution to the weaker lines, observed only at high temperatures.

b. furnace emission

The column of iron vapour at high temperatures has a measureable emission line spectrum. The importance of this depends on the relative intensity of the emission line and of the lamp at that wavelength. Blackwell et al (1975) established the correction for the 5127A line at 2400K as 1.5 per cent of the observed equivalent width. That is, the observed value had to be increased by this amount to take account of the emission line filling in the true absorption profile. For these measurements the correction was taken from that result. For a weak line the absorption width is

$$W \propto g_i f_{ij}$$

and the emission is $I_e \propto g_j f_{ji} \exp(-hc/\lambda kT)$

so that the ratio is $\Delta W/W \propto I_e/W \propto \exp(-hc/\lambda kT)$

and taking the result for 5127A to fix the constant:

$$\Delta W/W = 0.015\exp(-hc/\lambda kT)/\{\exp(-hc/5127A \cdot k \cdot 2400)\}$$

As the correction is greater at longer wavelengths it reached as much as 2.5 per cent for the weaker lines measured. This corresponds to 0.01dex in the measured oscillator strength. But the uncertainty in the correction is smaller and does not amount to a major source of error.

c. curve of growth correction

The reduction involved an approximate solution of the equation of transfer through the furnace tube which was interpreted as a curve of growth: the equivalent widths observed were corrected to the value they would have had if the equivalent width of the line was given simply by:

$$w = \text{const} \cdot gf \cdot (\text{number of absorbing atoms})$$

This curve of growth correction was about 1mA for stronger lines with equivalent widths of up to 15mA and therefore corresponds to a considerable adjustment to the oscillator strength. Uncertainty arises because the correction depends on a knowledge of the physical conditions in the furnace. First the number density of iron atoms must be calculated, and this relies on the vapour pressure at the local tube temperature. The data for vapour pressure calculations is not very precise; and it is moreover questionable whether the effects of streaming can be ignored to determine the vapour pressure solely from the local temperature. However, it was found that very large changes in the assumed temperature dependence of the vapour pressure - by some orders of magnitude - had no significant effect on the derived oscillator strengths. This result relies on the very even temperature distribution along the tube.

Secondly the curve of growth calculation assumed a simple Gaussian profile. This ignores the natural damping (radiation damping) constant; and the possibility of collisional broadening by the inert gas. It is however a greater problem in terms of the photometry of the line (see below) as the error in the curve of growth correction for pressures up to 100 torr is less than 2 per cent.

In addition to these qualitative arguments and empirical tests the curve of growth correction was previously investigated by Blackwell et al (1975). It was found that the relative oscillator strength derived from furnace measurements was independent of the strength of the line over a very wide range of equivalent widths. It could thence be concluded that the curve of growth correction was accurately relating the observed equivalent width to the conceptual equivalent width proportional to (Ngf).

d. measurement of temperature

Where two lines from the same lower level were compared the derived oscillator strength was essentially independent of the temperature measurement. This was due to the fact that only the oscillator strengths differ between the two lines: the number density, given by the vapour pressure and Boltzmann equation, were common. As noted above, the curve of growth correction is not sensitive to the precise form of the variation along the tube of the number density, nor is it dependent on accurate temperatures for the profile. The accuracy of measurements of pairs of lines with the same lower excitation potential is therefore dependent only on the photometric accuracy.

Where however there was a difference between the excitation potentials the temperature, through the Boltzmann equation, determined the relative populations of the two lower states. Considerable effort was taken to measure the temperature distribution in the furnace accurately, but there remain perhaps five sources of uncertainty.

i. It was found that the Leeds and Northrup Optical Pyrometer (No. 1681810) could be set with a repeatable precision of less than 5°C over the range of temperatures used for the furnace measurements. There was nevertheless a greater uncertainty in the temperature because of the pyrometer calibration. Calibration at the National Physical Laboratory in 1966 established corrections to the reading of about 5°C at 1500°C; increasing to 20°C at 2500°C. Emerson (1970) reported that the correction had not changed when the calibration was repeated after three years. But the recalibration by the Harwell Instrument Test Laboratories shortly after these measurements were made indicated increased corrections: about 4°C more at 1900°C and 8°C at 2400°C. Taking this into account the uncertainty from the pyrometer measurements was about 5K at 1500K and some 15K at 2600K.

ii. The pyrometer could only measure the temperature corresponding to the radiation from the carbon blocks after transmission through the quartz window. Absorption and reflection by the window would be expected to reduce the intensity of the light, and hence the measured temperature. This was confirmed by replacing the window used in the measurements with a spare, and measuring the temperature through that alone; and through the combined optical thickness of the two windows. The results, for two furnace temperatures, are shown in figure 5.6(a). From these two values corrections to the reading at other temperatures were obtained by assuming that the pyrometer measured the intensity at an effective wavelength of 5500A - defined by the internal filter and the response of the eye. For black body radiation:

$$I = c_1 (\exp(c_2/T) - 1)^{-1}$$

where the wavelength dependence is taken into the radiation constants as only one wavelength is considered.

If the window absorbs or reflects a fraction w of the incident light at 5500A the measured temperature T' is determined by

$$(1 - w)I = c_1 (\exp(c_2/T) - 1)^{-1}$$

and rearranging

$$w = 1 - \frac{\exp(c_2/T) - 1}{\exp(c_2/T') - 1}$$

From the observed differences (T-T') the mean value of w was 8 per cent. This value was then used to calculate the correction, shown in figure 5.6(a), for other temperatures.

There was however an uncertainty in the measured w which would admit of, say, 9 per cent rather than 8. The correction for the higher value is shown by the broken line in figure 5.6(a).

iii. Although measurements were not made until the furnace had reached a stable temperature there were small variations due to the very great thermal capacity of the system and to fluctuations in mains voltage. From the measurements made before, during and after the sets of scans, this was estimated to amount to about 5K at low temperatures, and some 10K at the highest temperatures used.

iv. It was assumed that the four measured temperatures defined the variation along the tube. Two broad factors might invalidate this assumption. First the temperature need not be symmetrical about the centre if, for instance, the flow of cooling water through the furnace gave different temperature gradients at different ends. This was checked when sighting blocks for the pyrometer were placed at the centre, and at -15, 15, and 30 cm from the centre. No

significant temperature difference was observed between the two blocks at ± 15 cm.

Second there were from time to time visible places in the tube where the temperature was higher than the surrounding. Such local hot spots arose because the carbon tube was gradually eroded by the action of the iron and, presumably, of other pollutents. Where the tube was thinner the Ohmic heating was anomalously high. However these effects were readily seen by their bright appearance against the background of the rest of the furnace, and a new tube fitted.

v. Finally there is the question of whether the temperature of the carbon tube is the temperature of the iron vapour. Heuristically the competing processes are collisions with the furnace wall and diffusion along the length of the tube. As the length of the tube greatly exceeds the diameter, and the temperature changes little for a distance along the tube comparable with the diameter, it is felt that temperature of the vapour was determined by measurements of the tube.

In figure 5.6(b) the three estimated uncertainties in the temperature are shown, together with the total value, for a range of furnace temperatures. In making these estimates it was assumed that the window correction was determined by the measured values and did not change with time, eg because of iron being deposited.

Corresponding to the uncertainty in the temperature there were uncertainties in the measured relative oscillator strengths which depended on the difference in the excitation potentials and the temperature at which they were measured. The Boltzmann

equation gave the relative populations of two levels with excitation potentials χ_1, χ_2:

$$\log_e(n_1/n_2) = \text{const.} - (\chi_1-\chi_2)/kT$$

As the derived oscillator strength depended on the ratio of the products (ngf) the effect of an error ΔT in T was an error in log gf:

$$\Delta(\log gf)_{12} = T\cdot(\chi_1-\chi_2)/kT^2\cdot\log_e 10$$

$$= 5040(\chi_1-\chi_2)\Delta T/T^2$$

where χ_1, χ_2 are in eV

For the lines from the a^5D level the greatest difference was 0.12eV. At a furnace temperature of 2500K the uncertainty in T then corresponded to less than 0.003 dex in the oscillator strength. At lower temperatures the error might be more because of the T^2 term in the denominator; but even at 1500K an error in the relative oscillator strength of 0.02 dex would have required an error in T of more than 70K. For these ground state lines there was therefore little possibility of errors arising from the temperature measurements. Indeed it is worth noting that the excitation potentials themselves needed to be expressed with accuracy comparable to the temperature. Approximate values, such as 0.12eV, are cited here for convenience. But more precise values were used in the reduction of the furnace measurements and lead to significantly different results: for example the a^5D_3 level has an excitation potential of 0.0515eV. If the rounded value 0.05eV were used at 1500K the resulting oscillator strength might have an error of 0.005 dex which, though small, would be systematic.

Comparisons between the a^5D and a^5F lines were however more dependent on the accuracy of the temperature. A difference of leV for instance would require an uncertainty of less than 4K in 2000K if the oscillator strength was to be subject to less than 1 per cent uncertainty. For the measurements reported here the actual uncertainty in such a case would be some 0.02 dex. For this reason alone the results for the excited group of lines must be considered no more than provisional values. Random errors in the temperatures used will, to some extent, be removed by the closures round the matrix of measurements. But there is the possibility of systematic errors which would not be detected.

The determination of the furnace temperature was therefore an important source of uncertainty for some at least of the lines. Since these measurements a photometric pyrometer has been installed (Shallis, 1978) with a significant improvement in the accuracy of the temperatures. Even so there are uncertainties in the accepted temperature scale (Blackwell, 1974) which may amount to some 5K at about 2500K.

e. photometry

In view of the accuracy of the temperature measurements and of the curve of growth correction, the number of absorbing atoms was effectively established. But the derived oscillator strength depended also on accurate measurement of the equivalent widths in the furnace spectrum. One factor in this was the possibility of broad wings to the lines. These might be introduced by the instrumental profile but Blackwell et al (1971) and Collins (1970) showed that the Oxford spectrometer would be free from significant wings. If the lines were broadened by collisons with the Argon in the furnace there would be a Voigt profile with extended wings of the form a/v^2 (see section 2.4). These would not be measured accurately because the line depth would be comparable with the noise level; and because the continuum would have been fitted to the wings rather than the true level.

As indicated the pressure was kept below values where damping would be important. There were nevertheless at least two further sources of uncertainty in the measured equivalent widths. First the background scans of the lamp spectrum gave corrections of the order of $\pm$0.25 mA although the mean value was very much less. The mean absolute value was about 0.07mA. Taken overall the background corrections improved the consistency of the measured oscillator strengths. It was not possible though to interpret them as real features in the spectrum from the lamp. Figure 5.7 shows that the total set from the two spectrometers could be explained as random errors about a zero mean value. And table 5.3 shows that the values for a particular line (5060·1A) from many measurements vary greatly. It is therefore felt that the background corrections were caused by the curvature of the continuum introduced by the monochromators; and by the fitting of a straight line to that continuum when measuring the equivalent widths. As the background scans were time consuming, more especially because the furnace had to be cooled first, it would be an advantage to dispense with them. This might be justified by taking more measurements of the oscillator strengths, on the grounds that the different background corrections would average to zero. However a more interesting idea uses a system of mirrors to bypass the furnace tube and pass light through the same optical system with the furnace still at working temperature.

The second possibility was the effects of scattered light in the spectrometers. Scattered light tends to fill in the absorption lines, and thereby reduces the measured equivalent width. If the effect was uniform all lines would be equally affected and the oscillator strengths would be determined accurately. But the amount of scattered light might be different in the two spectrometers; and in each might vary differently with the wavelength of the line. This was seen as perhaps the explanation of the substantial differences between the measured relative oscillator strengths according to the spectrometer configuration. If, for instance, the scattered light were greater in the upper spectrometer then the equivalent widths

there would be reduced more. It is reassuring though that the mean value of the two measurements would, provided the equivalent widths were about the same in the two configurations, give the correct value.

However plausible this explanation was, the measured amount of scattered light in the Oxford spectrometers (Mallia, 1967; Blackwell et al, 1967; Ibbetson, private communication) was both small and independent of wavelength: laboratory measurements and comparisons of the central depths of solar lines with the measurements by double-pass systems suggested a constant level of less than 1 per cent.

It was therefore necessary to adopt a more empirical approach, and to look for any correlations between the observed difference and the wavelength, excitation, strength, etc of the lines. As figure 5.8 shows, the differences themselves formed a slightly skewed distribution about a well-defined mean of about -0.02. The only correlation found though was with the magnitude of the oscillator strength difference; or more precisely with the ratio of the equivalent widths of the pair of lines. But even this correlation was only barely significant.

Tests were therefore made of the spectrometer-detector system by observing the same line in the furnace spectrum in both upper and lower simultaneously. Previous work had shown that there was no systematic difference between the two. But the range over which the scanning slit may move is very much greater than the distance traversed when actually measuring a single line. Thus it was found that the strength on, say, the lower spectrometer measured with respect to the upper depended on the part of the lower scanning range used. The part used was varied by small adjustments to the grating angle, comparable to the differences which arise when setting the grating to find a particular line.

These differences in the measured equivalent width arose, it appeared, because the distance moved by the slit varied very

slightly with the position in its range of travel. If for example the step between two points at the centre of a line was less than expected, the measured depth would be ascribed to a greater wavelength interval than actually moved, and the derived equivalent width would be too large. For stronger lines the central depth and error would be greater. However, there were indications that the slit angle also changed slightly from time to time and this would introduce more complex effects.

This interpretation of the differences observed is supported by the evidence of later measurements (Blackwell et al, 1978; Shallis, 1978) with a new pair of slit assemblies. No mean differences are now found. It should be emphasised though that the magnitude of the suspected irregularities was very small. The differences of 0.02 dex correspond to errors of the order of 5 per cent in a slit movement of about 0.002 mm.

f. the assumption of LTE

The uncertainties and errors at a. - e. above were at least amenable to analysis and could be reduced or eliminated. There remained then the question whether lines in the furnace spectrum were formed in LTE. The possibility of non-LTE populations and source functions arose because the column of vapour was illuminated by the intense beam from the Xenaon arc, which had moreover considerable intensity in the far blue and near ultra-violet. Radiative processes might then affect the equilibria.

In principle this may be seen from the term diagram (figure 5.9) for the multiplets measured. The a^5F term is metastable and populated by downward transitions from, for example, $^7D^o$, $^7P^o$, $^5F^o$, $^5D^o$. Those levels will in turn be populated by transitions upwards from the ground state term a^5D which has of course many strong lines in the furnace spectrum. It is conceivable then that the pumping would lead to an overpopulation of the a^5F term. The measured oscillator strengths from that term, using the LTE populations, would then be overestimated.

Such simple effects are perhaps unlikely. But the only prior evidence for LTE was the observation that the relative oscillator strnegth did not change with the pressure of inert gas in the furnace. The argument was that the gas tended to give LTE populations by collisional processes; and that any departures from LTE would decrease with increasing pressure, so that the derived log gf would change. Since these results were obtained however Shallis (1978) has investigated the effect of introducing a filter in front of the arc to remove the blue and ultraviolet energy. In this way the equivalent widths of lines at longer wavelengths were found to be independent of the energy at shorter wavelengths, which suggests that the strong, blue transitions do not cause non-LTE effects.

Leaving aside the question of LTE the oscillator strengths of the low excitation lines were certainly determined with errors less than 0.02 dex. That value for the uncertainty is the figure suggested by the adjustments to the measured values for the weakest lines; but is adopted more generally because of the errors in the photometry which cannot yet be assumed to have averaged to zero over the full set of comparisons.

Turning to the lines from the excited levels, the errors in temperature measurement contribute greater uncertainty; there are fewer overdetermined measures by which to assess the accuracy; and many of the lines were very weak in the furnace spectrum and subject to greater photometry problems. For those lines therefore the uncertainty might be as much as 10 per cent.

The arguments of internal consistency are however not a firm test of the accuracy of the measured oscillator strengths; and additional evidence will be given from comparisons with other measurements (in the next section) and from analysis of the lines in the solar spectrum (in the next chapter).

5.9 Comparison with other measurements

Many measurements of the oscillator strengths of FeI lines have been made, over a period of fifty years or more. The great majority were however very inaccurate and have been superseded by later work. In particular the absolute oscillator strengths were greatly revised some ten years ago following the results of improved arc measurements (eg Garz and Kock, 1969) and confirmation of the suspected errors in the results of the many measurements by Corliss and Warner (1964, 1966) and Corliss and Bozman (1962). Earlier values are therefore of historical interest only and comprehensive references have been given in the bibliographies of Glennon and Wiese (1966) and Miles and Wiese (1970), supplemented by Fuhr and Wiese (1971, 1973). In addition the compilations of oscillator strengths by Corliss and Warner (1964, 1966) and by Prokof'ev et al (1964) cite many previous reports of arc, furnace and shock tube measurements.

Accordingly only some of the more reliable, more recent results have been used in table 5.4 to show the oscillator strengths from the furnace measurements reported here alongside the values from other methods and authors. The results from other authors are chosen to represent the various methods: arc emission; shock tube; anomalous dispersion (hook) methods; calculation. The values given by Corliss and Warner (1964) and by Prokof'ev et al (1964) would not qualify on those grounds. But they represented the best results at the time of their compilation. Moreover the Corliss and Warner values still constitute the most complete and homogeneous set of oscillator strengths for FeI and have been widely used in astrophysics. It has long been realised though that these early, predominantly arc measurements were subject to systematic errors. Corliss and Tech (1968) revised the normalisation of the arc measurements of Corliss and Warner (1964) and Takens (1970) found that further corrections were necessary to the scale provided by Corliss and Bozman (1962). Allen (1971) used the theoretical constraints on the sums of f-values from LS coupling calculations further to

revise the Corliss and Warner values. But as shown by Bell and Upson (1971) there were probably errors in both the assumed temperature and the photometry used in obtaining the original experimental values. As the later corrections, which result in very substantial downward revisions of these values, must rely on comparisons with later, more accurate measurements, the original values are used here to allow direct comparison with the furnace results.

A major contribution to the revision of the earlier results came from the arc measurements of Garz and Kock (1969), Richter and Wulff (1970) and Bridges and Wiese (1970). All of these measurements claimed uncertainties less than 30 per cent and showed very large differences from the values of Corliss and Warner. In part this was due to the use of more stable arcs; but there was also more attention paid to maintaining LTE (eg Garz et al, 1970; Kock and Richter, 1968). These measurements were however limited to comparatively few lines; and relied on photographic measurement of the emission line strength. Bridges and Kornblith (1974) on the other hand used photoelectric detection and measured the oscillator strengths of 534 lines of FeI from a stabilized arc. Using lifetime measurements for 36 levels to establish the absolute scale, the accuracy was estimated to be better than 25 per cent; with 10 per cent claimed for many lines. Spectrophotometry was also used by May et al (1974) to measure more than 1000 FeI lines from an arc similar to that used by Richter and Wulff (1970). The oscillator strengths were calibrated using the values of Bridges and Kornblith (1974) so that the two sets of measurements are directly comparable. For astrophysical purposes this is particularly useful as May et al give values for many more weak lines than Bridges and Kornblith; and quote maximum experimental errors of only some 0.15 dex (40 per cent).

By comparison with the arc measurements, shock tubes have yielded few oscillator strengths though some important and

accurate. Wolnik et al (1970, 1971) derived absolute values for some 150 lines, including high-excitation FeI and 12 FeII lines. These differed significantly from the results of Byard (1967) and Huber and Tobey (1967) but the later results of the Harvard program (Huber and Parkinson, 1972; Huber, 1974) used anomalous dispersion in shock tube lines to derive more accurate oscillator strengths. In contrast the results of Gilbert et al (1974) using a glass shock tube appear to differ by a factor two from other results.

The Harvard group have also used absorption methods involving a furnace. The Russian work with the hook method (Penkin, 1964; Valters and Startsev, 1964) has been developed by Huber (1971) and applied by inter alia Banfield and Huber (1973) who measured more than 100 low excitation FeI lines in the blue and ultraviolet. The hook method is however restricted to relatively strong lines and Huber and Tubbs (1972) combined iron population densities derived from the anomalous dispersion of 3719.9A with the absorption strength of weak lines. In this way oscillator strengths over a range of about six decades were linked direct to the resonance line.

Apart from arc measurements however the only sources of many oscillator strengths are the calculations for various model atoms. Theoretical transition probabilities from the Coulomb approximation have usually been suspect for atoms as complex as FeI. The results of Rogerson (1969) and Goldman (1969) for instance ignored configuration interactions and gave values which do not agree well with experimental oscillator strengths. Ross (1973) applied intermediate coupling calculations to the lines of the FeI ground state and chose the coupling parameter so as to reproduce the experimental values of the strong lines. The good agreement for the weaker lines may however be accidental as Roth (1970) gave a very different value for the coupling parameter. Ross (1973) also ignored the configuration interaction, unlike the computations of scaled Thomas-Fermi-Dirac wave functions developed by Kurucz et al (1973). Biemont

(1974ab, 1975) showed that this method should be useful for iron group elements and the results given by Kurucz (1974) and Kurucz and Peytremann (1975) contain semi-empirical oscillator strengths for many FeI lines which have never been measured.

The calibration of observed oscillator strengths on absolute scales had also improved with more numerous and more precise lifetime measurements. Experimental values are now available for more than 30 levels of FeI from a variety of methods, eg beam foil (Whaling et al, 1969; Martinez-Garcia et al, 1971; Smith et al, 1970; Andersen and Sorensen, 1971); optical double resonance (Wagner and Otten, 1969); Hanle effect (Hilborn and Zafra, 1973); electron excitation (Klose, 1971); phase shift (Assousa and Smith, 1972); high frequency deflection (Erman et al, 1974); and of course absolute atomic beam work (Bell and Tubbs, 1970). Some of these results have been used above to determine the absolute gf value of the 3719A line, which determined in turn the absolute scale of the furnace measurements. But as an example of the other values the lifetime of FeI y^5F_5 can be derived from the oscillator strength measurements and compared with direct methods. The principal decay is to a^5F_5 (3734A) but there are also transitions to a^5D_4, a^5F_4 and a^3F_4, corresponding to lines at 2967A, 3798A and 4602A. Using the oscillator strengths of Corliss and Warner (1964, 1966) the lifetime is found as 6.11 n sec. Substituting the value for 3734A found here this becomes 9.47. The gf value of 2967A must also be considered though, and using the result of Banfield and Huber (1973) the lifetime is further amended to 7.48. Direct measurements include 11.5 $\pm$ 1.5 (Klose, 1971), 8.4 $\pm$ 0.9 (Assousa and Smith, 1972) and 7.9 $\pm$ 1.2 (Andersen and Sorensen, 1971). In view of the uncertainty of the provisional furnace results for the excited lines, and the possible errors in the gf value of 2967A, this broad agreement is satisfactory. But the comparison is presented here more to show the scope for the use of lifetimes than to prove the furnace measurements.

Quantitative comparisons with other experimental results are less easy. Figure 5.10 therefore shows the differences in log

gf between the results from the Oxford furnace given above and the results of other authors. As a bench mark figures (a) and (b) plot the values from the compilations of Corliss and Warner (1964, 1966) and of Prokof'ev et al (1964). Both sets of values show very large and systematic deviations from the furnace values. As the lines here are all from low excitation levels this cannot be attributed to errors in the furnace temperature. As far as the furnace is concerned, it has been seen that only the photometry (or perhaps non-LTE effects) could account for substantial error. For the predominantly arc measurements of these other authors however there is the possibility of errors in the temperature (since the emission lines have different upper levels) or the photometry; and of the presence of self-absorption. It is interesting therefore to note that the results of Bridges and Kornblith (1974) (figure 5.10(c)) and of May et al (1974) (figure 5.10(d)) show far less divergence. These later arc measurements may be considered together as they are on a common scale and suggest that emission methods are being adjusted towards the values from the furnace absorption method. Nevertheless there is in both these and the shock tube results a systematic divergence which is substantial for weak lines. And the scatter of the May et al values is not significantly less than that of the Corliss and Warner (1964, 1966) data.

Figures 5.10 (e), (f), (g) and (h) compare the furnace measurements of this work with results from other furnace methods. Agreement with the hook method of Valters and Startsev (1964) in figure (e) is generally very good although the Russian authors give results only for the stronger lines. And even the pioneering work of King and King (1938) would appear from figure (f) to be better than many of the measurements made in the following 30 years. The main comparisons are though with the results of Huber and Tubbs (1972) and Banfield and Huber (1973) in figure (g) and (h) respectively.

The hook measurements of Banfield and Huber (1973) confirm the agreement for the strong lines seen in figure (h). Figure (g) however is more significant. The hook method was used by Huber and Tubbs (1972) only to define the number of iron atoms in the column of vapour, and the oscillator strengths of the weak lines were then linked direct to the absolute value of 3719A by their equivalent widths. This may be seen as bypassing the successive comparisons used in the Oxford furnace measurements described above. Despite this different method, the quoted values agree over almost 6 decades with a maximum deviation of 0.09 dex. The standard deviation about a linear relation is only some 0.02 dex. From this it is felt that the furnace absorption methods give the more accurate oscillator strengths; and that the arc and shock tube emission methods are still perhaps subject to temperature and self-absorption errors. Furthermore the excellent agreement with Huber and Tubbs (1972) is indirect evidence of the absence of significant non-LTE effects in the Oxford furnace: it would be an unlikely coincidence that two different furnaces and lamps, operated at different temperatures and pressures, should give such precisely similar non-LTE populations.

Finally the theoretical values of Ross (1973) and Kurucz (1974) are clearly subject to considerable uncertainties (figures (i) and (j) respectively). Oscillator strengths from the intermediate coupling calculations are skewed in figure (i) and revising the coupling parameter can reduce but not remove this trend. In contrast the gf values given by the scaled Thomas-Fermi-Dirac calculations show no trend with respect to the furnace values. The absolute offset may be removed by adjusting the absolute scale; and the increasing scatter towards weaker lines should be seen against the comparable spread for experimental emission measures.

In conclusion there is from the internal experimental results and from these comparisons no reason to doubt that the measured

oscillator strengths from the low excitation levels are determined to 5 per cent or better (0.02 dex). And from that conclusion the errors of the excited lines are likely to be known and, as described above, amount to about 10 per cent. On the other hand there is evidence of systematic errors with respect to line strength for even the more accurate and elaborate emission methods.

Table 5.1

The table lists the lines compared; the number of scans, relative oscillator strength & standard deviation for each configuration; the mean and difference; adopted value & residual.

from	to	N1	(log gf)	s.d.	N2	(log gf)	s.d.	diff.	(log gf) mean	(log gf) fitted	residual
3719.9	3745.6	25	0.324	.012	25	0.340	.015	-.016	0.332	0.332	.000
3859.9	3745.6	25	0.041	.008	25	0.072	.012	-.031	0.057	0.056	.001
3679.9	3526.0	25	0.295	.015	25	0.325	.018	-.030	0.310	0.308	.002
3679.9	3920.2	25	0.140	.014	25	0.168	.013	-.028	0.149	0.151	-.002
4375.9	4461.7	25	0.189	.012	25	0.175	.015	.014	0.182	0.179	.003
5110.4	4489.7	25	0.179	.010	25	0.190	.016	-.011	0.185	0.191	-.006
5166.3	5204.6	30	0.122	.016	30	0.128	.014	-.006	0.125	0.122	.003
5166.3	4347.2	65	1.337	.028	45	1.298	.032	.039	1.318	1.313	.005
5060.1	4347.2	35	0.019	.011	35	0.040	.016	-.021	0.030	0.032	-.002
3922.9	3526.0	22	0.246	.012	28	0.271	.017	-.025	0.259	0.261	-.002
3922.9	3895.7	30	0.009	.015	30	0.037	.013	-.028	0.023	0.024	-.001
3922.9	3906.5	25	0.583	.011	35	0.600	.015	-.017	0.592	0.592	.000
3922.9	3920.2	30	0.122	.017	25	0.104	.015	.018	0.113	0.103	.010
4427.3	4482.2	25	0.454	.013	40	0.466	.013	-.012	0.460	0.461	-.001
4389.3	5247.1	20	0.346	.014	30	0.358	.014	-.012	0.352	0.371	-.019

from	to	N1	(log gf)	s.d.	N2	(log gf)	s.d.	diff.	(log gf) mean	(log gf) fitted	residual
4389.3	4232.7	25	0.347	.013	25	0.357	.016	-.010	0.352	0.351	.001
4389.3	5250.2	25	0.348	.013	25	0.367	.012	-.019	0.358	0.355	.003
3745.6	3679.9	30	0.826	.015	29	0.828	.016	-.002	0.827	0.821	.006
3745.6	3886.2	25	0.281	.008	25	0.292	.007	-.011	0.287	0.293	-.006
3745.6	3722.6	25	0.501	.007	25	0.513	.010	-.012	0.507	0.512	-.005
3745.6	3748.3	21	0.243	.012	30	0.254	.012	-.011	0.249	0.243	.006
3722.6	3679.9	25	0.301	.017	25	0.320	.017	-.019	0.311	0.309	.002
3722.6	3899.7	25	0.224	.013	25	0.241	.011	-.017	0.233	0.235	-.002
3722.6	3526.0	25	0.623	.015	25	0.610	.021	.013	0.617	0.618	-.001
3899.7	3679.9	15	0.064	.018	25	0.079	.020	-.015	0.072	0.074	-.002
3526.0	4375.9	25	1.123	.013	25	1.108	.014	.015	1.116	1.118	-.002
4461.7	4216.2	33	0.132	.011	27	0.152	.013	-.020	0.142	0.137	.005
4461.7	4482.2	30	0.280	.015	35	0.310	.013	-.030	0.295	0.297	-.002
4258.3	5204.6	23	0.009	.014	27	0.005	.016	-.004	0.007	0.009	-.002
4258.3	4435.2	28	0.057	.012	28	0.071	.014	-.014	0.064	0.065	-.001

from	to	N1	(log gf)	s.d.	N2	(log gf)	s.d.	diff.	(log gf) mean	(log gf) fitted	residual
5204.6	4435.2	25	0.051	.012	25	0.060	.011	-.009	0.056	0.056	.000
5247.1	5060.1	22	0.514	.014	25	0.524	.015	-.010	0.519	0.518	.001
5247.1	4445.5	35	0.467	.011	30	0.465	.016	.002	0.466	0.487	-.021
4445.5	5060.1	41	0.021	.013	41	0.043	.012	-.022	0.032	0.028	.004
3748.3	3722.6	30	0.261	.020	23	0.273	.017	-.012	0.267	0.269	-.002
3748.3	3722.6	25	0.258	.017	25	0.290	.009	-.032	0.274	0.269	.005
3748.3	3895.7	30	0.652	.010	40	0.652	.016	.000	0.652	0.650	.002
3748.3	3745.9	20	0.324	.012	20	0.336	.012	-.012	0.330	0.328	.002
3906.5	4375.9	25	0.779	.012	25	0.796	.017	-.017	0.788	0.788	.000
3906.5	4427.3	32	0.791	.015	25	0.816	.018	-.025	0.804	0.803	.001
4482.2	5168.9	25	0.467	.013	25	0.469	.014	-.002	0.468	0.471	-.003
5255.0	5225.5	30	0.021	.011	15	0.015	.017	.006	0.018	0.020	-.002
5255.0	4232.7	30	0.177	.013	30	0.167	.014	.010	0.172	0.170	.002
5225.5	4232.7	25	0.144	.015	25	0.156	.017	-.012	0.150	0.149	.001
5225.5	5250.2	25	0.154	.013	20	0.146	.016	.008	0.150	0.153	-.003

	from	to	N1	(log gf)	s.d.	N2	(log gf)	s.d.	diff.	(log gf) mean	(log gf) fitted	residual
	5060.1	4471.7	25	0.534	.013	25	0.545	.019	-.011	0.540	0.545	-.005
	5060.1	4471.7	15	0.515	.011	15	0.573	.016	-.058	0.542	0.545	-.003
	3265.1	4461.7	32	0.098	.016	25	0.092	.017	.006	0.095	-	-
	4445.5	5060.1	35	0.015	.016	38	0.011	.011	.004	0.013	0.028	-.015
	4445.5	5060.1	15	0.014	.011	15	0.019	.012	-.005	0.017	0.028	-.011
	4445.5	4471.7	15	0.578	.021	11	0.593	.017	-.015	0.586	0.573	.013
	4445.5	4471.7	15	0.566	.018	15	0.570	.017	-.004	0.568	0.573	-.005
*	3734.9	3679.9	15	1.925	.015	15	1.948	.016	-.023	1.937	1.931	.006
*	3734.9	3679.9	15	1.920	.018	15	1.928	.014	-.008	1.924	1.931	-.007
	3734.9	3820.4	15	0.214	.014	15	0.192	.014	.022	0.203	0.194	.009
	3734.9	3820.4	15	0.181	.012	15	0.206	.013	-.025	0.194	0.194	.000
	3734.9	3749.5	15	0.170	.015	15	0.161	.010	.009	0.166	0.176	-.010
*	3734.9	3906.5	15	2.547	.017	15	2.608	.017	-.056	2.575	2.570	.005
*	3734.9	3906.5	15	2.569	.015	15	2.564	.011	-.009	2.567	2.570	-.003
*	3820.4	3906.5	15	2.368	.013	15	2.379	.017	-.011	2.374	2.376	-.002

	from	to	N1	(log gf)	s.d.	N2	(log gf)	s.d.	diff.	(log gf) mean	(log gf) fitted	residual
*	5269.5	4216.2	25	2.050	.024	25	2.058	.008	-.008	2.054	2.043	.011
*	5269.5	5110.4	25	2.456	.015	15	2.414	.016	.042	2.440	2.458	-.018
*	4939.7	5060.1	25	2.145	.021	25	2.177	.017	-.032	2.161	2.142	.019
	4939.7	6280.6	26	1.058	.021	25	1.082	.019	-.024	1.070	1.077	-.007
	6280.6	6358.7	24	0.042	.014	15	0.060	.014	-.018	0.051	0.050	.001
*	6280.6	5060.1	15	1.071	.014	13	1.036	.012	.035	1.054	1.065	-.011
*	6280.6	5060.1	25	1.071	.030	25	1.095	.020	-.024	1.083	1.065	.018
	6280.7	6498.9	15	0.332	.025	15	0.344	.023	-.012	0.338	0.343	-.005
*	6358.7	5060.1	20	0.961	.032	20	1.039	.031	-.078	1.000	1.015	-.015
	6358.7	5956.7	25	0.188	.013	25	0.169	.009	.019	0.179	0.170	.009
*	5956.7	5060.1	26	0.850	.025	25	0.856	.026	-.006	0.853	0.846	.007
	5956.7	6574.2	15	0.417	.018	15	0.450	.021	-.033	0.434	0.427	.007
$	5956.7	6609.7	10	1.078	-	10	1.110	-	-.032	1.094	1.097	-.003
	3749.5	3820.4	15	-0.003	.016	15	0.018	.017	-.021	0.008	0.018	-.010
$	6498.9	6574.2	15	0.297	-	15	0.299	-	.002	0.298	0.303	-.005
$	6574.2	6609.7	10	0.684	-	10	0.662	-	.022	0.673	0.671	.002

from	to	N1	(log gf)	s.d.	N2	(log gf)	s.d.	diff.	(log gf) mean	(log gf) fitted	residual
4232.7	5060.1	25	0.537	.022	31	0.542	.018	-.005	0.540	0.537	.003
4232.7	4445.5	28	0.494	.016	31	0.526	.017	-.032	0.510	0.507	.003
3745.9	3922.9	25	0.289	.019	25	0.316	.012	-.027	0.304	0.298	.006
3745.9	3920.2	25	0.393	.015	30	0.400	.014	-.007	0.397	0.401	-.004
3920.2	4375.9	25	1.277	.022	26	1.296	.018	-.019	1.287	1.276	.011
4489.7	5166.3	25	0.237	.012	25	0.237	.012	.000	0.237	0.241	-.004
4489.7	4258.3	30	0.346	.021	25	0.356	.021	-.010	0.351	0.354	-.003
5250.2	4445.5	55	0.494	.025	45	0.512	.023	-.018	0.503	0.503	.000

Notes: * lines compared from a^5D and a^5F with large excitation difference

$ mean scan used to determine the equivalent width: provisional gf value only

Table 5.2

Absolute oscillator strengths of FeI lines from the furnace measurements.

Multiplet No.	Wavelength	E.P. low	E.P. high	J	log(gf)	
1	5166.286	0.00	2.39	4-5	-4.173	
	5247.052	0.09	2.44	2-3	-4.938	
a^5D-z^7D	5254.956	0.11	2.46	1-2	-4.749	
	5250.212	0.12	2.47	0-1	-4.922	
	5110.414	0.00	2.41	4-4	-3.742	
	5168.901	0.05	2.44	3-3	-3.956	
	5204.582	0.09	2.46	2-2	-4.296	
	5225.533	0.11	2.47	1-1	-4.769	
	5060.079	0.00	2.44	4-3	-5.455	
	5127.68	0.05	2.46	3-2	-6.110	
2	4375.932	0.00	2.82	4-5	-3.009	
	4427.312	0.05	2.84	3-4	-3.024	
a^5D-z^7F	4461.654	0.09	2.85	2-3	-3.188	
	4482.171	0.11	2.86	1-2	-3.485	
	4489.741	0.12	2.87	0-1	-3.933	
	4347.239	0.00	2.84	4-4	-5.487	
	4445.48	0.09	2.86	2-2	-5.426	
	4471.68	0.11	2.87	1-1	-5.999	* provisional
	4389.244	0.05	2.86	3-2	-4.567	
	4435.151	0.09	2.87	2-1	-4.351	

Multiplet No.	Wavelength	E.P. low	E.P. high	J	log(gf)
3	4216.186	0.00	2.93	4-4	-3.326
	4258.320	0.09	2.99	2-3	-4.287
a^5D-z^7P	4232.724	0.11	2.99	1-2	-4.918
4	3859.913	0.00	3.20	4-4	-0.705
	3886.284	0.05	3.23	3-3	-1.054
a^5D-z^5D	3899.709	0.09	3.25	2-2	-1.508
	3906.482	0.11	3.27	1-1	-2.221
	3895.658	0.11	3.28	1-0	-1.654
	3922.914	0.05	3.20	3-4	-1.630
	3920.260	0.12	3.27	0-1	-1.733
5	3719.935	0.00	3.32	4-5	-0.43 **
	3737.133	0.05	3.35	3-4	-0.578
a^5D-z^5F	3745.561	0.09	3.38	2-3	-0.762
	3748.264	0.11	3.40	1-2	-1.004
	3745.901	0.12	3.42	0-1	-1.332
	3679.915	0.00	3.35	4-4	-1.583
	3705.567	0.05	3.38	3-3	-1.312
	3722.564	0.09	3.40	2-2	-1.273

** assumed absolute value

Multiplet No.	Wavelength	E.P. low	E.P. high	J	log(gf)	
6 a^5D-z^5P	3526.039	0.09	3.59	2-3	-1.791	
8 a^5D-z^3D	3265.046	0.09	3.87	2-3	-3.093	
13 a^5F-z^7F	6358.692	0.86	2.80	5-6	-4.439	
	6609.68	0.99	2.85	2-3	-5.707	*
	6280.625	0.86	2.82	5-5	-4.390	
	6498.950	0.95	2.85	3-3	-4.733	
	6574.238	0.99	2.86	2-2	-5.036	*

Multiplet No.	Wavelength	E.P. low	E.P. high	J	log(gf)
14 a^5F-z^7P	5956.702	0.86	2.93	5-4	-4.609
15 a^5F-z^5D	5269.541	0.86	3.20	5-4	-1.283
16 a^5F-z^5F	4939.69	0.86	3.35	5-4	-3.313
20 a^5F-y^5D	3820.428	0.86	4.09	5-4	+0.155
21 a^5F-y^5F	3734.867	0.86	4.16	5-5	+0.349
	3749.487	0.91	4.20	4-4	+0.173

Table 5.3

Measured background correction equivalent widths from 9 comparisons involving the line FeI 5060.1A.

upper spectrometer mA	lower spectrometer mA
0.045	0.032
-0.080	0.096
-0.013	0.009
0.214	0.059
0.240	-0.076
-0.025	0.074
0.064	0.044
0.009	0.047
-0.008	0.131

Table 5.4

Comparisons of measured gf values with other data.

eV	A	Oxford	calculation		compilation		furnace		shock	arc				shock
		1	2	3	4	5	6	7	8	9	10	11	12	13
0.00	3719.9	-0.430	-0.490	-0.43	-0.32	-0.43	-0.43	-0.43	-0.43	-0.43	.	-0.43	-0.43	-0.60
	3859.9	-0.705	-0.787	-0.59	-0.54	-0.67	.	-0.70	-0.60	-0.75	.	.	.	.
	3679.9	-1.583	-1.629	-1.41	-1.27	-1.44	-1.58	-1.57	-1.51	-1.55	.	.	.	.
	4375.9	-3.009	-3.123	-2.99	-2.59	-2.65	.	.	.	.	.	.	.	-3.00
	4216.2	-3.326	-3.443	-3.23	-2.98	-2.93	.	.	.	-3.14	.	.	.	.
	5110.4	-3.742	-3.740	-3.86	-3.34	-3.33	-3.77	.	.	.	.	.	.	.
	5166.3	-4.173	-3.972	-4.17	-3.68	-3.68	-4.25	.	.	.	.	.	.	.
	5060.1	-5.455	-6.155	-5.58	-5.34	.	.	.	.	.	.	.	.	.
	4347.2	-5.487	-5.691	-5.20	-5.01	-3.87	.	.	.	.	-5.32	.	.	.
0.05	3737.9	-0.578	-0.644	-0.58	-0.49	-0.56	-0.58	-0.58	-0.57	-0.57	.	-0.58	-0.59	.
	3886.3	-1.054	-1.141	-0.92	-0.90	-0.99	.	-1.06	-0.96	-1.07	.	.	.	.
	3705.6	-1.312	-1.386	-1.22	-1.12	-1.22	-1.32	-1.29	-1.27	-1.30	.	.	.	.
	3922.9	-1.630	-1.704	-1.45	-1.41	-1.50	.	-1.60	-1.52	-1.60	.	-1.58	-1.58	-1.54
	4427.3	-3.024	-3.113	-2.99	-2.51	-2.58	.	.	.	-2.50	.	-2.48	-2.35	-2.89
	5168.9	-3.956	-3.911	-4.05	-3.49	-3.48	-4.01	.	.	.	.	.	.	.
	4389.2	-4.567	-4.568	-4.67	-3.90	-3.81	.	.	.	.	-4.39	.	.	.
	5127.7	-6.110	-7.674	-6.14	.	.	-6.06	.	.	.	.	.	.	.

eV	A	Oxford	calculation		compilation		furnace		shock	arc				shock
		1	2	3	4	5	6	7	8	9	10	11	12	13
0.09	3745.6	-0.762	-0.837	-0.76	-0.62	-0.73	-0.74	-0.76	-0.80	-0.77	.	.	.	.
	3722.6	-1.273	-1.348	-1.21	-1.08	-1.20	-1.25	-1.26	-1.22	-1.28	.	.	.	.
	3899.7	-1.508	-1.593	-1.37	-1.30	-1.42	.	-1.50	-1.40	-1.50	.	-1.48	-1.35	-1.44
	3526.0	-1.791	-2.080	-2.05	-1.61	-1.73	.	.	.	.	.	.	.	.
	3265.1	-3.093	-3.095	.	-2.12	-2.71	.	.	.	.	.	.	.	.
	4461.7	-3.188	-3.268	-3.18	-2.71	-2.80	.	.	.	.	.	.	.	-3.03
	4258.3	-4.287	-4.376	-4.33	-3.67	-3.68	.	.	.	.	-4.28	.	.	.
	5204.6	-4.296	-4.227	-4.41	-3.77	-3.77	-4.35	.	.	.	.	.	.	.
	4435.2	-4.351	-4.368	-4.46	-3.79	-3.86	.	.	.	.	-4.20	.	.	.
	5247.1	-4.938	-5.121	-5.14	-4.50	-4.42	-4.97	.	.	.	.	.	.	.
	4445.5	-5.426	-5.652	-5.02	-4.87	-4.11	.	.	.	.	-5.23	.	.	.
0.11	3748.3	-1.004	-1.082	-0.99	-0.87	-0.97	-1.02	-1.02	-0.98	-1.01	.	.	.	.
	3895.7	-1.654	-1.745	-1.49	-1.47	-1.56	.	-1.62	-1.50	-1.61	.	-1.60	-1.48	-1.59
	3906.5	-2.221	-2.290	-2.06	-1.89	-1.98	.	-2.09	.	-2.12	.	.	.	-2.03
	4432.2	-3.485	-3.537	-3.48	-2.85	-2.95	.	.	.	.	.	.	.	.
	5254.9	-4.749	-4.760	-4.88	-4.23	-4.22	-4.74	.	.	.	.	.	.	.
	5225.5	-4.769	-4.628	-4.87	-4.26	-4.25	-4.77	.	.	.	.	.	.	.
	4232.7	-4.918	-4.962	-5.05	-4.10	-3.87	.	.	.	.	.	.	.	.
	4471.7	-5.999	-6.203	-5.57	-5.14	.	.	.	.	.	-5.62	.	.	.

eV	A	Oxford	calculation		compilation		furnace		shock	arc				shock
		1	2	3	4	5	6	7	8	9	10	11	12	13
0.12	3745.9	-1.332	-1.408	-1.30	-1.15	-1.24	-1.40	-1.35	-1.35	-1.29	.	.	.	.
	3920.3	-1.733	-1.809	-1.55	-1.49	-1.60	.	-1.68	-1.61	-1.71	.	.	.	-1.62
	4489.7	-3.933	-3.976	-3.96	-3.40	-3.56	.	.	.	.	-4.20	.	-3.98	.
	5250.2	-4.922	-4.837	-5.03	-4.46	-4.40	-4.98	.	.	.	.	.	.	.
0.86	3734.9	+0.349	+0.406	.	+0.55	+0.46	.	+0.72	+0.30	+0.31	.	.	.	.
	3820.4	+0.155	+0.154	.	+0.41	+0.28	.	+0.56	+0.24	+0.13	.	.	.	.
	5269.5	-1.283	-1.414	.	-1.35	-1.02	.	.	.	-1.36	.	.	.	.
	4939.7	-3.313	-3.057	.	-3.18	-2.86	.	.	.	.	.	.	.	.
	6280.6	-4.390	-4.264	.	-3.99	.	.	.	.	.	-4.36	.	.	.
	6358.7	-4.439	-4.738	.	-4.00	.	.	.	.	.	-4.28	.	.	.
	5956.7	-4.609	-5.442	.	-4.06	.	.	.	.	.	-4.55	.	.	.
0.91	3749.5	+0.173	+0.254	.	+0.43	+0.33	.	+0.59	+0.18	+0.17	.	.	.	.
0.95	6498.9	-4.733	-4.657	.	-4.22	.	.	.	.	.	-4.63	.	.	.
0.99	6574.3	-5.036	-5.016	.	-4.64	.	.	.	.	.	-4.94	.	.	.
	6609.7	-5.707	-5.505	.	.	.	.	.	.	.	.	.	.	.

Notes to table 5.3

a. the first two columns give the excitation potential and wavelength of the line.

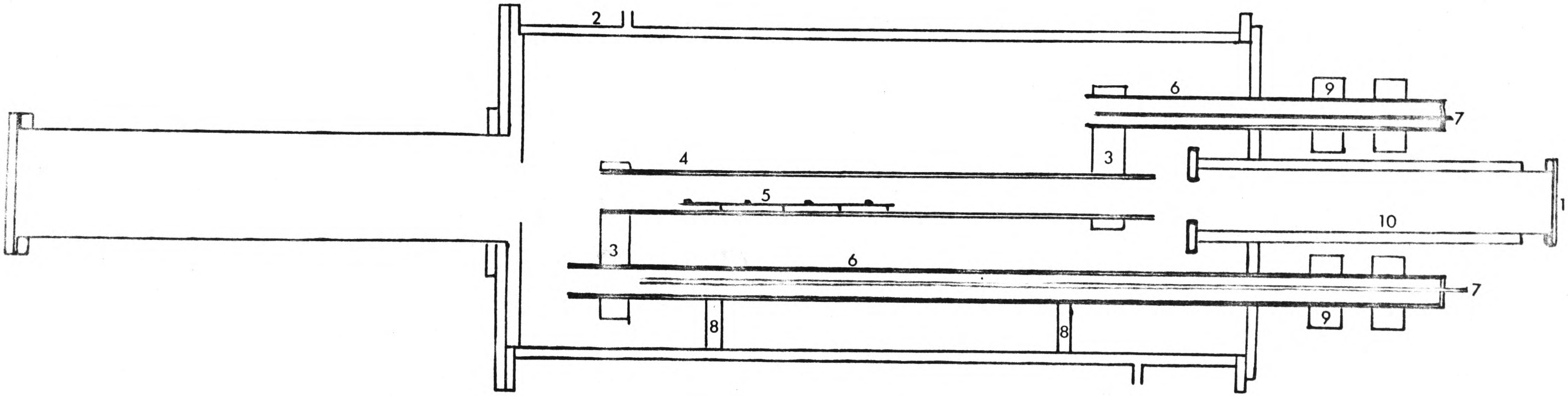
b. columns 1 to 13 give the absolute oscillator strengths from the following references:

1	this work	8	Huber and Parkinson (1972)
2	Kurucz (1974)	9	Bridges and Kornblith (1974)
3	Ross (1973)	10	May et al (1974)
4	Corliss and Warner (1964)	11	Bridges and Wiese (1970)
5	Prokof'ev (1964)	12	Garz and Kock (1969)
6	Huber and Tubbs (1972)	13	Wolnik et al (1970)
7	Valters and Startsev (1964)		

c. scales are adjusted to give log gf(3719)= -0.43 except for column 4 (the measurments of Corliss and Warner) and column 12 (the absolute shock tube values of Wolnik et al).

Figure 5·1

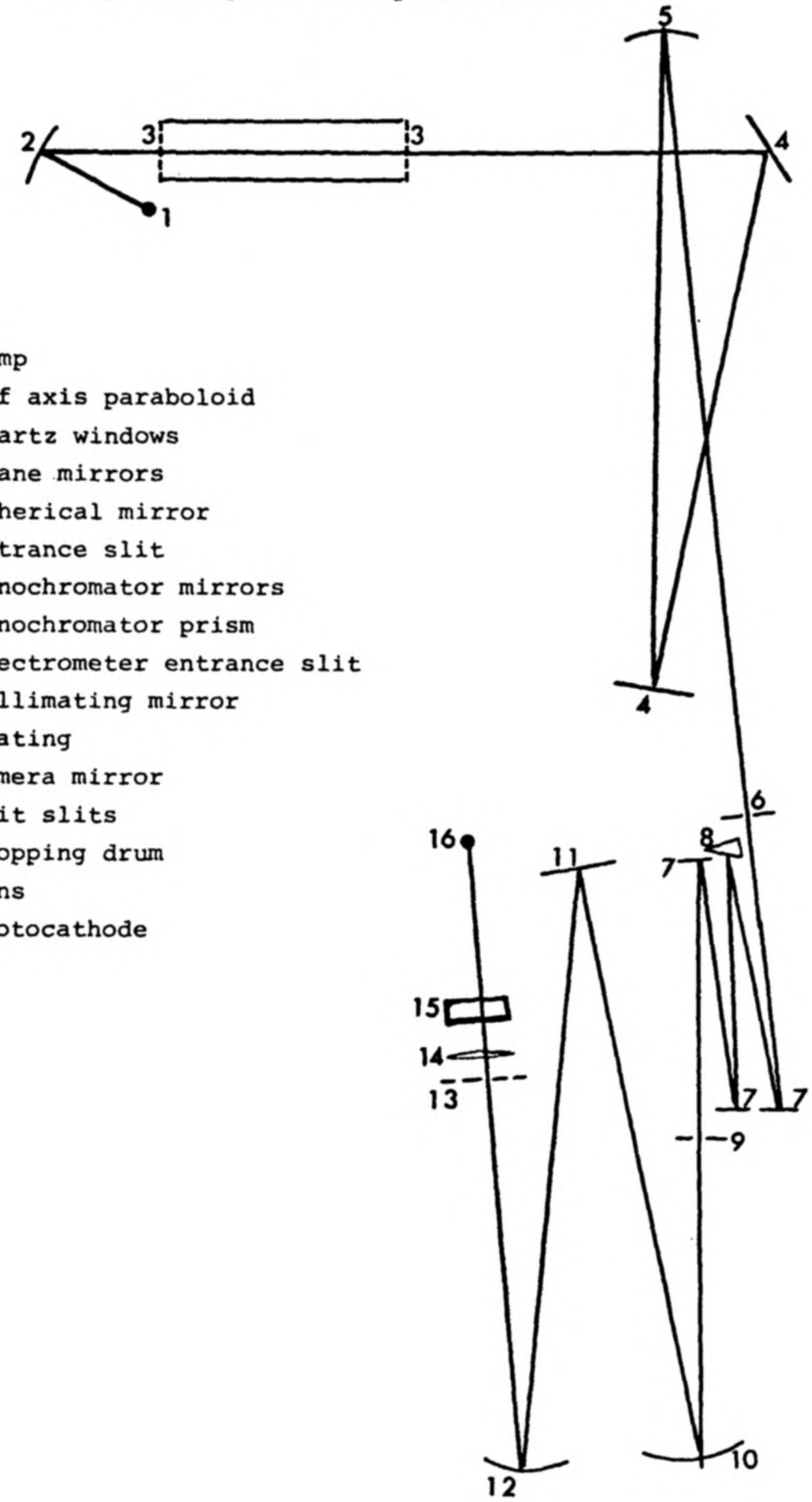
SIMPLIFIED TRANSVERSE SECTION OF FURNACE



1. window
2. water cooled vacuum tank
3. carbon end block
4. carbon heater tube
5. carbon sighting blocks
6. copper busbar
7. busbar cooling pipe
8. insulating support
9. copper busbar clamp
10. water cooled end tube

Figure 5.2

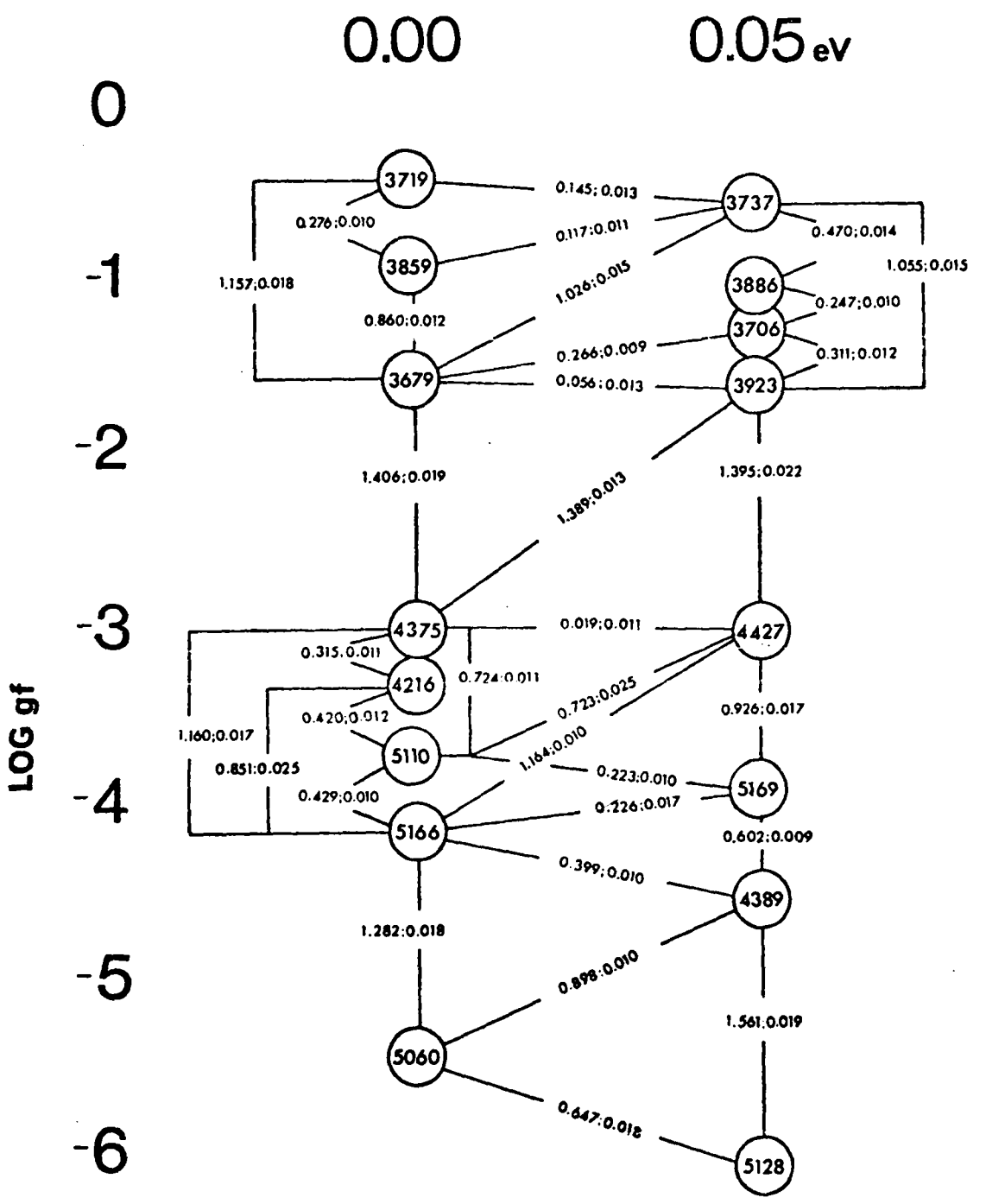
Furnace optical system and spectrometers.



1. lamp
2. off axis paraboloid
3. quartz windows
4. plane mirrors
5. spherical mirror
6. entrance slit
7. monochromator mirrors
8. monochromator prism
9. spectrometer entrance slit
10. collimating mirror
11. grating
12. camera mirror
13. exit slits
14. chopping drum
15. lens
16. photocathode

Figure 5.3

Previously measured relative oscillator strengths of FeI lines using the Oxford furnace, from Blackwell, Ibbetson & Petford (1975).



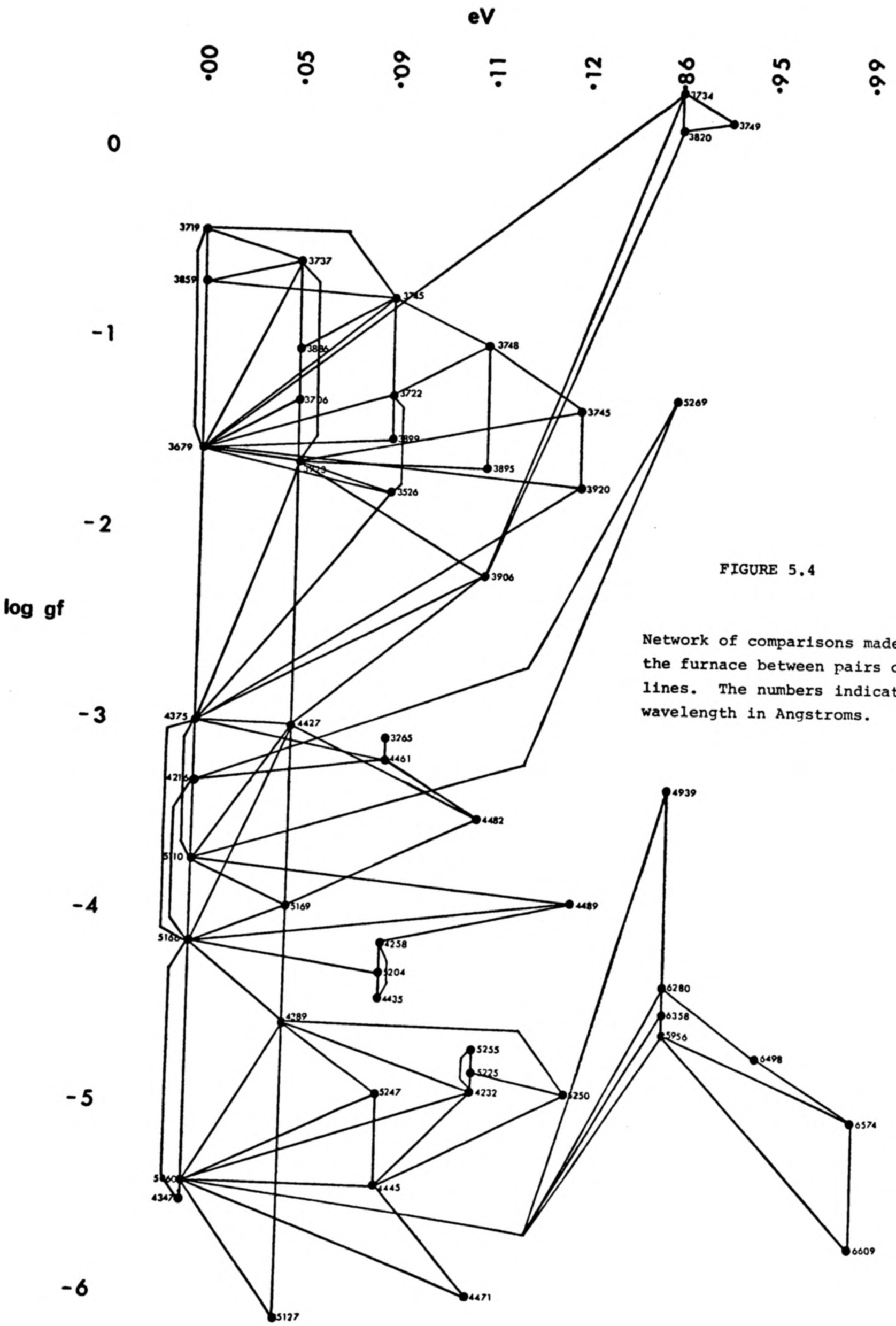


FIGURE 5.4

Network of comparisons made with the furnace between pairs of FeI lines. The numbers indicate the wavelength in Angstroms.

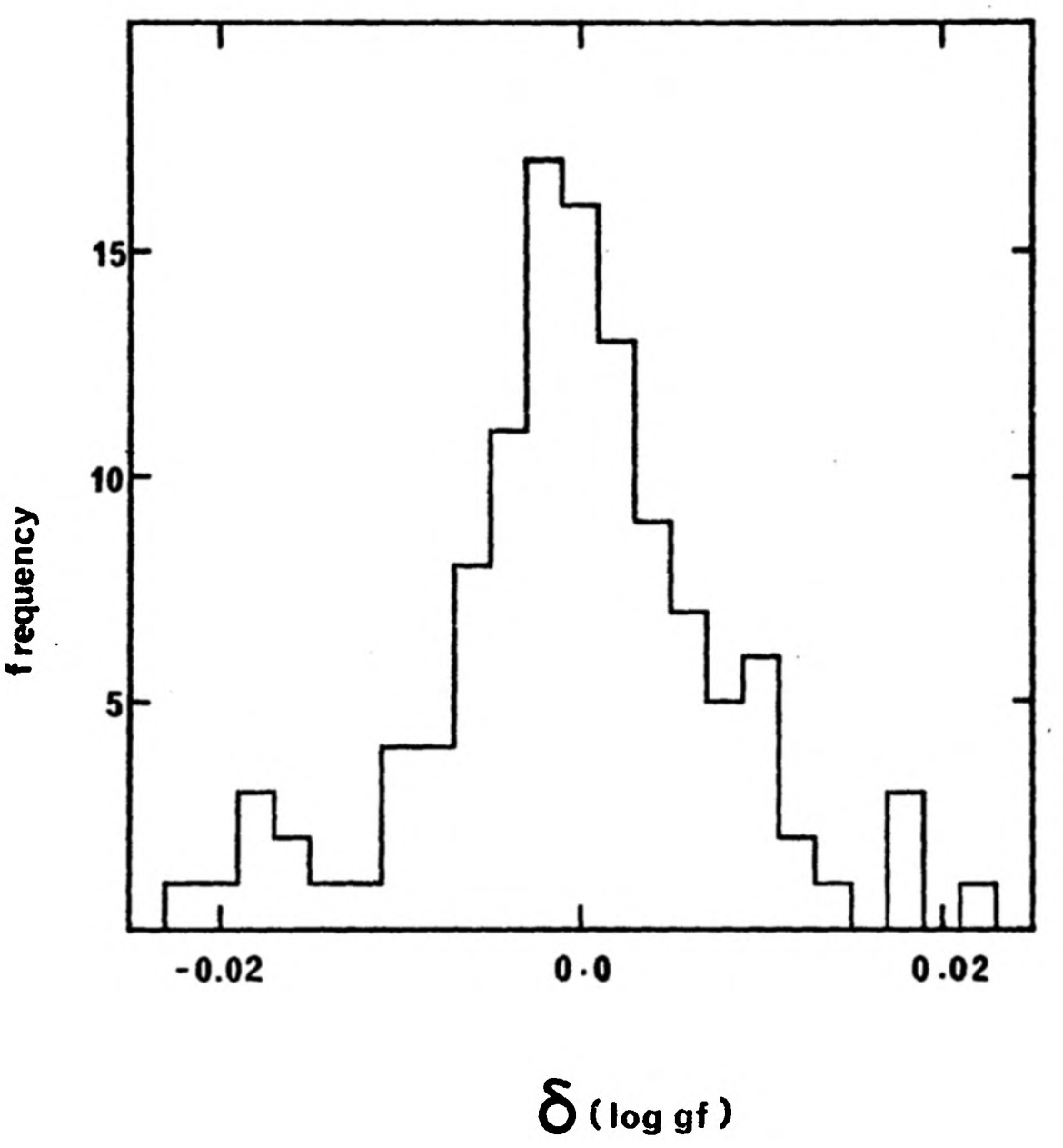
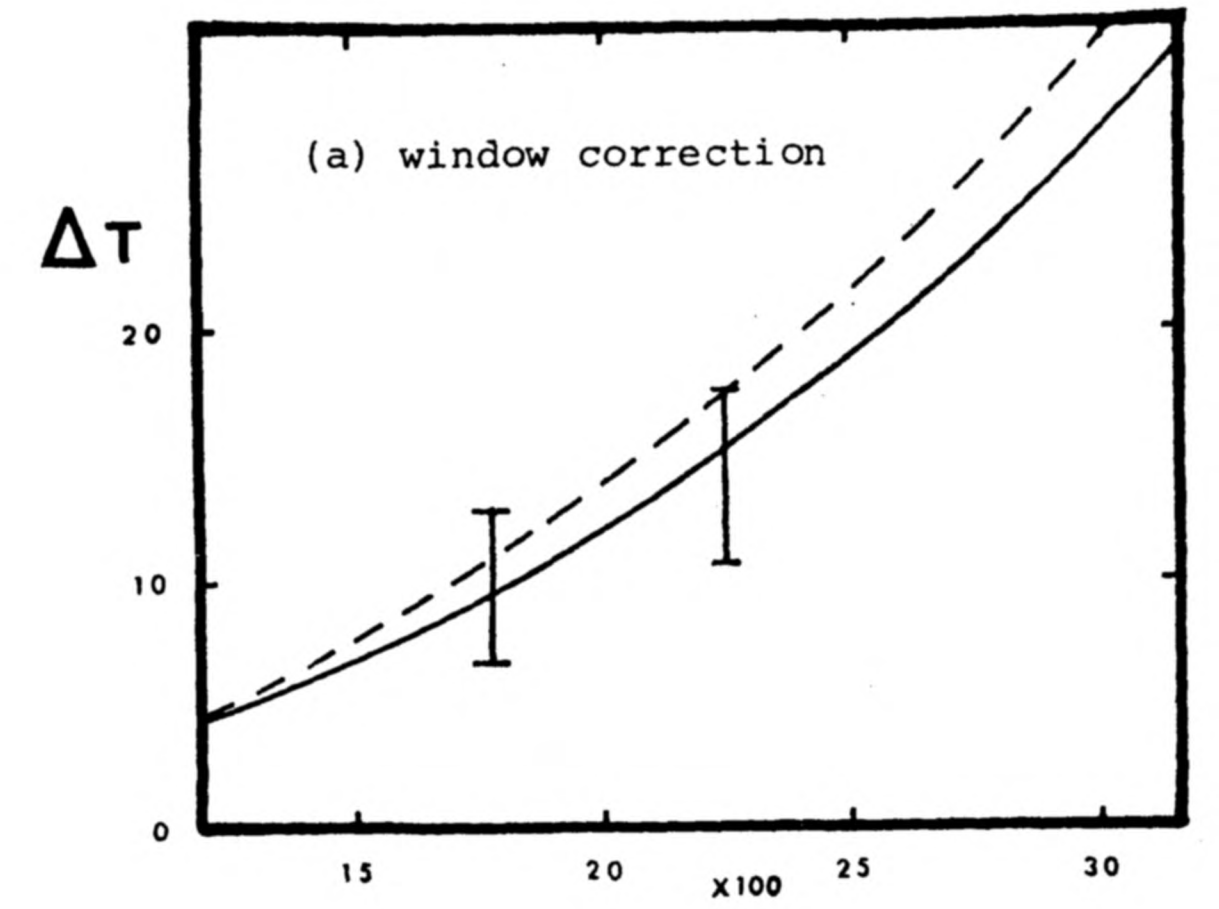
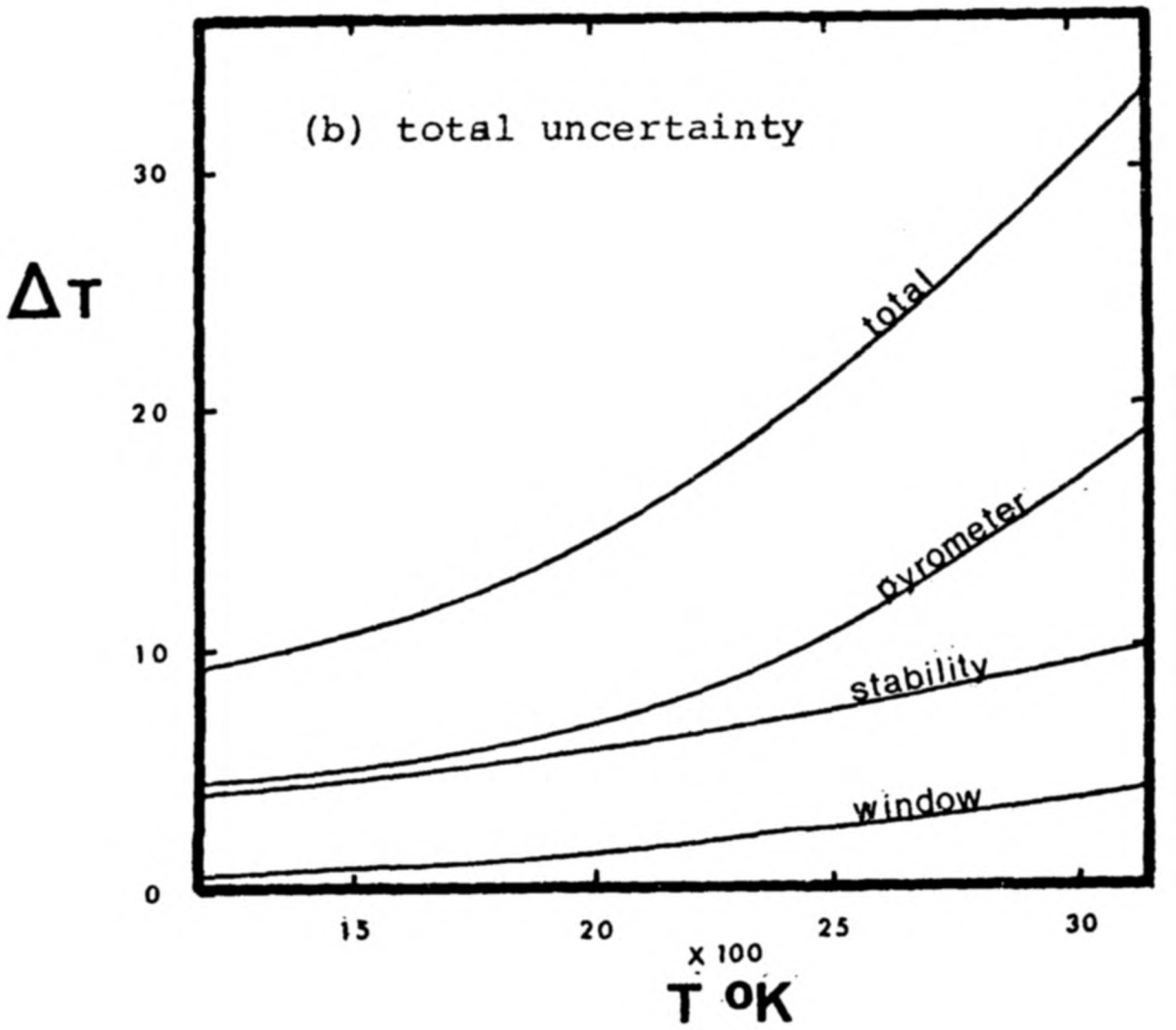


Figure 5.5

Residuals between the measured and adopted relative oscillator strengths.

Figure 5.6





(a) observed window correction and theoretical curves fitted to that data;

(b) total uncertainty in temperature and the 3 contributing factors.

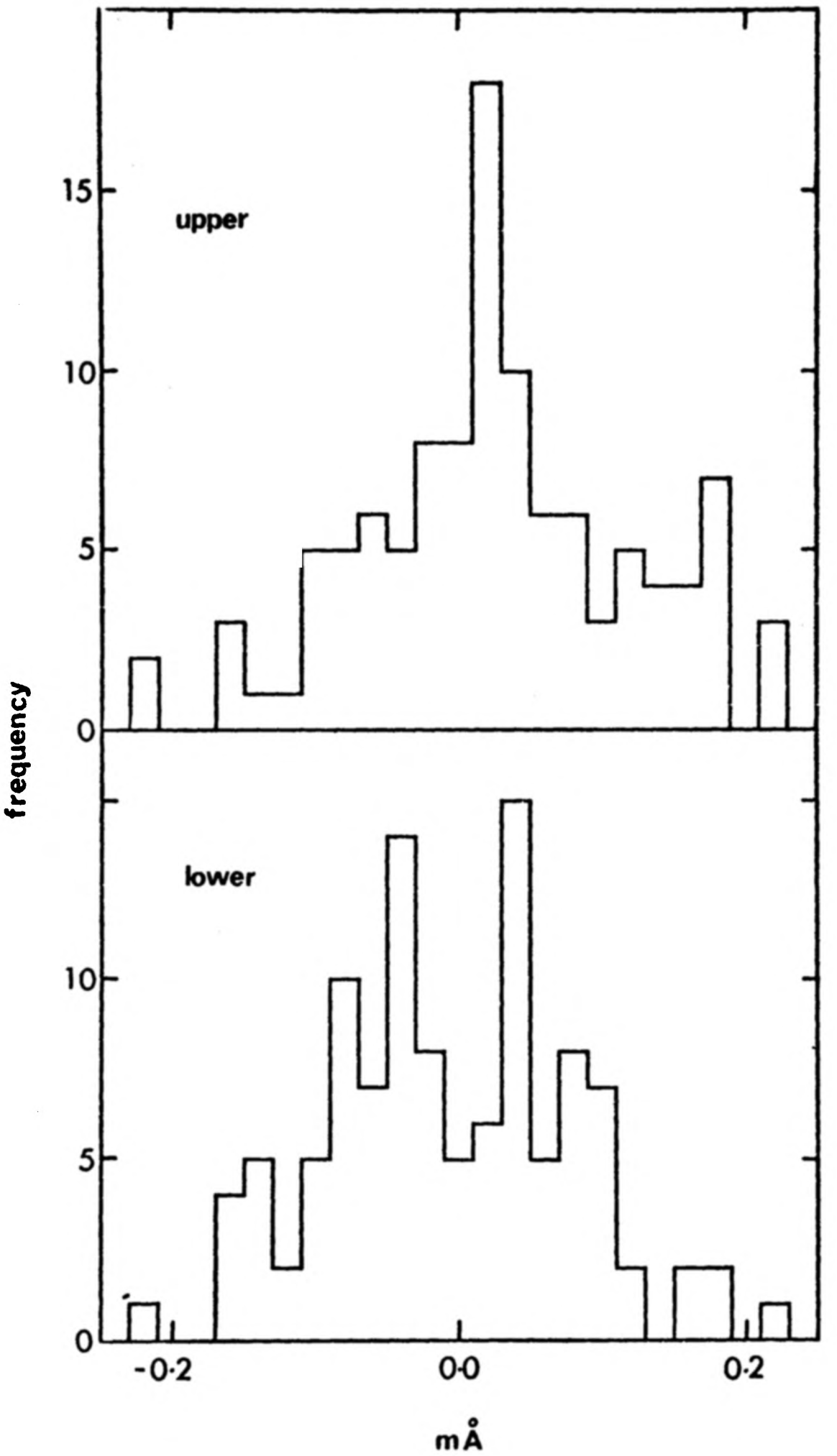


Figure 5.7

Histograms of the background corrections found for the two spectrometers.

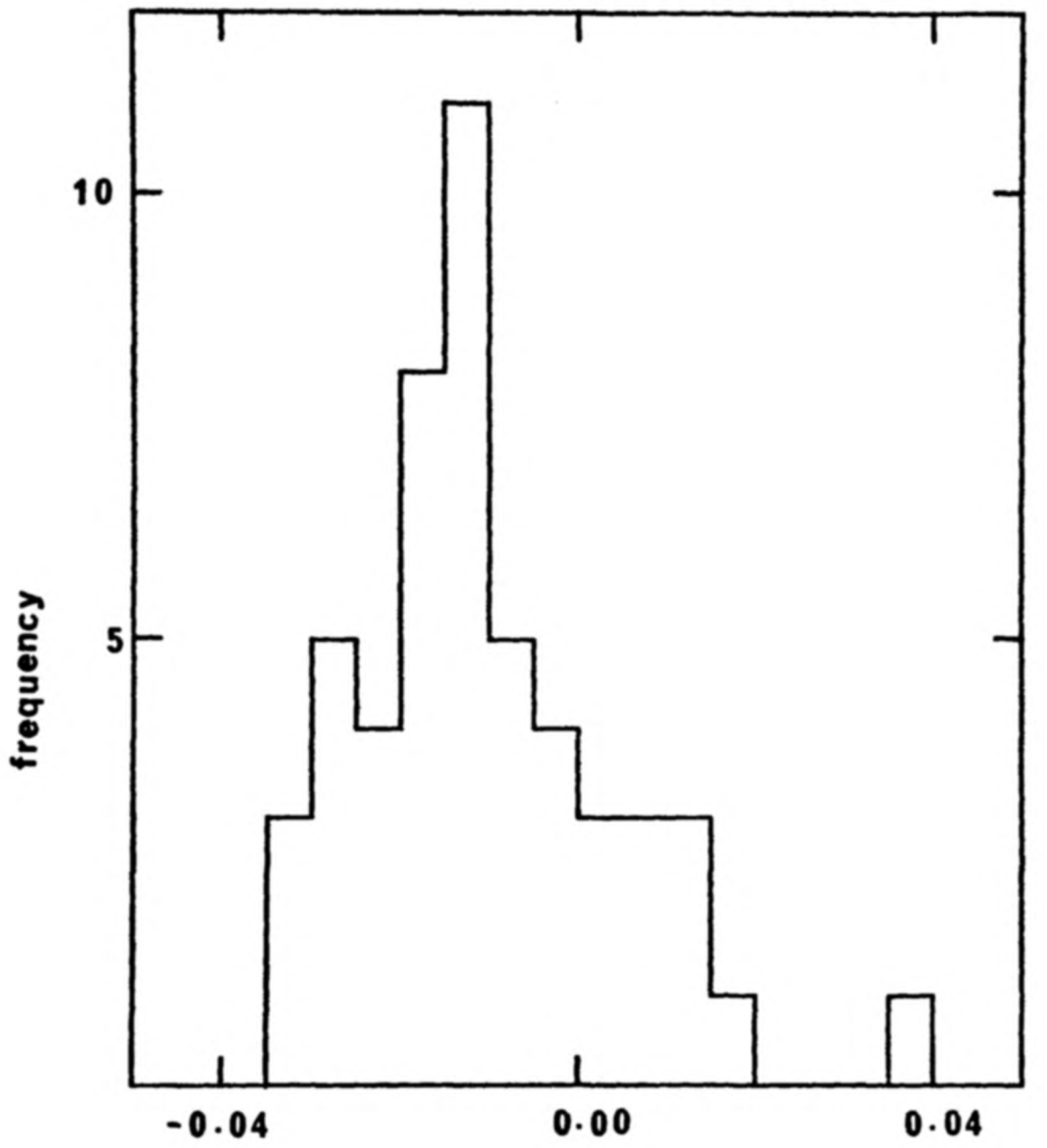


Figure 5.8

Histogram of the differences between the pairs of oscillator strengths according to the spectrometer configuration, showing the systematic difference.

Figure 5.9

Term diagram for the transitons measured, giving multiplet numbers.

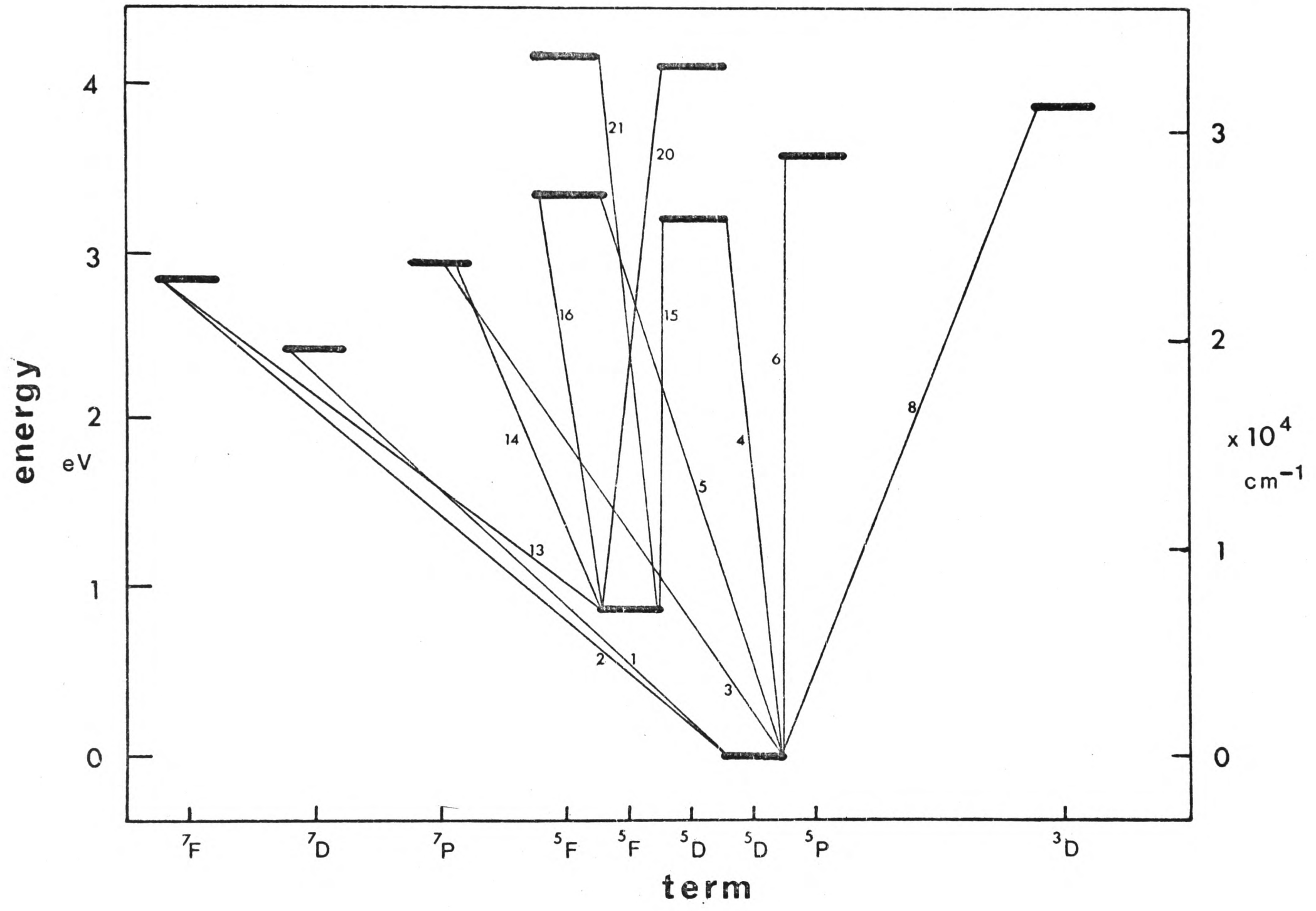
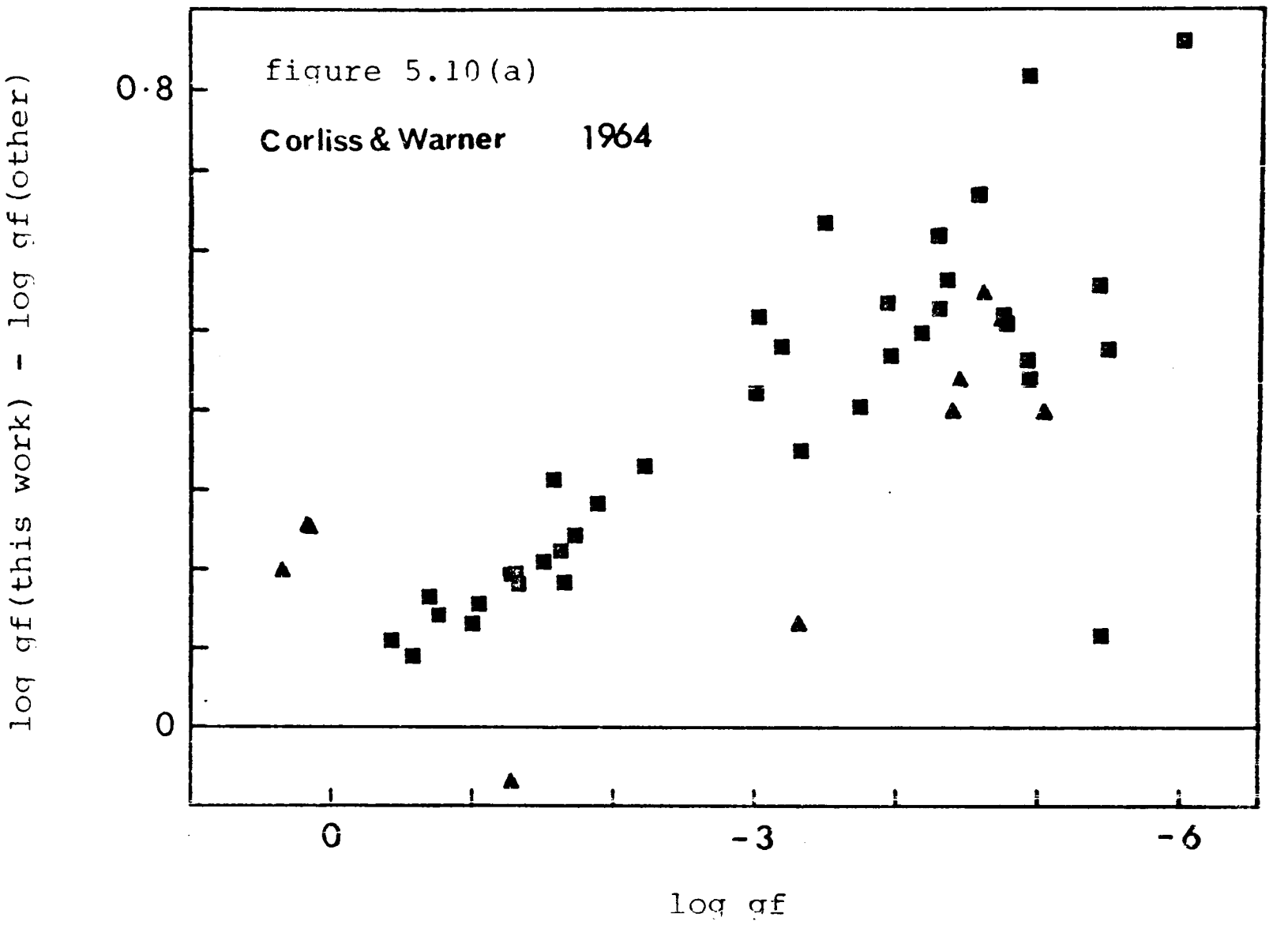


Figure 5.10

Comparisons between the measurements reported in this and the results of other authors: lines from a^5D and a^5F terms are identified by squares and triangles respectively.

a. Corliss and Warner (1964) - arc compilation
b. Prokof'ev et al (1964) - compilation
c. Bridges and Kornblith (1974) - arc
d. May et al (1974) - arc
e. Valters and Stratsev (1964) - furnace hook
f. King and King (1938) - furnace absorption
g. Huber and Tubbs (1972) - furnace absorption
h. Huber and Banfield (1973) - furnace hook
i. Ross (1973) - calculation
j. Kurucz (1974) - calculation


figure 5.10(a)
Corliss & Warner 1964
0·8
0
0
-3
-6
log gf(this work) - log gf(other)
log gf

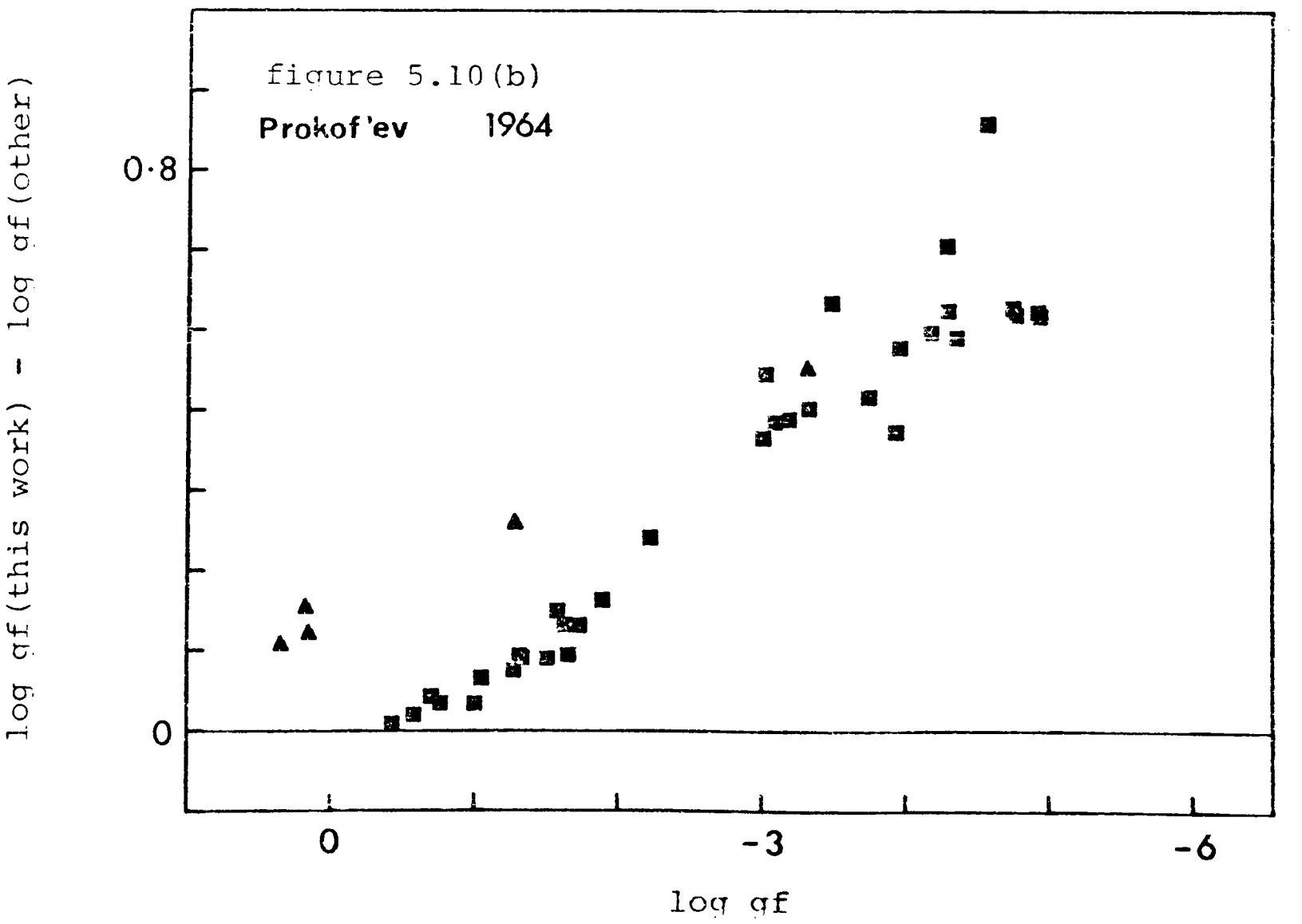

figure 5.10(b)
Prokof'ev 1964
0·8
0
0
-3
-6
log gf(this work) - log gf(other)
log gf

figure 5.10(c)

Bridges & Kornblith 1974

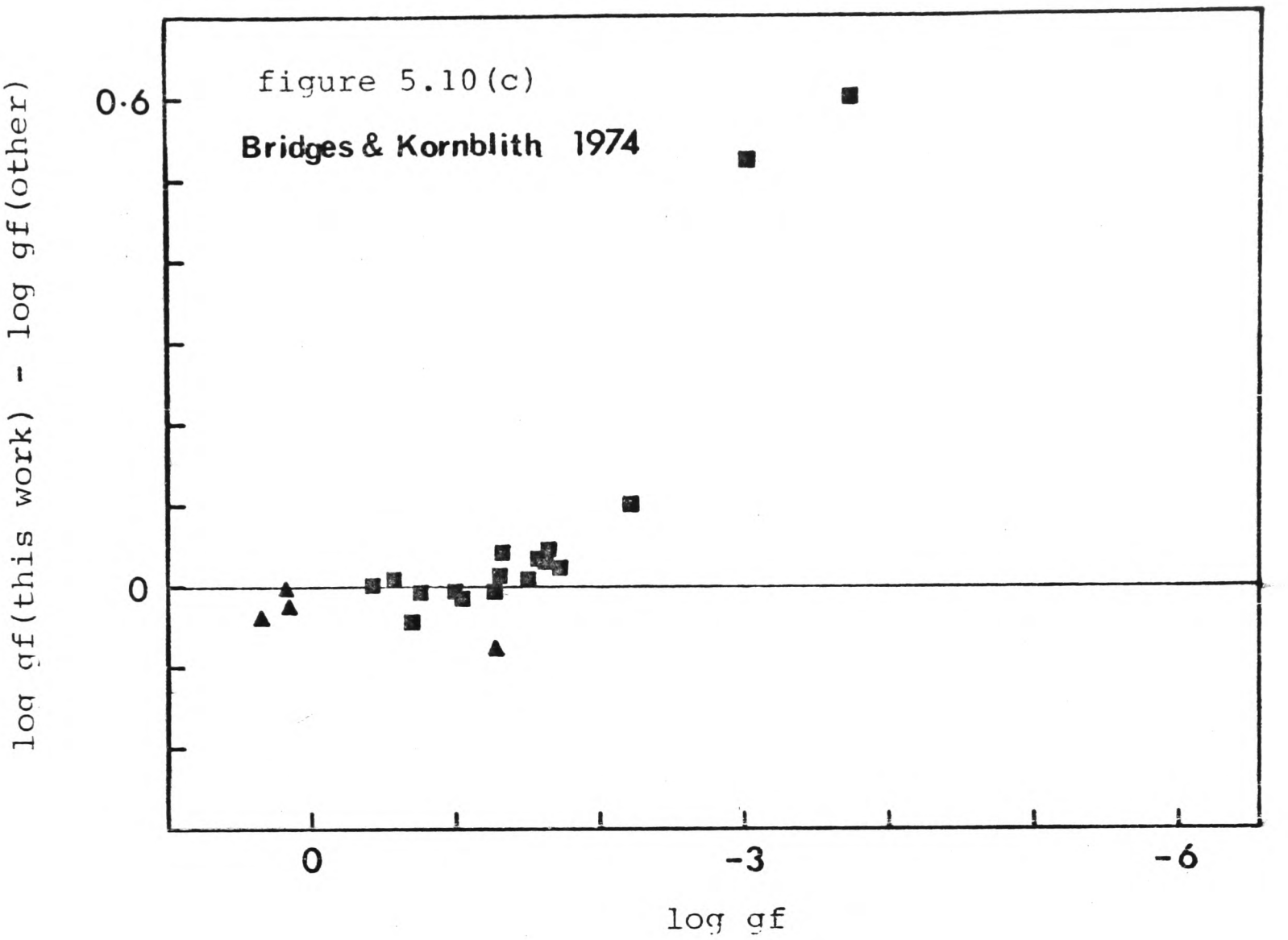
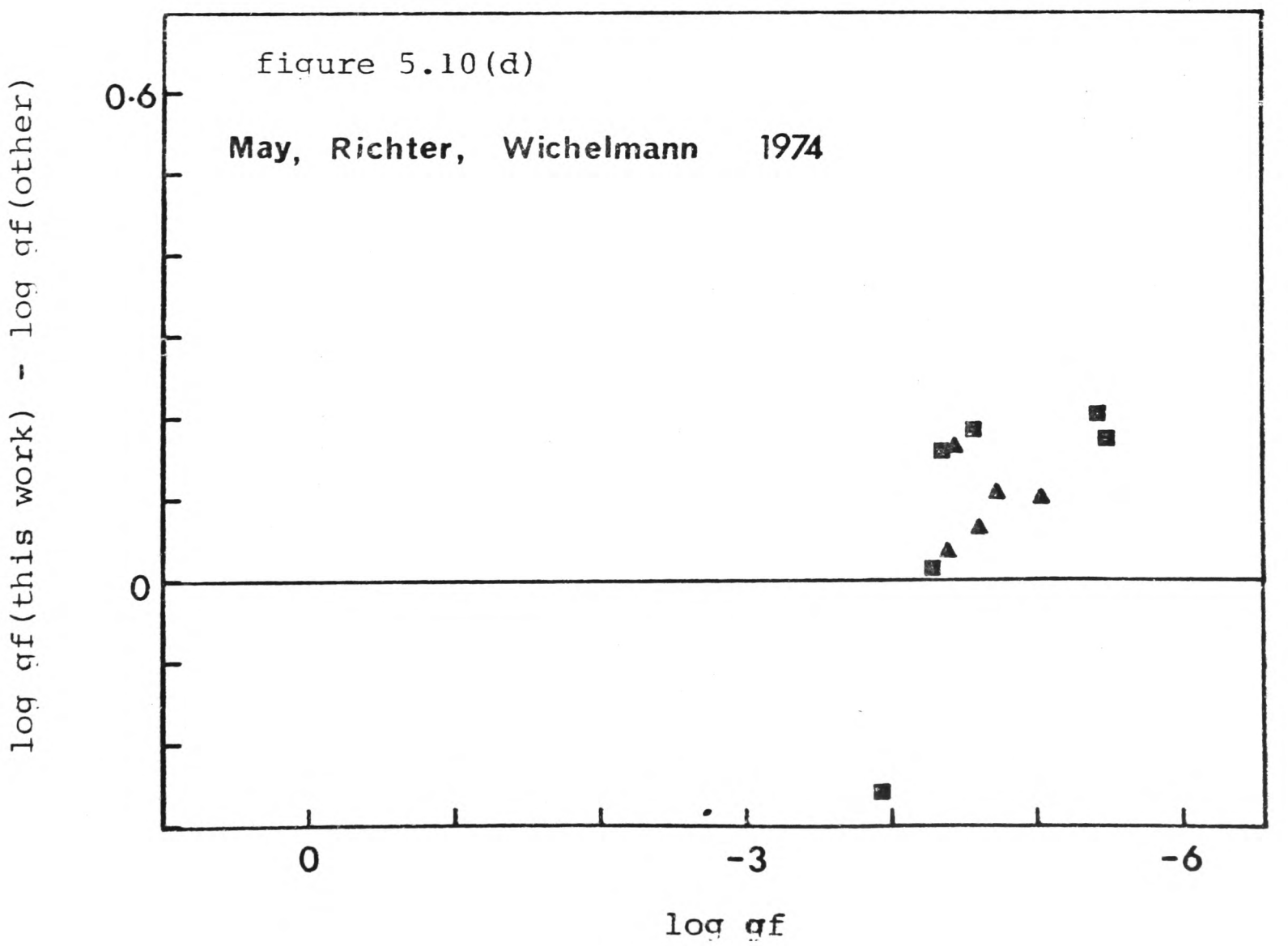
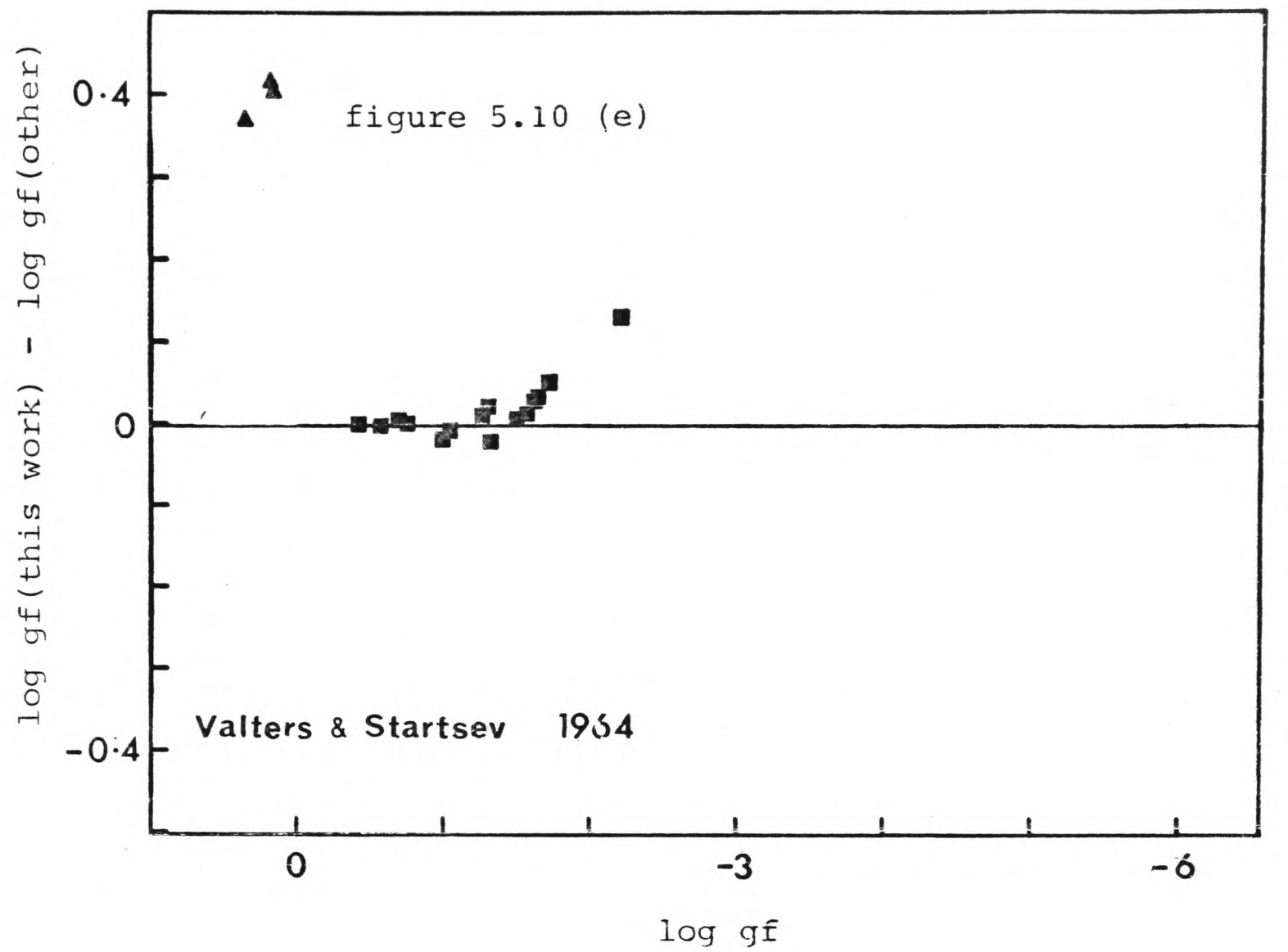


figure 5.10(d)

May, Richter, Wichelmann 1974




figure 5.10 (e)
0·4
0
-0·4
log gf(this work) - log gf(other)
Valters & Startsev 1964
0
-3
-6
log gf

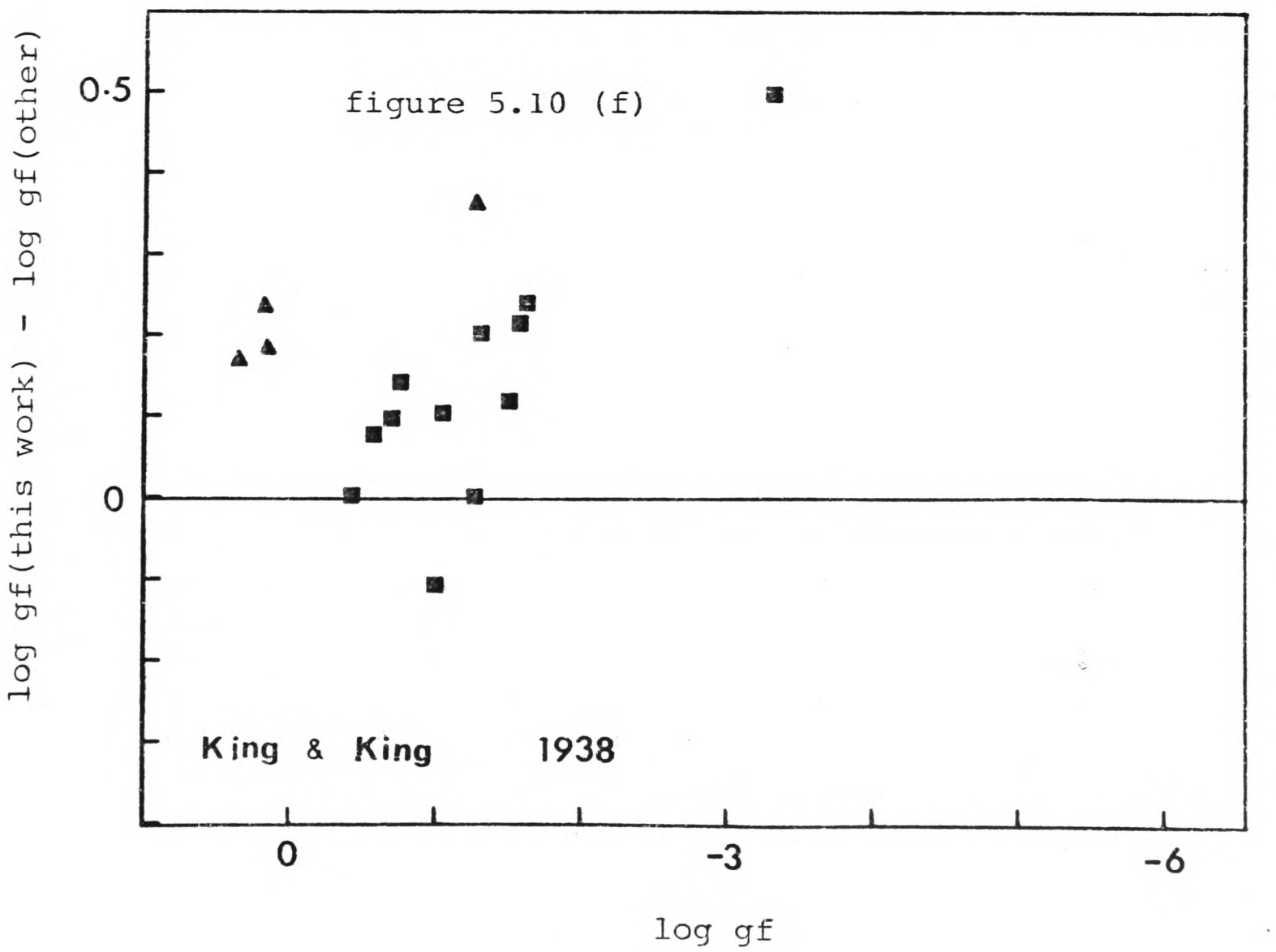

figure 5.10 (f)
0·5
0
log gf(this work) - log gf(other)
King & King 1938
0
-3
-6
log gf

figure 5.10 (g)

Huber & Tubbs 1972

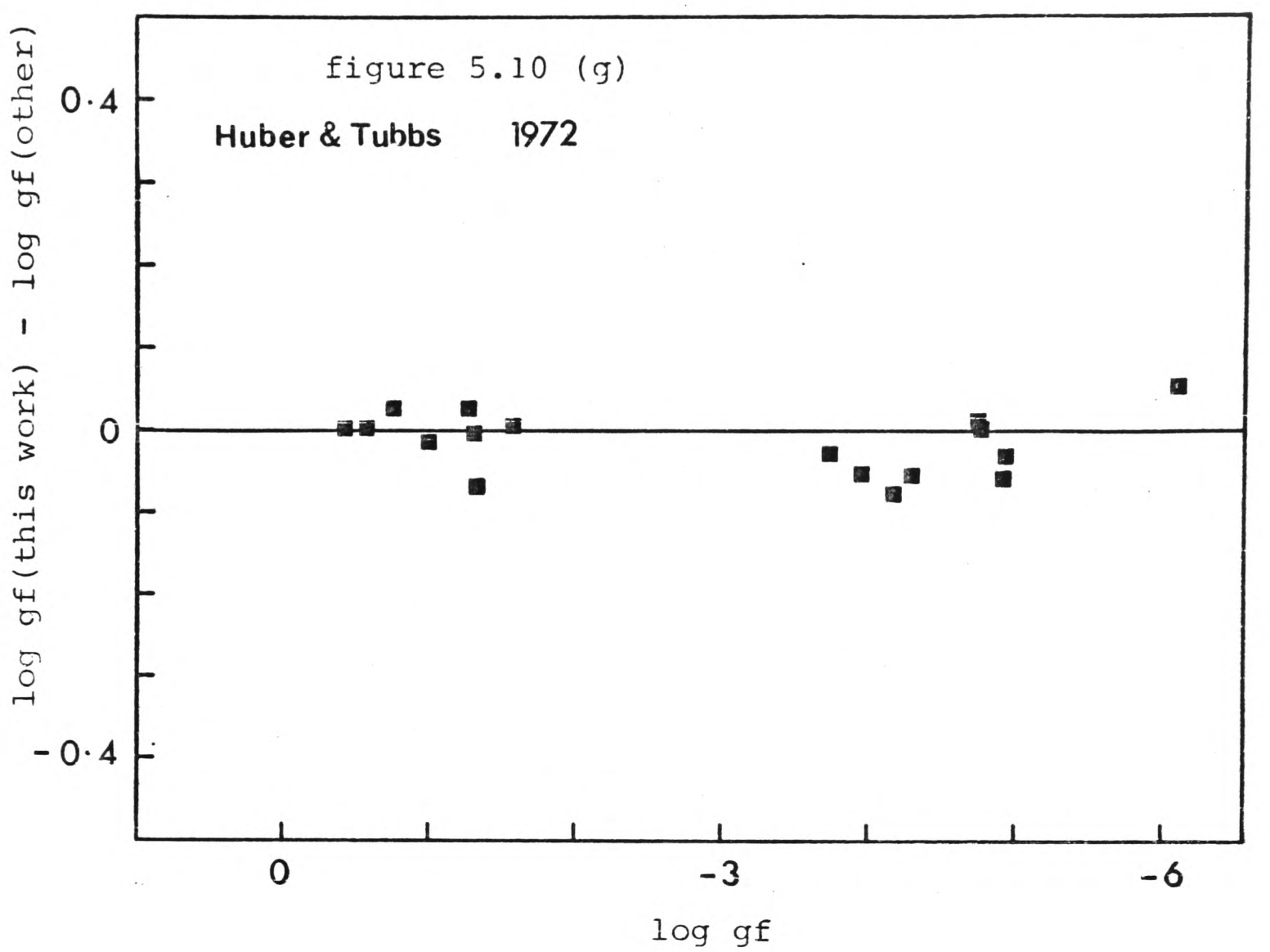


figure 5.10 (h)

Huber & Banfield 1973

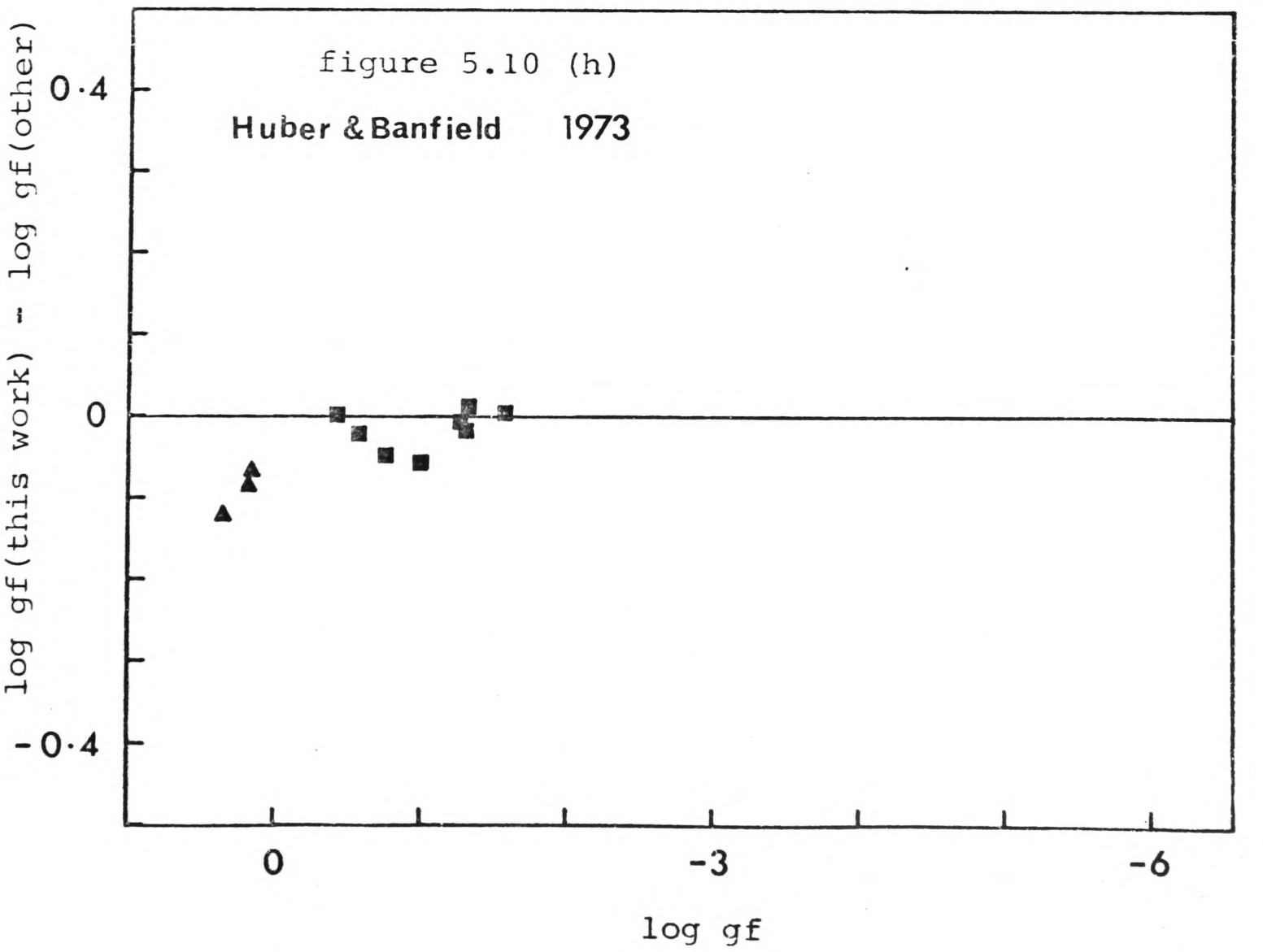


figure 5.10 (i)

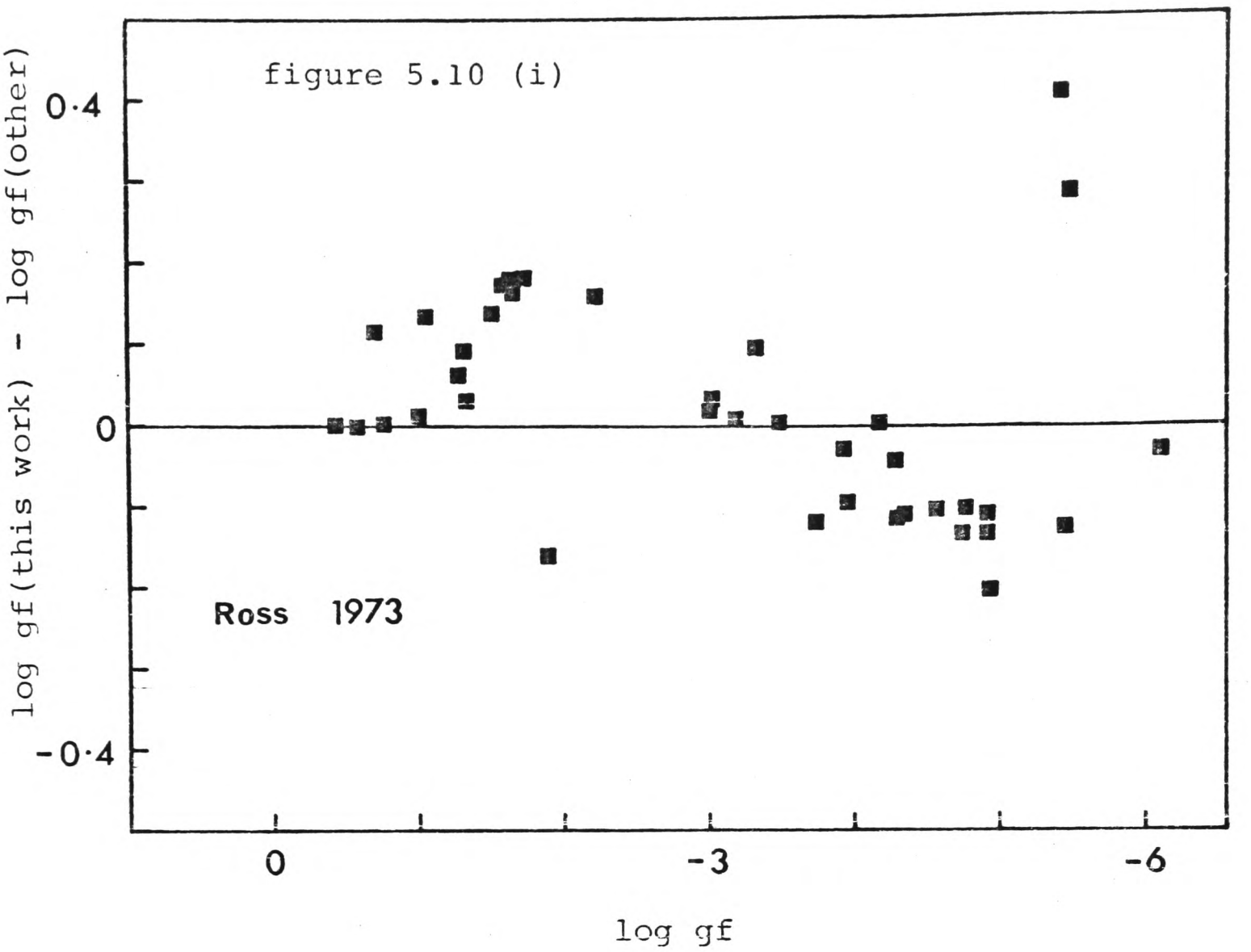
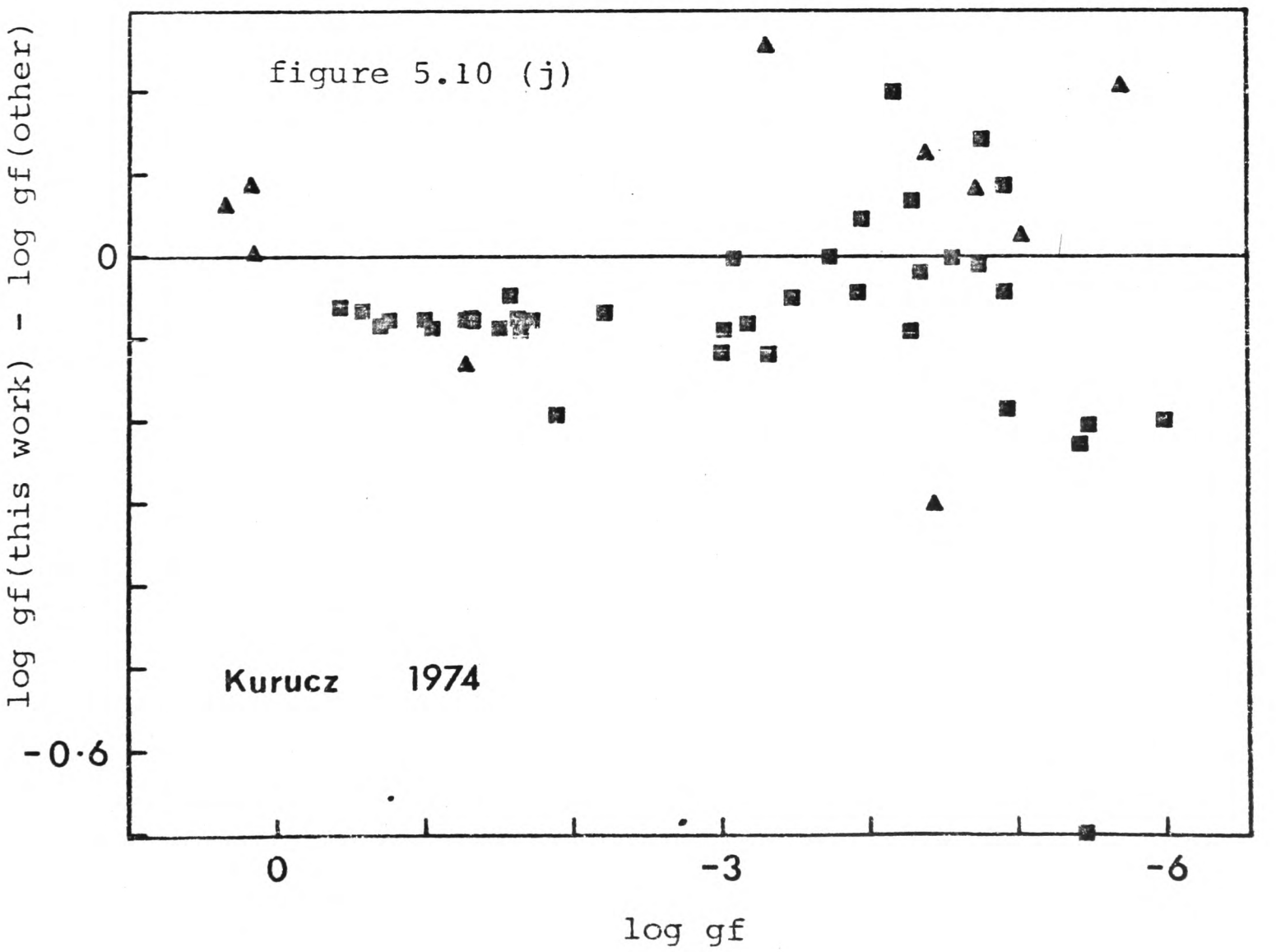


figure 5.10 (j)



6. SOLAR SPECTRUM : FE I ABUNDANCE AND MICROTURBULENCE

6.1 Solar data

6.1.1 Selection of lines

Not all of the lines with measured oscillator strengths could be used to determine the abundance. First the very strong lines were rejected because their profiles and equivalent widths were determined by the damping which was to be found. Secondly, the desired precision would be impossible if the lines were blended with other transitions where the strength or even the identity of the contaminant was unknown; or if the position of the continuum was uncertain. Blends were identified from the symmetry of the observed profile, and from the line lists of, inter alia, Moore et al (1966). Even so there was one line (FeI 0.00eV 5060A) which appeared from the solar line lists and spectrum to be free from blends, but which gave - from its observed equivalent width - an anomalous abundance. On further investigation it was found (Moore, 1959) that it was blended with a high excitation FeI line (multiplet no. 1095, 4.28eV). From the observed strength in the sun the oscillator strength could be obtained, and this agreed within the expected limits with the calculated gf value (Kurucz and Peytremann, 1975). But it is impossible to rule out the possibility, however remote, of some small blending from other, similarly unexpected lines.

Selection of strong lines was less straightforward. Of those measured in the furnace only FeI 5269A was free from serious blends in the solar spectrum. And the other lines were also at wavelengths below 4000A where the continuum was uncertain. The 5269A line was therefore adopted as the principal line for the damping measurements, which are described in the next chapter. 9 of the strong lines in the blue region were also investigated and provisional results for their damping constants also reported below.

6.1.2 Measured equivalent widths

A total of 19 relatively unblended, weak lines were left when blends etc were excluded: 13 from the 0.00-0.12 eV levels and

6 from the excited group. These lines were interpreted in terms of their equivalent widths at a number of disk positions in the range $\mu = 1.0$ to $\mu = 0.2$. Equivalent widths were measured from the published spectra of Delbouille et al (1973) and of the "Preliminary edition of the Kitt Peak solar atlas" (Brault and Testerman, 1972). Both of these were obtained at high altitude with photo-electric, double pass spectrometers, and both exhibit low noise, narrow instrumental profiles and an absence of scattered light. Lines in the former, disk centre spectrum were planimetered from the paper atlas, using where appropriate the expanded (0 - 20 per cent) absorption scale. For the Kitt Peak atlas on 35mm film, large scale prints were made to allow measurements of the two profiles: at disk centre and at $\mu = 0.2$.

Observations made at the Gornergrat Observatory of the Department of Astrophysics, Oxford (Blackwell et al, 1969) were used to find the equivalent widths at $\mu = 1.0$, 0.5 and 0.3. The spectra had very low noise levels and high resolution but came from a single pass spectrometer. It was necessary therefore to correct the measured equivalent widths for the effects of scattered light. A correction factor was found from the residual intensities at the core of strong lines measured at the Gornergrat, by the double pass systems mentioned above, and by Lites and White (1973). As an independent check, weak lines in unblended regions of the spectrum were also measured in both the Gornergrat and double pass spectra, and the ratio of equivalent widths used to determine the amount of scattered light. The mean value was 3 per cent and the equivalent widths were adjusted by this amount. Although this correction was uncertain by perhaps 1 per cent, and reduced the absolute accuracy of the Gornergrat values, there was a compensating advantage. The spectra were recorded in digital form, and equivalent widths were measured using a visual display unit forming part of the DGC NOVA computer system at the Department of Astrophysics, Oxford. Apart from making the planimeter redundant, this allowed the profile of the line to be checked for symmetry (by reversing the fitted profile); and the observed line could be compared with calculated profiles, eg a convolution of a Voigt function and the approximate instrumental profile.

Published measurements were also taken into account and values for some or all of the 19 lines were given by Moore et al (1966), Holweger (1967), Smith (1974), Huber and Tubbs (1973), Muller and Mutschlechner (1964) and Withbroe (1968). These are listed, together with the equivalent widths measured from the spectra, in table 6.1.

6.1.3 Correction for molecular blends

It was not practicable to exclude all blended lines. Many of the measured FeI lines coincided with vibration-rotation transitions of molecules which might exist in the solar atmosphere. If all of the potential blends were rejected the number of lines left for the abundance and microturbulence would be greatly reduced. Lines contaminated by blending with a molecular line were therefore used if the strength of the FeI line was very much greater than that of the molecular: and if also the correction to the measured equivalent width for the blend could be determined with sufficient accuracy.

Possible blends were considered from the line lists of Phillips and Davis (1968) for the Swan bands of C_2; Moore and Broida (1959a) for CH; Davis and Phillips (1963) for the red system of CN; Balfour (1970) for MgH; Moore and Broida (1959b) for OH; Sotirovski (1971, 1972) for MgH, MgO, CN, TiO, CaH, AlH and O_2. Many coincidences were found with the wavelengths of the FeI lines but these were not necessarily evidence of real blending. In the case of TiO for instance, Sotirovski (1972) concluded that the molecule did not exist in the solar spectrum. It was therefore safe to ignore the lines $Q_1(3)$ at 5254.9A and $R_1(5)$, $R_1(8)$ at 5250.2A. Results are accordingly reported here only for the molecules where a significant correction for blending was applied.

a. CH

From the extensive tabulation of CH lines given by Moore and Broida (1959a) two transitions, both from the (2,2) band, gave rise to blends with the chosen FeI lines: $Q_{1d}(26)$ at 4347.2A and $P_{1dc}(21)$ at 4427.3A. Estimates of the equivalent widths

of these two CH lines were obtained first from the observed equivalent widths of other lines from the same band. Within a given vibration-rotation band the line strength is given by:

$$W_J = S_J \cdot C \cdot \exp(-BJ(J+1)/kT) \qquad (6.1)$$

where J is the rotational quantum number, W_J the equivalent width (for weak lines), C a constant, and B the energy level scaling constant. The Honl-London factors S_J were taken from Bennet (1970) and Kovacs (1969) throughout this work, and the normalisation of Schadee (1971) adopted. B was found from the data given by Gaydon (1968) and by Rosen (1970). Then writing equation (6.1) as:

$$\log (W_J/S_J) = C' - \log e \cdot BJ(J+1)/kT \qquad (6.2)$$

plotting $\log(W_J/S_J)$ against J(J+1) should yield a straight line. Equivalent widths for CH lines from the (2,2) band were taken from Moore and Broida (1959a) whose values agreed well with the later results of Grevesse and Sauval (1973). Figure 6.1 shows the result. For the weaker lines at high J the observed equivalent widths were uncertain and the line poorly defined. The value of B was therefore used, with the rotational temperature of Laborde (1961), to predict the gradient and to draw in the line shown in figure 6.1. From this the equivalent widths of the 4347A and 4427A blends were estimated to be 2.8 and 6.4mA respectively.

Line strengths were also estimated from the corresponding transitions in the (0,0) vibration band, using the relationship:

$$W(2,2) = W(0,0 \ (q/q') \exp(-Ghc/kT) \qquad (6.3)$$

where q and q' are the Franck-Condon factors and G a molecular constant calculated from the standard spectroscopic data. Using the values for the Franck-Condon factors given by Sotirovski (1971) and the equivalent widths of lines in the (0,0) band of Moore and Broida (1959a) the blending correction for FeI 4427A was 4mA. The correction for 4347A was less precisely determined because of the lack of observed lines in the lower band, and a limit of 6mA was the only conclusion. The values adopted, taking account of the two determinations, were 3mA for FeI 4347A and 5mA for FeI 4427A.

b. C_2

Many of the lines of FeI measured in the furnace coincided with lines in the Swan bands of the C_2 molecule. The blends considered were FeI 5127A with $P_1(8)$, $P_1(22)$, $P_2(7)$ and $P_3(6)$ from the (1,1) band; FeI 4347A with $R_1(13)$ from (4,2) and $R_1(27)$ from (2,0); FeI 4375A with $P_3(40)$ from (2,0) and $R_3(33)$ from (8,6); FeI 4389A with $R_3(9)$ from (8,6).

Particular attention was given to the 5127A blends because the solar equivalent width of the iron line was small and the line ideal for abundance determination. The blending correction was however significant. Using first the observed lines from the same band figure 6.2 was constructed. Equivalent widths were taken from Moore et al (1966) and the gradient of the line computed using the rotational temperature of Persi (1975) which is some 200K less than the value given by Schadee (1964). The line shown in the figure assumes that the equivalent widths are overestimated, due to other blends. But with the value of $\log(W_O/S_O)$ found by Persi (1975) the line is moved up and the correction to FeI 5127A became 2.5mA.

Huber and Tubbs (1973) gave 2mA for the same lines using the higher rotational temperature, and equivalent widths measured from solar spectra at the Kitt Peak National Observatory. This may be a more precise value in view of the greater resolution of the observations. It was not possible however to confirm the source of the difference as the equivalent

widths were not given. Nor was it possible to derive equivalent widths for all the lines from the (0,0) band in the case of C_2 because the lower band was heavily blended. A value of 2.5mA was therefore adopted with an estimated uncertainty of at least 0.5mA.

For the lines from other bands it was less easy to estimate the equivalent width in the solar spectrum. Where possible observed equivalent widths were used to plot line strength against energy as before, but in some instances this could only be done using the intensities in laboratory spectra. Accordingly there were very great uncertainties in the adopted corrections, which amount to upper limits, of 5mA in 4346A; 0.9mA in 4375A; 1.7mA in 4389A.

c. MgH

The only important MgH blend was $Q_1(7)$ from the (2,2) band at 5127.69A (Sotirovski, 1972). The equivalent width of this was derived using the observed strength in the solar spectrum of the corresponding line in the (0,0) band. The ratio of the Franck-Condon factors is 0.772 (Sotirovski, 1971) and the relative Boltzmann factor 0.424 using T_{exc}= 4700K. Then

$$W(2,2) = 0.327\ W(0,0) \qquad (6.4)$$

Huber and Tubbs (1973) followed the same procedure and used 2.2mA for the equivalent width of the $Q_1(7)$ (0,0) line. It was noted by those authors that Schadee (1964) gave 4.5mA but the superior spectrum was an argument for the lower value. However many other measurements favour a higher value than 2.2. Moore et al (1966) also quote 4.5; Laborde (1961) gives 5.7; Withbroe (1968), Mallia (1968) and Lambert et al (1971) give 4.0, 3.4 and 4.1 respectively. Perhaps the most significant measurement though was by Grevesse and Sauval (1973) who found 3.9mA from the double pass spectrometer at the Jungfraujoch

(Delbouille and Roland, 1969). Taking account of the uncertainty in the observed equivalent width a value 1.1 $\pm$ 0.3 was adopted for the blending correction.

Finally the corrections found for the disk centre equivalent width were used to estimate the values at other disk positions. In order to take account of the particular centre-limb behaviour of molecular lines, the variation at different line strengths was derived from the equivalent widths listed by Baschek et al (1967) and by Withbroe (1967, 1968).

6.1.4 Adopted equivalent widths

From the measured equivalent widths of the FeI lines, corrected for molecular blends, mean values were taken. Greatest weight was given to the measurements from the Jungfraujoch, Kitt Peak and Gornergrat spectra where the noise level was low and the resolution high. The uncertainties are given for the adopted values in table 6.2, and arise from the different measurements and reported values. The major part of this uncertainty was due to the position of the continuum which differs from spectrum to spectrum. In addition the uncertainty quoted in table 6.2 reflects the difference between the measurements of this author and the equivalent widths found by Professor D E Blackwell from the same spectra.

6.2 Calculation of equivalent widths

6.2.1 Line formation

Equivalent widths of the FeI lines were calculated assuming LTE and a pure absorption mechanism. As indicated above, the assumption of LTE ionisation and excitation is not significant for the method proposed; and the weak lines are unlikely to have departures from simple absorption due to scattering. It was important though that the calculations should preserve the precision of the measured oscillator strengths and the observed equivalent widths. Particular care was therefore taken with the FORTRAN program used with the ICL 1906A computer of the Oxford University Computing Laboratory. The factors determining the accuracy of the computed profile and equivalent width are considered further in Appendix I but, broadly speaking, approximate methods were avoided; accurate values used for all physical constants; and numerical methods chosen to avoid rounding errors. As a further check on the calculations, equivalent widths were compared with the results of an independent computer code written by Dr Peter Craven.

6.2.2 Line opacity

Of the factors determining the line opacity, the oscillator strength was measured, and the iron abundance one of the values to be found. Ionisation and excitation were determined by the solar atmosphere (see next section) and by the physical data, such as partition functions, assumed in the computation. The profile function however depended on the assumed values of the damping of the line and of the microturbulence in the atmosphere. The weak lines were found, as expected, to be insensitive to the damping constant but care was taken to calculate the natural damping accurately from the measured oscillator strengths and from the data of Kurucz (1974). Collisional broadening was taken into account using the relation given by Unsold (1955) discussed in chapter 7 below:

$$\Gamma_6 = 17.0\ C_6^{0.4}\ V^{0.6}N$$

where C_6 was taken from the approximate formula given by Unsold (1955):

$$C_6 = 1.61 \times 10^{-33} (13.52/X)^2$$

where X is the energy, in eV, needed to ionise the atom from the level in question. Similarly the collisional broadening by helium was calculated from the corresponding formulae. The damping from the Stark effect is negligible for the low excitation FeI lines (Panter and Foster, 1937).

The other contribution to the profile function, Doppler broadening, combined the thermal velocity in the atmosphere with a microturbulent velocity. The latter was assumed to be anisotropic but could be specified separately for different disk positions; in the majority of the calculations it was also assumed to be independent of optical depth although any depth dependence could be specified by defining the values at the discrete optical depths used in the model atmosphere.

6.2.3 Model solar atmospheres

The second major input for the line calculations was the model of the solar atmosphere: the variation with depth of the temperature, gas and electron pressures; and the abundances. Model photospheres fall into three broad categories - empirical, semi-empirical and theoretical - according to how they were constructed. And further divisions are possible, eg to distinguish models which take account of inhomogeneities.

As representatives of the more recent and widely used atmospheres, four were used: the Harvard Smithsonian Reference Atmosphere (HSRA) (Gingerich et al, 1971); the ELSTE10 model (Elste, 1967); the atmosphere of Holweger (1967) as revised by Holweger and Mueller (1974) (HOLWEGER); and the theoretical, line blanketed model of Kurucz (1974a) (KURUCZ).

In addition a variant of the HSRA model (Lites, 1973) with the same broad structure but non-LTE populations for FeI was also used and is denoted hereinafter as HSRA NLTE. Calculations with this model were unique only in so far as the computed number densities of FeI atoms in the relevant lower level were scaled by the correction factors necessary to take account of the departures from LTE (Lites and Brault, 1973).

The four models are compared in figure 6.3 (a) - (f) which shows the variation with the standard optical depth at 5000A of temperature, pressure (gas and electron), opacity and the number density of iron atoms for 0eV and 1eV excitation potentials. In the following sections these figures will be drawn on to explain the results of detailed calculations, but a number of qualitative points may be made here. First, the temperature structures are very similar, more especially for optical depths greater than about 0.5. Next the gas pressure shows almost constant differences over a very wide range. The order by decreasing pressure is ELSTE10, KURUCZ, HSRA and HOLWEGER but the total spread is less than 0.2 dex.

Turning to the electron pressure, there is again a small range, but the HOLWEGER model has the higher values and the ELSTE10 the lower. As H^- dominates the opacity, this explains, at least qualitatively, the differences in the continuous opacity shown in figure 6.3(d).

In contrast to the physical properties, the concentration of iron atoms in the particular lower levels shown in (e) and (f) exhibits very large differences from model to model. These differences may be interpreted as the effect of the small differences in temperature and pressure on the ionisation and excitation of the atoms, and show how sensitive the Saha-Boltzmann equation is to those values. And of course the abundance and number of iron atoms enter the line opacity together, so that, for the same equivalent widths different models will require different abundances.

6.3 Determination of abundance and microturbulence

It was apparent from the measured equivalent widths that it would not be possible to determine the abundance from a line or lines from a single, lower level. Blackwell et al (1972) had shown that the uncertainty in the abundance for a given uncertainty in microturbulence increased sharply with equivalent width. Similar uncertainty in the damping constant also made the derived abundance uncertain. The quantitative results are shown in figures 6.4 and 6.5. If the abundance was to have a precision comparable to the gf values only lines less than 20mA or so would suffice. But only 5127A qualified, and its width was uncertain because of blending. Accordingly it was necessary to determine the microturbulence as well as the abundance. Anticipating the results below, a precision of 0.1 km s^{-1} and 60mA would correspond to about 0.03dex in the abundance.

The method used to determine the abundance (A) and microturbulence (ξ) was conventional, and consisted of varying the assumed microturbulence until the abundances required to reproduce the equivalent widths of the lines showed no gradient (in the best straight line sense) with respect to line strength. The mean abundance could then be found. But of course the abundance would not relate to a single lower level if lines from different excitations were used. It was felt though that the groups of levels within a single term were sufficiently close in energy for collisional processes to maintain LTE equilibria. That is, the term might be populated by non-LTE effects, but the relative populations would be given by the Boltzmann equation.

As shown by figure 6.5, uncertainty in the damping would also lead to errors in the abundance if stronger lines were used. In computing lines the results of the next chapter were anticipated, but the lines measured were nevertheless reviewed to see if damping would introduce errors. For this purpose the gradient of abundance with microturbulence and damping

was considered, the latter being varied by enhancing the value from the Unsold formula by a constant factor (E_6, see chapter 7). Results from calculations using the HSRA model are given in table 6.3. From these it was apparent that the stronger lines would be sensitive to errors in the damping, and that these errors would be passed on to the derived abundance. Moreover the abundances derived from the stronger lines were not particularly sensitive to microturbulence, and would not therefore determine the microturbulence more precisely. Accordingly the five strongest lines from the 0.00-0.12eV levels were excluded. The lines are indicated in tables 6.1 and 6.2 also.

Only the 8 weakest lines from the ground state term were used; together with the 6 lines from excited level. The two groups were however treated separately because of the difference in excitation, and because of the less precise gf values for the excited lines. Furthermore the 6609A line had only a very provisional gf value, and was given reduced weight. The 5127A line was excluded altogether from the abundance determination because of the uncertainty in its equivalent width, but is shown below as an illustration of the behaviour of a very weak line from the lower levels.

The results of the calculations are illustrated in figures 6.6 and 6.7 which show the variation of abundances with microturbulence for the two groups of lines at two disk positions. All of the curves intersect in a small area, corresponding to the microturbulence for that model and disk position. Two points are clear however: first, the microturbulent velocity is greater towards the limb than at disk centre; second, the vertical scatter of the curves is greater, indicating a greater scatter in the abundances. The first point is confirmed by the full results from all five models. These show that there is essentially no difference between the microturbulence derived from the ground state lines and from the lines of higher excitation. Furthermore the values, listed in table 6.4 for each disk position are, within the experimental error, independent of the model.

Table 6.5 gives the mean abundance and standard deviation at the derived values of microturbulence, and the values of individual lines are shown in figure 6.8, for the four disk positions and five models. (Here, as elsewhere, the abundance is defined by $A = \log (N_{Fe}/N_H) + 12$).) The results show certain common features: at disk centre there is very little scatter and the two groups of lines give much the same abundance. Towards the limb however there is a systematic difference, with the excited lines giving higher abundances. This is however difficult to interpret because the scatter of all the measurements also increases. In addition the mean value of the abundance may also change with disk position, and the amount and direction of the change depends on the model. This is seen more clearly in figure 6.9 which shows the abundance and associated error for each model, disk position, and the two groups of lines. The errors here are a measure of the maximum combined uncertainties in oscillator strength, microturbulence and equivalent widths.

The accuracy of these measurements reflects the precision of the oscillator strengths and equivalent widths. Assuming errors of 5 per cent in the gf values and 2 per cent in the equivalent widths at disk centre, the corresponding error in log A would be about 0.03. Abundances for all 5 models at disk centre show standard deviations smaller than this. Such consistency suggests:

a. that the oscillator strengths measured are indeed accurate to 5 per cent or less; and

b. that the simple LTE computation of the line profiles is valid for solar atmospheres and weak FeI lines.

It was shown that the consistency was not a spurious result of the many factors by deriving abundances in the same way using the gf values from May et al (1974). These are among the best of the arc measurements, but the derived abundance showed a standard deviation of almost 0.2 dex. This is attributed to errors in the oscillator strengths, and supports the conclusion at (a) above.

For the measurements away from disk centre however the position

is less satisfactory. All the models show standard deviations on the abundance that increase towards the limb. A large part of this is undoubtedly due to errors in the equivalent widths, eg since limb spectra are subject to scattered light. However there is also the possibility of inadequacies in the model atmospheres, which would become more apparent as the lines at the limb probe higher, and less well-determined, levels in the photosphere: figure 6.3(e,f) shows how the populations of the absorbing states from the different models diverge at higher levels.

6.4 Significance of the microturbulence measurement

The measured equivalent widths and subsequent analysis confirmed that an additional broadening is needed to reproduce the observed line strengths with a unique abundance. But the concept of a turbulent velocity as this broadening agent has been questioned. In particular Worrall (1972, 1973) and Worrall and Wilson (1972, 1973) have questioned the existence of velocity fields with the required scale and magnitude; and have suggested that departures from LTE, magnetic enhancement, hyperfine structure and erroneous temperature distributions account for the observed lines. Holweger (1973) finds however that the non-LTE effects are not a function of line strength. Lites (1973) derived a finite microturbulence from detailed non-LTE computations of FeI lines. And of course FeI has no hyperfine structure.

On the other hand it is quite likely that many of the reported values of microturbulent velocities in the sun and in other stars are not real velocity fields in the atmospheres. This is partly due to the difficulties of measuring the effects. Gray and Evans (1973) suggest that the only reliable measurements come from line profiles; and Gray (1973) has examined the effects of rotation, micro- and macroturbulence in this way. There is moreover little doubt that the very high velocities found for some stars are the result of forcing lines with systematic errors in their oscillator strengths to produce a unique abundance. This may explain the very high values found in surveys by Glebocki (1973) and Andersen (1973) which Hearn (1974) showed were unlikely given the energy required and the amount generated by convection. For example, the curve of growth analysis of FeI lines by Chaffee (1970) gave 3.5 km s^{-1} for the solar type star CVN. But Hearnshaw (1974) used higher dispersion spectra and revised data for the FeI lines to find 1.3 for the same star, which agrees reasonably well with the value found - 1.1 ± 0.3 - from the oscillator strengths and lines measured for this work.

There is however direct and indirect evidence for the hydrodynamic nature of the broadening of weak lines. In particular, the correlation between the width of weak lines in Cepheids and supergiants with the radial velocity (Paradijs, 1972) suggests that similar convective motions in normal stars could account for the microturbulence.

The measurements here, based on accurate oscillator strengths, are also evidence for some broadening mechanism. The value at disk centre, 0.8 km s^{-1}, is not inconsistent with many other measures: eg Huber and Tubbs (1973) used their own gf values to derive 0.5, though the damping constants used were too high. Cowley and Toney (1973) used oscillator strengths from Wolnik et al (1970) and Bridges and Wiese (1970) to find 1.1; Foy (1972) and Yamashita (1972) used similar compilations of gf values to derive 0.5 and 1.0 respectively. These two authors also used the same equivalent width data and the difference in the results is due to the very great scatter in their curves of growth. This arises in part from their damping constants. Erroneous damping also accounts for the very high value (3.4 km s^{-1}) given by Rogerson (1969). Other references are given in table 6.6.

Table 6.4 shows the increase towards the limb in the derived velocities. Conventionally this is interpreted as a microturbulence with horizontal (tangential) and vertical (radial) components so that:

$$\xi^2(\mu) = (\xi_v^2 - \xi_h^2)\mu^2 + \xi_h^2 \qquad (6.5)$$

Recent measurements of microturbulence in the solar atmosphere have tended to concentrate on this model, and to propose also a depth dependent microturbulence. The latter might explain the results here, which do not fit the form of equation (6.5). Broadly speaking the complex models are constructed from the behaviour from centre to limb of lines formed at different depths in the atmosphere (eg Gonczi and Roddier, 1971; Holweger, 1967; Dunn and Olson, 1971; Altrock and Cannon, 1972, 1973; Gail and Sedlmayr, 1974; Stenholm, 1977). Generally the results show that the microturbulence increases at high levels, to match the established values in the chromosphere (eg Canfield, 1971; Fosbury, 1974); and also rises again for optical depths greater than about 0.1.

These results do not however prove that there is a micro-turbulence, and the effects of assuming a spectrum of velocities and scale lengths has been investigated (eg Edmonds and Webb, 1972; Hundt, 1973; de Jager, 1974; Frisch, 1975). The more complex, and perhaps more realistic, velocity fields modify the behaviour predicted for solar lines. But these predictions rest on the elimination of other uncertainties and there is in particular a need to use only the most precise oscillator strengths, as in this work.

Finally it should be said that the work of Wilson and Guidry (1974) suggested that temperature inhomogeneities could explain the centre-limb behaviour of the Na D lines without microturbulence. The proposed model had two streams with a temperature difference of some 500K. But for the weak FeI lines used here this would not suffice because the lines of different strengths would be similarly effected. This was confirmed by calculations using a three stream model developed from the Elste 10 (David, 1961; Elste, 1967). Following the same analysis as above, a microturbulent velocity was still needed to make the abundance independent of line strength.

6.5 The solar iron abundance

In so far as damping constants are the aim of these measurements, the absolute value of the iron abundance is not important. The few lines measured; the simple LTE analysis; and the use of lines from a very small range of excitations reduce the significance of the results. Furthermore the abundances vary with disk position and from model to model. In view of the greater precision of the disk centre measurements however these are taken from table 6.2 to define the iron abundance for the five atmospheres (table 6.7).

These values depend on the microturbulence but this has been determined accurately. And the form of the microturbulence has little effect. The anisotropic depth-dependent model of Lites (1973) was used in the HSRA NLTE model, for which it was derived, to determine the depth variation and scaled to minimise the error on the abundance. The results in table 6.8 show there was no significant difference from the previous results.

The differences between the models are due principally to the different degrees of ionisation (see fig 6.3 (e,f)) and hence to the temperature and pressure structures (fig 6.3 (a,b,c)). It should be noted however that certain abundances must be assumed in computing a model; and that the iron atoms are themselves important contributors to the electron pressure in the solar photosphere. Ideally therefore the model should be revised to take account of, and to reproduce, revised abundances (as previously was the HOLWEGER model used here (Holweger and Mueller, 1974)).

In contrast the difference of 0.13 between the HSRA and HSRA NLTE models is due almost wholly to the non-LTE ionisation and excitation, as the atmospheres are otherwise very similar. It should not be assumed however that the same correction for non-LTE effects can or should be applied to the results from other models. The HSRA model was derived solely from observations of the solar continuum; and differs in several important

respects from the HOLWEGER model based on the centre-limb variation of spectral lines. Indeed it may not be a coincidence that the abundances from the HOLWEGER AND HSRA NLTE models are consistent: many of the lines used by Holweger (1967) to construct the model were of FeI, and the atmosphere may therefore have been constrained to simulate non-LTE conditions for lines in the solar spectrum.

Notwithstanding the caveats of the few lines and LTE analysis, the results contribute usefully to the still vexed question of the photospheric abundance of iron. Reviews of determinations for the photosphere, chromosphere and corona have been undertaken by Hauge and Engvold (1970); Withbroe (1971); Cameron (1973); Blackwell (1974) and Engvold and Hauge (1974). As the photosphere values before about 1969 relied on inaccurate gf values (see Chapter 5) early results are of historical interest only. But even the more recently reported values (table 6.9) cover a wide range, even for a single model atmosphere. These differences arise in part from the different oscillator strengths used: for example, Yamashita (1972) derived a value of 7.26 with the gf scale of Wolnik et al (1970, 1971) but 7.54 if the measurements of Bridges and Wiese were taken.

A further source of uncertainty are the damping coefficients, since many of the lines in abundance measurements are not so weak that they are independent of damping. As there are no experimental measurements of the damping constants it is usual to use theoretical values from the theory of Unsold (1955), increased by some factor to account for the believed enhancement (see section 7.4 below). Thus Garz et al (1969) used an enhancement factor of 2.5 and found an abundance of 7.60; Foy (1972) has 4.0 and 7.28 respectively; Rogerson (1969) 5 and 6.85. There were also of course different gf values, but this should be compared with the calculations of Blackwell et al (1972) which showed that a typical FeI line (4000A, 100mA, 3eV) and a factor 3 uncertainty in the damping gave rise to an uncertainty of 0.25 dex in the abundance. Similarly Lites (1973) and Athay and Lites (1972) derived an abundance of 7.2 from the broadening theory of Brueckner (1971) but

remarked that their observations could be equally interpreted with reduced damping constants and an abundance of 7.5 to 7.6.

Measurements independent of the line shape parameters are rare since they require very weak lines for which there are few oscillator strengths. Huber and Tubbs (1973) used the 5127A FeI line to derive abundances for the Holweger (1967), HSRA and HSRA NLTE models of 7.61, 7.48 and 7.59 respectively. These are close to the values found from the Oxford oscillator strengths since the two sets of gf values are very close. But as noted above, the 5127A line is contaminated by C_2 blends. This problem at least was avoided by Biemont and Grevesse (1975) who examined weak infra-red lines. Oscillator strengths were taken from Kurucz (1974b) and the scatter of these semi-empirical values reduced by using a total of 40 lines. The result was an abundance of 7.57 ± 0.11 for the HSRA model and a microturbulence of 0.5 km s^{-1}. These two measurements are therefore in close agreement with the provisional results obtained here. On the whole, the evidence from the use of weak FeI lines and precise oscillator strengths and observations is a high value (log A 7.5 $\sim$ 7.7) for the photospheric iron abundance. Greater precision in the absolute photospheric abundance must however await improvements in the model atmospheres as there is at present no firm evidence by which to prefer one over others. Moreover there is scope for developing inhomogeneous models (eg Turon, 1975) to take account of the obvious inhomogeneities in the photosphere; and for more non-LTE analyses. These improvements may be assisted by the use of precise oscillator strengths, eg from different excitation potentials so as to test the temperature distribution on the model. But at present abundances must be considered as precisely determined for a given model, rather than for the atmosphere itself.

Table 6.1

Solar equivalent width sources

1. Moore et al. (1966)
2. this author: from "Photometric Atlas of the Solar Spectrum", Delbouille et al. (1973)
3. this author: from "Preliminary Kitt Peak Atlas", Brault & Testerman (1972)
4. this author: from Oxford observations at the Gornergrat out-station
5. Holweger (1967)
6. Smith (1974)
7. Huber & Tubbs (1972)
8. Muller & Mutschlechner (1964)
9. Withbroe (1968)

In the tables below, the first two columns give the excitation (eV) and wavelength (A) of the line. The remaining columns show the measured equivalent width in mA. before correction for blending, with the source indicated by reference to the list above.

Table 6.1(a)

Equivalent width measurements for disk centre: mA.

X	λ	1	2	3	4	5	6	7	8	9
0.00	4375.9	152	157	163	153	...	...	...	153	...
	4216.2	130	...	130	132	...	...	...	...	...
	4347.2	41	47	48	46	...	...	...	...	...
0.05	4427.3	147	172	173	173	...	180	...	171	...
	4389.3	67	73	73	72	...	75	...	...	...
	5127.7	20	20.4	19.4	20.6	...	...	19.9	...	...
0.09	4461.7	116	139	137	134	...	133	...	137	...
	5247.1	59	65	64	65	68	...	66	...	...
	4445.5	30	39.5	38.6	39	37	...	...	...	...
0.11	5225.5	68	72.5	70	70.5	71	...	73	...	...
	4232.7	58	...	57.5	56	...	...	...	...	...
0.12	4489.7	81	96.5	94.5	95	89	...	...	...	...
	5250.2	62	66.5	64.5	66	70	...	67	...	...
0.86	4939.7	96	104	103	103	...	...	...	...	...
	6280.6	52	63.1	63.8	63.9	...	...	...	...	...
	5956.7	60	50.8	50.2	53	...	52	...	...	54.3
0.95	6498.9	43	44.2	45.3	43.5	...	...	...	...	43.7
0.99	6574.3	22	27.2	25.8	27.2	24	...	...	...	24.1
	6609.7	5	6.2	6.0	5.6	...	...	...	...	...

Table 6.1(b)

Equivalent width measurements for limb positions μ = 0.5, 0.3, 0.2

		0.5			0.3					0.2
χ	λ	4	8	9	4	8	5	6	9	3
0.00	4375.9	160	158	...	160	160	...	185	...	171
	4216.2	145	139	...	151	141	...	...	...	140
	4347.2	56	...	...	61	...	...	...	...	63
0.05	4427.3	186	179	...	186	180	...	180	...	185
	4389.3	80	...	...	85	...	...	91	...	91
	5127.7	26.5	...	...	29.8	...	...	...	...	34.6
0.09	4461.7	145	140	...	151	140	...	167	...	156
	5247.1	73.5	...	...	78.5	...	76	...	...	80.5
	4445.5	48	...	...	55.5	...	51	...	...	61
0.11	5225.5	78	...	...	84	...	83	...	...	89.5
	4232.7	68	...	...	72	...	...	...	...	76.5
0.12	4489.7	107.5	...	...	111.5	...	102	...	...	114.5
	5250.2	75	...	...	80.5	...	83	...	...	83.5
0.86	4939.7	109	...	...	114	...	...	...	...	115
	6280.6	67.8	...	...	76.6	...	...	...	...	76
	5956.7	59.1	...	60.1	63.7	...	...	61	66.6	64.6
0.95	6498.9	50.6	...	56.2	55.1	...	...	...	56.5	58.4
0.99	6574.3	34	...	29.6	37.8	...	35	...	37.8	39.6
	6609.7	8.8	...	...	9.7	...	...	...	...	9.8

Table 6.2
Adopted equivalent widths and uncertainties.

		equivalent widths and errors (mA)								W (μ)/W(1.0)		
χ	λ	μ=1.0		μ=0.5		μ=0.3		μ=0.2				
* 0.00	4375.9	159.0	4.0	160.0	5.0	160.0	5.0	171.0	6.0	1.006	1.006	1.075
*	4216.2	130.7	1.0	142.0	3.0	151.0	3.0	140.0	4.0	1.086	1.155	1.071
	4347.2	41.1	2.5	47.6	3.0	51.4	3.0	53.0	3.5	1.158	1.251	1.290
* 0.05	4427.3	167.9	1.0	179.0	3.0	176.0	3.0	176.7	3.0	1.066	1.048	1.052
	4389.3	72.5	1.0	80.0	2.0	85.0	2.0	91.0	2.0	1.103	1.172	1.255
	5127.7	16.4	2.0	24.1	2.5	26.7	3.0	28.3	3.0	1.470	1.628	1.726
* 0.09	4461.7	136.5	2.2	145.0	2.5	151.0	2.5	156.0	2.0	1.062	1.106	1.143
	5247.1	64.8	0.7	73.5	1.5	78.5	1.5	80.5	1.0	1.134	1.211	1.242
	4445.5	39.1	0.8	48.0	1.5	55.5	1.5	61.0	1.0	1.228	1.419	1.560
0.11	5225.5	71.2	1.3	78.0	2.0	84.0	2.0	89.5	1.5	1.096	1.180	1.257
	4232.7	57.1	0.5	68.0	1.0	72.0	1.0	76.5	1.0	1.191	1.261	1.340
* 0.12	4489.7	95.0	1.3	107.5	2.0	111.5	2.0	114.5	1.5	1.132	1.174	1.205
	5250.2	66.0	1.2	75.0	2.0	80.5	2.0	83.5	2.0	1.136	1.220	1.265
0.86	4939.7	102.3	2.0	109.0	3.0	114.0	3.0	115.0	3.0	1.065	1.114	1.124
	6280.6	63.6	1.0	67.8	2.0	76.6	2.0	76.0	2.0	1.066	1.204	1.195
	5956.7	51.1	1.5	59.1	2.0	63.7	2.0	64.6	1.5	1.157	1.247	1.264
0.95	6498.9	44.9	1.0	50.6	2.0	55.1	2.0	58.4	2.0	1.127	1.227	1.301
0.99	6574.3	25.8	1.5	34.0	2.0	37.8	2.0	39.6	1.5	1.318	1.465	1.535
	6609.7	5.6	0.6	8.8	1.0	9.7	1.0	9.8	1.0	1.571	1.732	1.750

* lines not used in the abundance determination (see text)

Table 6.3

The gradients of the logarithmic iron abundance with respect to microturbulence, equivalent width, and damping as calculated for the H.S.R.A. at disk centre. Assumed values are E_6 = 1.25 and ξ = 0.8 km/sec.

χ eV	λ A	W_λ mA	$\frac{dA}{d\xi}$	$\frac{dA}{dW_\lambda}$	$\frac{dA}{dE_6}$
0.00	4375.9	159	.14	.010	.37
	4216.2	131	.33	.013	.33
	4347.2	41	.19	.023	.01
0.05	4427.3	168	.11	.007	.36
	4389.3	73	.64	.030	.07
	5127.7	16	.04	.035	.00
0.09	4461.7	137	.27	.014	.34
	5247.1	65	.43	.025	.03
	4445.5	39	.16	.022	.01
0.11	5225.5	71	.52	.025	.04
	4232.7	57	.44	.028	.03
0.12	4489.7	95	.63	.024	.17
	5250.2	66	.45	.025	.03
0.86	4939.7	102	.67	.020	.16
	6280.6	64	.33	.021	.02
	5956.7	51	.22	.020	.02
0.95	6498.9	45	.16	.019	.01
0.99	6574.3	26	.06	.023	.00
	6609.9	6	.01	.084	.00

Table 6.4

microturbulent velocities (km s^{-1}) from combined results of 0.00-0.12 and 0.86-0.99eV lines.

μ	HSRA	HSRA NLTE	HOLWEGER	ELSTE10	KURUCZ
1.0	0.8	0.9	0.9	0.8	0.8
0.5	1.1	1.2	1.2	1.1	1.1
0.3	1.3	1.4	1.4	1.4	1.4
0.2	1.5	1.7	1.7	1.7	1.8

Table 6.5

Abundance and standard deviation for the 5 models, 4 disk positions, and the two groups of FeI lines.

	μ									
lines from 0.00-0.12eV	1.0	7.509	.018	7.638	.020	7.656	.018	7.481	.020	7.433	.021
	0.5	7.502	.044	7.654	.044	7.658	.043	7.465	.043	7.419	.046
	0.3	7.487	.047	7.646	.060	7.665	.064	7.432	.056	7.420	.074
	0.2	7.415	.065	7.615	.070	7.605	.070	7.350	.069	7.369	.079
lines from 0.86-0.99eV	1.0	7.522	.023	7.663	.022	7.635	.027	7.485	.027	7.428	.023
	0.5	7.516	.041	7.693	.028	7.685	.027	7.484	.040	7.497	.021
	0.3	7.517	.022	7.712	.026	7.727	.039	7.467	.017	7.516	.066
	0.2	7.518	.023	7.782	.030	7.841	.054	7.493	.022	7.663	.093
combined values	1.0	7.524	.031	7.654	.029	7.664	.029	7.492	.030	7.441	.026
	0.5	7.513	.044	7.669	.042	7.668	.039	7.499	.044	7.456	.044
	0.3	7.514	.052	7.705	.064	7.722	.069	7.494	.064	7.488	.090
	0.2	7.482	.063	7.670	.075	7.724	.080	7.431	.070	7.501	.104

Table 6.6

Examples of measurements of the solar microturbulence.

author	(ξ)	notes
Wright (1944)	0.9	FeI, TiI
Waddell (1958)	1.8 v	FeI, VI, TiI
	3.0 h	
Cowley & Cowley (1964)	1.4	general curve of growth
Elste (1967)	1.0	FeI
Holweger (1967)	2.3	for τ=1.0, μ=1.0
	3.0	μ=0.3
Athay & Canfield (1969)	1.0 v	for τ=1.0
	1.6 h	
Garz et al (1969)	1.0	for τ=1.0 from FeI
Rogerson (1969)	3.4	FeI
Baschek et al (1970)	0.7	FeII
Nissen (1970)	1.0	
Gurtovenko & Troyan (1971)	1.3	for τ=0.8 from FeI
Ross & Aller (1972)	0.	AgI
Foy (1972)	0.5	FeI
	0.65	FeII
Yamashita (1972)	1.0	FeI
Cowley & Toney (1973)	1.1	FeI
Grevesse & Sauval (1973)	0.5	molecular lines
Huber & Tubbs (1973)	0.5	FeI
Kuli-Zade & Guseinov (1973)	0.7	FeI
Lites (1973)	1.0 v	for τ=0.1 from FeI
	2.2 h	.. ..
Ross (1973)	0.0	for FeI abundance 7.55
	0.8	7.35
Holweger & Muller (1974)	1.6	for τ=1.0
Foy (1975)	0.5	TiI,II
Stenholm (1977)	2.2	for τ=1.0 from FeI,CaI,TiI

h - horizontal component of ξ
v - vertical component of ξ

Table 6.7

Adopted values for the abundance of FeI in the 5 model solar atmospheres.

HSRA	7.52
HSRA NLTE	7.65
HOLWEGER	7.66
ELSTE10	7.49
KURUCZ	7.44

Table 6.8

Abundances and standard deviations determined from the HSRA NLTE model with (i) depth-independent microturbulence; (ii) scaled velocity distribution of Lites (1973).

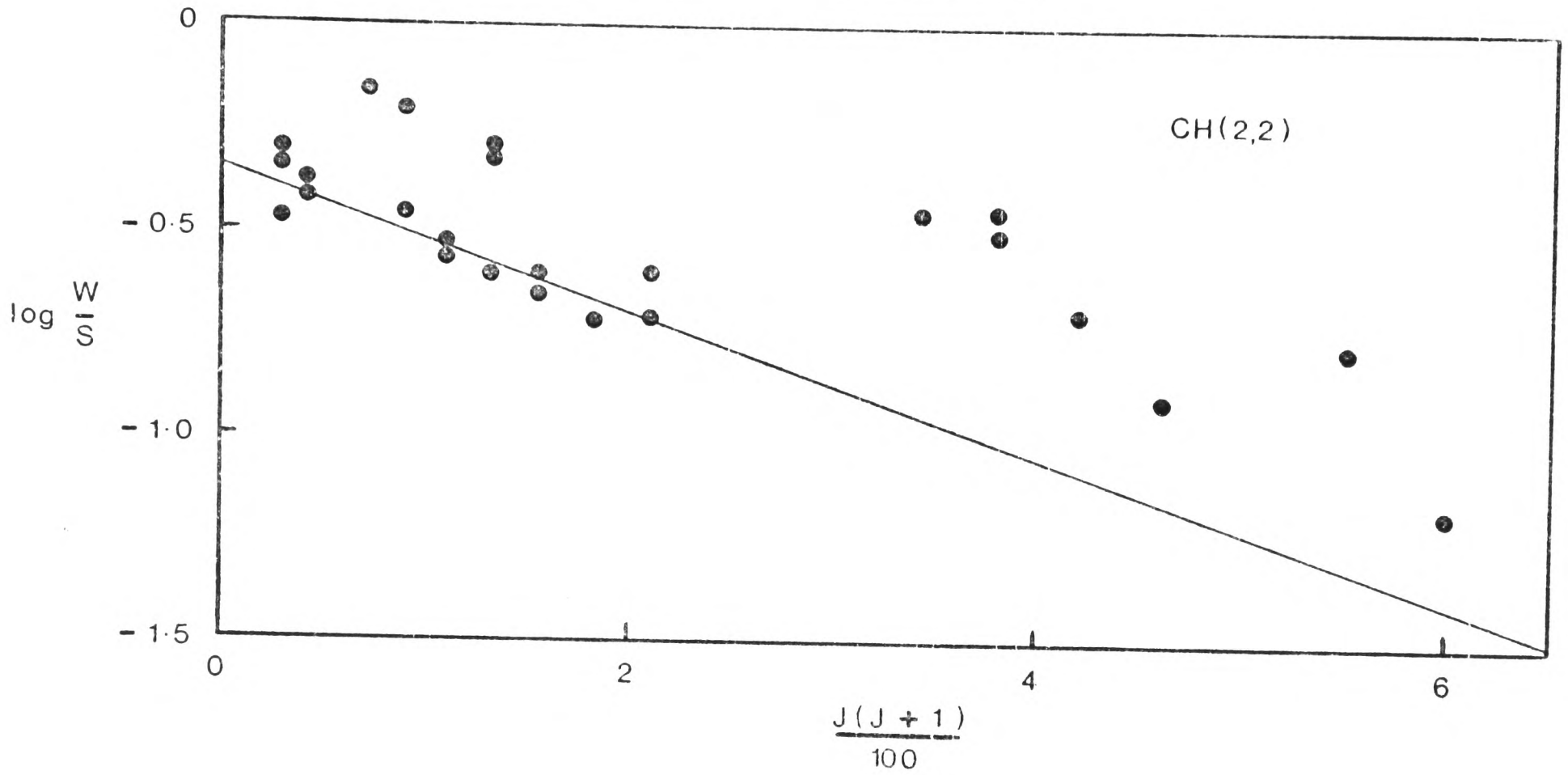
	μ	(i) A_{Fe} & s.d.	(ii)	mean difference (a)-(b)
0.00-0.12 eV	1.0	7.638 .020	7.640 .020	
lines	0.5	7.654 .044	7.667 .045	-0.004
	0.3	7.646 .060	7.645 .057	
	0.2	7.615 .070	7.617 .085	
0.86-0.99 eV	1.0	7.663 .022	7.671 .022	
lines	0.5	7.693 .028	7.731 .026	
	0.3	7.712 .026	7.729 .036	-0.025
	0.2	7.782 .030	7.818 .042	

Table 6.9

Measurements of the solar iron abundance.

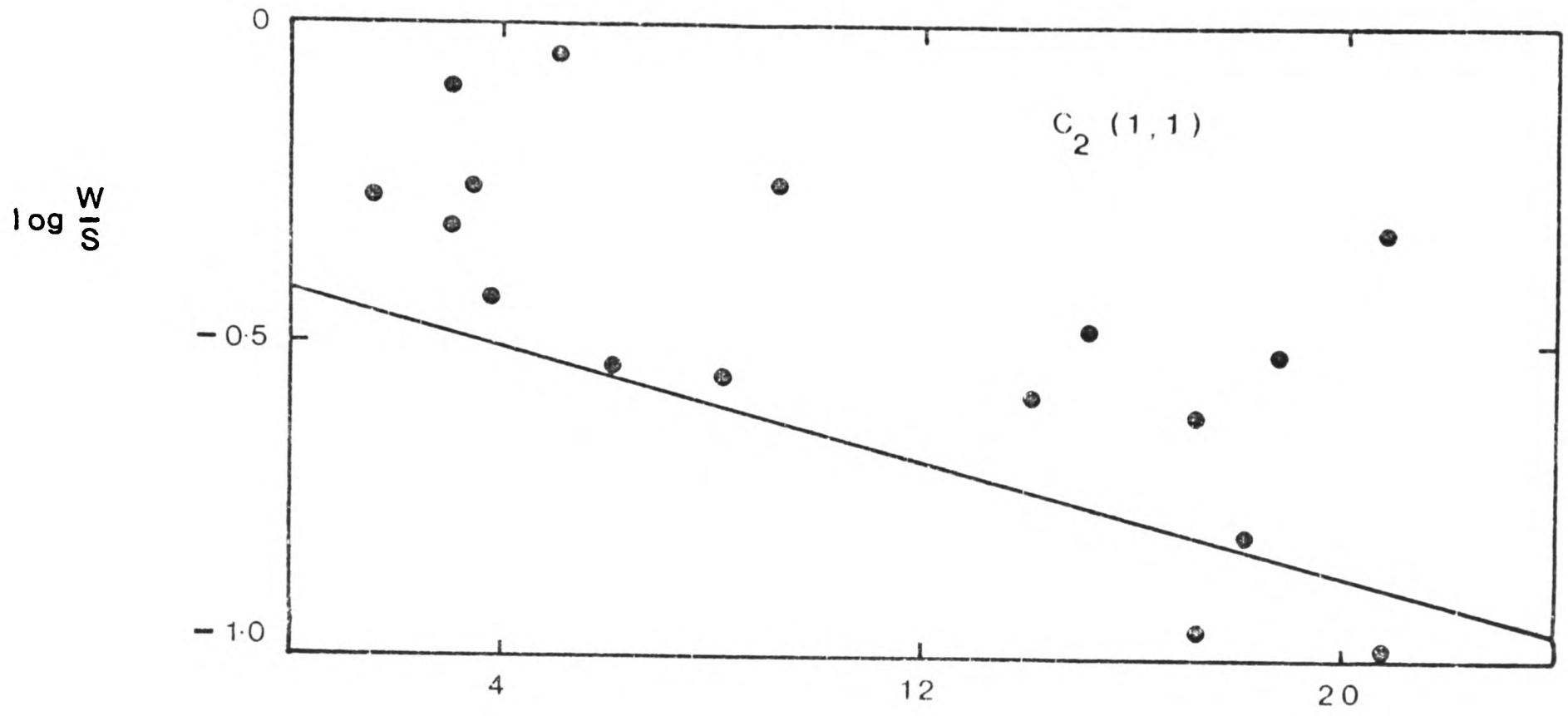
author	abundance	notes
Grevesse & Swings (1969)	7.5	forbidden FeII
Garz et al (1969)	7.60	
Ross (1969)	6.9 - 7.2	
Baschek et al (1970)	7.63	
Cowley (1970)	7.00	
Richter & Wulff (1970)	7.55	
Tanaka (1971)	7.7	chromosphere
Fort et al (1972)	7.88	corona
Foy (1972)	7.28	
Yamashita (1972)	7.37	
Huber & Parkinson (1972)	7.4	
Fichtel et al (1972)	7.1	solar particles
Huber & Tubbs (1973)	7.64	
Lites (1973)	7.2	
Smith & Whaling (1973)	7.4	
Ross (1973)	7.35-7.55	
May et al (1974)	7.52	
Biemont & Grevesse (1975)	7.57	

Figure 6.1



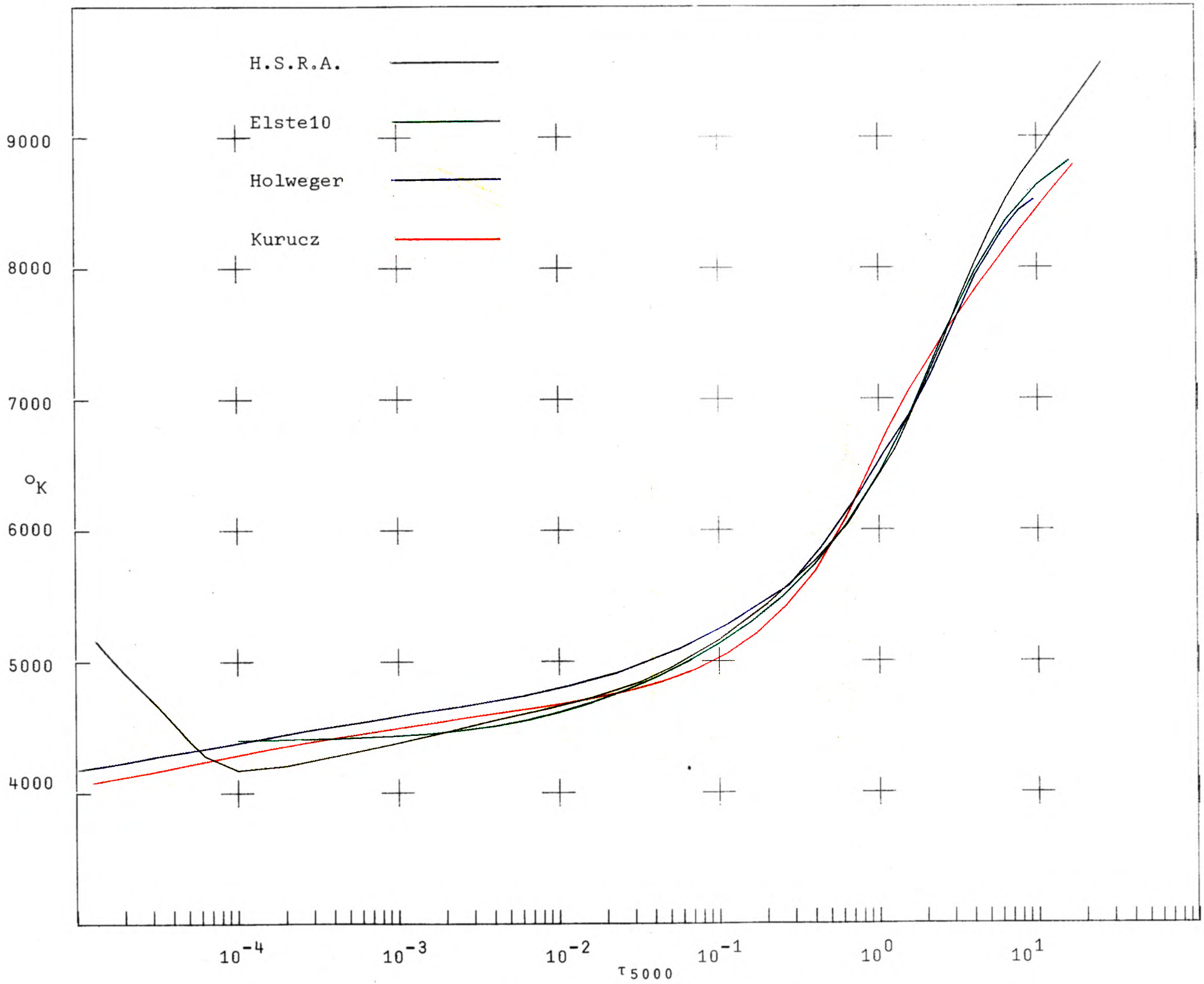
The ratio of observed solar equivalent width to line strength is plotted against excitation potential for the (2,2) band of the CH molecule. The line drawn through the data has the theoretically predicted gradient.

Figure 6.2



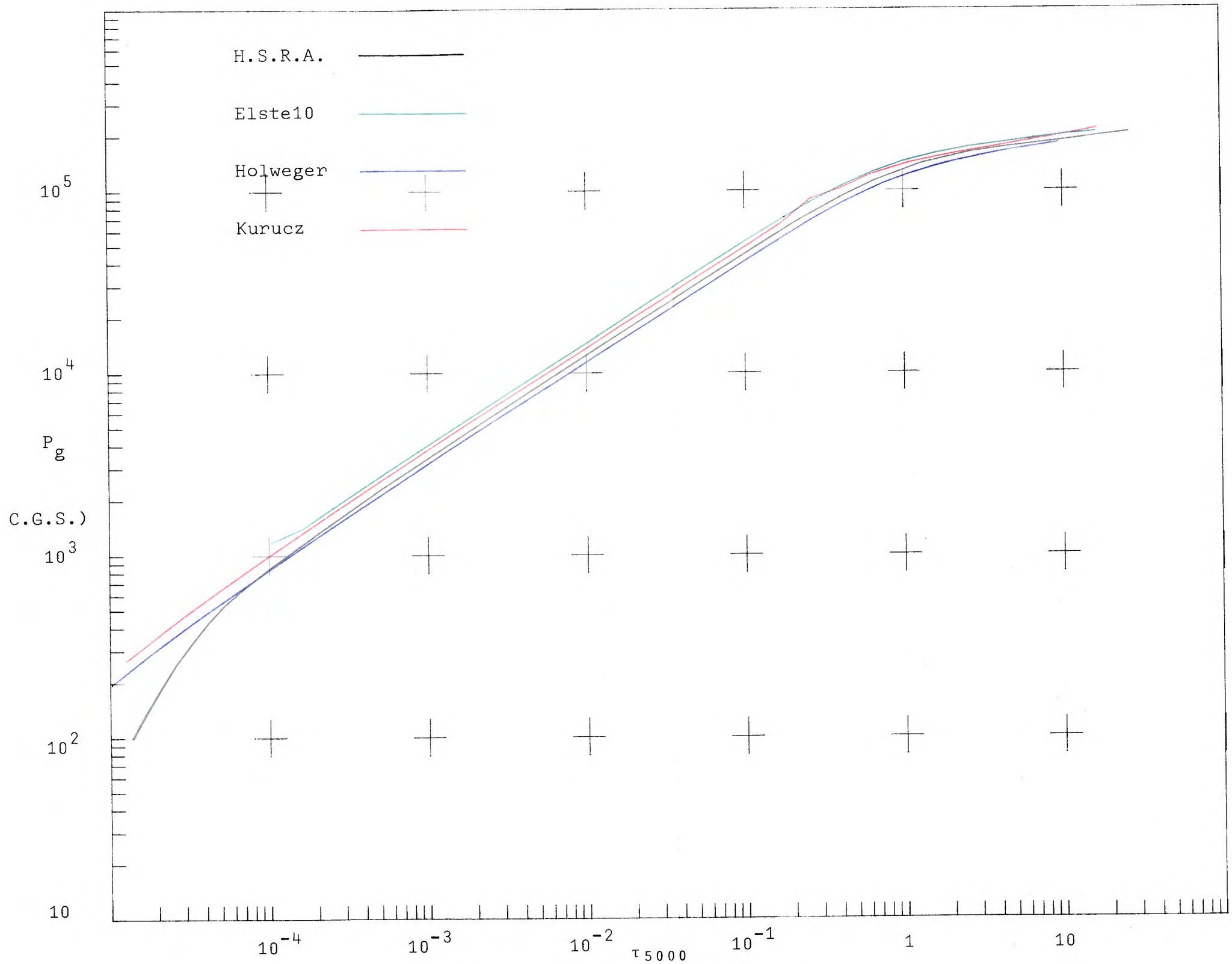
The ratio of observed solar equivalent width to line strength is plotted against excitation potential for the (1,1) band of the C_2 molecule. The line drawn through the data has the theoretically predicted gradient.

Figure 6.3(a)



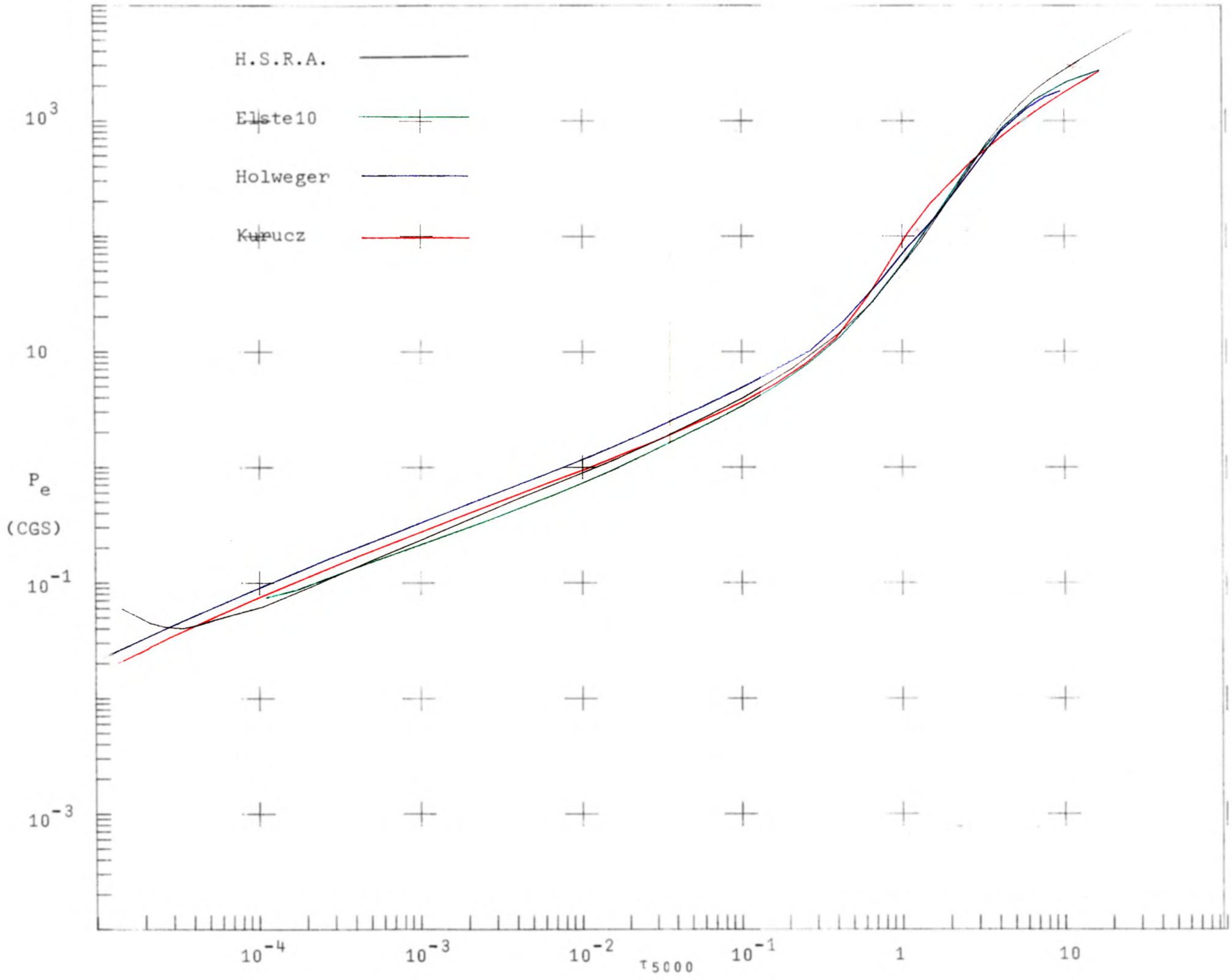
The variation of temperature with optical depth for the four solar model atmospheres.

Figure 6.3(b)



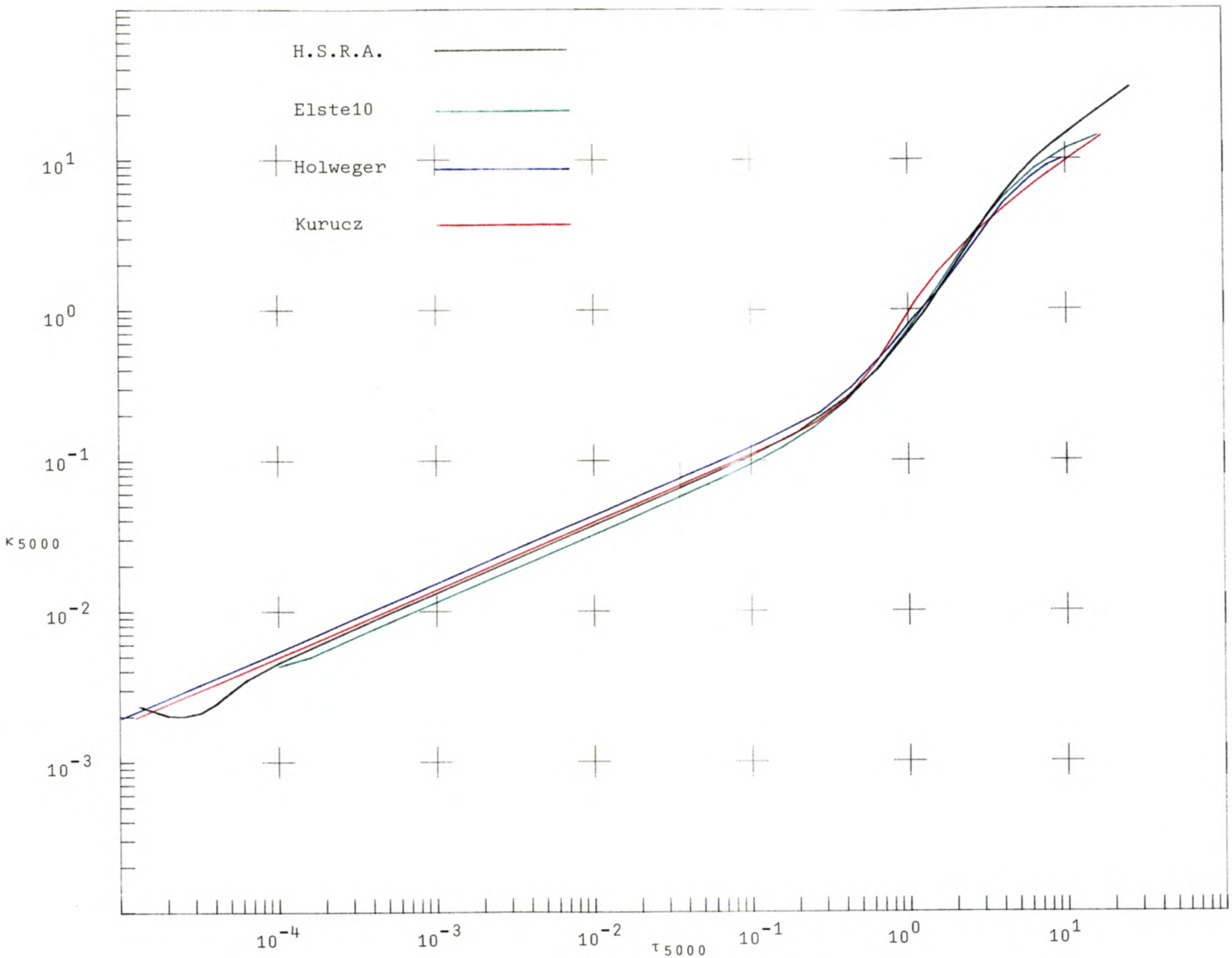
The variation of gas pressure with optical depth
in the four model atmospheres.

Figure 6.3(c)



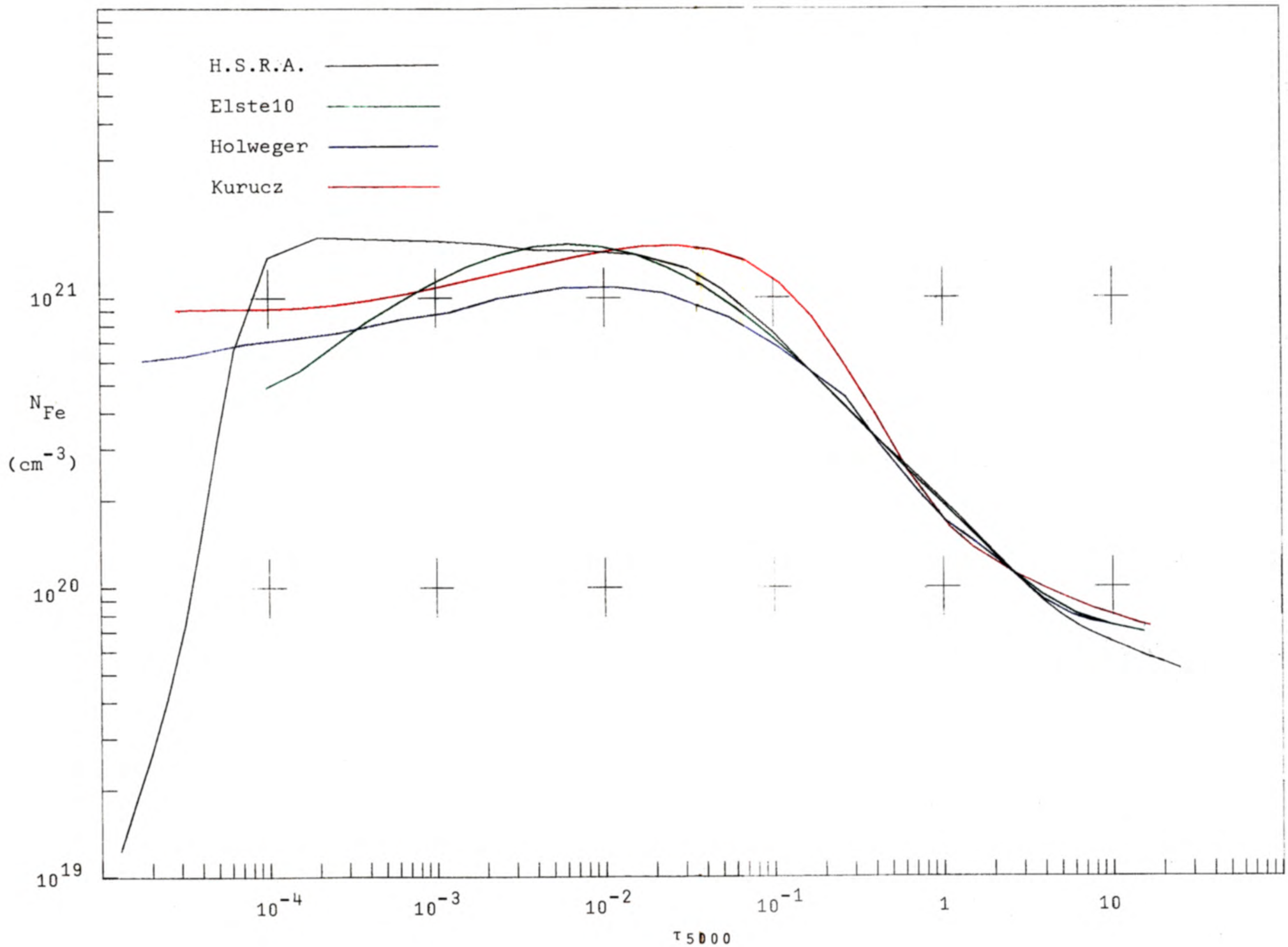
The variation of electron pressure with optical depth
in the four model atmospheres.

Figure 6.3(d)



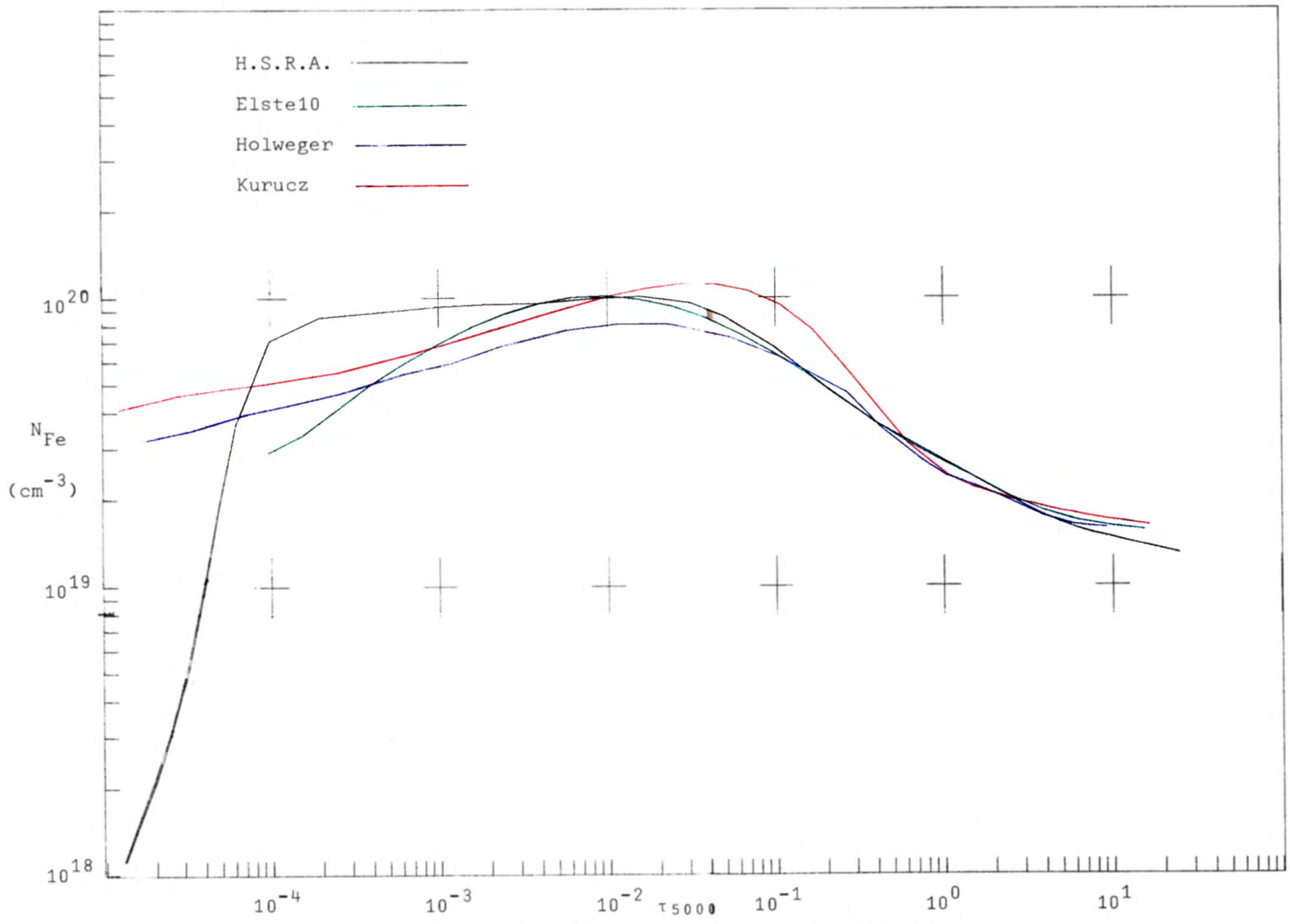
The variation of continuous opacity with optical depth at the tsandard wavelength, for the four atmospheres.

Figure 6.3(f)



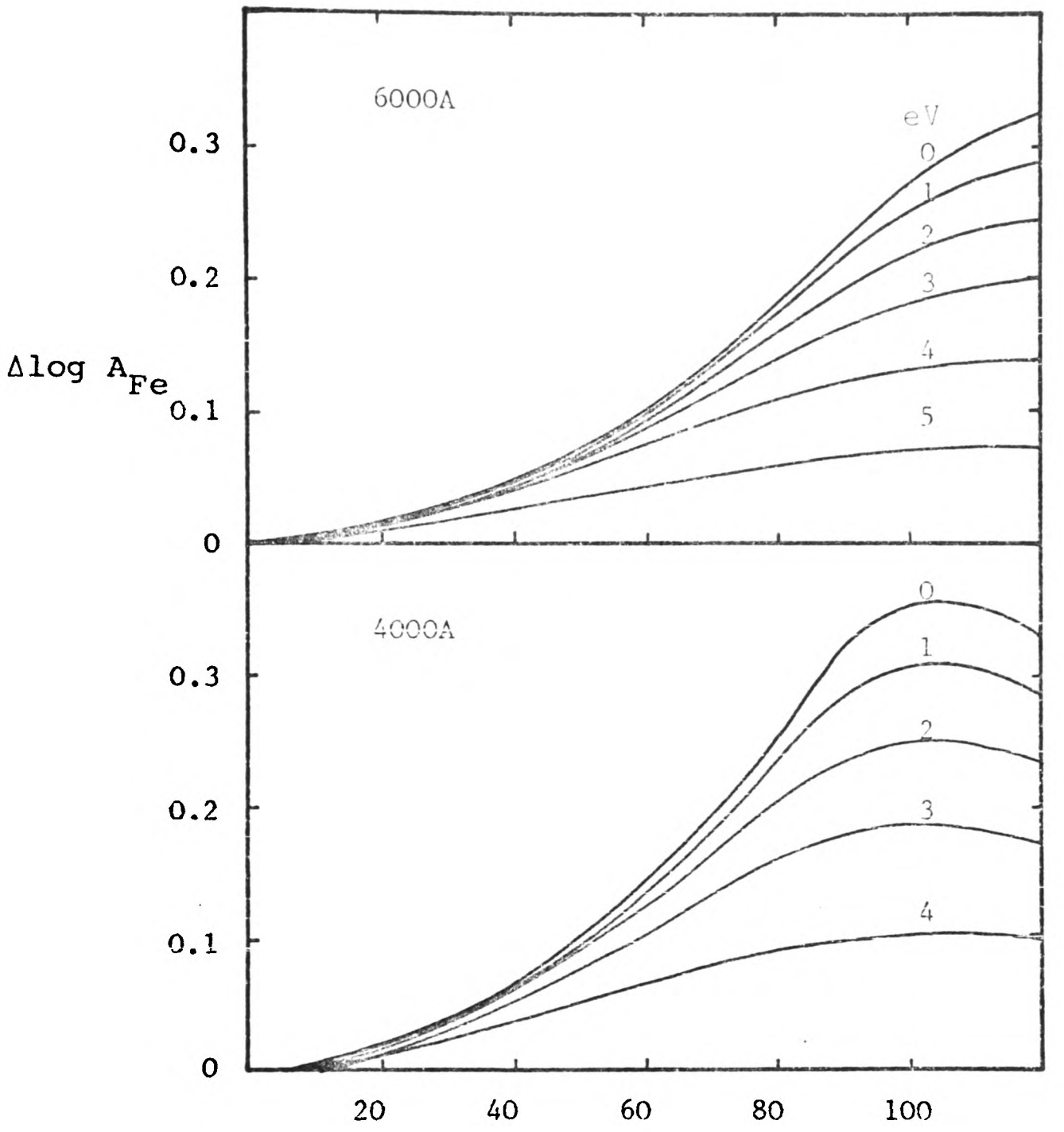
The variation with standard optical depth of the number density N_{Fe} for a line of excitation 0.0 eV.

Figure 6.3(f)



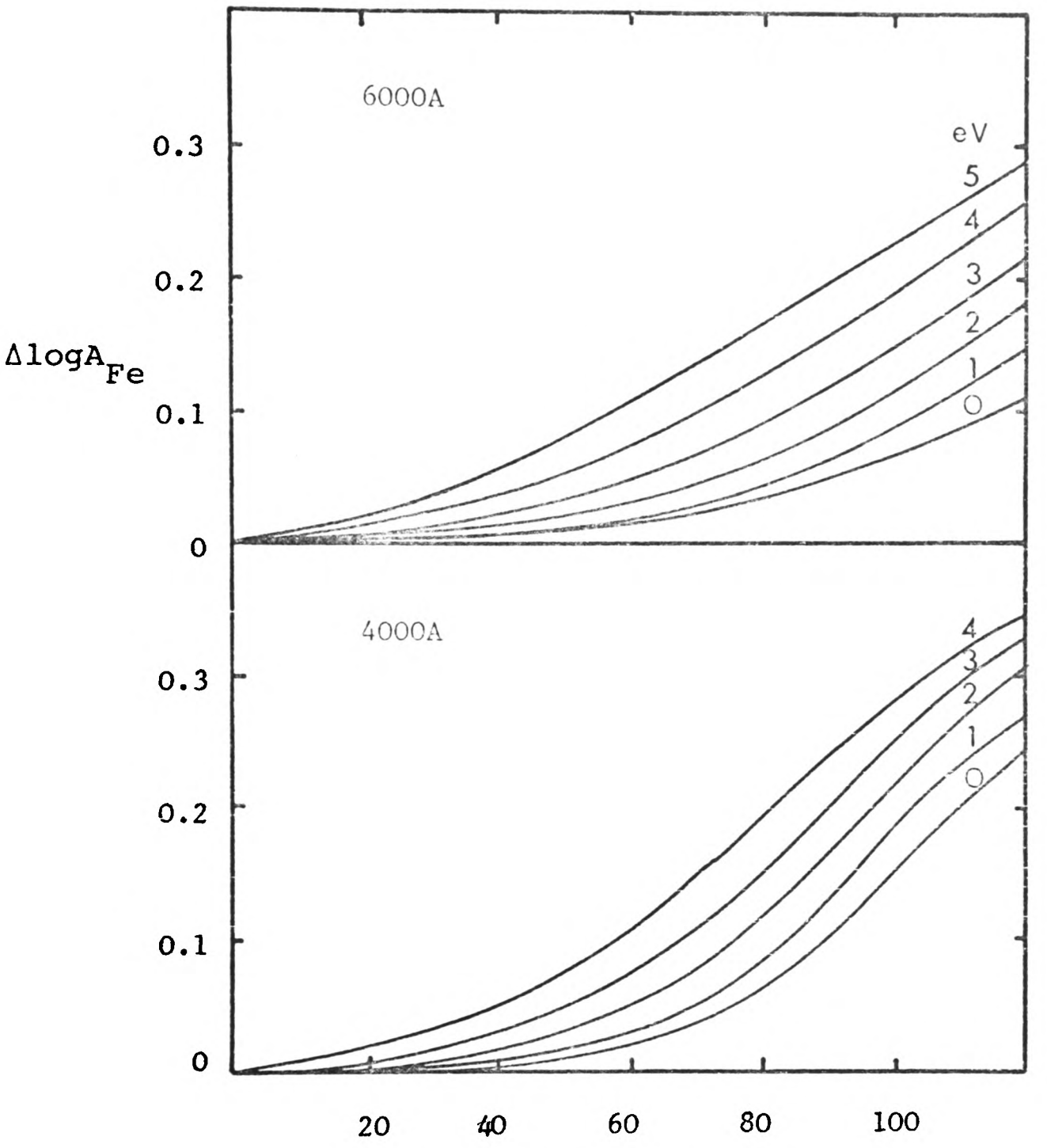
The variation with standard optical depth of the number density N_{Fe} for a line of excitation 1.0 eV.

Figure 6.4



Uncertainty in the abundance derived from Solar FeI lines at 4000A & 6000A due to uncertainty in the microturbulence: $1.3 < \xi < 1.9$ km s^{-1}.

Figure 6.5



Uncertainty in the abundance derived from Solar FeI lines at 4000A & 6000A due to the uncertainty in damping: $0 < \log E_6 < 0.5$

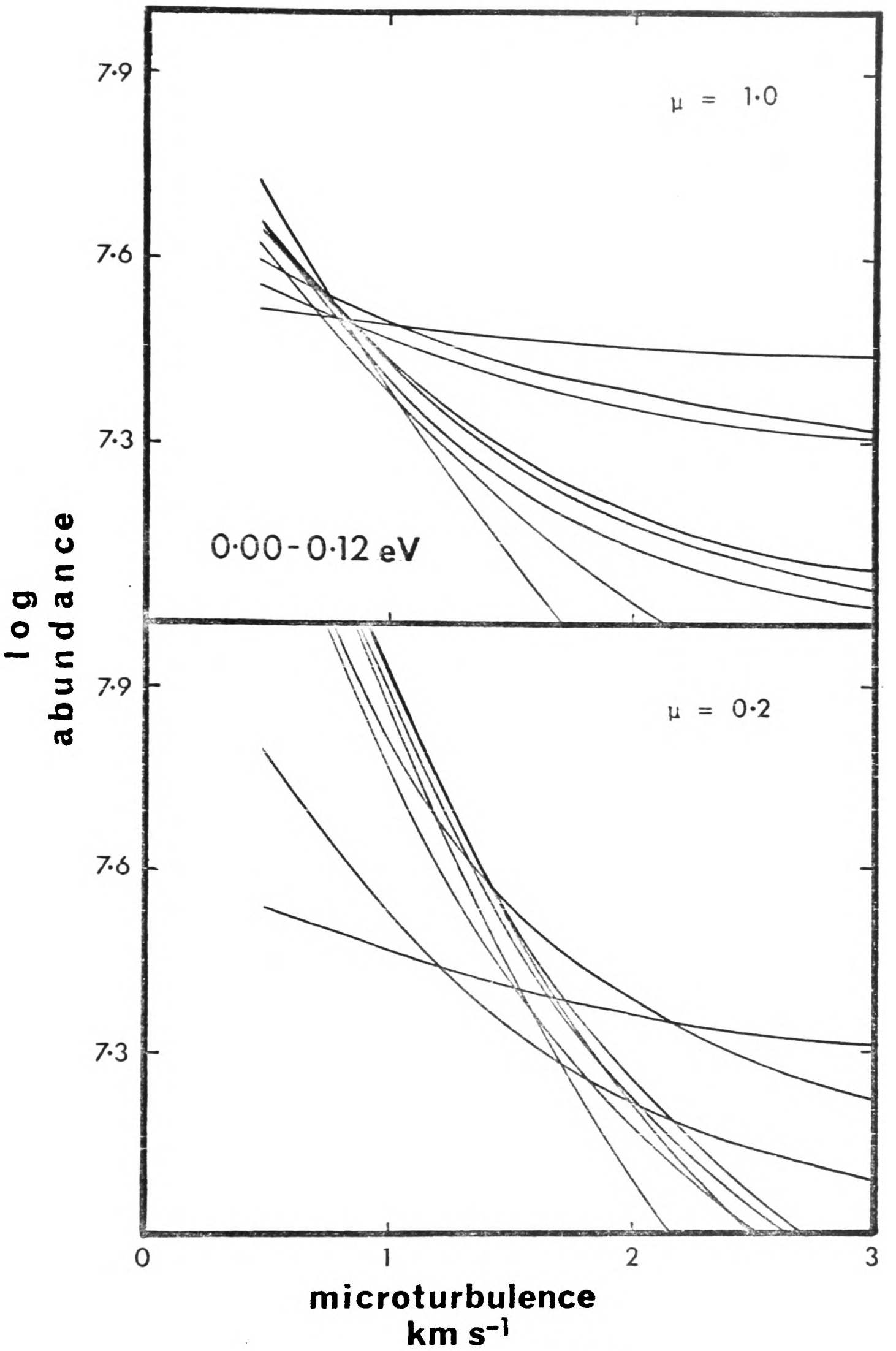


Figure 6.6

The variation of derived abundance with microturbulence is shown for the eight weak lines of the ground state group. The model is the H.S.R.A. at disk centre (upper) and at $\mu = 0.2$ (lower).

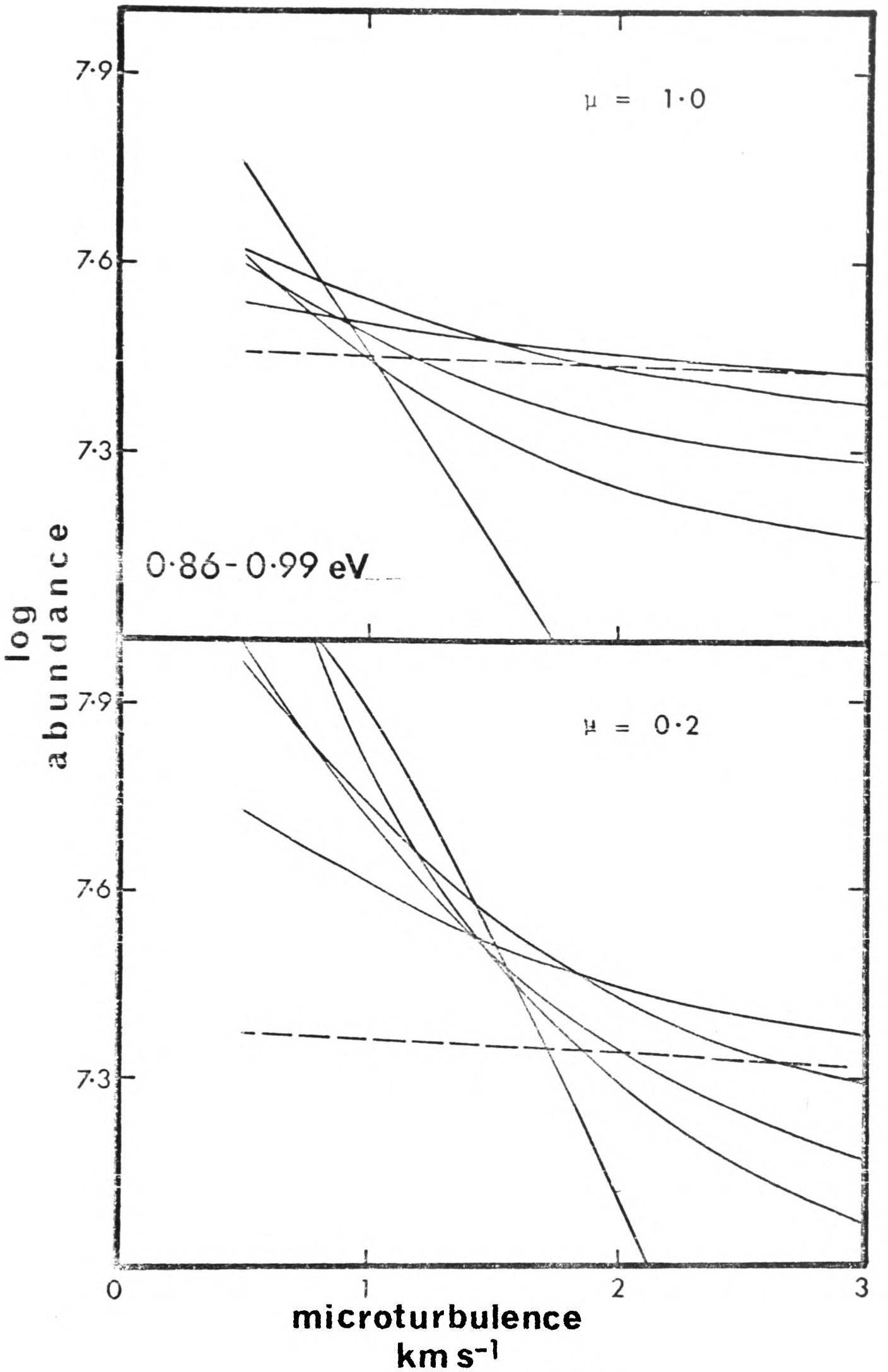
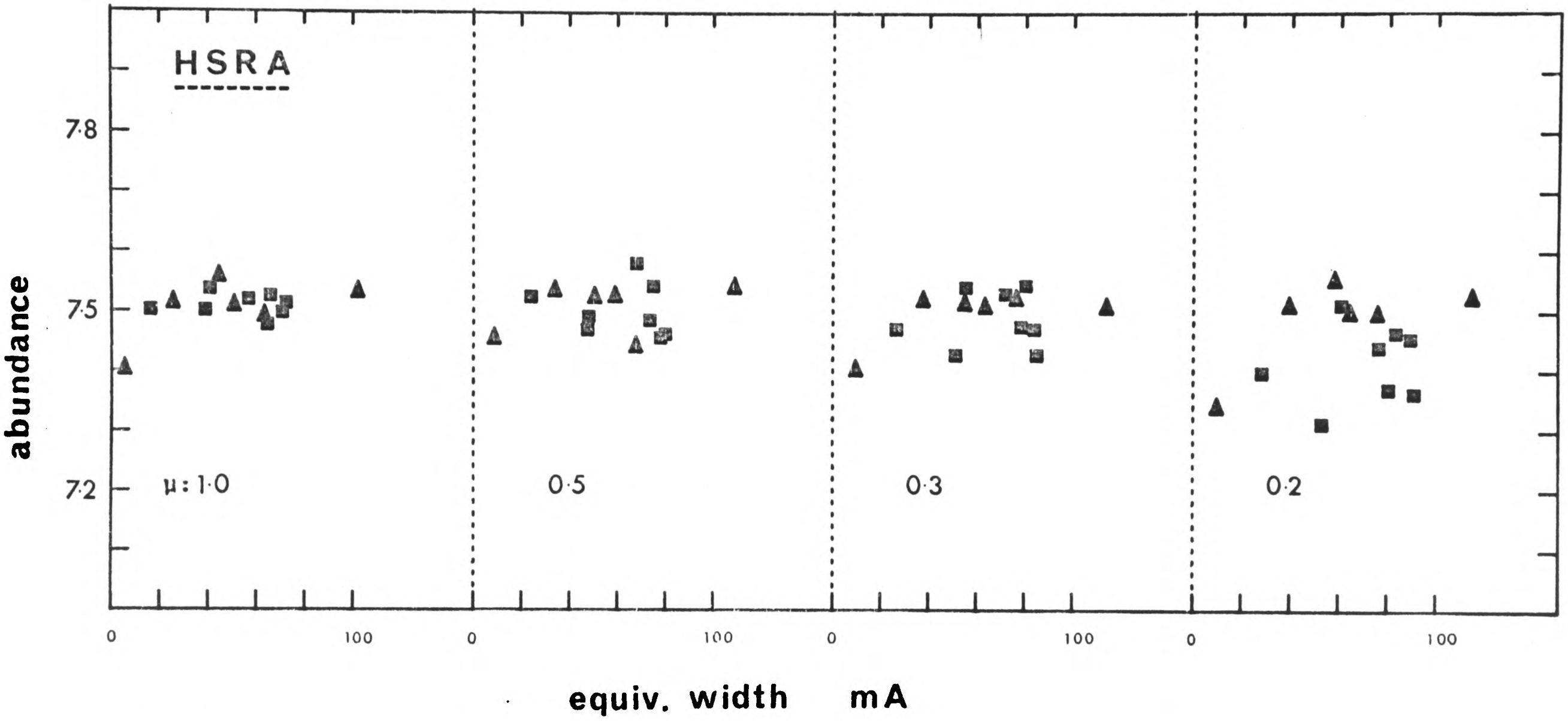


Figure 6.7

The variation of the derived abundance with microturbulence is shown for the six weak lines of the first excited group of lines. The model is the H.S.R.A at disk centre (upper) and at μ = 0.2 (lower) dashed line is 6609A,- see text

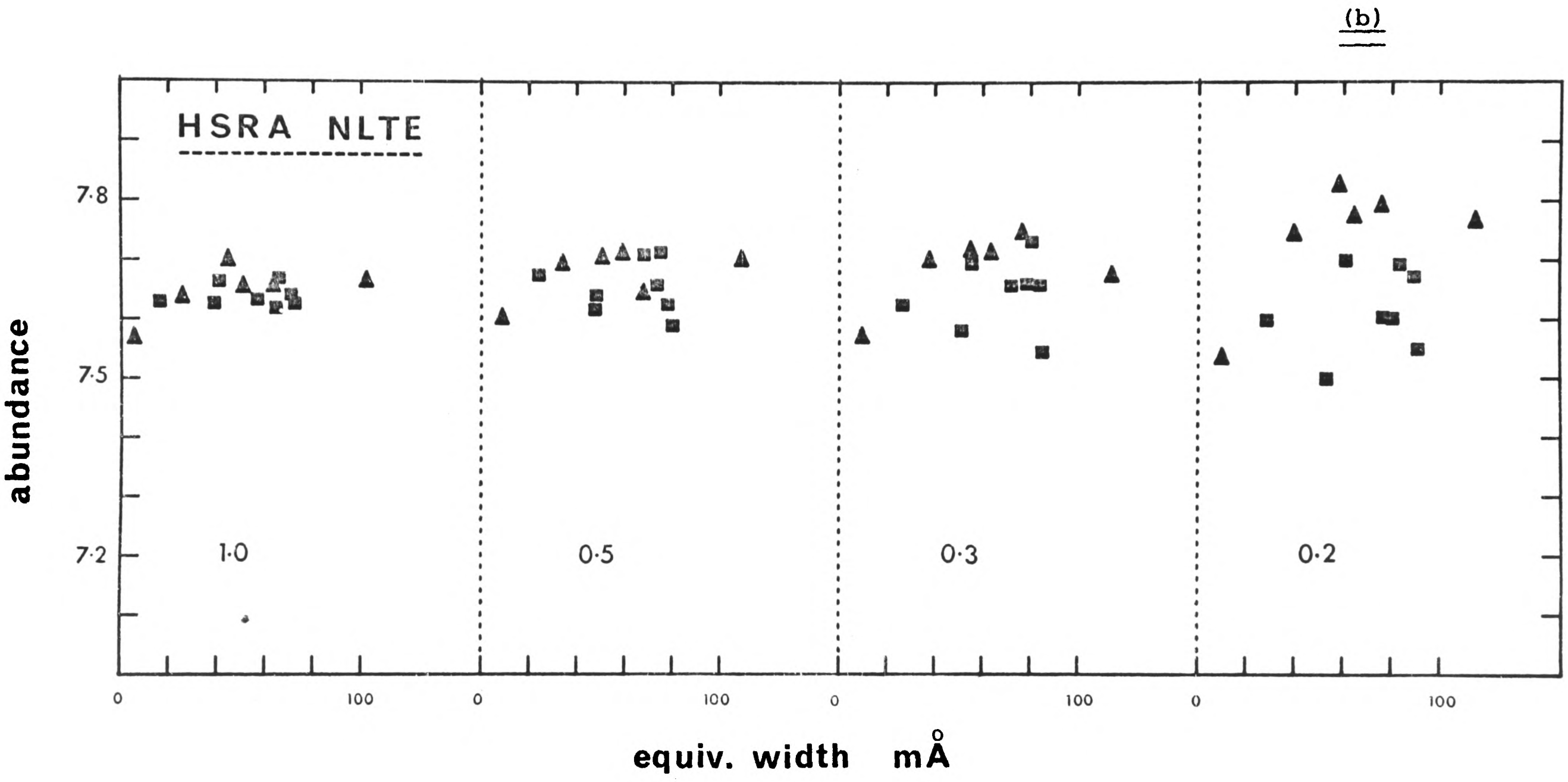
Figure 6.8

(a)

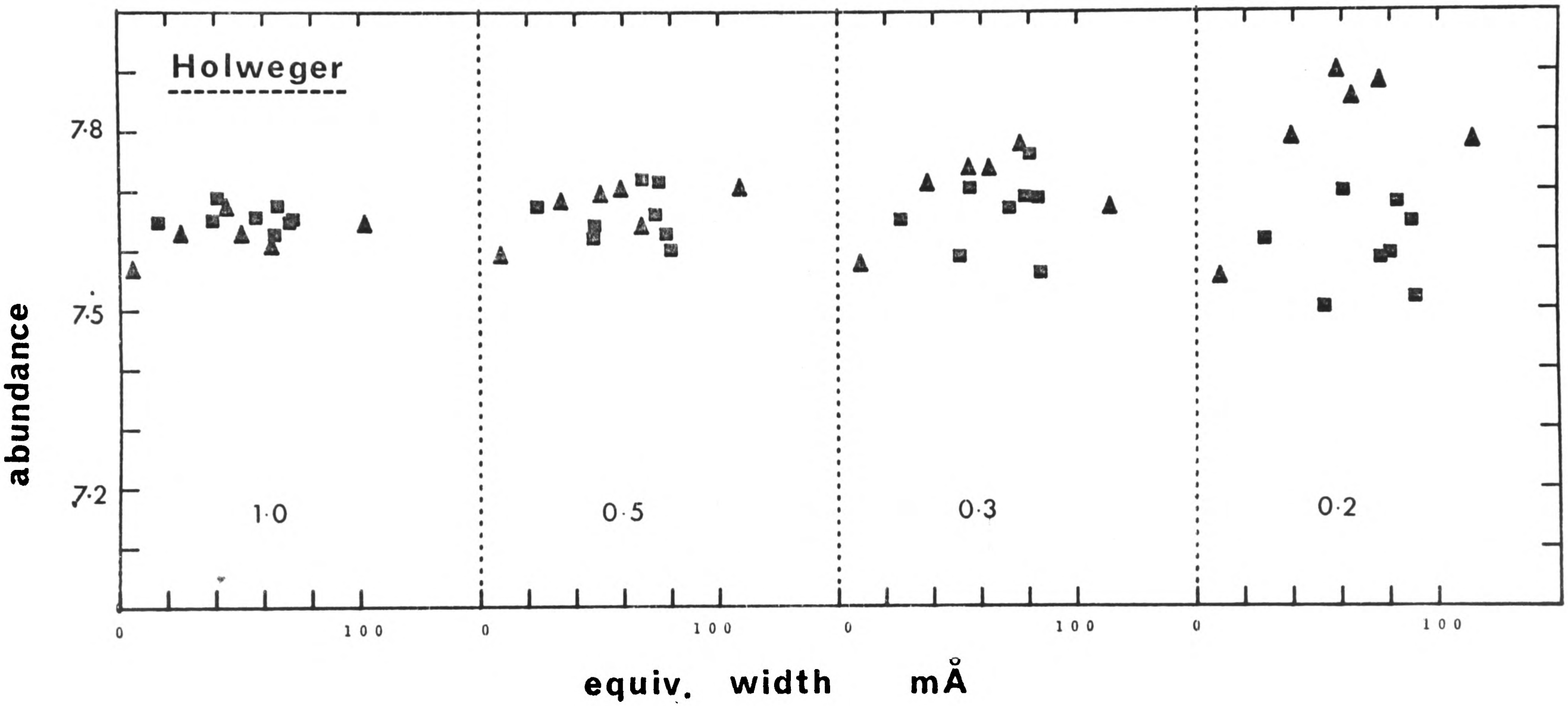


The derived abundances for each line, at the adopted microturbulences, for the 5 models and 4 disk positions; a^5D & a^5F lines are distinguished as in figure 5.4. The line 5127A is included for illustrative purposes only.

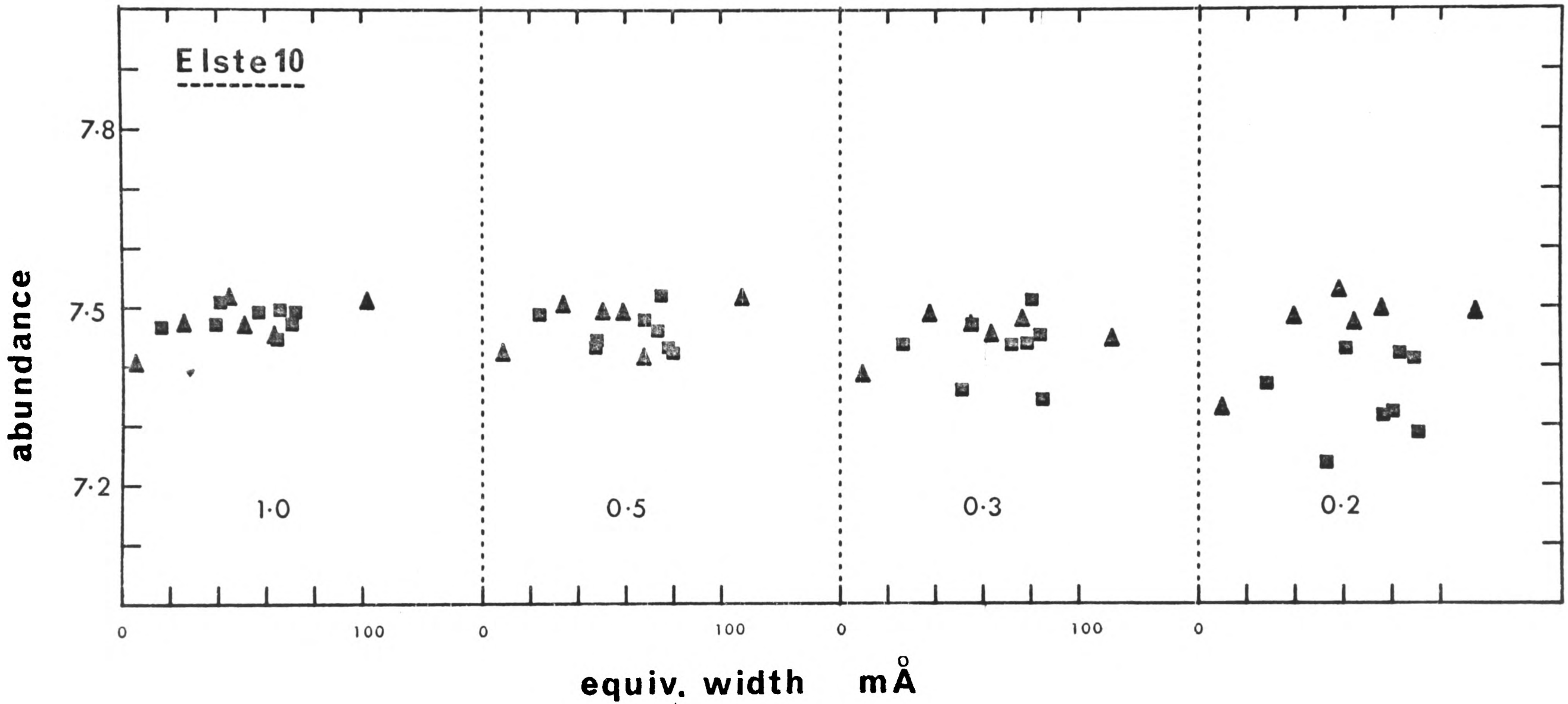
(b)


HSRA NLTE
7·8
7·5
7·2
abundance
1·0
0·5
0·3
0·2
0
100
0
100
0
100
0
100
equiv. width mÅ

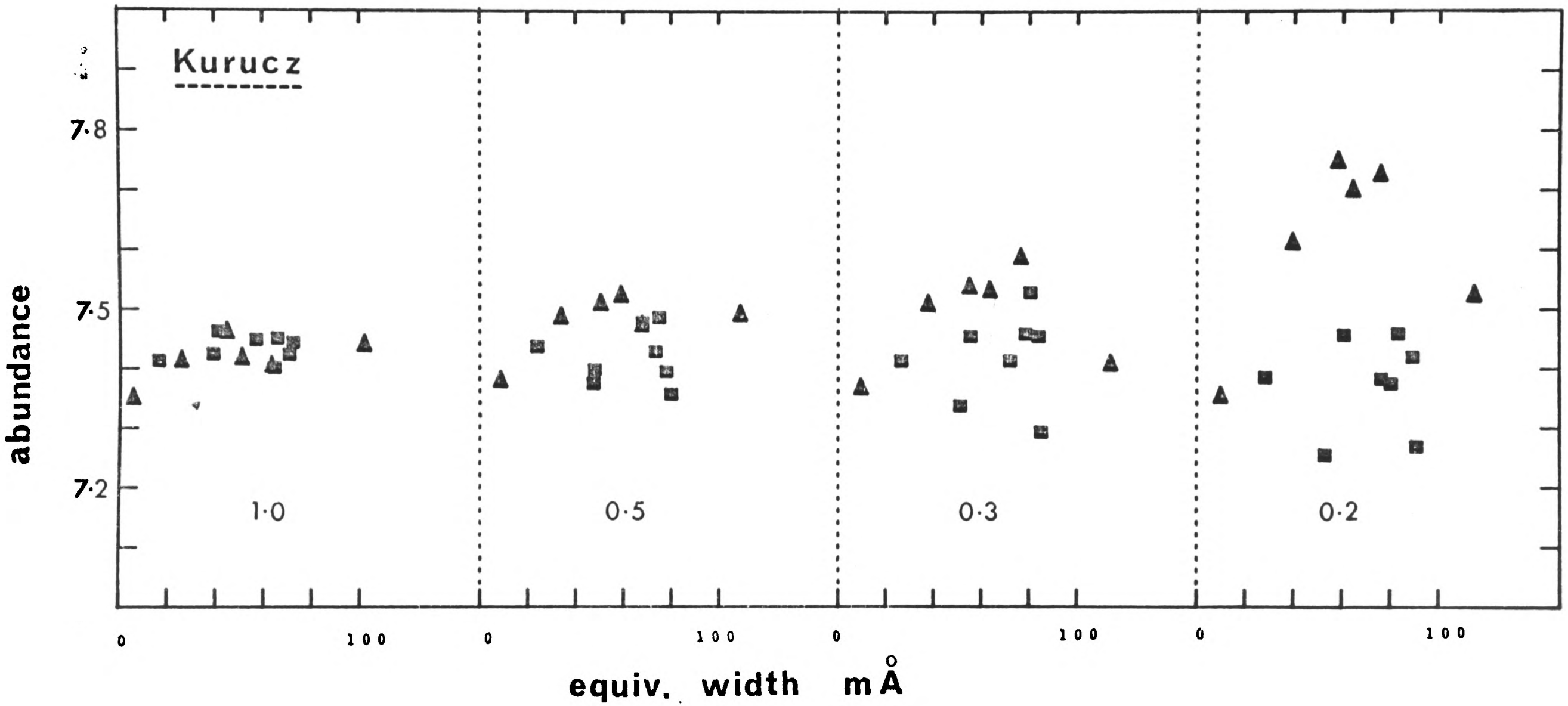
(c)


Holweger
7·8
7·5
7·2
abundance
1·0
0·5
0·3
0·2
0
100
0
100
0
100
0
100
equiv. width mÅ

(d)


Elste 10
7·8
7·5
7·2
abundance
1·0
0·5
0·3
0·2
0
100
0
100
0
100
0
equiv. width mÅ

(e)


Kurucz
7·8
7·5
7·2
abundance
1·0
0·5
0·3
0·2
0
100
0
100
0
100
0
100
equiv. width mÅ

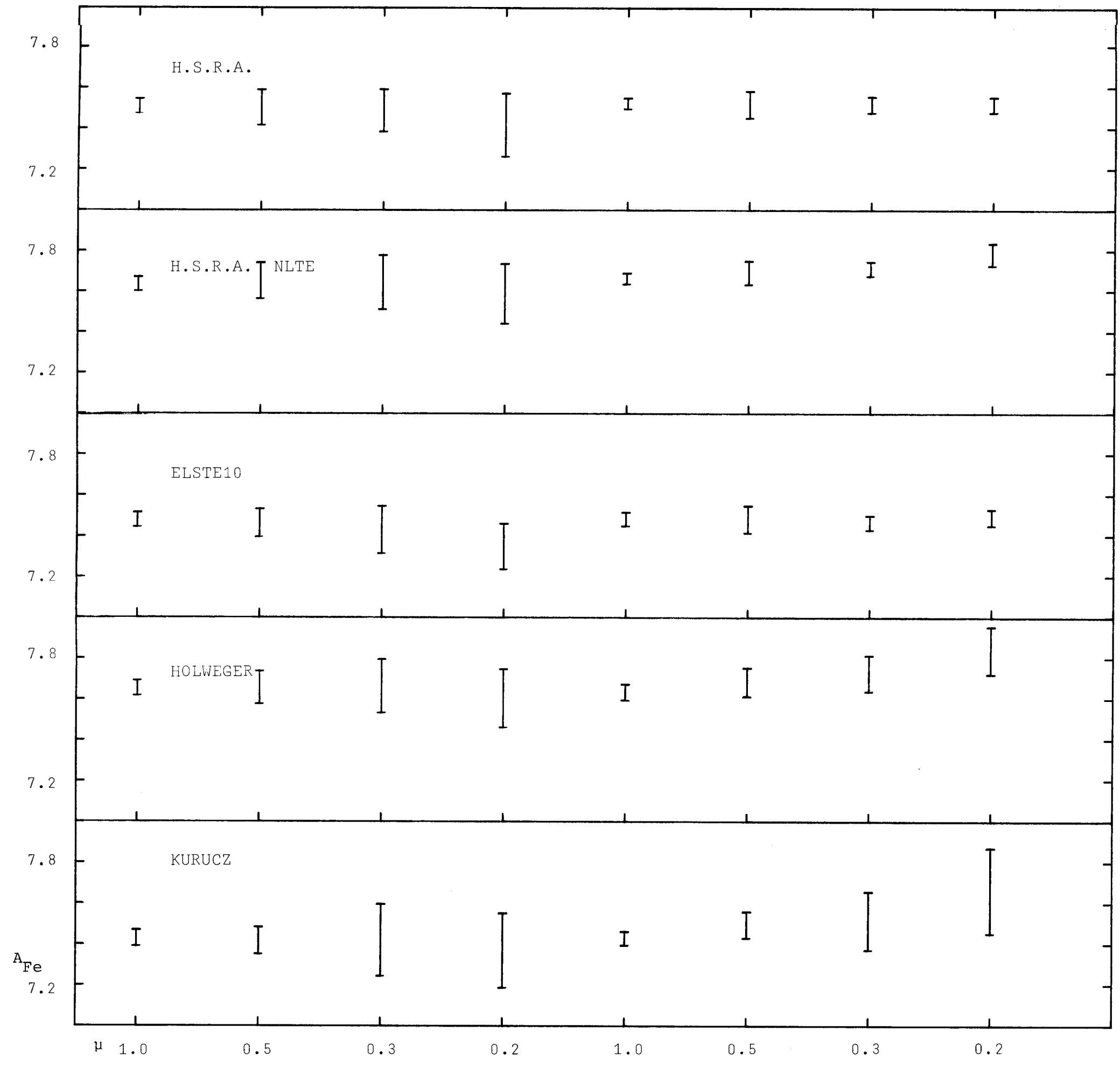


Figure 6.9

The derived solar iron abundance and the associated maximum error is shown for the ground state and first excited groups of lines. The abscissa indicates the disk position, and the ordinate the abundance on the scale $\log(n_H) = 12$.

7. SOLAR SPECTRUM: FEI DAMPING CONSTANTS

7.1 Introduction

As indicated in section 4.2 above, the abundance used to compute profiles of strong lines should be measured from a line with the same lower level. However the weak lines used were not independent of microturbulence. Hence the abundance from any one line depended on the value adopted for the microturbulence, and therefore on the other lines.

It was therefore necessary to relax the ideal condition, and to take the abundance defined by weak lines from the same lower term as the strong line. This was justified because:

a. the microturbulence was well-defined and the abundances from the different lines differed by very little; and

b. the levels within the terms were closely spaced and likely to have relative populations maintained in LTE by collisional processes, especially as they are formed comparatively deep in the solar atmosphere.

The abundances were therefore taken from the results in table 6.5 for each of the two groups. Damping constants were then found for a total of 14 lines, falling into 3 groups as follows.

7.2 Medium strong lines

Table 6.3 showed 4 lines from a^5D levels with equivalent widths greater than 100 mA, which were sensitive to the damping constant. Each had a relatively clear profile in the solar spectrum but this could not be used to derive the damping constant because the line shape also depends on macrotubulence which is not known accurately (Evans et al, 1975). The equivalent width on the other hand is independent of macroturbulence.

Damping constants were found by the value of C_6 needed to give the observed equivalent width. As the line strength also depends on the microturbulence, the values in table 6.4 were used according to the model and disk position. The abundances derived for the particular model and limb position were also used, because these may reflect effects, such as scattered light, which also act on the stronger lines. And it was indeed found that the measured damping coefficients at different values of μ were closer than if the disk centre abundance had been used.

The weighted mean results for the 4 lines and 5 models are given in table 7.1. The use of $(\log_{10}C_6 + 33)$ as a measure is explained below. For the present however it should be noted that the uncertainty in these results, about 0.1 to 0.15 in $\log C_6$, corresponds to only some 10 per cent in the damping. The results are also remarkably consistent between models, which may be taken to endorse the use of abundances and microturbulences derived for the particular models from lines from the same lower level. Such residual differences as do remain are probably the result of the different assumptions about abundances etc, used when constructing the models.

7.3 The line FeI 5269.5A

Profiles for the strong lines were taken from the spectra of Delbouille et al (1973), Brault and Testerman (1972) and from the Gornergrat observations, for the same disk positions as above. In addition profiles of many of the lines were taken from the results of Lites (1972) which show absolute and relative intensities at up to 10 disk positions (Lites and White, 1973).

Particular attention was given to the 5269A line from the 0.86eV level as this was the only strong line with a clearly defined continuum and wings free from blending. The line is included in the more general results below, but was also examined separately. Profiles were computed, using the same assumptions as in chapter 6, for all the models and disk positions heretofore discussed, and compared with all of the available spectra. Agreement between observations and theoretical profiles was assessed by inspecting the two when plotted on the same scale and overlayed; and qualitative but nonetheless clear conclusions were that the HOLWEGER and HSRA models were better able to reproduce the observed behaviour. The KURUCZ model in particular was less successful.

The adopted value for C_6 was 9.0×10^{-33} ($\log C_6 + 33 = 0.95$). Figure 7.1 illustrates the resulting fit to the observed profile for the HSRA model using the abundance derived in chapter 6 and the spectrum from the Preliminary Kitt Peak Atlas.

For a given model atmosphere the position of the continuum determined the uncertainty in the damping constant which was estimated to be less than 0.1 in $\log C_6$.

7.4 Damping of strong lines

The more general treatment of strong lines (which included 5269.5A for reference) had to take account of the fact that lines were below 4000A where the position of the continuum is quite uncertain (Labs and Neckel, 1972) and where solar models do not reproduce the observed intensities (Bell, 1973; Mount and Linsky, 1974, 1975; Lites, 1973). However the centre to limb variation of the profiles of these lines is itself a test of the model atmosphere (Athay et al, 1972). This was therefore used to find provisional C_6 values for 9 of the strong, blue lines.

Profiles were first computed for each of the lines, each model, and for each disk position; and for a range of C_6 values. The abundances and microturbulence were taken from chapter 6 above.

These computed profiles were then compared with the observed lines by projecting both on a visual display driven by a DGC NOVA computer. Although this required the redigitizing of the spectra, it allowed interpolated profiles from the computations to be displayed in a matter of seconds; and the best fit could be chosen for the many combinations of line, model atmosphere etc. This is illustrated in figure 7.2 which shows the observed spectrum from the Preliminary Kitt Peak Solar Atlas and the computed profiles of FeI 3719A. The particular assumptions are discussed below, but in each case the profile is shown for disk centre and the limb spectrum; and for 5 values of the damping: 0.75, 1.0, 1.5, 2, and 4 times the theoretical value of Warner (1969).

The centre-limb data was also used to examine the change in depth of the line at a particular wavelength and figure 7.3 is an example of the NOVA display for the same line (3719A) and damping constants as before. In both the use of the full profile and the centre-limb variation it was necessary to avoid obvious blends. And no regard was had to the cores of the lines which cannot be computed reliably with simple LTE models.

Figure 7.2(a, b) shows that the observed profile was not reproduced by straightforward calculations using the model atmosphere and the abundance derived above. But the models predicted intensities in the continuum much greater than those observed.

Three approximate adjustments for the discrepancy were tried. First the H^- opacity in the models was scaled by a constant factor such that the predicted intensity agreed with the measurements of Houtgast (1972) at wavelengths close to the line. The scaling factors, which differed from model to model, are given in table 7.2. Profiles computed for 3719A are shown in figure 7.2(c, d) and are, as a result of the increased opacity, closer to the observed line shape.

Damping constants derived from the profiles are given in tables 7.3 and 7.4. The values found from the limb spectra differ according to which abundance was used: the abundance from the disk centre observations or from the particular limb position. For the medium strong lines it was argued that the latter was correct. But these strong lines do not share the sensitivity to microturbulence or suffer the same observational uncertainties. There was therefore no firm evidence for taking one set of abundance over another. Ideally the damping constant should of course be independent of the limb position. But the mean differences between centre and limb - -0.12 in table 7.3 and +0.18 in table 7.4 - were not significantly different. Subsequently the disk centre abundance was used throughout.

Next the profiles from the unamended model atmospheres were compared with the observations assuming that the true continuum was at the predicted level rather than the perceived. Figure 7.2(e, f) illustrates the effect of drawing the continuum at 3719A 20 per cent higher. The profiles were not close to the observed line shape but, for completeness, table 7.5 records the mean damping constants which gave the closest approximation to the observed spectrum.

These two adjustments to the continuum correspond to two extreme forms of additional opacity: the H^- opacity is a greater proportion of the whole at greater optical depths; raising the continuum is equivalent to an extra opacity at the top of the atmosphere. The discrepancy between models and observed intensities has been explained however (Labs and Neckel, 1968; Carbon et al, 1968; Holweger, 1970, 1971; Zwann, 1974; Dreiling and Bell, 1975) by the opacity introduced by the very many weak lines present, but not observed, at these wavelengths. The third and final method therefore used a pseudo-line opacity, the sum of fictitious lines of FeI,II and SiI,II from a number of excitations, to simulate a "line haze". This quite arbitrary opacity was then scaled to give the correct continuum intensity for the level drawn on the observed spectra (figure 7.2(g, h)). The distribution of the extra opacity with depth was then more realistic and the results showed better agreement between the limb and disk centre values, as well as qualitatively better fits. As the three models with better approximations to the true profile, calculations in this way were carried out for the HSRA, ELSTE10 and HOLWEGER models and the values derived are given in table 7.6.

These very approximate calculations can only indicate what might be done with more sophisticated methods: eg inversion of the observed profiles to derive simultaneously the extra opacity and the damping. However the scarcity of other measurements of damping constants based on precise oscillator strengths and abundances makes even the provisional values useful. C_6 values adopted from the better fits are therefore given in table 7.7. The uncertainty in these suggested by the measurements is about 0.2 dex, due mainly to the different values from different model atmospheres. There may of course be very much larger errors due to the simple assumptions in the analysis or to inaccuracies in the models.

There was however little likelihood of errors due to the derived abundance of iron. In section 4.1 it was argued that one of the advantages of the proposed method would be similar depths of formation for the weak and strong lines. This was confirmed by calculations for the HSRA model using the adopted abundance, microturbulence and damping constants and the method of Gurtovenko (1974, 1975ab) to define the depth of formation. Results for 3719A and 5127A, both from the 0.05eV level, are shown in figure 7.4. As expected the optical depth for a given absorption depth is much the same in the two lines. The strong line is formed somewhat deeper because the absorption depends on the product of the population n_i and the damping (and hence pressure) whereas the weak line is, broadly speaking, determined only by n_i. But the difference is small and the abundance found from the weak lines is clearly the value for the depth where the strong line is also formed.

7.5 Calculated damping constants and other measurements

As the damping constants have been presented here in an unusual form it may be helpful to refer briefly to the great amount of previous work on the broadening of FeI lines in the solar spectrum; and to the laboratory and theoretical values for the van der Waals damping.

The general theory of the interaction of a radiating atom and perturber (Szudy and Bayliss, 1975) is rarely tractable. Classical approximations (Lorentz, 1915; Weisskopf, 1933; Lindholm, 1945) and quantum mechanical theories (Baranger, 1958; Kolb and Griem, 1958) have often been reviewed (Traving, 1960; Griem, 1964; Cooper, 1966). The simple classical theory gives (Unsold, 1955)

$$\Gamma_6 = 17.0\, C_6^{0.4}\, v^{0.6}\, N \qquad (7.1)$$

where
$$C_6 = (e^2/h)\cdot\alpha\bar{r}^2 \qquad (7.2)$$

Bates and Damgaard (1949) used Coulomb wave functions to calculate approximate mean square radii

$$\bar{r}^2 = (n^{*2}/2z^2)\cdot\{5n^{*2}+1-3l(l+1)\} \qquad (7.3)$$

and Unsold (1955) developed more crude expressions; first by neglecting the (1 - 31(1+1)) term; second by using only approximate expressions for the effective principal quantum number n*. More accurate values of $\bar{r}^2$ have been attempted by Warner (1967, 1969) and Hofsass (1975) using scaled Thomas-Fermi wave functions.

The more advanced theories generally give damping constants greater than from the simple Unsold theory of the van der Waals interaction. This arises in part from the more complex potentials which are used to approximate to the interatomic interaction. For example, Hindmarsh et al (1967) used a Lennard-Jones potential and later (Hindmarsh et al, 1970) potentials with terms proportional to r^{-6}, r^{-8}, and r^{-12}. Other potentials have been proposed by Griem (1964), developed by Fullerton and Cowley (1970, 1971); and by Smirnov (1967) developed by Roueff (1970, 1974) and Roueff and van Regemorter (1969, 1971) among others. The results of the latter authors were applied by Deridder and Rensbergen (1974) and Rensbergen et al (1975) but the subsequent tabulations of damping constants (Deridder and Rensbergen, 1976) must be treated with caution as there was an error in the calculated potentials. In any case there is no generally accepted formalisation of the problem. Brueckner (1971), for instance, has given results for FeI which Smith et al (1973) felt were based on dubious assumptions.

Nevertheless the theoretical evidence suggests that damping constants calculated from the simple Unsold formulae are too low by a factor of the order two or more. This is supported by the laboratory measurements of collisional broadening (eg Grasdalen et al, 1969; Copley and Camm, 1973). But these use inert gases as the perturbing atom and only Kusch (1958) has presented results for FeI lines broadened by atomic hydrogen. His results show an enhancement over the Unsold value of as much as 1.1 dex, but are subject to very great uncertainties and are not now widely accepted.

Observations of the solar spectrum have therefore been used to test the theories or to derive empirical damping constants. In principle this should be a reasonable method. And Blackwell et al (1972b) showed that the solar model atmospheres and LTE mechanisms were able to reproduce the NaI D profile with the accurate theoretical damping coefficient of Lewis et al (1971, 1972). Unfortunately the majority of other applications have not been so precise. For example Foy (1972) and Yamashita (1972) both derived damping constants from the curve of growth of FeI lines in the solar spectrum. But both also used oscillator strengths obtained by quite unexplained shifts in the values reported by the originating authors. Uncertainties in the oscillator strengths have also been a source of error in the results of other authors, eg Chamaraux (1967); Cowley et al (1969); Cowley (1970); Holweger (1971ab, 1972, 1973); Blackwell et al (1972a); Lites (1973); Evans et al (1975); Edmunds (1975ab).

The results of these solar determinations are generally quoted as enhancements over the classical van der Waals damping. The consensus perhaps is that an enhancement of about a factor 2 is required. But it is not always clear what classical value is being taken as the basis for the enhancement. At least four "Unsold values" are in general possible for a given transition, according to the formulae used for $\bar{r}^2$ and for n*. In particular very few authors appear to take account of the parental term for the optical electron.

For this reason the factor E_6 has been eschewed in this work and C_6 given direct, although the value of C_6 must be seen as no more than a parameter for use in equation (7.1). The damping might also be given in absolute units which would however be less convenient for application to other astrophysical spectra. Accordingly table 7.8 gives the C_6 values found for the FeI lines alongside the values from the Unsold equations, the van der Waals theory with Warner's (1967, 1969) wave functions, and the calculations of Brueckner (1971) as interpreted by Edmunds

(1975ab). This shows that for these lines the full Unsold (1955) formulae are a very good approximation to the observed values: the mean difference corresponds to an enhancement factor 0.83.

This result was not surprising in view of the abundance derived in chapter 6 and used in the damping determination. The depression in the wing of a strong line depends, other things being equal, on the product:

damping x abundance x oscillator strength

so that an observed line will correspond to a lower damping if the abundance is increased. This relationship was used by Cowley (1970) and by Blackwell et al (1972a) to revise the damping constants found by Cowley et al (1969) for FeI lines in the solar spectrum. The original results of Cowley et al (1969) assumed an iron abundance of 6.55 (Warner, 1968) and the oscillator strengths of Corliss and Tech (1968). As both are subject to large errors the E_6 values were again revised, using the abundance (7.52) found herein for the HSRA model which is not unlike the Revised Bilderberg Model (Elste, 1968) used in their derivation. The oscillator strengths were taken from Bridges and Kornblith (1974) which the comparisons in chapter 5 suggested were perhaps the best of the emission measurements. The results of this simple correction are given in table 7.9. The damping enhancement is clearly no longer necessary, and the mean value of E_6 only -0.01. It should be noted however that this is the enhancement with respect to values calculated without the l(l+1) term and without taking account of the parental term.

It was felt unsatisfactory to adjust the damping constants and abundance over such large ranges in this way, so the gf values of Bridges and Kornblith (1974) were also used to compute profiles of a number of excited FeI lines for a range of C_6. The profiles and equivalent widths obtained were than compared

with the spectrum of Delbouille et al (1973) to derive the empirical damping constant from the solar line strength. The calculation assumed the microturbulence and abundance, and the HSRA model, as in chapter 6. The values for 18 lines where the oscillator strengths had errors of 10 per cent or less according to the authors are given in table 7.10. It must be emphasised that these are very tentative results. But they support the conclusion that the damping of FeI lines in the solar spectrum is very much less than previously believed. And that the full Unsold formula a good first approximation.

The success of the Unsold formula is undoubtedly accidental, and should not be assumed for other elements. But there is perhaps a need to reconsider the theoretical approximations which give very much higher values. These could only be accepted if the solar iron abundance was very much lower. Lites (1973) for instance found that the Brueckner (1971) damping corresponded to an abundance of 7.2. This would imply errors in the oscillator strengths measured in the furnace of the order of 0.4 dex which is most improbable. On the other hand, the results for the low excitation FeI lines are the only ones which are presented here with any confidence. Smith (1976, private communication) has pointed out that the low damping for these lines is quite consistent with the laboratory measurements and should not be taken to imply similarly low values at high excitations.

The damping constants at high excitations need similarly precise abundances from weak lines from the same lower levels, and must await more precise oscillator strengths. For the low excitation FeI lines measured here though it would appear that the damping coefficients determined from the solar spectrum are, as expected, more precise than the theoretical values.

Table 7.1

C_6 values from the comparisons of observed and calculated equivalent widths.

	$\log_{10} C_6 + 33$					
wavelength A	HSRA	HSRA NLTE	ELSTE10	HOLWEGER	KURUCZ	mean
4427.3	0.89	1.09	0.95	1.08	0.85	0.97
4375.9	0.54	0.71	0.57	0.76	0.47	0.61
4461.7	0.57	0.73	0.63	0.78	0.51	0.64
4216.2	0.71	0.91	0.81	0.94	0.72	0.82

Table 7.2

Enhancement factors for the H^- opacity to produce the observed continuum intensity. (in order of increasing wavelength)

line Å	continuum Å	H.S.R.A.	Elste10	Holweger	Kurucz	
3679.9	3675.1	1.66	1.70	1.88	1.88	
3719.9	3715.0	1.64	1.70	1.88	1.88	
3722.6	3715.0	1.64	1.76	1.88	1.88	
3734.9	3740.9	1.67	1.73	1.84	1.84	
3749.5	3755.8	1.65	1.69	1.80	1.81	
3820.4	3811.5	1.42	1.46	1.51	1.56	
3859.9	3852.0	1.42	1.43	1.48	1.52	
3886.3	3883.9	1.55	1.62	1.73	1.73	
3899.7	3898.6	1.46	1.50	1.59	1.61	
3906.5	3909.2	1.42	1.50	1.50	1.53	
3920.3	3923.8	1.91	1.98	2.15	2.08	
5269.5	5261.1	1.00	1.00	1.00	1.00	* assumed

Table 7.3

Empirical damping constants deduced from disk centre profiles (left of column) and from the centre-limb behaviour (right of column). The abundances derived at individual limb positions were used for the latter.

λ	$\log_{10} C_6 + 33$									
Å	HSRA		HSRA NLTE		Elste10		Holweger		Kurucz	
3820.4	1.11	0.56	0.71	0.23	0.69	0.64	1.41	0.76	0.79	0.21
3722.6	1.08	0.88	0.76	0.38	0.83	0.86	1.23	1.40	0.88	1.21
3679.9	0.91	-	0.58	-	0.71	-	1.01	-	0.66	-
3719.9	0.91	0.88	0.58	0.51	0.68	0.71	1.01	1.36	0.66	1.01
3906.5	0.91	1.08	0.71	0.58	0.78	0.81	0.98	1.23	0.78	0.96
3920.3	1.03	1.08	0.83	0.63	0.93	1.16	1.18	1.36	0.91	1.26
3899.7	0.73	0.73	0.46	0.23	0.58	0.56	0.88	1.11	0.63	0.76
3886.3	0.91	0.63	0.71	0.23	0.93	0.48	1.26	1.31	0.78	1.26
3859.9	0.86	0.83	0.53	0.33	0.66	0.36	1.03	1.23	0.71	1.16
5269.5	1.00	0.90	0.83	0.23	0.78	0.68	0.90	0.55	0.68	0.28

Table 7.4

Empirical damping constants deduced from the disk centre profiles (left of column) and from the centre-limb behaviour (right of column). The disk centre abundance was used for all limb positions.

λ	$\log_{10} C_6 + 33$									
Å	HSRA		HSRA NLTE		Elste10		Holweger		Kurucz	
3820.4	1.11	0.55	0.71	0.53	0.69	0.65	1.41	1.38	0.79	0.80
3722.6	1.08	0.65	0.76	0.32	0.83	0.53	1.23	1.27	0.88	1.08
3679.9	0.91	-	0.58	-	0.71	-	1.01	-	0.66	-
3719.9	0.91	0.65	0.58	0.45	0.68	0.38	1.01	1.23	0.66	0.85
3906.5	0.91	0.85	0.71	0.52	0.78	0.48	0.98	1.10	0.78	0.80
3920.3	1.03	0.85	0.83	0.57	0.93	0.83	1.18	1.23	0.91	1.10
3899.7	0.73	0.50	0.46	0.17	0.58	0.23	0.88	0.98	0.63	0.60
3886.3	0.91	0.40	0.71	0.17	0.93	0.15	1.26	1.18	0.78	1.10
3859.9	0.86	0.60	0.53	0.27	0.66	0.03	1.03	1.10	0.71	1.00
5269.5	1.00	0.89	0.83	0.53	0.78	0.70	0.90	1.05	0.68	0.87

Table 7.5

Empirical damping constants derived from disk centre and limb profiles with the continuum drawn above the apparent level to allow for depression by weak lines.

	$\log C_6 + 33$				
Å	HSRA	HSRA NLTE	Elste10	Holweger	Kurucz
3820.4	0.96	0.99	0.99	1.34	0.91
3722.6	0.96	0.86	0.91	0.98	0.76
3679.9	1.18	0.76	0.73	1.01	0.73
3719.9	1.03	0.76	0.86	1.21	0.76
3906.5	1.13	0.71	0.81	1.16	0.68
3920.3	1.26	0.81	0.93	1.26	0.96
3899.7	1.13	0.71	0.81	1.01	0.68
3886.3	1.08	0.71	0.81	1.23	0.81
3859.9	0.88	0.56	0.71	1.01	0.68
5269.5	1.00	0.83	0.78	0.90	0.68

Table 7.6

Empirical damping constants derived from centre profile and limb behaviour using a continuum opacity enhancement which simulates a weak metallic line "haze".

	$\log_{10} C_6 + 33$					
Å	HSRA		Elste10		Holweger	
3820.4	1.20	1.26	1.08	1.08	1.20	1.08
3722.6	1.18	1.00	0.90	1.00	1.15	1.23
3679.9	1.08	-	0.85	-	0.78	-
3719.9	0.95	1.08	0.90	0.95	0.90	0.95
3906.5	1.08	0.90	0.78	0.70	0.78	1.00
3920.3	1.08	1.08	0.78	0.95	0.90	1.02
3899.7	0.90	0.95	0.70	0.78	0.78	0.86
3886.3	1.05	1.00	1.08	0.90	1.20	1.23
3859.9	1.00	0.90	0.85	0.90	0.90	1.08
5269.5	1.00	0.89	0.78	0.70	0.90	1.05

Table 7.7

C_6 values adopted for the 10 strong FeI lines.

wavelength A	$\log_{10} C_6 + 33$
3820.4	1.15
3722.6	1.09
3679.9	0.90
3719.9	0.96
3906.5	1.04
3920.3	0.98
3899.7	0.83
3886.3	1.08
3859.9	0.94
5269.5	0.95

Table 7.8

C_6 values from the interpretation of the solar spectrum and from calculations.

wavelength A	log C_6 + 33				
	measured (1)	Unsold (2)	Unsold (3)	Warner	Brueckner
4427.3	0.97	0.30	0.84	0.54	1.51
4375.9	0.61	0.30	0.84	0.54	1.50
4461.7	0.64	0.29	0.84	0.54	1.51
4216.2	0.82	0.38	0.87	0.58	1.54
3820.4	1.15	0.80	1.09	0.86	1.85
3722.6	1.09	0.66	1.00	0.73	1.70
3679.9	0.90	0.64	0.99	0.73	1.69
3719.9	0.96	0.62	0.98	0.73	1.69
3906.5	1.04	0.58	0.96	0.68	1.66
3920.3	0.98	0.58	0.96	0.68	1.66
3899.7	0.83	0.57	0.95	0.68	1.64
3859.9	0.94	0.56	0.95	0.68	1.63
5269.9	0.95	0.45	0.91	0.55	1.66

(1) mean values. (2) without 1-31(l+1) term. (3) with 1-31(l+1) term.

Table 7.9

Enhancement factors for damping from Cowley et al. (1969) are corrected to the oscillator strengths of of Bridges & Kornblith (1974), and for the revised iron abundance.*

RMT	λ	log gf_{CT}	log gf_{BK}	E_6	E_6'
15	5405.8	-1.75	-1.80	0.75	-0.25
	5397.1	-1.88	-1.98	0.73	-0.22
	5434.5	-1.97	-2.07	0.77	-0.18
41	4404.8	0.25	-0.15	0.58	-0.07
318	4920.5	0.30	0.10	0.78	-0.07
	4891.5	0.17	-0.10	0.81	0.03
	4890.8	-0.09	-0.39	0.78	0.03
553	5324.2	0.47	-0.18	0.38	-0.02
	5302.3	-0.04	-0.78	0.56	0.25
686	5586.8	0.34	-0.15	0.48	-0.08
	5615.7	0.51	-0.10	0.70	0.26
	5576.1	-0.31	-0.90	0.65	0.19
	5569.6	0.07	-0.56	0.67	0.19
1146	5383.4	1.17	0.57	0.29	-0.16
1165	5415.2	1.20	0.53	0.27	-0.11

* $\log (N_{Fe}/N_H) + 12 = 7.52$ assumed

Table 7.10

Provisional C_6 values found from the HSRA model and the gf values of Bridges & Kornblith (1974)

wavelength and multiplet no.		log C_6 + 33				
		measured	Unsold[1]	Unsold[2]	Warner	Brueckner
5328.0	15	0.60	0.46	0.91	0.55	1.67
5405.8	15	0.78	0.47	0.92	0.55	1.69
3758.2	21	1.00	0.87	1.13	0.89	1.91
3763.8		1.00	0.87	1.13	0.89	1.92
3727.6		1.00	0.87	1.13	0.89	1.92
3767.2		1.18	0.88	1.14	0.89	1.93
4383.6	41	1.26	0.83	1.11	0.89	1.93
4404.8		1.48	0.85	1.13	0.89	1.95
4325.8	42	0.95	0.90	1.16	0.92	2.00
4045.8	43	1.30	0.95	1.19	1.00	2.03
4063.6		1.00	0.98	1.21	1.00	2.06
3815.8	45	1.40	1.05	1.26	0.80	2.12
5232.9	383	1.95	1.59	1.51	1.58	2.60
4919.0	318	1.89	1.62	1.55	1.59	2.64
4890.8		1.51	1.63	1.56	1.59	2.66
4871.3		1.51	1.63	1.56	1.59	2.66
5572.9	686	1.91	1.70	1.63	1.69	2.81
5415.2	1165	2.41	1.81	2.03	1.92	3.45
mean (measured-calculated)			0.23	0.05	0.32	-0.73

(notes as in table 7.8)

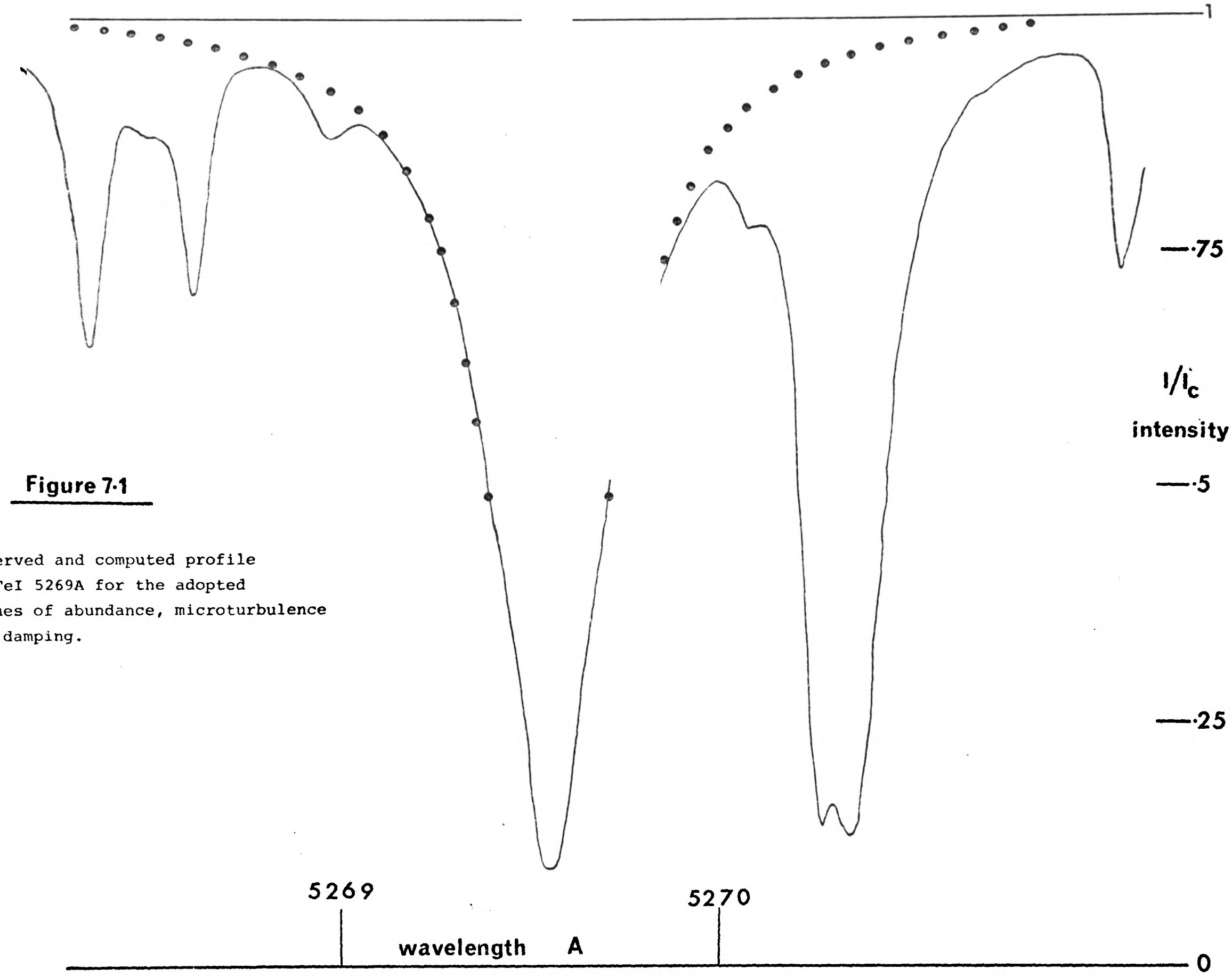
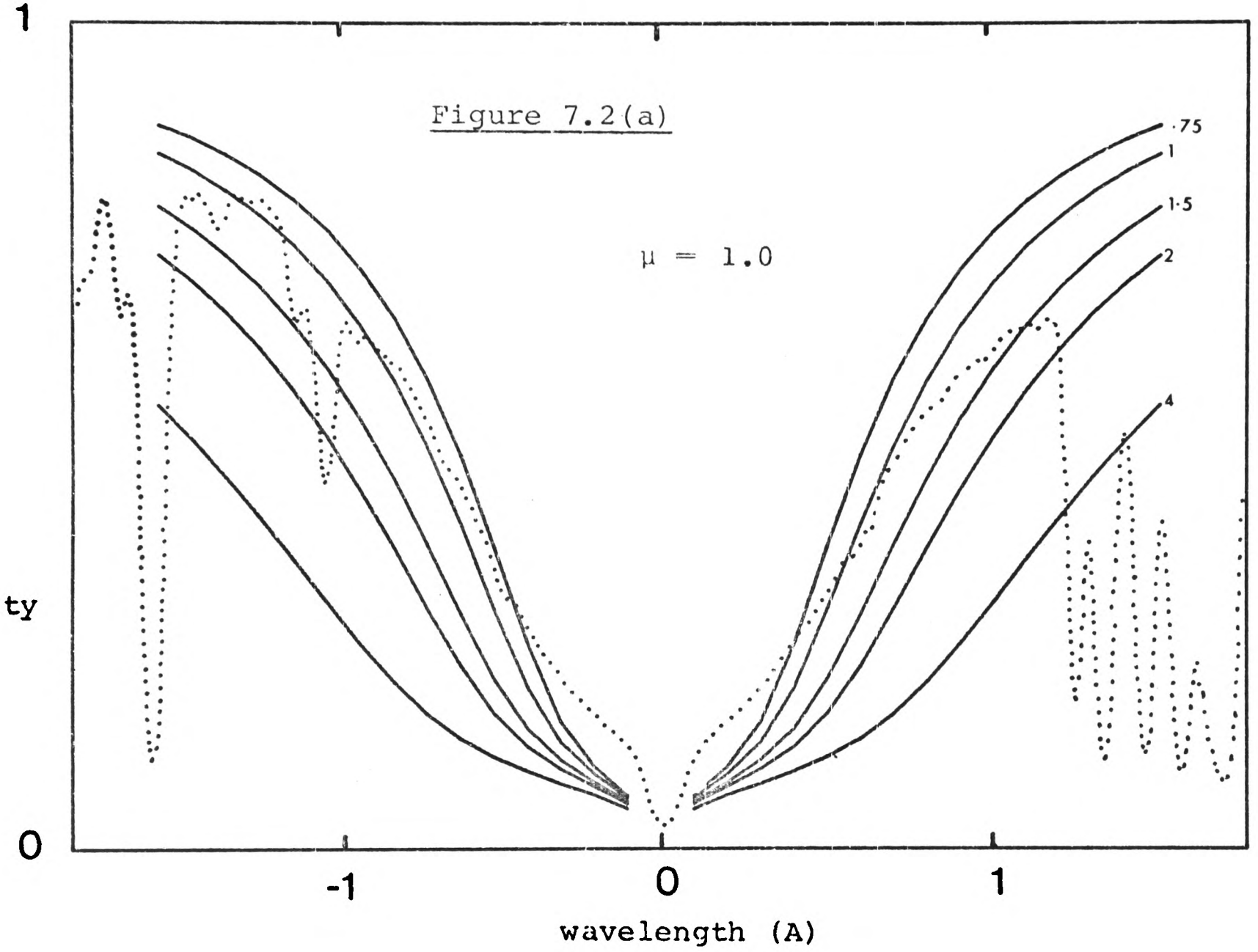


Figure 7·1

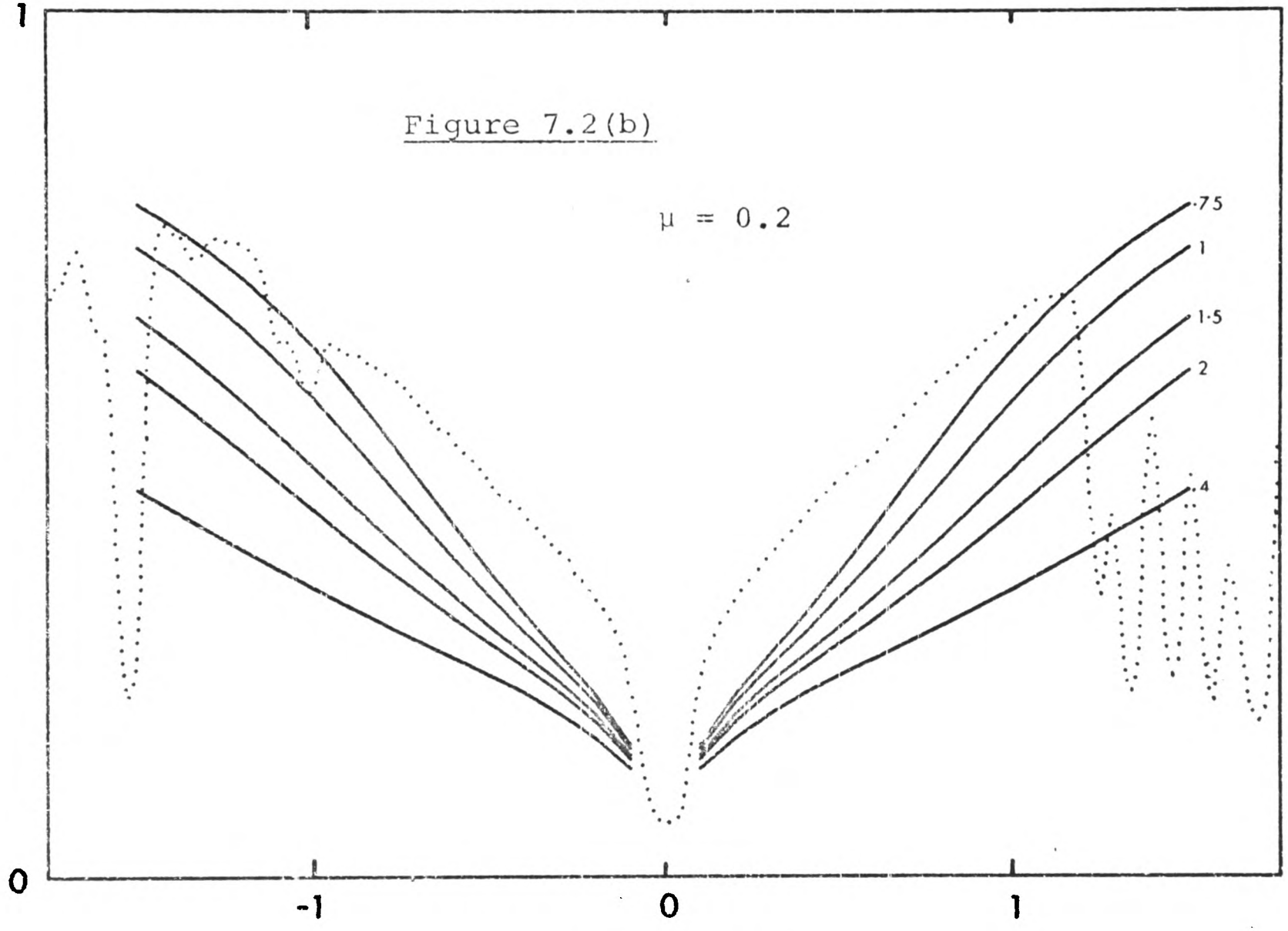
Observed and computed profile of FeI 5269A for the adopted values of abundance, microturbulence and damping.

line is FeI 3719A

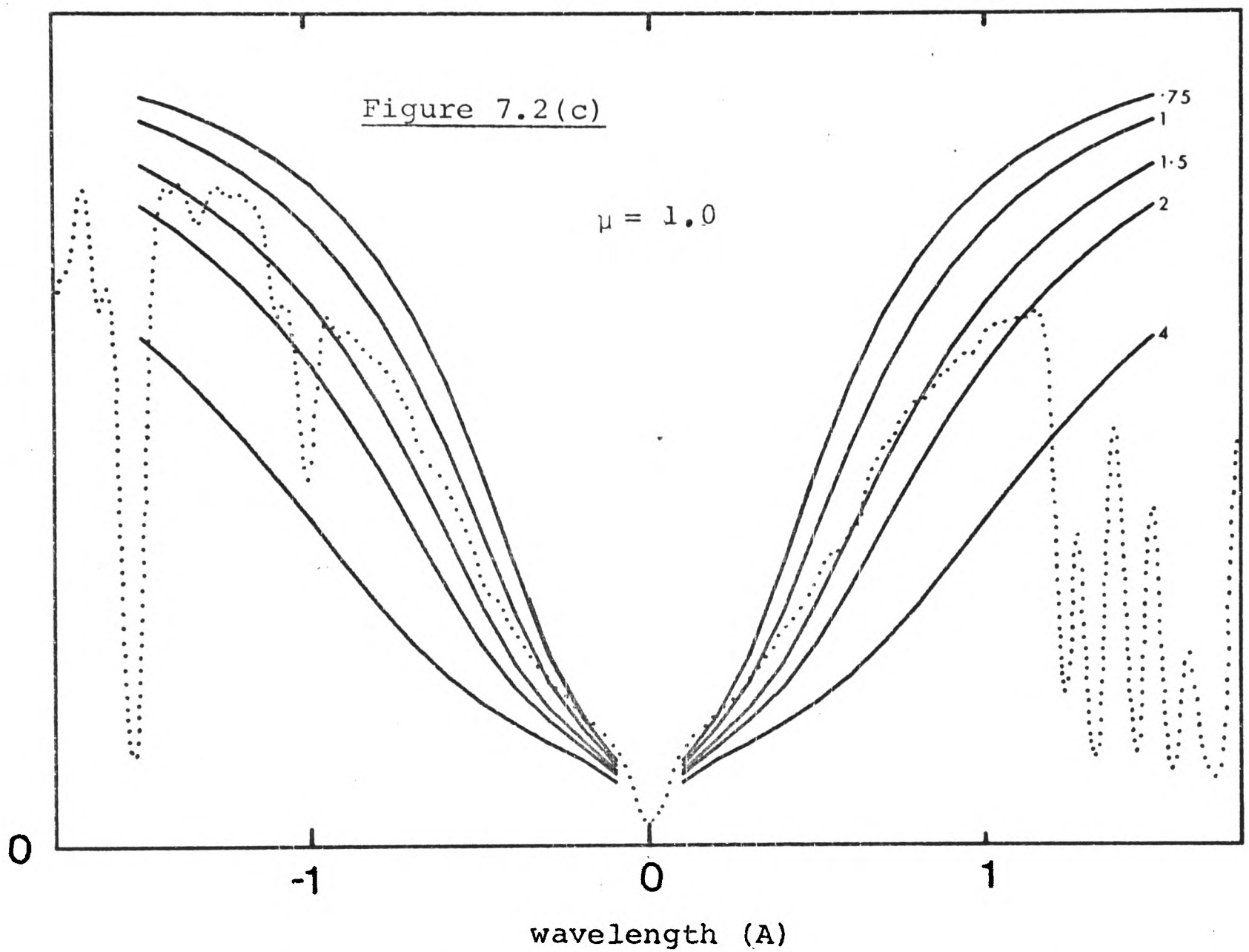


Profiles with "normal" continuum and opacities

Figure 7.2(b)

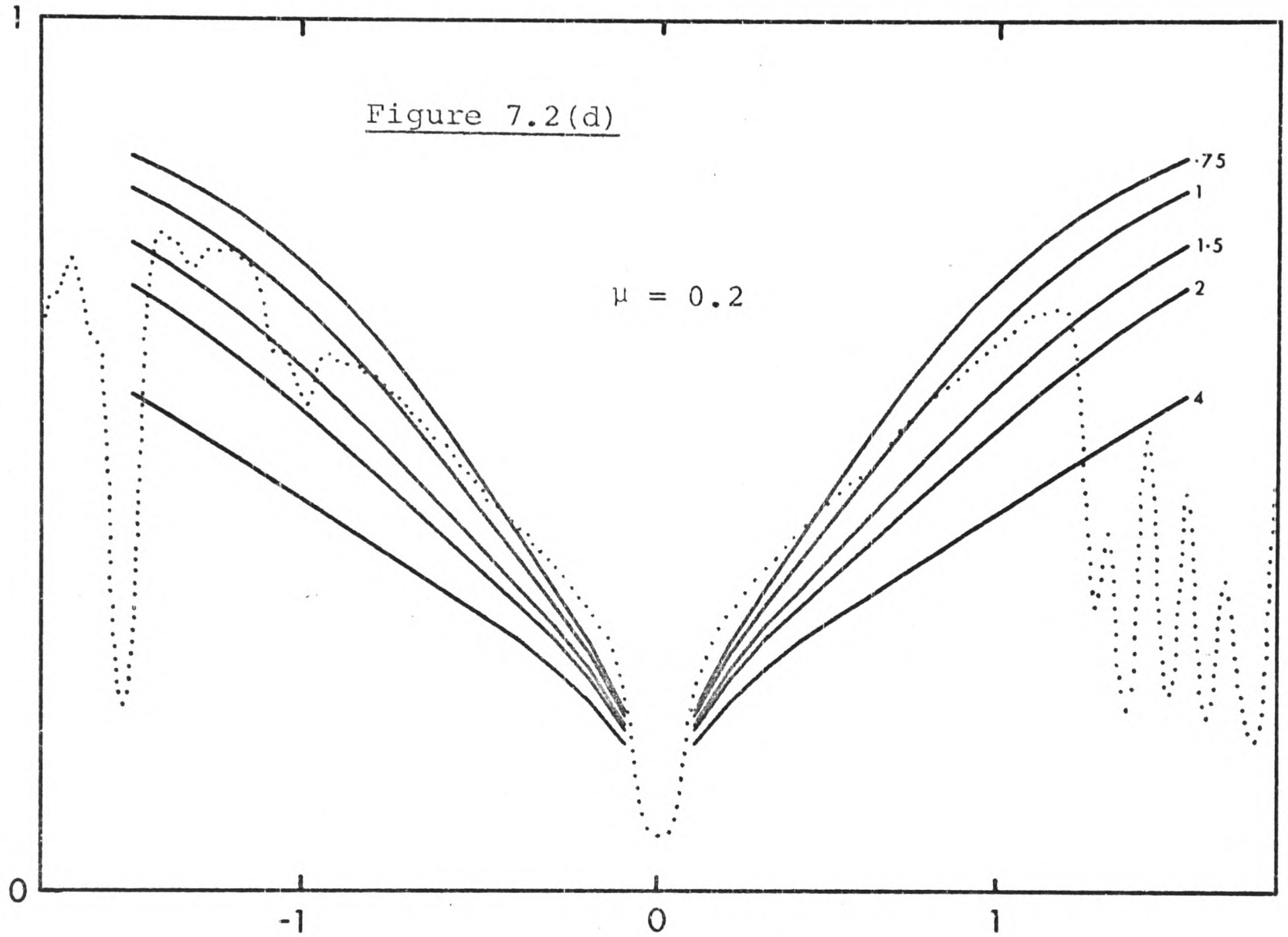


Profiles with "normal" continuum and opacities.

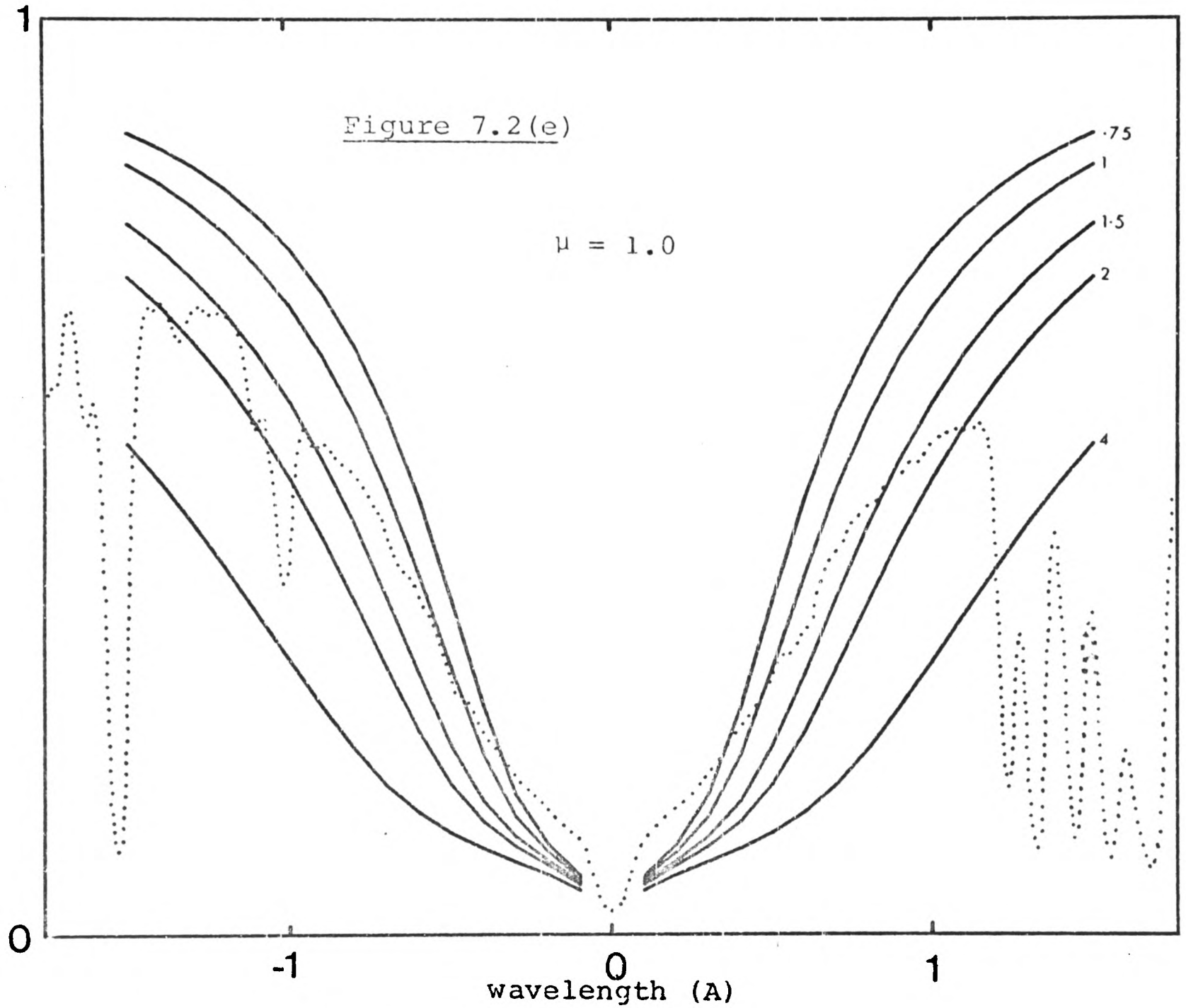


Profiles with "normal" continuum level but H^- opacity increased by a factor 1.75.

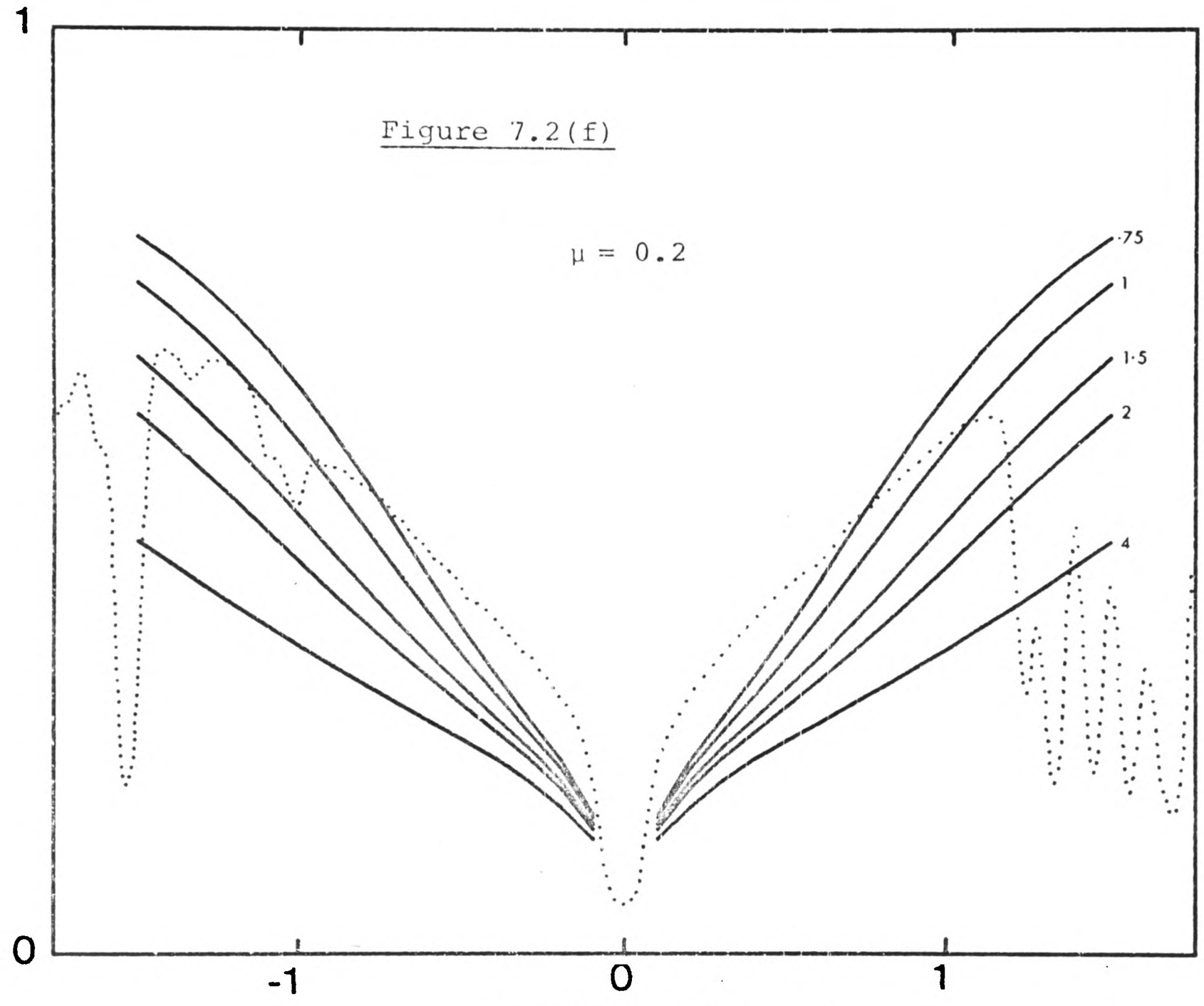
Figure 7.2(d)



Profiles with "normal" continuum level but H^- opacity increased by a factor 1.75.

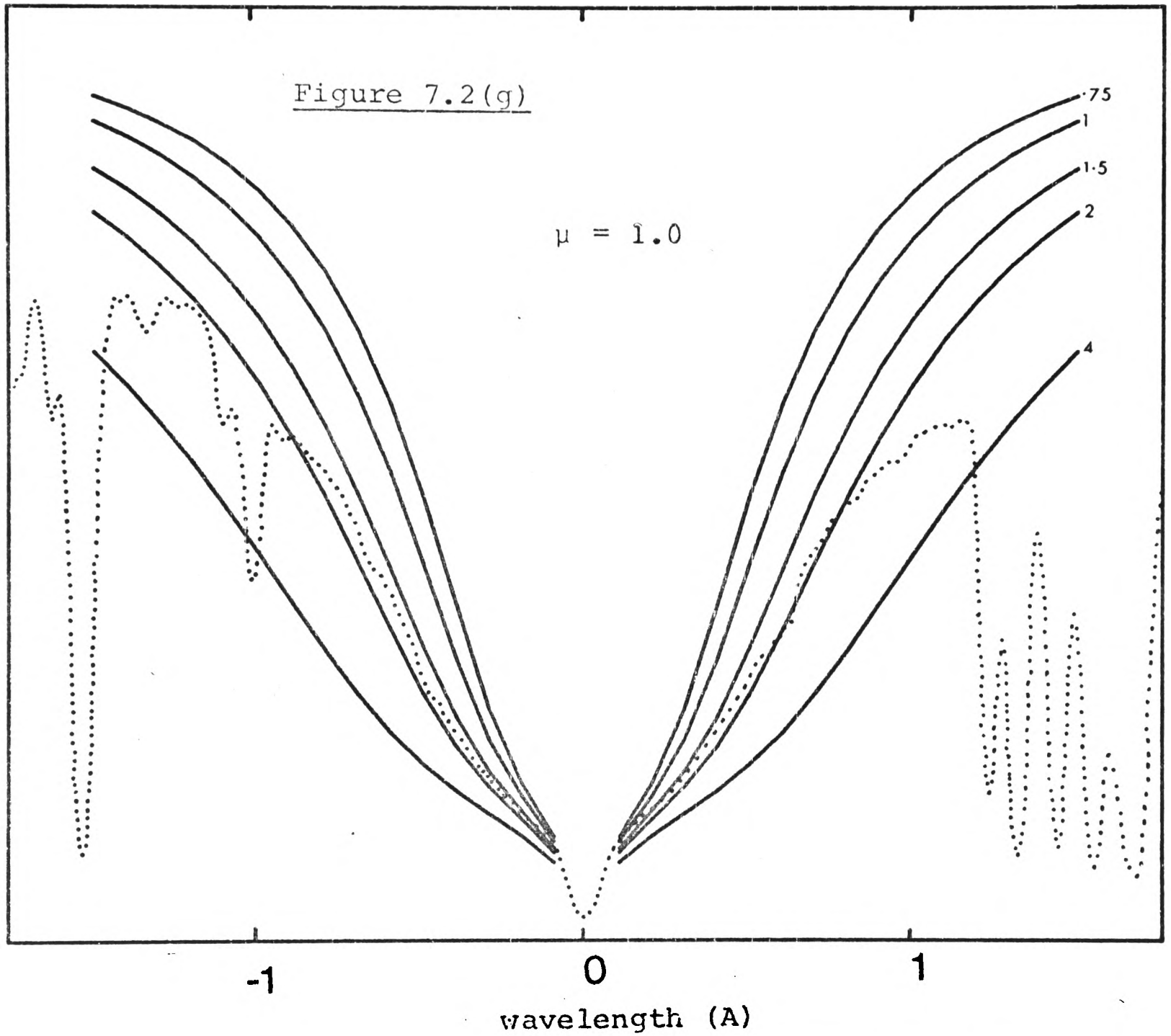


Profiles with normal opacities but the continuum level raised by 20 per cent.

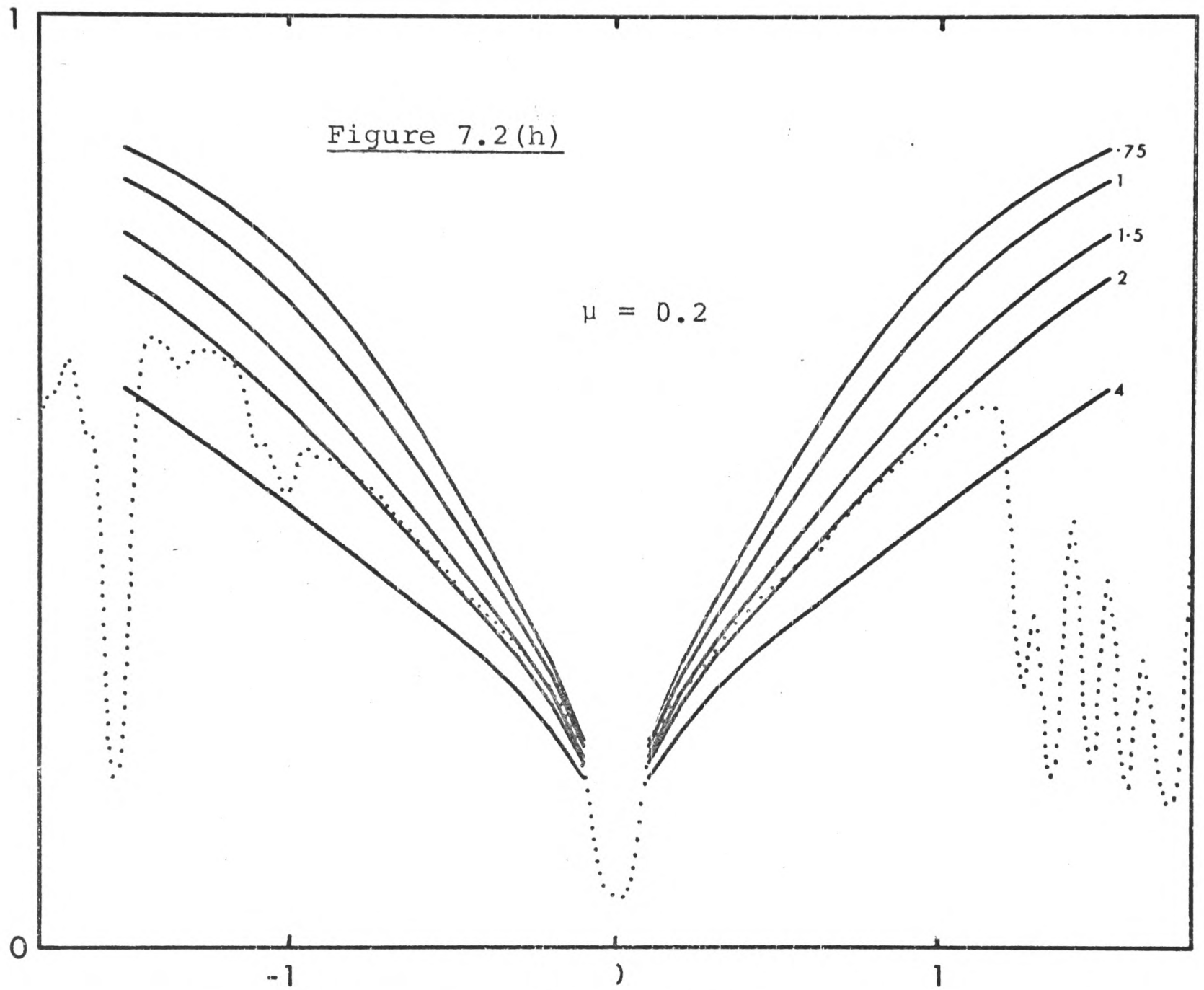


Profiles with normal opacities but continuum level raised by 20 per cent.

Figure 7.2(g)



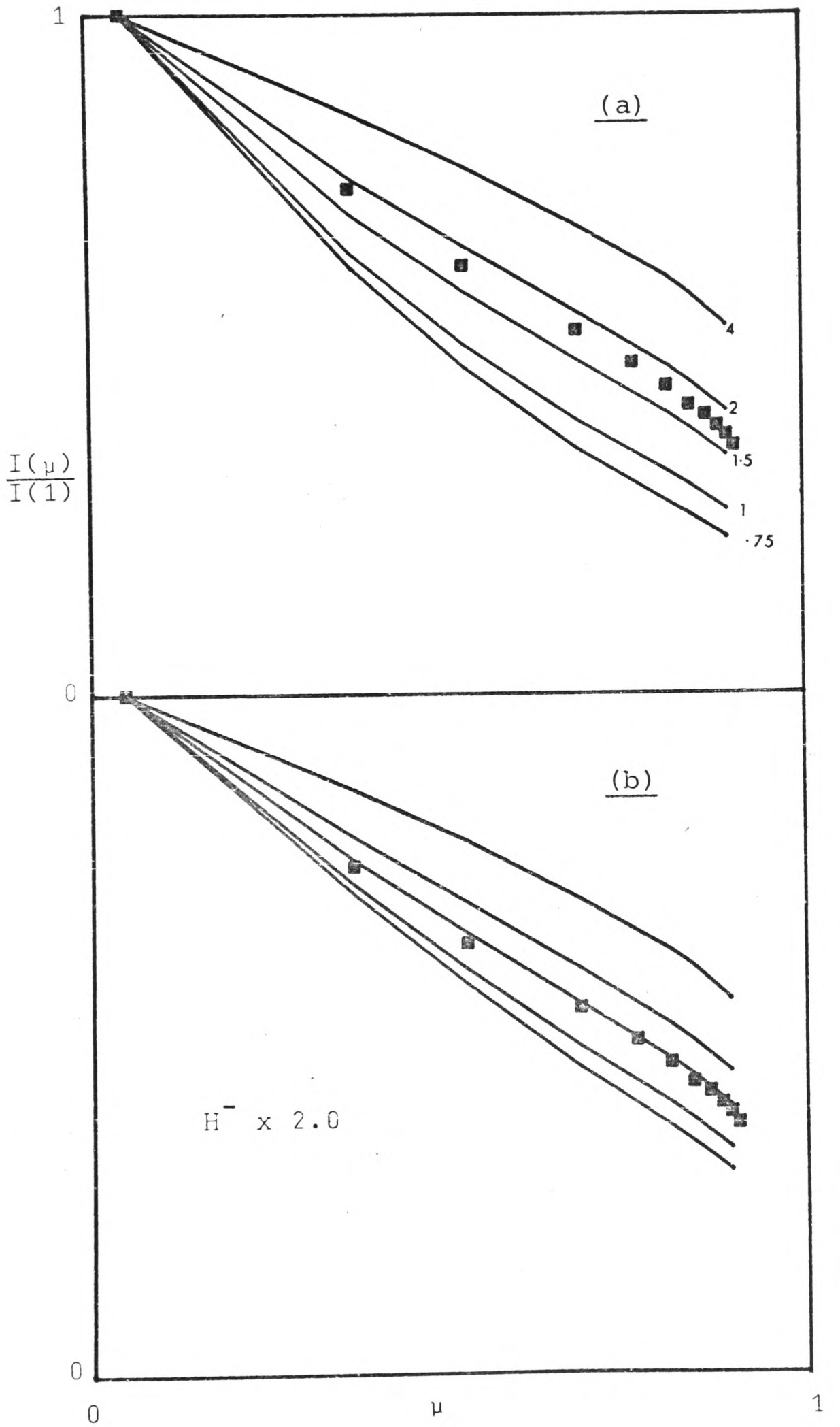
Profiles with opacities simulating a weak line "haze".



Profiles with opacities simulating a weak line "haze".

Figure 7.3

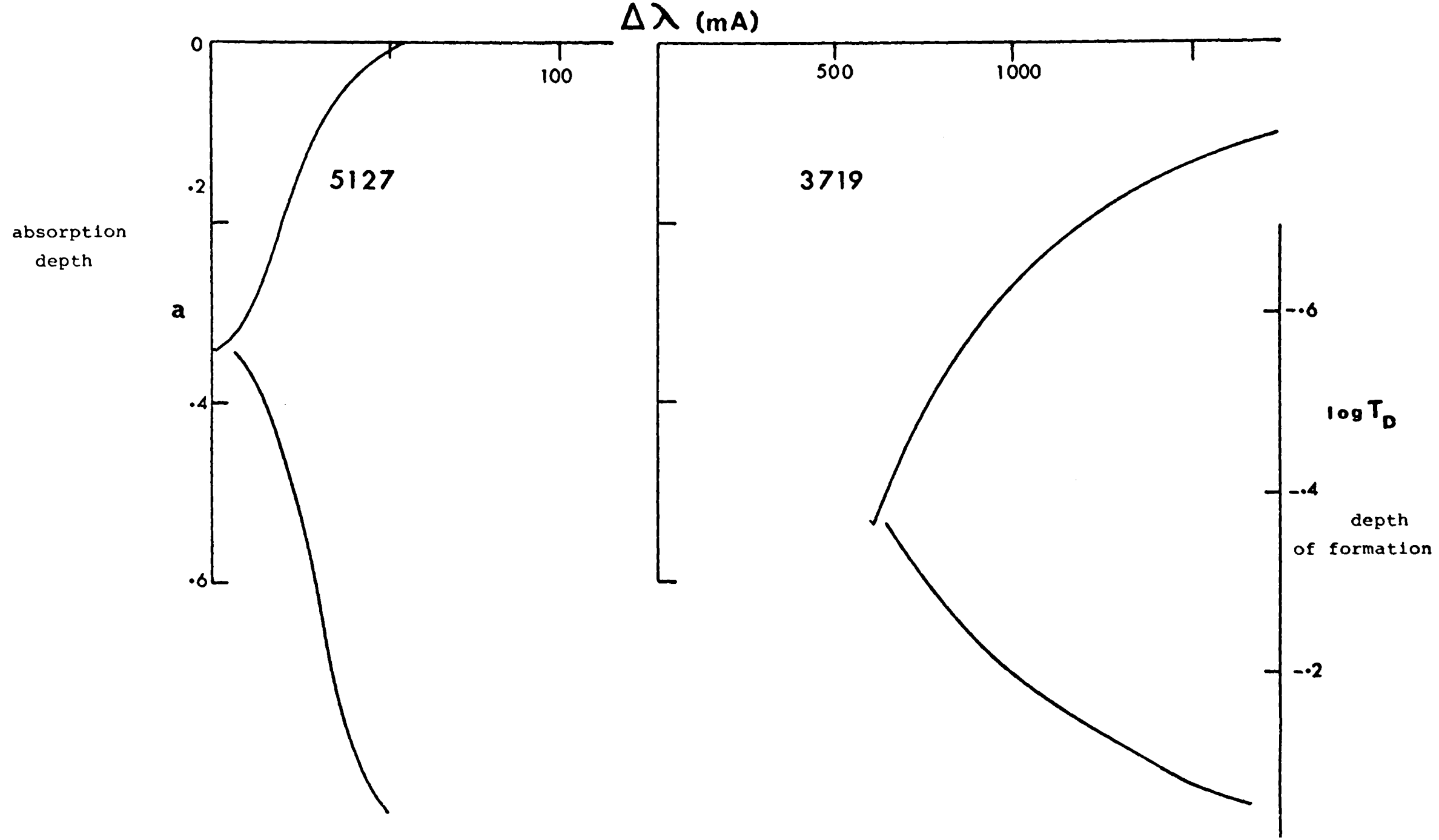
Centre-limb variation 0.5A from the centre of FeI 3719A from obsevations of Lites and White (1973) and calculations with HSRA model and (a) normal opacities; (b) opacity of H^- increased by factor 2.



$\Delta\lambda = \overset{\circ}{0}.5$ A

Figure 7.4

Profiles of FeI 5127A & FeI 3719A from the a^5D level, showing how the depth of formation of the weak and strong lines is very similar.



8. APPLICATION OF THE LABORATORY AND SOLAR MEASUREMENTS TO STELLAR SPECTRA

8.1 Introduction

The interpretation of the solar spectrum gave the damping constants needed (section 4.1) to measure the pressure in the atmosphere of a star from the wing of a strong line; and thence to find the surface gravity. In addition the results showed the precision of the measured oscillator strengths - indicated by the consistent abundance from different lines. These abundances differed from model to model but the derived damping constants were largely independent of the model. This was evidence of the advantages of the proposed method: because the abundance used to measure the C_6 values was derived from the weak lines from the same lower level the differences between the models in temperature and electron pressure were far less significant.

Given the measured values of C_6 and oscillator strengths, the method outlined in chapter 4 could be applied to the spectrum of a star. The practical application cannot however be quite so simple. Ideally there would be 5 discrete steps, as follows:

a. observations of the spectrum;

b. observations of the flux, or flux distribution, to determine the effective temperature;

c. a model atmosphere computed for that effective temperature [and, initially, assumed abundances and gravity];

d. abundance derived from weak lines;

e. comparison of observed and calculated profiles of strong line(s) and if they do not agree adjust gravity and the abundances and go to (c).

These operations are on all fours with the solar analysis. The element of iteration arises because where the solar model was defined and the C_6 value to be found, the position is reversed with C_6 known and the model (which includes log g) to be derived. As the model also depends on the assumed abundances, these also must be adjusted for changes in log g: as shown in section 2.5.3, the ionisation equilibrium, and hence the abundances derived from weak lines, can be very sensitive to the surface gravity. In principle the effective temperature might also be revised to take account of different gravities and abundances since these will change the predicted flux from the model. But the change is often very small and may be neglected if the starting value of log g is chosen carefully.

8.2 Choice of stars

The aim was to test the method rather than to measure surface gravities and derive masses or mass-luminosity ratios for a whole range of stars. Furthermore the whole emphasis on precision and freedom from uncertainty in the laboratory and solar measurements, and in the principle of the gravity determination, would be frustrated by poor observations of the stellar spectrum; or by inadequate model atmospheres. As good high-dispersion spectra are only available for bright stars, and model atmospheres not generally reliable for stars later than about K5, the choice of objects was restricted somewhat. However the parallel purpose of the work was to improve the reliability of the data for stars used as references for differential measurements: eg, differential abundance analyses. These considerations predetermined a very few bright, late type stars which are widely used as secondary standards.

Of these Arcturus (αB00) was chosen because of its wide use as a secondary standard; and because of the excellent quality of the published spectrum (Griffin, 1968); which is itself intended and used as a standard reference. Arcturus was also one of the few stars with accurate direct measurements, so that the full properties could be derived using the relationships in section 1.4. This explored the practical limitations of the ideal procedure discussed in chapter 1 but also established the importance of precision in the measured surface gravity in relation to other observations.

Arcturus was however a very severe test of the method and of the measurements made. The spectral type of Arcturus (K2III: see table 8.1) indicated:

a. the atmosphere of Arcturus is very much cooler than the sun's. The fraction of the iron atoms in the neutral state is therefore very much greater than in the sun, so that the lines of FeI will tend to be stronger. Changes in excitation

reinforce this effect for lines with low excitation potentials so that what were weak lines in the sun become correspondingly stronger in Arcturus' spectrum.

b. Arcturus is a giant star with, at a given optical depth, a pressure very much less than in a main sequence star such as the sun. The damping due to collisional interactions with hydrogen atoms is correspondingly small and difficult to measure.

8.3 Effective temperature and model atmospheres for Arcturus

Although any model atmosphere must take account of the final values of abundances and surface gravity, by far the most important determinant of the continuum flux is the effective temperature T_e. Conversely if T_e is measured from the flux the result is almost independent of gravity and abundance. The effective temperature can therefore be looked at separately.

8.3.1 Flux measurements

Effective temperatures from direct measurements use absolute fluxes and an angular diameter (equation 1.19). For Arcturus absolute fluxes had been given by Willstrop (1965), Komarov and Pozigun (1970) and Kharitonov and Knyazeva (1969) in narrow bands from 3300A to 9000A; and by Johnson (1963, 1965), Johnson et al (1966, 1967), Gillett et al (1968, 1971) and Gehrz and Woolf (1971) in wide bands (defined by filters in most cases) for wavelengths as great as 13 μ .

The observed flux must be corrected for the energy removed by absorption lines to find the true continuum. The blanketing corrections are very large for the many lines in the spectrum of Arcturus, especially at shorter wavelengths (less than 5000A). As there are deep, relatively narrow lines the convolution of relative intensity with the response across the band depends on the precise wavelengths observed, which are often not well-defined. Additional measurements were therefore made with the intention of finding the absolute flux incident at the earth from narrow, precisely known sections of the spectrum.

The further flux measurements were made on 5 nights during April 1973 at the Florence and George Wise Observatory of the University of Tel Aviv, Israel. The Cassegrain focus of the Observatory's Boller and Chivens 40" telescope was used to give an f/15 image at the entrance aperture of a scanning spectrometer designed and constructed at Oxford. Ellis (1974) has described in detail the observations and analysis for Arcturus but it may be helpful to record briefly the optical system (figure 8.1) and associated electronics (figure 8.2).

In operation the program star was imaged in the plane of the entrance aperture, which excluded other nearby objects and reduced the area of sky contributing background light. The size of the entrance aperture could be adjusted, according to seeing conditions, but the system was essentially a slitless spectrometer comprising a Bausch and Lomb grating, ruled at 600 mm^{-1} and blazed at $n\lambda$ = 16 000A, and two precisely figured off-axis paraboloids with focal lengths of 59.4 cm (camera) and 59.6 cm (collimator) in a Czerny-Turner arrangement. As observations were made in the second and third orders this gave dispersions of 12 A mm^{-1} and 8 A mm^{-1} respectively at the exit slits. The slits could be set to an accuracy corresponding to less than 0.15 A so the bandwidth was precisely defined. The response across that band was moreover essentially rectangular since the entrance aperture (ie the star's image) was always very much larger than the exit slit.

However the absolute wavelength of the band must also be known. This was measured from the position of the grating. A stepping motor rotated the grating to bring the required spectrum on to the exit slits, and the grating table was in turn linked to a potentiometer. This formed a potential divider for the standard and variable output to a ratio voltmeter with a resolution of 1:20 000. In this way the grating drive was isolated from the system determining its position; and when calibrated against lines of known wavelength, a setting accuracy of better than 1 A was achieved. The greatest uncertainty in the band measured was then the positioning of the stellar image in the entrance aperture. For this reason an eyepiece was included (not shown in figure) to examine, between observations, the entrance aperture and to adjust the telescope setting accordingly.

The final part of the spectrometer system imaged the exit slit on the photocathode of the detector: an EMI 9659A photomultiplier mounted in Peltier effect coolers to operate at a temperature c. - 20°C. In order to sort the overlapping spectral orders a set of filters was included in the light path. Unfortunately

an Ilford 621 filter was used to block the second order spectrum 5500-7500 AA when making observations in the range 3800-4500 AA from the third order. It was later found that this filter also transmits wavelengths beyond 6000A so that the observations were contaminated by light from the first order spectrum and, in the range 3800-4500 AA, could not be used.

Turning to the right hand side of figure 8.1, a spectrosil plate behind the entrance aperture passed a fraction of the incident light to a narrow band interference filter and second photomultiplier. This defined a constant bandwidth around 5200A which monitored changes in atmospheric transparency.

The associated circuits for the grating drive, grating position and photomultiplier power supply were mounted in a separate unit to reduce the weight on the telescope and the electrical coupling. The preamplifiers for the photomultipliers were however placed within their mountings, to reduce detection of spurious pulses.

The detector circuitry itself was a conventional pulse-counting system, duplicated for the two channels, and is simply shown in schematic (figure 8.2).

Because the response function of the telescope-spectrometer-detector combination could not be measured the fluxes were determined by comparison with a standard star with a known, absolute flux. α Leo and α Lyr were used as Hayes (1970) had presented accurate results for those stars and they were well placed for observations in Israel during April. The principle was to set the grating and exit slit to define the desired band; and then to measure the flux from Arcturus and from the standard star. Then, as the detector is linear, the ratio of the counts gives the ratio of the fluxes from the two stars incident on the telescope. In practice however the time taken to reset the grating and slits was so much less than the time to position a different star in the aperture that measurements

for a series of bands were made for first one star and then the next. Measurements were also made of the background sky illumination, and of the photomultiplier dark currents, so that there was an interval of an hour or more between the two measurements of the same band. Variations in the atmospheric transmission during this time would introduce errors in the flux ratio. However the monitor band provides a measure of this change and the first order effects can be eliminated by using only the ratio of the count for a given band to the count for the monitor channel, and by observing, say star A, then B, then A again: the mean ratio of the observations of A will then correspond to the conditions during the observations of B for linear changes in atmospheric conditions.

Finally the observed flux must be corrected for atmospheric extinction to give the absolute flux incident on the earth. However the effective temperature is determined from the flux distribution with greater precision than from the absolute value. As details of the interpretation of the observations have been given by Ellis (1974) and Blackwell et al (1975) the results are assumed here. The discussion in those references of the various flux measurements makes the following points:

a. the large blanketing corrections are reflected in the scatter in the results for wavelengths below 5000A;

b. between 5000A and 8000A the flux curve is defined consistently by the Oxford measurements, and by the values of Willstrop (1965), which differ significantly from the results of Kharitonov and Knyazeva (1968) and Komarov and Pozigun (1970);

c. the 13 colour photometry of Johnson et al (1967) does not agree well with the flux curve from more precise bands;

d. the flux is very poorly defined in the range 12 000 - 22 000AA.

These discrepancies are shown in figures 8.3 and 8.4; and account for the uncertainty in the total flux, found from integrating a smooth curve through the data to be $5.08 \pm 0.08 \times 10^{-12}$ W cm^{-2} (Blackwell et al, 1975).

8.3.3 Effective temperature from flux and angular diameter

The measured angular diameter (see table 8.1) must be corrected for limb darkening. Hanbury Brown et al (1974) give 10 per cent as the correction for the intensity interferometer, using the model atmospheres of Carbon and Gingerich (1969). But Blackwell and Shallis (1977) find a factor 1.12 is predicted by the theoretical blanketed models of Bell et al (1976). This correction is therefore uncertain and must be treated with caution; furthermore Worden (1976) quotes a result from speckle interferometry as 0."019 for a uniform disk, but 0."027 for a limb darkened disk - apparently a factor of 1.42.

Uncertainties in the measured diameter translate into very considerable uncertainties in the derived effective temperature. Thus Pease (1931) found 0."020 which gives T_e as 4419K with the above value for the flux. A 10 per cent correction makes this 0."022, and gives 4213K. Similarly the two values cited by Worden (1976) correspond to 3803K and 4534K respectively: Gezari et al (1972) find 0."022 which would also give 4213K but after 10 per cent correction to atrue diameter of 0."024 the derived T_e becomes 4035K.

The uncertainty due to the limb darkening correction is also independent of, and in addition to, the uncertainty in the measured angular diameter. Gezari et al (1972), for instance, quote the probable error as 0."003 so that the effective temperature, after correction to a true diameter, is 4035K (+277/-231K). With some allowance for uncertainty in the 10 per cent factor applied, the effective temperature is not determined with a precision of even 300K. The other measurements are given with even less precision, and have correspondingly greater uncertainties in the final effective temperature.

8.3.4 Effective temperature from the flux distribution

The shape of the flux curve apparently determines the effective temperature of Arcturus more precisely, although this method does rely on the use of model atmospheres. It is therefore necessary to seek models which are realistic representations of the real atmosphere. Line blanketing presents particular difficulty. Line-blanketed models by Carbon and Gingerich (1969), and Peytremann (1974) were used by Blackwell et al (1975) to compute the flux distribution which was then compared with the observed continuum curve. The comparison showed, for wavelengths less than about 5000A, discrepancies which were in excess of the uncertainty in the observed flux. As it is the flux at these wavelengths which is most sensitive to changes in T_e the comparisons do not define a precise effective temperature, and the models themselves become subject to some doubt. The models of Peytremann were superior to those of Carbon and Gingerich in approaching, though not reaching, the low flux observed at short wavelengths. But neither gave good agreement with the observed flux curve and this was reflected in the uncertainty in the quoted effective temperature: 4500K (+50/-120).

Line blanketed models were also given by Bell et al (1976) for a grid of values (T_e, g). The model for 4500K gave too great a flux at shorter wavelengths (Blackwell and Willis, 1977) (see figure 8.5). No models were published for temperatures between 4000K and 4500K but by scaling down the computed flux in the ratios found from scaled Carbon and Gingerich models at 4500K and 4400K an effective temperature of 4400K (+60/-30K) was derived. Nevertheless the flux curve deviated from that observed, and temperatures in the range 4300-4500K could not be excluded.

8.3.5 Adopted value of effective temperature

Ayres and Johnson (1977) suggested that the effective temperature derived as above by fitting the flux distribution is uncertain

because of the blanketing corrections; and because the models were not derived for the particular composition and gravity of Arcturus. A value of 4250K was preferred, derived from comparing the flux computed to include the line blanketing, using a line-blanketed model of Arcturus with the particular properties, (Johnson et al, 1976). This is very close to the effective temperature of 4260K ($\pm$50K) adopted by Mackle et al (1975) from comparisons of photometric data with the fluxes predicted by scaled solar models. However it is not clear whether the model of Mackle et al is flux-constant. Scaled models have, where the temperature change is large, the possibility of errors in $T(\tau)$. Gustaffson et al (1974) for instance found flux-constant atmospheres to be more than 100^{o} cooler for optical depths 0.1 - 1.0, which would require a higher value for T_e to produce the same flux as a scaled model. Figure 8.6 shows that there are similar differences between the temperature structure of the models of Bell et al (1976) and of Mackle et al (1975).

Other determinations tend to be less sophisticated and do not resolve the discrepant values. Williams (1971) and Van Paradijs and Meurs (1974) give 4338K and 4380K respectively from broad band colours; the latter authors also use the flux curve to find 4030K, though with the Russian data questioned above, and the variation of FeI line strengths with excitation potential to find 4370K. Earlier results are shown in table 8.2.

In all the above measurements there is great uncertainty because the flux depends on the particular model used, and there are large discrepancies even for the same effective temperature. As described in section 1.4 however Blackwell and Shallis (1977) have used the flux at infrared wavelengths which is almost independent of the model used. Their effective temperature was 4410 $\pm$ 88K, which is consistent with the values found from the flux distribution. In view of this an effective temperature of $4400 \pm^{60}_{80}$ is adopted hereinafter. Even so the greater

agreement with the value found by Blackwell and Willis (1977) an

uncertainty about the value of T_e must be borne in mind, especially when considering the values of log g derived from methods which are sensitive to the temperature structure.

8.3.6 Model atmospheres

Both the method outlined at 8.1 above and the arguments of Ayres and Johnson (1977) favour model atmospheres computed for the particular star and parameters being considered. However there are as yet no published programs for the construction of flux-constant, line-blanketed models. It was therefore necessary to use models from the grids published by various authors, and in view of their better agreement with the observed flux from Arcturus, the models of Bell et al (1976) were chosen. These were however available only for discrete values of (T_e, g), and from the effective temperature adopted and previous values of the gravity, the more likely models had T_e = 4000K, 4500K; log g = 0.75, 1.50, 2.25, 3.0; [A/H] = -0.5, -1.0.

Table 8.1

Arcturus: summary of basic data & measurements.

star:	Arcturus (αBoo)
	HD 124897
	HR5340
parallax:	0".092 ± 0.005 [1]
	0".09 [2]
angular diameter:	0".020 [3]
	0".022 ± 0.003 [4]
	0".026 ± 0.004 [5]
	0".019 [6]
	0".0201 ± 0.0010 [7]
spectral type:	K1III [1]
	K2III [2]
apparent magnitude:	$-0^m.05$ [1]

---

references: [1] Wooley et al (1970)
[2] Hoffleit (1964)
[3] Pease (1921, 1931)
[4] Gezari et al (19720
[5] Currie et al (1974)
[6] Worden et al (1976)
[7] Blackwell & Shallis (1977)

Table 8.2

Reported values of effective temperature of Arcturus.

author	T_e	notes
Kuiper (1938)	4074	total flux
Popper (1959)	4400	
Gasson (1966)	4720	excitation
Conti et al (1967)	4150	OI lines
Griffin & Griffin (1967)	4168	total flux
Williams (1970)	4280	
	4370	total flux
Warren (1971)	4300	mean
	4305	FeI excitation
Williams (1971)	4338	RIK colours
Simon (1971)	4250	
Linsky & Ayres (1973)	4250	
Paradijs & Meurs (1974)	4350	
Mackle et al (1975)	4260	
Blackwell et al (1975)	4500	
Paradijs et al (1976)	4290	
Johnson et al (1976)	4250	
Blackwell & Shallis (1977)	4400	

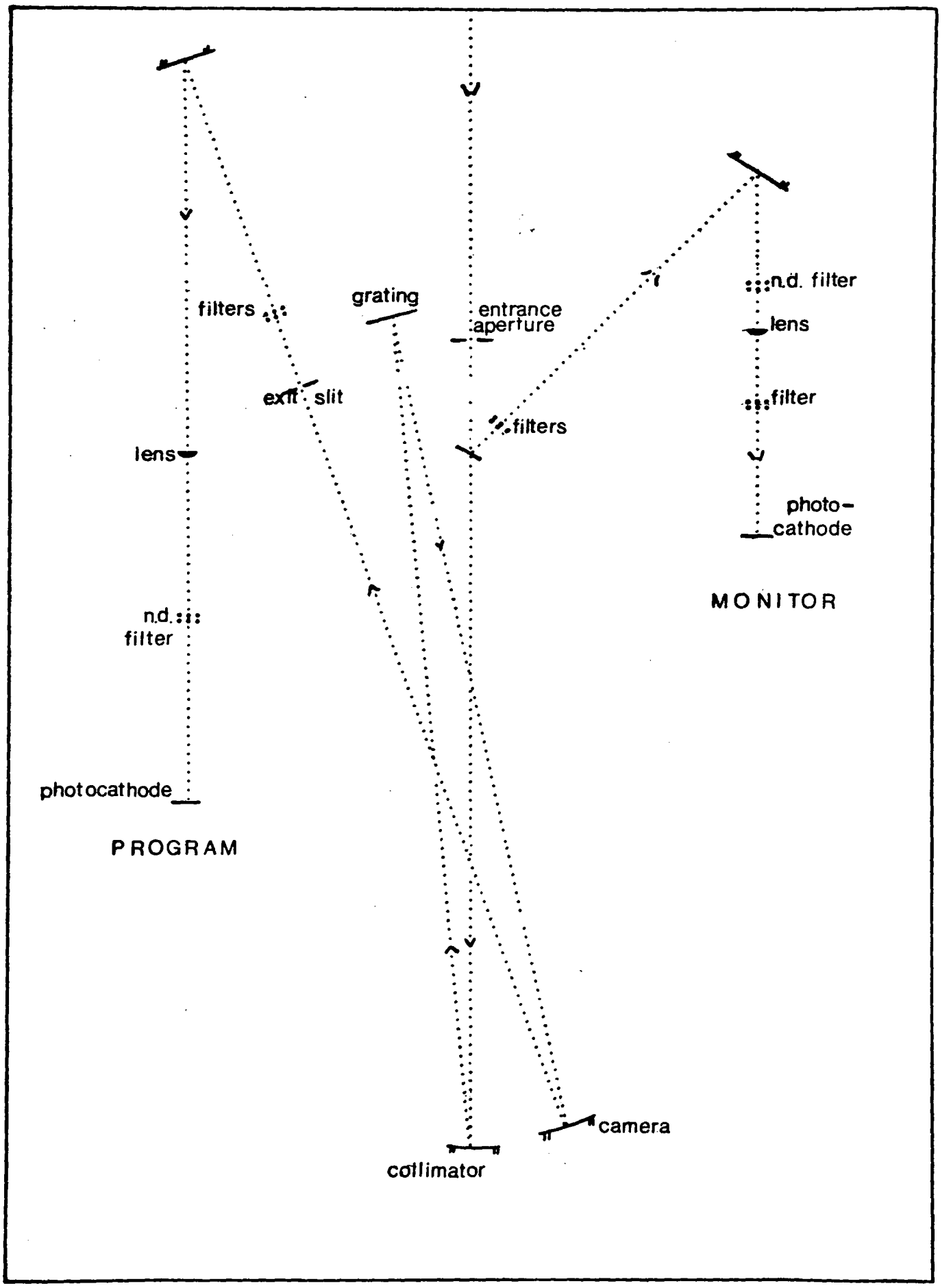


Figure 8.1

Spectrometer optical system (to scale).

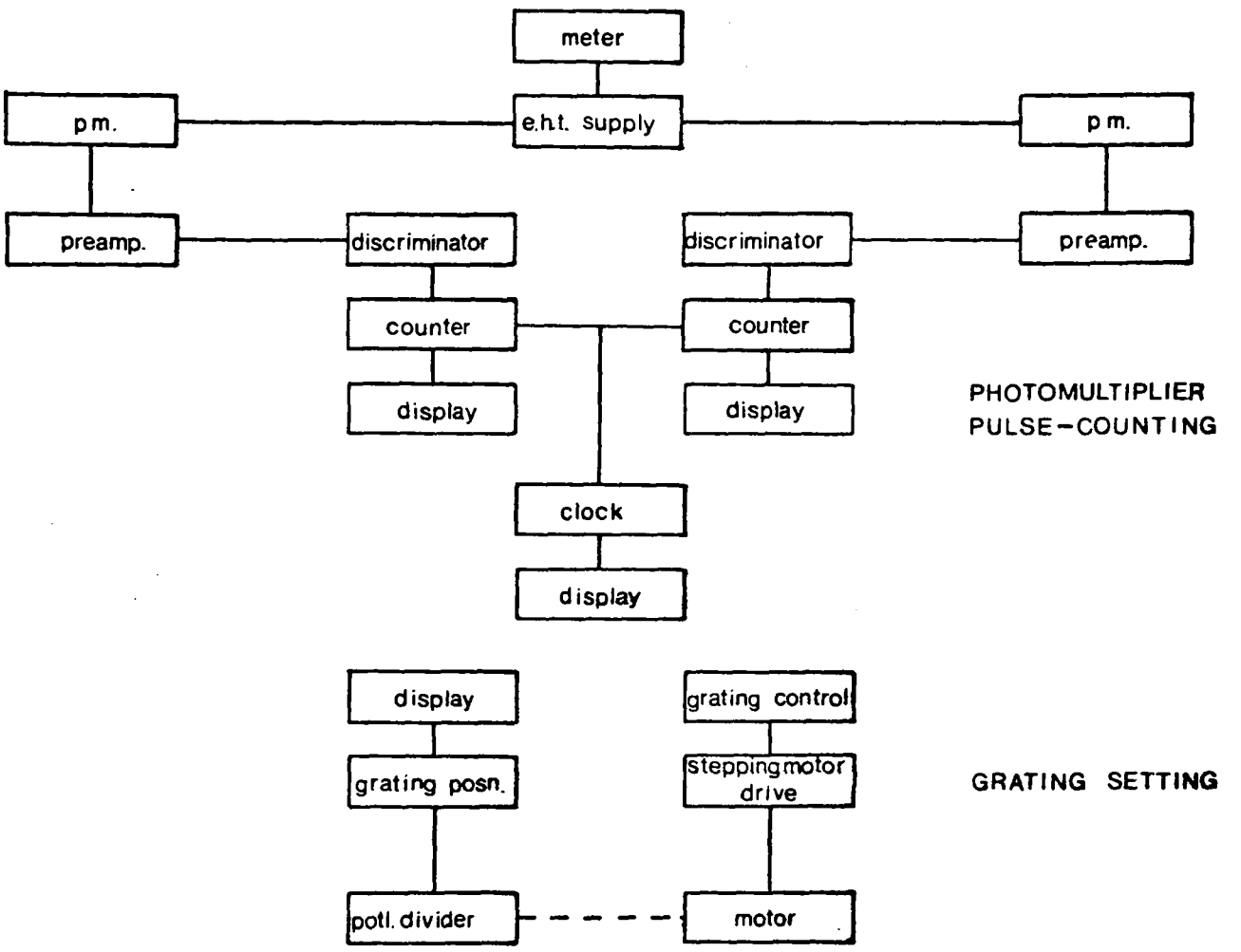


Figure 8.2

Schematic of units for spectrometer control
and pulse counting.

Figure 8.3

Observed continuum flux from Arcturus, from Blackwell, Ellis, Ibbetson, Petford & Willis (1975).

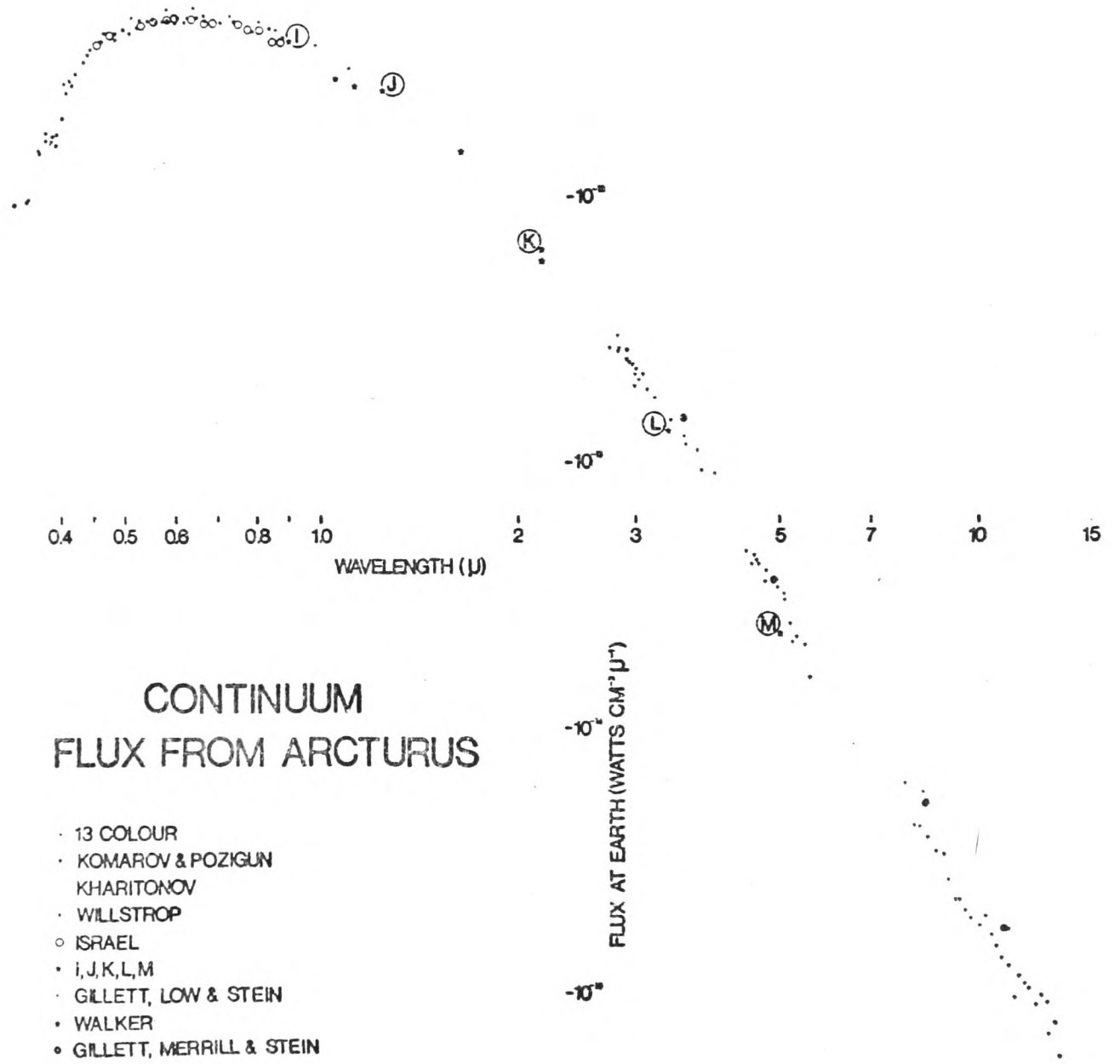


Figure 8.4

Observed continuum flux from Arcturus, from Blackwell, Ellis, Ibbetson, Petford & Willis (1975).

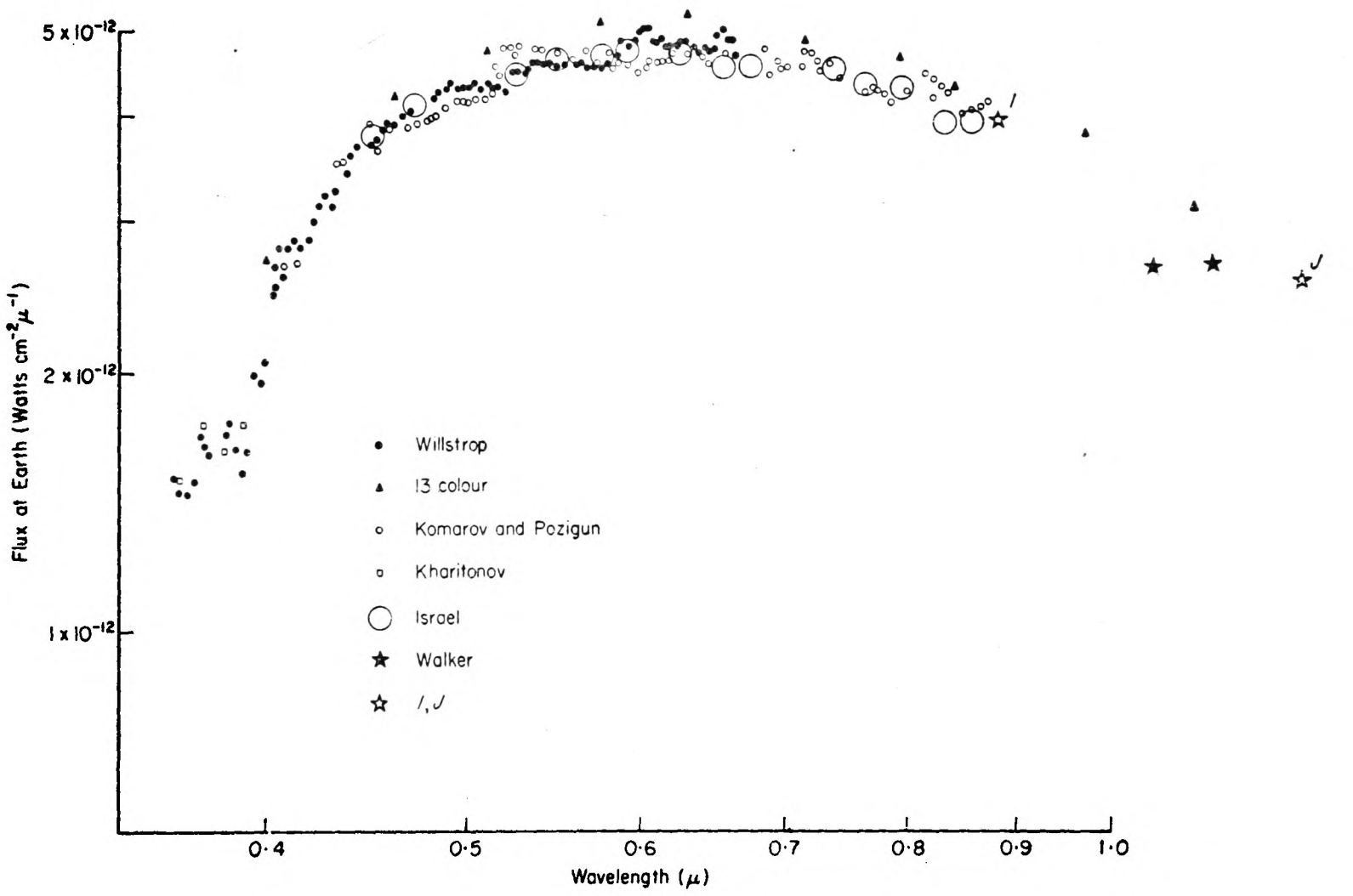
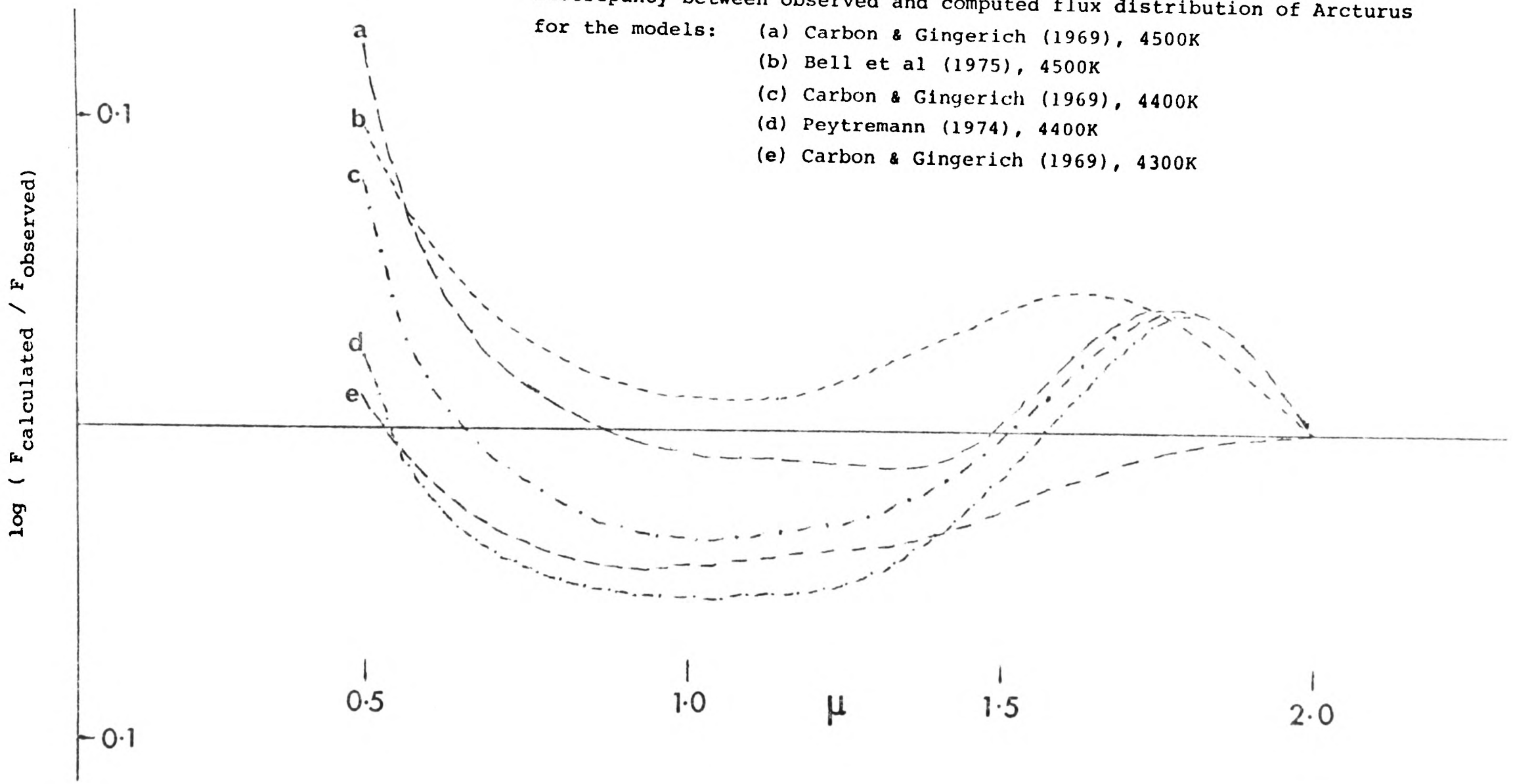
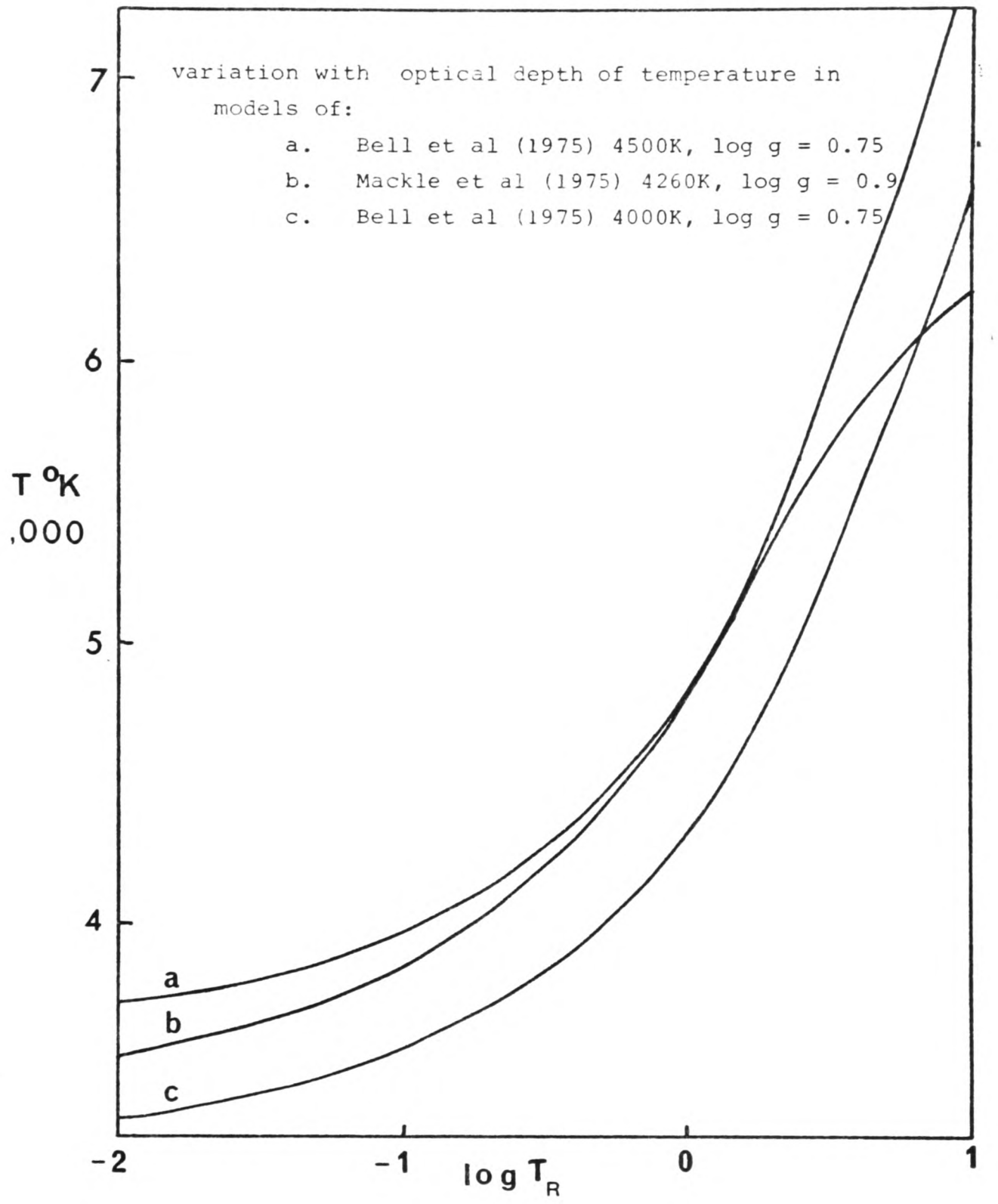


Figure 8.5



Discrepancy between observed and computed flux distribution of Arcturus for the models:
(a) Carbon & Gingerich (1969), 4500K
(b) Bell et al (1975), 4500K
(c) Carbon & Gingerich (1969), 4400K
(d) Peytremann (1974), 4400K
(e) Carbon & Gingerich (1969), 4300K

Figure 8·6



Mean (Rosseland) optical depth

9. INTERPRETATION OF THE FEI SPECTRUM OF ARCTURUS

9.1 Spectroscopic data

The observational data came entirely from the "Photometric Atlas of the Spectrum of Arcturus" (hereinafter "the Atlas") of Griffin (1968) which probably represents the limits of photographic detection. From the Atlas it was apparent first that the low excitation lines of FeI were far stronger than in the sun; that they were more heavily blended with other lines; and that the continuum was less well-defined, especially for wavelengths below 5000A: in the region of the strong ground state lines the continuum was perhaps no more than a plausible level. Each of the lines with a measured oscillator strength was therefore examined in the spectrum and reassessed in term of blends, both from visible lines and those suggested by line lists. Fifteen (15) lines were selected as reasonably clear and free from contamination (table 9.1).

It was apparent also that the lines in Arcturus were too strong to permit an abundance determination independent of microturbulence; and indeed that the microturbulence could not be measured accurately with only the lines used in the solar analysis. The smallest observed equivalent width in table 9.1 is 97 mA. From the discussion in section 6.1 this line would be sensitive to both microturbulence and damping in the solar atmosphere. Quantitative results for the sun cannot be applied to Arcturus but certainly the effect of microturbulence on the smaller thermal Doppler width in the cooler atmosphere would be at least as great.

It was therefore decided to consider the use of oscillator strengths derived from the strengths of lines observed in the solar spectrum. This might appear a major abrogation of the absolute precision demanded of the line data. But it was felt to be justified because:

i. the lines measured in the Oxford furnace had determined, for a given model photosphere, a very precise value of the FeI abundance;

ii. if lines were chosen with the same lower level as those used to measure the abundance, the effects of the temperature structure and of non-LTE populations would again largely be eliminated;

iii. the lines would be very weak in the solar spectrum, and therefore-

a. have equivalent widths essentially independent of microturbulence (and damping); and

b. have equivalent widths essentially proportional to the value of (log gfA): ie, the curve of growth correction would be very small.

This very last comment reflects the fact that the solar atmosphere was used as a "furnace" to derive the oscillator strengths relative to lines with absolute values, in the same way as the laboratory measurements. In practice this entailed measuring the equivalent widths of the weak lines at the centre of the solar disk from the spectra of Delbouille et al (1973), Brault and Testerman (1972) and from observations at the Gornergrat Observatory of the Department of Astrophysics, Oxford (Blackwell et al, 1969). Equivalent widths for these lines were then computed using the model atmospheres and the derived abundances and microturbulences for those models given in chapter 6. The value of log gf used in the computation could then be adjusted until the observed equivalent width was obtained, thus determining the oscillator strength on a scale defined by the absolute furnace measurements.

The lines and the measured oscillator strengths are given in table 9.2.(ii), together with the solar equivalent widths. In view of the uncertain equivalent widths of these very weak lines

the uncertainty in log gf may be as much as 0.1 dex. However they are all from the a^5F term, as is 5269A for which the damping was derived.

Tables 9.1 and 9.2 also give the measured equivalent widths in the spectrum of Arcturus. These were found by estimating the wings of lines which were blended and then planimetering the line in the Griffin Atlas. Published measures (Mackle et al, 1975b) were included to give mean values where appropriate. Griffin (1969abc) had demonstrated that the very broad, shallow wings in the instrumental profile of this spectrum lead to underestimates of the true equivalent width. Despite counter arguments (Warren, 1970; Blackwell et al, 1971), Mackle et al (1975a) quantify this effect as 5 per cent, increasing to 10 per cent where the blanketing reaches 25 per cent. The equivalent widths given here do not take account of this correction, and must be considered to have a corresponding element of uncertainty in addition to that introduced by noise and the continuum position.

Profiles of the strong lines were also examined in the spectrum. As already indicated only 5269A had a clear profile showing damping wings. However 4 of the strong lines in the blue region were considered to merit very preliminary investigation: 3679.9A; 3719.9A; 3722.6A; 3899.7A.

9.2 Abundance and microturbulence determination

As the gravity was to be found from the 5269A line, the abundance and microturbulence should also have been determined by lines from the same lower level. As before, however, this condition was relaxed to allow lines from the same lower term; and moreover three lines from the a^5D term. This was necessary because the number of lines would otherwise have been too few to exclude a spurious value of the microturbulence where errors in the equivalent widths and oscillator strengths happened to combine to give zero gradient with respect to line strength in the derived abundance.

The lines used in the abundance and microturbulence determination are given in table 9.2 with the values of log gf and the equivalent widths. The method was as for the solar measurements. Equivalent widths were computed for a range of abundance and microturbulence, and the microturbulence defined by the value which gave abundances from the individual lines with no gradient with respect to line strength. The abundance was then defined by the mean of those abundances. However, in the case of Arcturus, the model could not be chosen until the gravity was fixed, so that the determination was carried out initially for 6 of the models of Bell et al (1976) (see section 8.6).

Figure 9.1 shows how the derived abundance varied with equivalent width for the models with T_e= 4500, [A/H] =-0.5 and log g = 1.5, 2.25. Clearly the microturbulence and abundance are not defined as precisely as was the case with the sun (compare figure 6.3). Typically the standard deviation on the abundance from the 13 lines was about 0.15 dex, although the models with T_e= 4000K had somewhat larger uncertainties. The microturbulence and the abundances determined are given in table 9.3.

Although the abundance is determined largely by the 6 weak lines with "solar" log gf's there will be some contribution from the

other lines which include those from the 0.00-0.12 eV levels. However a second, independent determination used all the lines with more accurate, laboratory oscillator strengths and the 6 weak lines to derive the microturbulence; but only the abundances from the 6 weak lines were averaged to determine log A_{Fe}. This amounts to using all but the 3 lines at the foot of table 9.1 (6498A; 6574A; 6609A) for which the values of log gf measured in the furnace were subject to exceptional uncertainty.

The results of this second determination are illustrated in figure 9.2. The variation of abundances with microturbulence is qualitatively the same as in figure 9.1; and the values derived were consistently about 0.1 km s^{-1} greater - that is, 2.1 km s^{-1} for T_e = 4000K, 2.2 km s^{-1} for T_e = 4500K. However the abundance was determined only by the 6 weak lines. These are relatively insensitive to microturbulence so that the derived values were little different: less than 0.03 dex in every case.

9.3 Determination of gravity

9.3.1 The gravity from the profile of FeI 5269A

As in the solar work, the microturbulence and abundance derived from the weak lines were used to compute profiles of the strong line FeI 5269A in each of the models. But where before the damping coefficient C_6 had been varied until the observed profile was obtained, the aim with Arcturus was to vary the gravity in the model whilst keeping constant the damping coefficient determined from the solar spectrum. Because only the six models were available this entailed interpolation among the profiles (initially for a given value of T_e). This is less satisfactory than recomputing the model atmosphere, but fortunately the absorption depth in the wing of the line is determined by the damping and hence the pressure. As the pressure depends in turn on the gravity (the underlying argument of course behind the method) the absorption depth is, to a first approximation, proportional to the gravity. Or more usefully, log a varies almost linearly with log g. Thus even linear interpolation would be a reasonable approximation. With the three models, somewhat better profiles could be deduced for intermediate gravities, so that the interpolation is not considered to be a major source of uncertainty.

For T_e = 4500K the best fit was obtained with log g = 1.52 with a corresponding abundance 7.13; at 4000K the iron abundance and gravity were both lower at 6.45 and 1.18 respectively. Figure 9.3 shows the observed and computed profiles for the former values.

9.3.2 Uncertainties in the derived gravity

a. continuum position

The profile was fitted using the continuum adopted by Griffin for the atlas. This is set at the level of the higher points of the spectrum, and could not be placed lower without assuming very great errors in the spectrum: these are most unlikely. A

higher continuum level might be plausible. But "line haze" would be the additional opacity depressing the observed continuum and, as was seen in chapter 7, this cannot be dealt with properly by simply raising the continuum level. In any case the line is fitted by the observed profile down to quite great absorption depths, and taking account of the full profile a change of a percentage point or two in the continuum level changes the derived gravity by only some 0.05 dex.

b. damping coefficient

Errors or uncertainties in the damping could arise from the solar measurement of C_6, from the assumed theory, or from neglect of other contributions to the profile function. The solar determination gave log C_6 = 32.05 with an uncertainty of perhaps as much as 0.2 dex for the absolute value. This corresponds to an uncertainty in the damping of 0.08 dex or 20 per cent, which will in turn cause the pressure in the atmosphere which fits the observed profile to be uncertain by 0.08 dex. For the models in question this corresponds to an uncertainty in log g of about 0.12 dex. But this is <u>not</u> the conventional probable error as the value of C_6 was determined consistently with smaller uncertainty; and 0.2 dex is an estimate taking account of possible errors in the abundance, microturbulence and log gf's .

Errors in the assumed theory will be most important if they affect the temperature dependence of the damping, and hence both its variation with depth in the atmosphere and the value for the cooler atmosphere of Arcturus found from the damping constant derived from the solar spectrum. Such errors are likely as the $T^{-0.7}$ factor in the simple van der Waals theory is not borne out by more sophisticated treatments. However Holweger (1971) has shown that even with the Lindholm theory, which uses an interatomic potential giving a phase shift C_{12}/r^{12}, the error in the damping due to the use of the van der Waals theory is proportional only to $T^{-0.11}$. Taking the temperature in the atmospheres of the sun and Arcturus to be the effective

temperatures, 5770K and 4400K respectively, the damping from the van der Waals theory would have $T^{-}0.7$ terms in the ratio 1.21; with the error proportional to $T^{-0.11}$ this becomes 1.17. This difference of 3 per cent is unlikely to be important in the gravity determination.

Significant errors could however be introduced if the radiation damping was ignored. As indicated above, the radiation damping constant was computed from the relationship:

$$\Gamma = \sum_i A_{iU} = \sum_i \frac{8\pi^2 \nu^2 g_i f_{iU}}{mc^3 \cdot g_U}$$

where the values of the oscillator strengths were taken from the Oxford measurements, supplemented by the data of Kurucz (1974) and Corliss and Warner (1964) (corrected to the Oxford scale) where lines had not been measured in the furnace. The value derived for the z^5D_4 level was 1.24×10^7 s^{-1}. This is very much less than the damping due to H and He in the solar atmosphere, at the depths where the line is formed. In Arcturus though the pressure is lower and the radiation damping more important. It amounts to some 15 per cent of the damping in the model with T_e = 4500K, log g = 1.5; and for log g = 0.75 is almost 40 per cent of the total. As the value determined is probably accurate to within 10 per cent the error introduced by radiation damping is not great for the derived gravities. In atmospheres of lower surface gravity however the radiation damping would clearly be a very important contributor to the profile function; and would make the profile relatively

insensitive to the collisional broadening, and hence insensitive to the pressure and gravity. In recognition of this danger the computations of the line profiles included, as part of the FORTRAN program used (see Appendix I), a listing of the contribution to the total at each level in the atmosphere from radiation, Stark, van der Waals (hydrogen), and van der Waals (helium) damping.

c. abundance

The abundance determinations show an internal uncertainty of about 0.04 dex. There are of course many more factors which make the absolute abundance much less precise. But the abundance for the particular model and the particular excitation is apparently determined to that accuracy. The corresponding uncertainty in log g was about 0.08 dex.

d. model atmospheres

It is difficult to assess the extent to which the value derived for the surface gravity depends on the particular grid of models used in its determination. The effect of using an erroneous abundance of helium has been mentioned above. It would moreover be desirable to ascertain what residual sensitivity to the temperature structure of the models remained even with the abundance determined for the same lower level as the strong line. Unfortunately there was available no set of models comparable to those of Bell et al which reproduced at all well the observed flux distribution. Very tentative calculations were therefore made using models computed from the program of Peytremann (1974) and made available by Cayrel de Strobel (private communication) for T_e = 4500K, 4400K; log g = 1.0, 2.0, 3.0.

First the abundance for the Peytremann models was found. The results were in very good agreement with the determinations described above. For 4500K and log g = 3.0 there was less than 0.02 dex difference in the two abundances; and the microturbulence agreed within 0.1 km s^{-1}. At lower gravities the abundancies

diverged a little, but the discrepancy was no more than 0.1 dex for log g = 1.0. The derived gravity however showed a more substantial difference: the value derived from the models with 4500K was 1.40 - ie 0.12 dex lower than from the Bell et al models. Without full details of the Peytremann models it was not possible to identify with confidence the cause of the different gravities but it appeared to arise from different opacities in the models, corresponding perhaps to the different electron pressures.

In the same way the abundances used to construct the model will affect the gravity derived. As Bell et al gave models for different values of the relative composition, [A/H], this could be examined within the single set of models. For example, the models used for 4500K had [A/H] =-0.5 which is consistent with the derived iron abundance of 7.13 (of solar values in chapter 6). Models with [A/H] = -1 on the other hand gave abundances lower by almost 0.1 dex; and further lead to changes in the derived gravity which were, for some values of (T_e, g), as much as 0.25 dex.

It is perhaps useful to look at this result in some detail as it provides a solid example of the effects of changes in the model atmosphere on the FeI lines. From chapter 2, a higher abundance of metals increases the electron pressure, and hence the continuous and line opacities, at a given temperature. The effect on weak lines therefore tends to be self-cancelling. But the gas pressure for a given optical depth will decrease. For the four models with T_e = 4500K; log g = 1.5, 2.25; [A/H] = -0.5, -1.0, and for optical depths around unity this amounts very broadly to:

$$\left.\frac{\delta \log P_e}{\delta \log g}\right|_{T_e,[A/H]} \sim 0.35$$

$$\left.\frac{\log P_g}{\log g}\right|_{T_e,[A/H]} \sim 0.6$$

$$\left.\frac{\delta \log P_g}{\delta [A/H]}\right|_{T_e,\ \log g} \sim 0.4$$

which suggests

$$\left.\frac{\delta \log g}{\delta [A/H]}\right| \sim 0.6$$

That is, the use of a model atmosphere with [A/H] = -1.0 rather than -0.5 would give a gravity too low by as much as 0.3 dex.

e. unresolved blends

Figure 9.3 shows that 5269A is blended in its wings with other lines. These could however be allowed for when drawing the position of the profile observed. Lines which are not resolved cannot be treated in the same way, and might lead to an over-estimate of the line strength. The derived gravity would then be too high. From the line list and oscillator strengths of Kurucz and Peytremann (1975) however it would appear that the known contaminants of the line have negligible effect (save of course for the lines clearly visible in the spectrum).

Taken together the above uncertainties admit some possibility of very large errors in the derived gravity. However the probable error is estimated to be no more than 0.10 - 0.15 dex.

9.3.3 Derived gravity from strong "blue" lines

The results for the strong lines in the region 3700-3900AA are given here to illustrate the possibilities for further work rather than to provide a measure of the surface gravity of Arcturus. Notwithstanding the very great uncertainty in the

continuum position, and the great blanketing corrections, it was possible to proceed by way of an analysis similar to that applied to the solar spectrum using a simulated "line haze". First the continuum flux for wavelengths near the lines was taken from the observations. As the absolute flux was not needed this was normalised to the flux at 2μ . The same simulated line opacity was then included in the model atmosphere and adjusted until the computed fluxes were in the observed ratio. (Of course the line haze affects only the flux at short wavelengths.)

Secondly profiles were computed, using the abundances and microturbulent velocities derived above, for the 4 lines which appeared to offer tractable profiles in the Griffin Atlas. These were in no case free from substantial blends but one, FeI 3722.6A, is particularly affected by the wing of FeI 3719.9A. As the latter was one of the lines being examined, its damping constant was known from the sun. The profiles of 3722.6A were therefore computed with the additional opacity due to the 3719.9A line included in the model atmosphere: ie, a very elementary form of spectral synthesis was applied.

As a preliminary investigation only, the profiles were found only for the models with T_e = 4500K and [A/H] =-0.5. The lines will however be no more susceptible to changes in temperature than the 5269A line although the correction to the model opacity would be very much smaller at the lower effective temperature. However, the results for the 4 lines (given in table 9.4) must be seen as no more than an indication that they are not inconsistent with the gravity derived from 5269A. The profiles adopted to fit the observations are shown in figure 9.4 and demonstrate how uncertain the measurements must be.

The lines are remarkably insensitive to the correction needed to fit the observed flux, at least in comparison with their sensitivity to the surface gravity. In figure 9.5 for example the computed profile of 3719A is shown for log g = 1.5 and 2.25; and for differences in the additional continuum opacity

amounting to 25 per cent in the flux. However results from these lines cannot be viewed with confidence until (i) the theoretical models are better able to reproduce the low fluxes observed at short wavelengths and (ii) a more sophisticated spectrum synthesis is used to take account of the blends in the wings of the lines. Care will also need to be taken in the use of these lines at low gravities since their radiation damping constants are larger than for 5269A, whilst the value of C_6 - and hence the collisional broadening - is much the same.

9.4 The surface gravity, FeI abundance and microturbulence of Arcturus

9.4.1 Measured values

The calculations were carried out with the atmospheres with effective temperatures of 4500K and 4000K. With the value adopted in chapter 8, 4400K, the values given in table 9.5 were given by interpolating. This confirmed that the method used to determine gravity was insensitive to the temperature adopted, as $d \log g / dT_e = 0.07/100K$. The uncertainty corresponding to that of the effective temperature is then only (+0.04/-0.02). In view of the other uncertainties discussed above though the accuracy claimed is 0.15.

The FeI abundance is more sensitive to temperature, as expected from changes in the ionisation equilibrium. The gradient is $d \log A / dT_e = 0.14/100K$ giving for the adopted value 6.99 (+0.08/-0.04). In view of the preliminary oscillator strengths and the few weak lines the uncertainty quoted is again greater: the iron abundance derived solely from the low excitation lines of FeI is 6.99 ± 0.15.

As the microturbulence was insensitive to changes in the effective temperature the value adopted is determined principally by the lines used. An uncertainty of 0.2 km s^{-1} is therefore attached to the adopted value of 2.1 km s^{-1}.

9.4.2 The surface gravity

The adopted surface gravity, $\log g = 1.45 \pm 0.15$, agrees well with the range 1.7 - 2.0 given by Griffin and Griffin (1967). Upson (1973) adopted 1.7 - 1.9; Gustaffson et al (1974) proposed 1.9 ± 0.2; van Paradijs and Meurs (1974) determined $\log g = 1.9 \pm 0.2$. However these values usually relied on approximate methods to find the gravity which gave the same abundance from neutral and ionised lines. This ionisation equilibrium is of course sensitive to temperature. Van Paradijs and Meurs, for

instance, found their derived gravity had d log g / d θ = 13 so that a change of, say, 4400K to 4460K would change the measured value by about 0.2 dex. This result and the measured gravity rested though on a differential curve of growth analysis with respect to α Tau.

In contradistinction Mackle et al (1975ab, hereinafter MHGG) derived a value of 0.9 $\pm$ 0.35 from a detailed model atmosphere analysis which (i) used models constructed for the particular effective temperature and abundances proposed for Arcturus and (ii) calculated the equivalent widths of individual, observed lines in order to derive the corresponding abundance. The MHGG value would therefore appear to be the most precise application of the ionisation equilibrium method, and more reliable than the earlier less rigorous results. There are however four factors which may account for the discrepancy between the value found herein and the MHGG result.

The first is the intrinsic sensitivity of ionisation equilibria to the effective temperature. MHGG used the ratios of FeI:II, TiI:II, CaI:II, and CrI:II to find that the observed line strengths were reproduced by a unique set of abundances for pairs of values (T_e, log g) of (4200K, 0.6), (4300K, 1.1), (4400K, 1.5). Their adopted temperature 4260K then fixes log g = 0.9. But if 4400K was used, as here, the value would be 1.5 in very good agreement with the 1.45 found from the FeI 5269A wings. On the other hand, the value from this work would decrease by only 0.1 to 1.35 if 4260K was used. The discrepancy can therefore be removed by the hypothesis that MHGG used too low a temperature, but not by decreasing the value adopted herein.

Second the ionisation equilibrium was assumed to be in LTE and MHGG cite the results of Cowley and Lites (1974) to support this assumption. But these results did not include stars with the low gravity of Arcturus. Ramsey (1976) has questioned the assumption of LTE in Arcturus and Ayres and Linsky found that non-LTE was inadequate, a comment supported by the work of Smith (1974b) which reported observable departures from LTE in the FeI spectrum of Arcturus.

Third the differential analysis with respect to the sun neglects the possibility of non-LTE effects there, effects which are predicted by inter alia Athay and Lites (1972); Lites (1972, 1973); Smith (1974a); Auer and Heasley (1976).

Fourthly the gravity derived from the ionisation rations depends also on the temperature structure. Ayres and Johnson (1977) showed that the MHGG model departs from a flux-constant, line-blanketed model (Johnson et al, 1976) in much the same way as in figure 8.6, so that the lines formed at different depths are differentially affected by the temperature error.

Ayres and Johnson (1977) pointed out that the use of weak lines to determine the ionisation equilibrium introduced many uncertainties (eg measurement of weak lines; turbulence; damping) and proposed a method using the ratio of the absorption in the wings of CaI 4227A and CaII (H) which is sensitive to gravity through the ionisation equilibrium and van der Waals damping. A detailed atmosphere for Arcturus (Johnson et al, 1976) was used with Te = 4250 $\pm$ 100K to obtain log g = 1.6 $\pm$ 0.2. But sensitivity to temperature persists in this method and the gradient with respect to effective temperature was found to be 0.25 / 100K. For 4400K then the derived gravity might be around 1.9 $\pm$ 0.2 which is not consistent with 1.45 $\pm$ 0.15. If 4250 is assumed for the method applied here the gravity becomes 1.35 $\pm$ 0.15, which is consistent with the value of Ayres and Johnson. Although this might indicate, contrary to the comparison with MHGG, that the lower temperature is more likely, there are fundamental uncertainties in the method used by Ayres and Johnson. The relative oscillator strengths are uncertain by some 10 per cent; 0.1 dex in the derived gravity is their estimate of the uncertainty in the line formation theory; and the damping constants, determined from the solar spectrum, introduce further possibility of error. Moreover the method assumes LTE.

In conclusion it is therefore suggested that the results from both weak and strong line methods relying on the ionisation equilibrium cannot be assessed fully unless and until the effective temperature is determined more firmly. Even if the temperature is fixed, the effects of non-LTE need to be examined in greater detail before the results of assuming LTE can be adopted with confidence. The results of the method proposed in chapter 4 and applied herein to the FeI line 5269A are however insensitive to the temperature used; and are independent of the assumption of LTE for the ionisation or for the degree of excitation to a particular term.

9.4.3 Microturbulence and FeI abundance

The microturbulence found is 2.1 $\pm$ 0.2 km s^{-1}, consistent with the 2.0 used by Warren (1970), Simon (1971) and Upson (1973). Griffin and Griffin (1967) and Gustaffson et al (1974) found 2.1, as did Ellis (1974) from TiI lines. Van Paradijs and Meurs (1974) give 2.2. Sikorski (1976) used the Goldberg Unno method to establish a depth-dependent microturbulence with 2.0 and 2.5 km s^{-1} at optical depths 0.1 and 0.001 respectively. Stenholm (1977) proposed 2.5, 1.5, and 1.2 km s^{-1} at 1, 0.1, and 0.01. As the low excitation lines are formed deep in the atmosphere these models seem consistent with the value found. MHGG found 1.8 km s^{-1} from lines of Fe, Ti, and Ni but, as shown below, this low value may result from the temperature adopted. (In any case Smith (1974b) has found that non-LTE effects introduce errors of 0.2 km s^{-1} into the microturbulence derived from some FeI lines, which may be relevant to some of these determinations.) Mount et al (1975) found 2.5 $\pm$ 0.2 from a non-LTE analysis of the CN 3883A system, close to the LTE value 2.4 $\pm$ 0.14 for CN 8000A (Day et al, 1973).

Abundances for Arcturus have usually been derived with respect to the sun: eg Van Paradijs and Meurs (1974) give [Fe] = -0.51 and Gustaffson et al (1974) -0.61. Adopting a solar abundance of 7.5 these become absolute abundances of 6.99 and

6.89. The abundance found above from the weak, low excitation FeI lines was 6.99. The MHGG abundance was [Fe] = -0.70 $\pm$ 0.08 but their analysis was with respect to the HOLWEGER model and the solar abundance found herein for that model was 7.66, to give 6.96 for Arcturus. Unfortunately this agreement of the separate values is probably spurious: the determinations used different temperatures which should give different abundances.

No sensitivity to temperature was given for the reported values. It was therefore decided to use the equivalent widths given by MHGG to look at the effects of using a value nearer 4400K. This turned out to reveal further evidence for a higher temperature.

295 FeI lines were used by MHGG, and data included the equivalent widths in the sun and Arcturus; and the values of [Fe] derived for each line. These differences showed no systematic trend with equivalent width in either the sun or Arcturus, reflecting the correct microturbulent velocities. There was however a very distinct variation with excitation potential (figure 9.6). The difference between the low and high excitation lines suggested too low a temperature had been used for Arcturus, though the lines with higher excitations are also weaker and therefore effects of microturbulence will not be equal at all excitations. Non-LTE in the sun or Arcturus might also be a factor. But it was felt that temperature effects were more plausible. An order of magnitude correction was therefore found from the mean abundance differences over ranges of excitation potential (see table 9.6). The mean difference for a 4 eV difference in excitation potential was 0.21 dex. Supposing this was due entirely to an error in T_e, and moreover that T_e determines the excitation, then:

$$\Delta[Fe] = -4 \cdot \Delta\theta$$

$$\theta + \Delta\theta = 1.18 - 0.05$$

$$= 1.13$$

and $$T_e = 4460K$$

It would be wrong to give any emphasis to this result alone. There was hoever at least qualitative confirmation from detailed re-analysis of the MHGG data. This was carried out using a model atmosphere with (4400K, 1.0) derived by Ellis (1974) by scaling the models of Carbon and Gingerich (1969), and consisted essentially of repeating the MHGG work: ie, equivalent widths were computed for the sun and Arcturus to find values of log gfA and the differences taken to define [Fe]. This was repeated for different microturbulent velocities until the derived abundance difference was independent of equivalent width. The result was a microturbulence of 2.0 km s^{-1} and abundances which varied with excitation potential but in the opposite sense, (see table 9.6).

With this very preliminary model atmosphere there can be no firm conclusion. But the very approximate calculations appear to agree with the temperature 4350K found by van Paradijs and Meurs (1974) from the variation with excitation of the FeI lines. And the MHGG model clearly had not reproduced the ionisation and excitation equilibrium of FeI.

Turning to the actual value of the abundance, the MHGG list included 57 lines with equivalent widths less than 25 mA in Arcturus. It is suggested that the abundance determined from these is more likely to be free from uncertainties in the microturbulence and damping constants, although they are very weak in the solar spectrum and may be subject to errors in the solar equivalent widths. In any case it is these weak lines which largely determine the microturbulence; and hence the abundance from the other lines. From these weak lines alone the MHGG data gives [Fe] = -0.72 $\pm$ 0.15 (s.d.). Using the 4400K Ellis model the corresponding value was -0.52 with respect to the HSRA model and -0.59 with respect to the HOLWEGER. Again using the abundances given in chapter 6, these become absolute abundances of 7.00 and 7.07. But the model atmosphere is unrealistic, the gravity too low, and the results

very uncertain. Moreover the 57 weak lines come from excitation potential in the range 2.41 - 5.04 eV and would not be similar in depth of formation or temperature dependence to the low excitation lines. It is therefore not possible to assess the absolute abundance; and the value 6.99 found herein is put forward solely as the abundance for low excitation FeI lines.

Table 9.1

Measured equivalent widths of lines with laboratory oscillator strengths.

wavelength A	E.P. eV	log gf	$W_{Arcturus}$ mA
4347.2	0.00	-5.49	158
4389.2	0.05	-4.57	200
5127.6	0.05	-6.11	155
5247.0	0.09	-4.94	181
4445.5	0.09	-5.43	162
5225.5	0.11	-4.77	198
4232.7	0.11	-4.92	160
4489.7	0.12	-3.93	225
5956.7	0.86	-4.61	162
6280.6	0.86	-4.38	198
4939.6	0.86	-3.31	199
6498.9	0.95	-4.73	163
6574.3	0.99	-5.04	118
6609.7	0.99	-5.71	97
5250.2	0.12	-4.92	203

Table 9.2

Lines used in combined abundance and microturbulence determination, with oscillator strengths from (i) laboratory measurements; (ii) solar spectrum.

	wavelength A	E.P. eV	log gf	W(sun) mA	W(Arcturus) mA
(i)	4347.2	0.00	-5.49	41	158
	4445.5	0.09	-5.43	39	162
	4232.7	0.11	-4.92	57	160
	5956.7	0.86	-4.61	51	162
	6498.9	0.95	-4.73	45	163
	6574.3	0.99	-5.04	26	118
	6609.7	0.99	-5.71	6	97
(ii)	6120.5	0.91	-6.08	4.4	68
	6648.1	1.01	-5.89	5.6	83
	6353.8	0.91	-6.57	1.54	38
	6221.6	0.86	-6.41	2.35	41
	6551.7	0.99	-5.99	4.7	73
	8204.1	0.91	-6.02	6.5	80

Table 9.3

Iron abundance and associated microturbulence from the lines in table 9.2 and the models of Bell et al (1976).

T_e K	[A/H]	log g	A_{Fe}	microturbulence km sec^{-1}
4000	-1.0	0.75	6.34	2.10
		1.50	6.53	2.05
		2.25	6.79	1.95
4500	-0.5	1.50	7.13	2.10
		2.25	7.26	2.10
		3.00	7.46	2.10

Table 9.4

Results of the illustrative interpretation of the profiles of strong, blue FeI lines in the spectrum of Arcturus: models used were T_e=4500K; [A/H]=-0.5; log g = 0.75, 1.50, 2.25, 3.00.

line (A)	log C_6+33	derived log g
3679.9	0.90	1.8
3719.9	0.96	1.6
3722.6 *	1.09	1.5
3899.7	0.83	1.4

* calculated as a blend with the line FeI 3719.9A.

Table 9.5

Values determined from the interpretation of the flux and spectrum from Arcturus.

effective temperature	4400 (+60/-30) K
log g	1.45 $\pm$ 0.15
microturbulence	2.1 $\pm$ 0.2 km s^{-1}
iron abundance	6.99 $\pm$ 0.15

Table 9.6

Relative iron abundance from the 295 FeI lines used by Mackle et al (1975) grouped by lower excitation potential: (i) the results of Mackle et al with an effective temperature of 4260K; (ii) the same data interpreted with a model with T_e= 4400K.

E.P. eV	number of lines	[Fe] (i)	[Fe] (ii)
0 - 1	10	-0.96	-0.43
1 - 2	9	-0.88	-0.45
2 - 3	64	-0.83	-0.57
3 - 4	50	-0.75	-0.62
4 - 5	151	-0.73	-0.64
5 - 6	11	-0.70	-0.57

Figure 9.1

Abundance of iron (A) is plotted as a function of equivalent width (W) for T_e = 4500K, and for log g = 2.25, 1.50; ξ = 2.4, 2.0, 1.8.

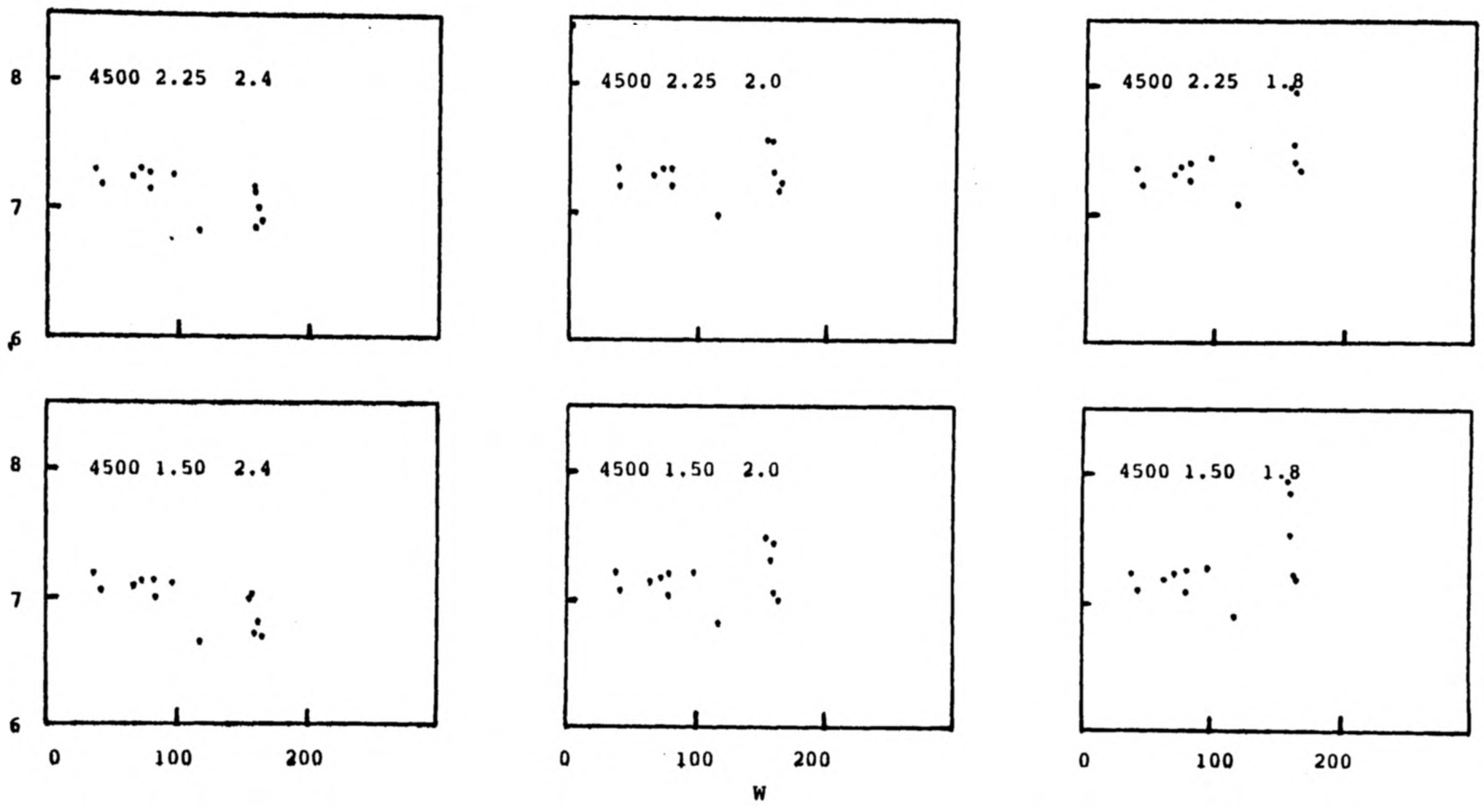
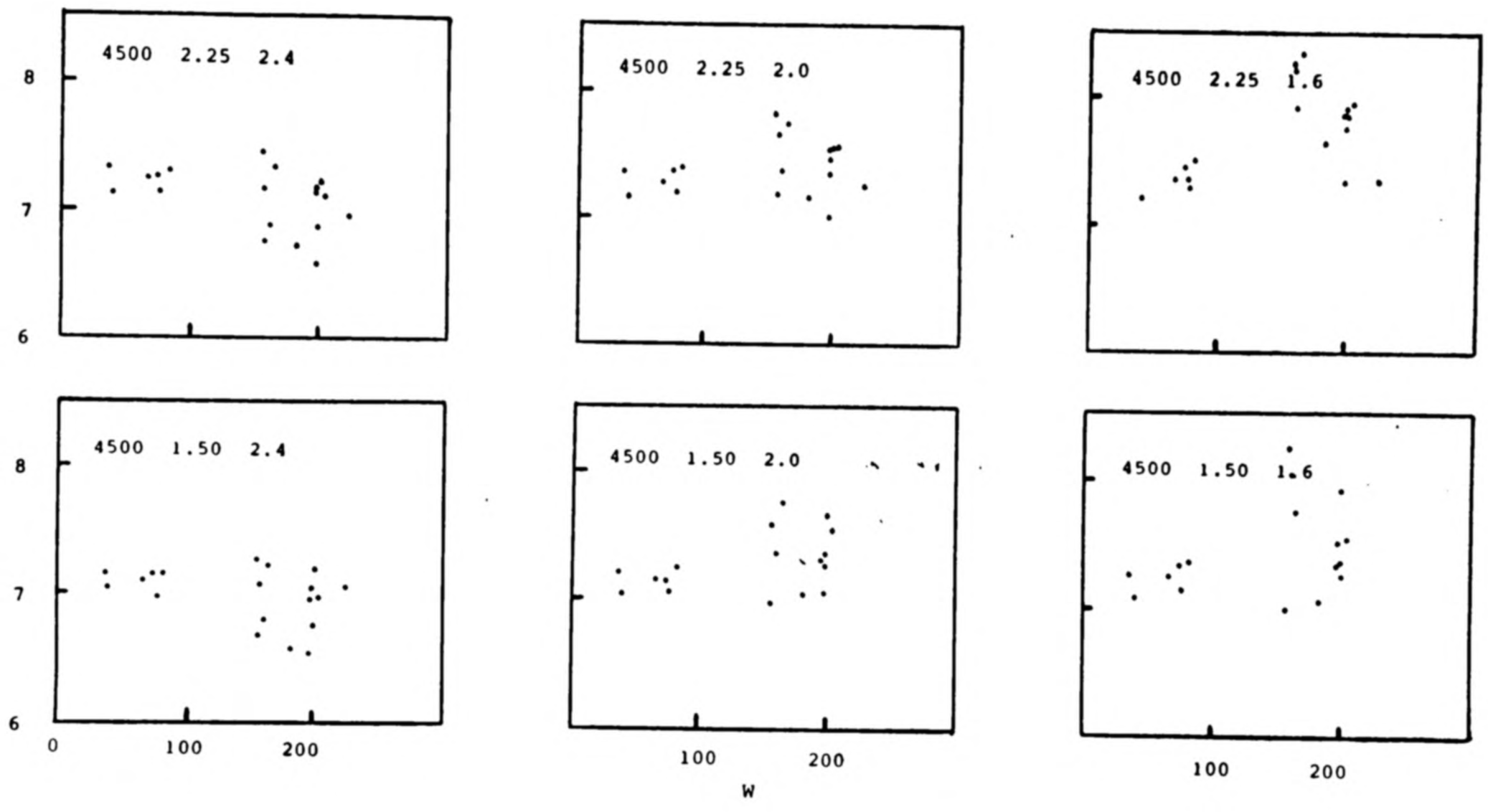


Figure 9.2

Abundance of iron (A) is plotted as a function of equivalent width (W) for T_e = 4500K, and for log g = 2.25, 1.50; ξ = 2.4, 2.0, 1.6.



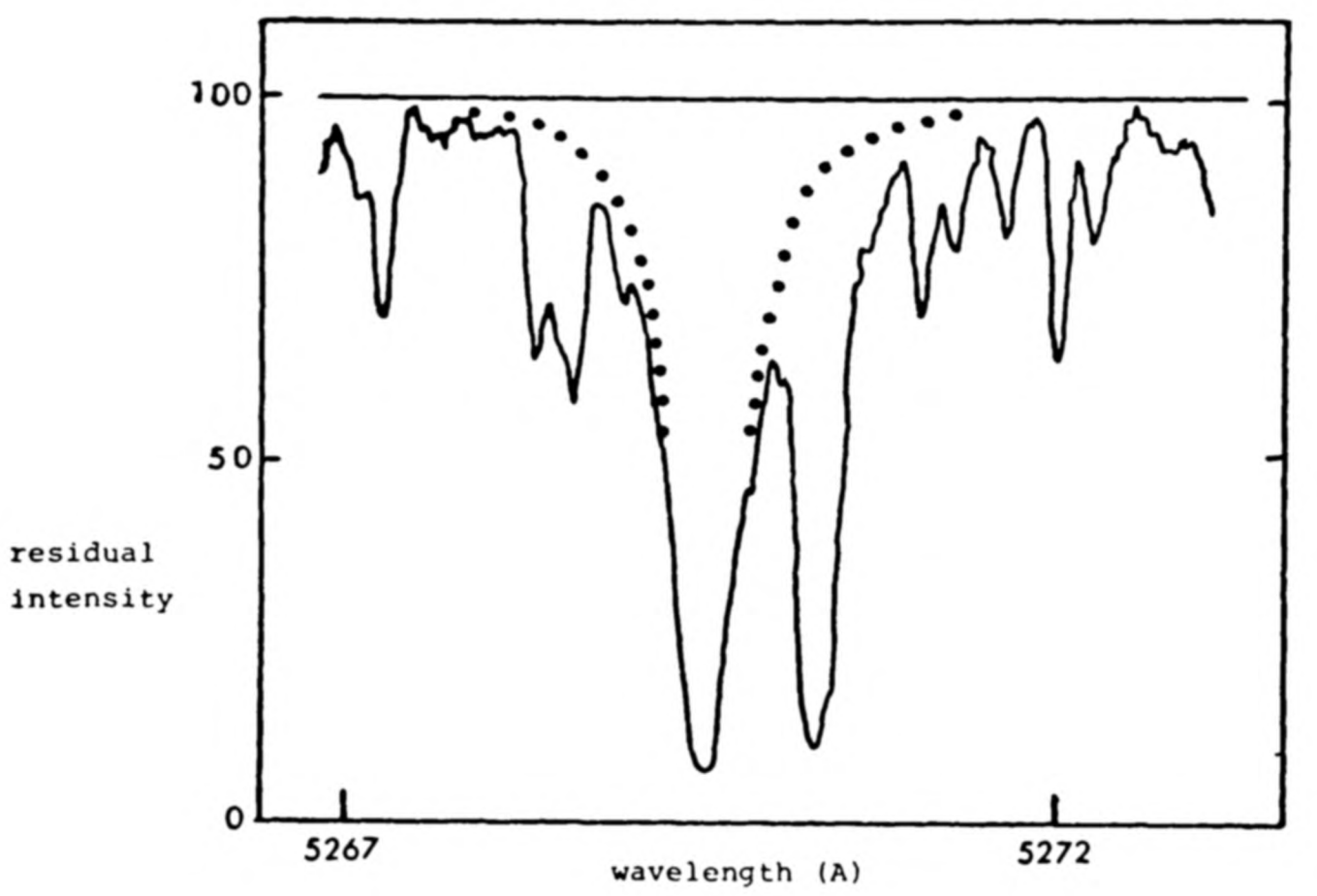


Figure 9.3

Observed and calculated profiles of FeI 5269A for the abundance and effective temperature adopted for Arcturus, and the adopted surface gravity.

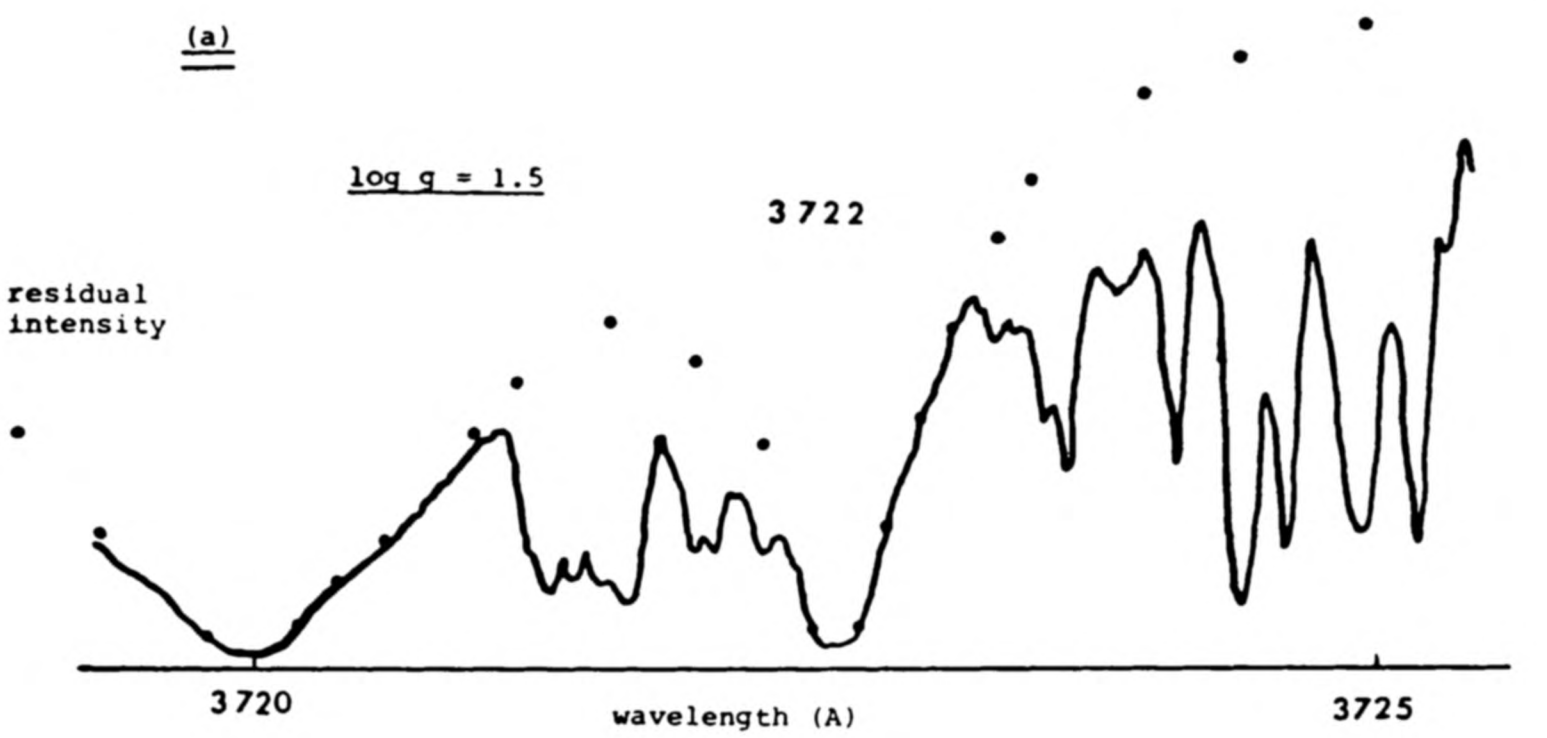
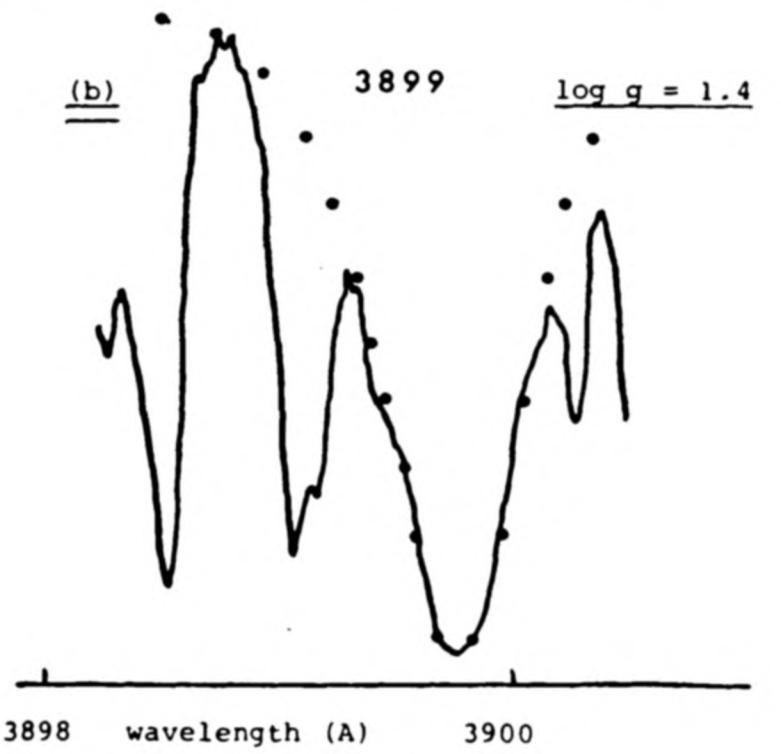
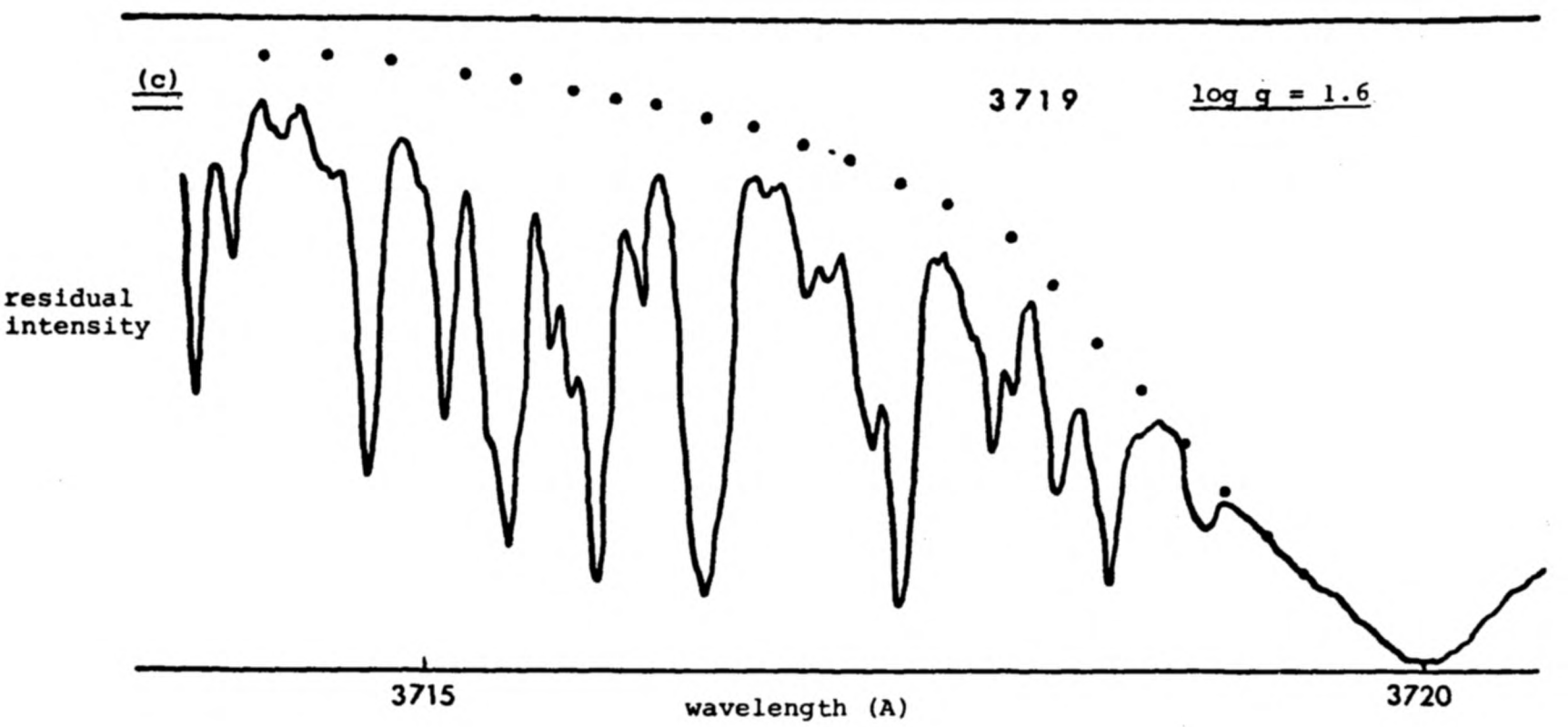


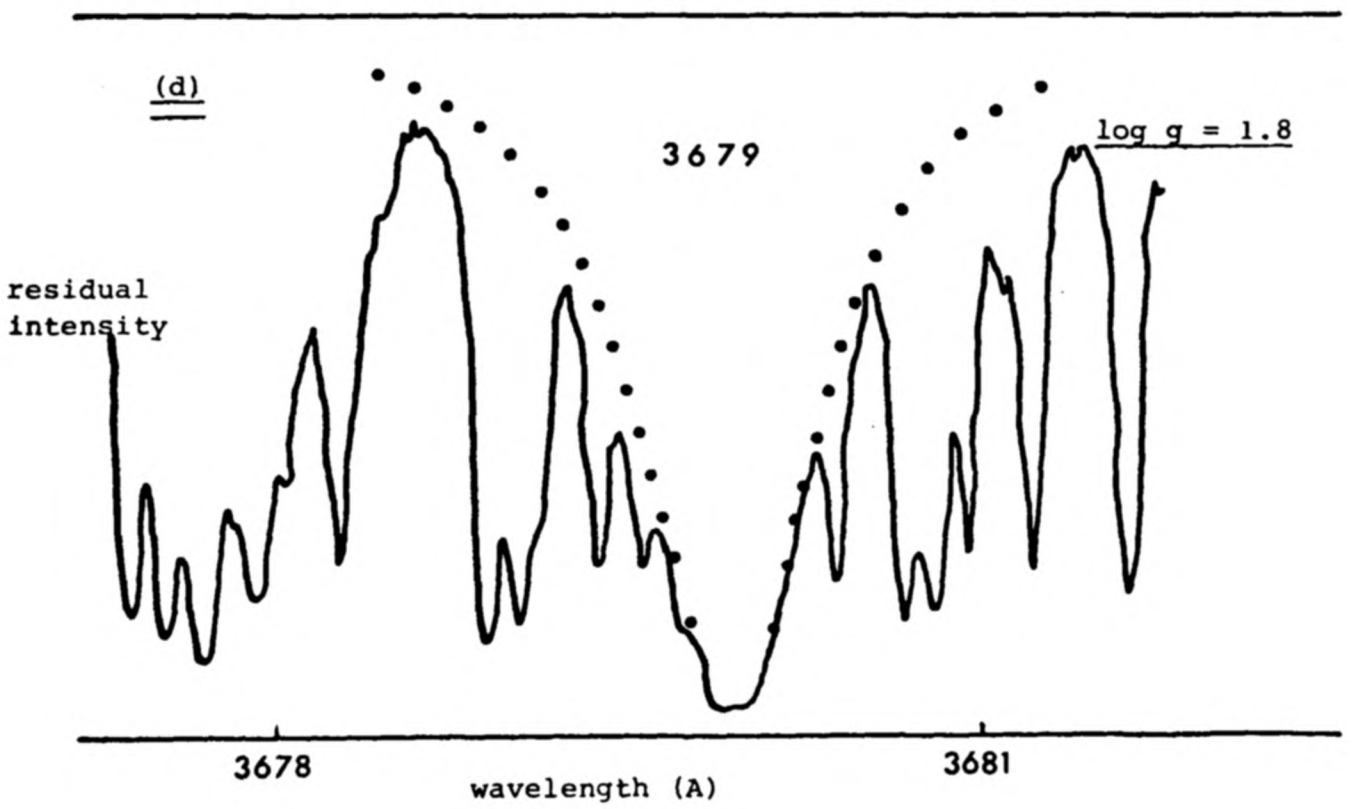
Figure 9.4

Observed and computed profiles of the strong blue lines for the adopted values of log g from models with T_e=4500K and [A/H]=-0.5.

(a) FeI 3722A
(b) FeI 3899A
(c) FeI 3719A
(d) FeI 3679A




(c)
3719
log g = 1.6
residual intensity
3715
wavelength (A)
3720


(d)
3679
log g = 1.8
residual intensity
3678
wavelength (A)
3681

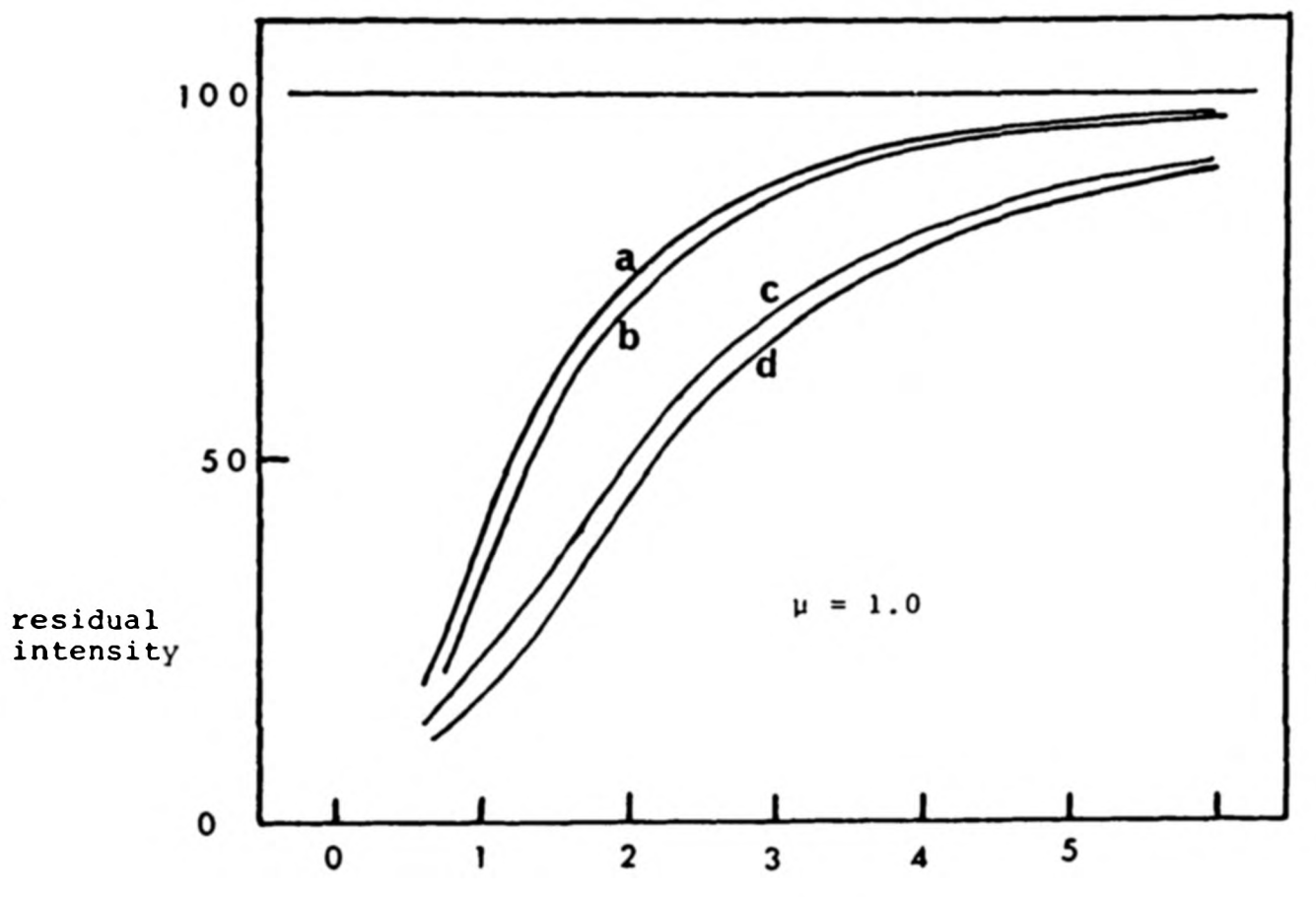


Figure 9.5

Computed profiles for the line FeI 3719A from the adopted abundances and damping constant and the Bell et al (1975) model with T_e=4500K and [A]=-0.5:

a & b - log g = 1.5 with opacity scaled to vary F_ν by 0.1 dex

c & d - log g = 2.25 . . . . . .

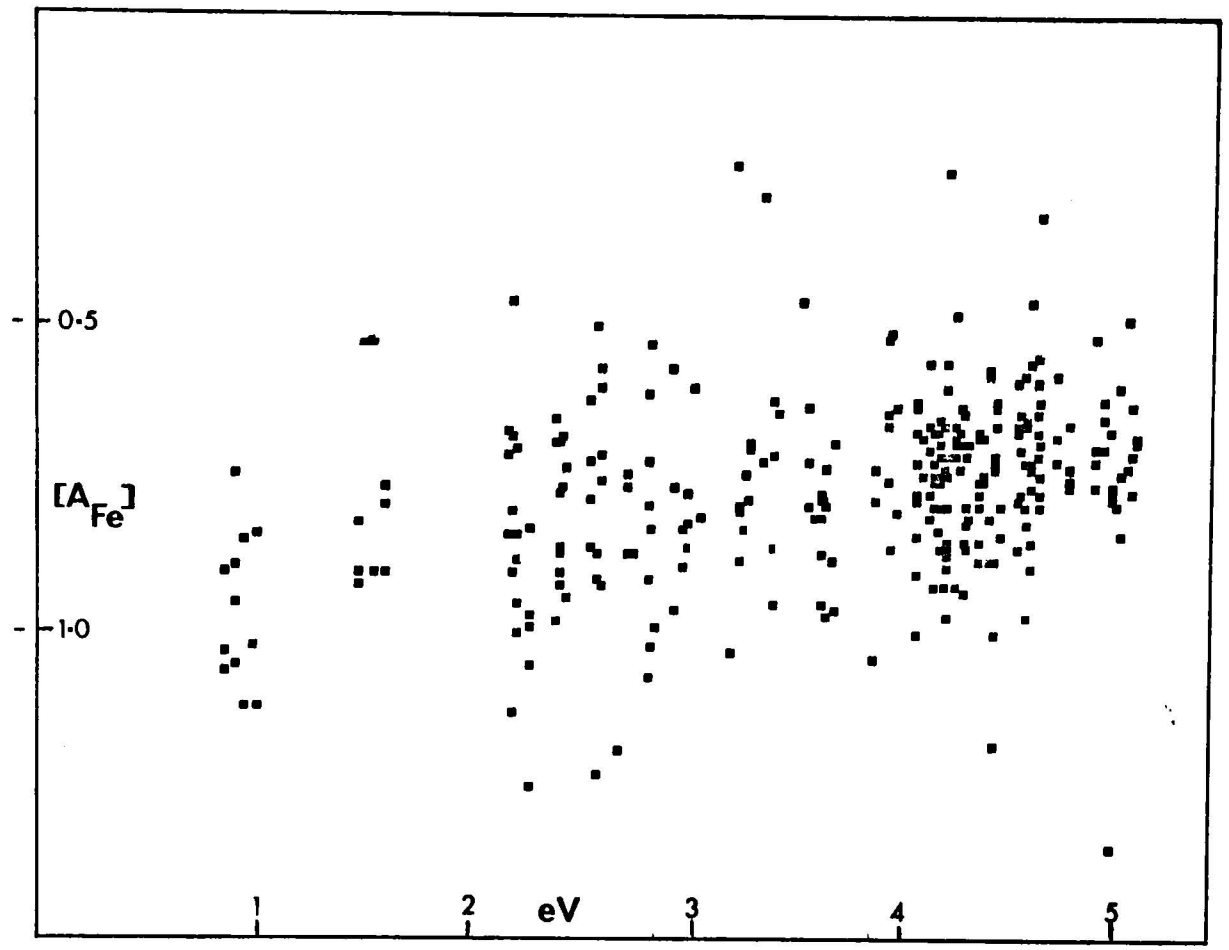


Figure 9.6

Values of [Fe] of Mackle et al (1975) are plotted against excitation potential of the FeI lines to show the systematic variation with the excitation potential of the lower level.

10. MASS, LUMINOSITY AND RADIUS OF ARCTURUS

10.1 Values derived from this work

The results from the interpretation of the spectrum of Arcturus may be combined with the various direct observations to find the mass, radius and luminosity. Following the discussion of the principles in chapter 1, the effective temperature and surface gravity determine the mass-luminosity ratio (equation 1.11). Using 4400K and 1.45 respectively the value found is:

$$[M/L] = -2.52 \pm 0.2 \qquad (10.1)$$

Using the absolute flux, as given in chapter 8, and the parallax (table 8.1) the luminosity is found from equation 1.12. The result, expressed in solar units, is:

$$L(\text{Arcturus}) = 184 \pm 15\ L(\text{sun}) \qquad (10.2)$$

where: $L(\text{sun}) = 3.90 \times 10^{33}$ erg s^{-1}

Combining these results (equation 1.13) gives the mass, determined solely from measurements of the flux as interpreted by means of model atmospheres, as:

$$M(\text{Arcturus}) = 0.56\ M(\text{sun}) \qquad (10.3)$$

with an uncertainty corresponding to a range 0.32 - 0.95.

Finally equation 1.14 is used to derive the radius, from the effective temperature, total flux and parallax, as:

$$R(\text{Arcturus}) = 23 \pm 2\ \ R(\text{sun}) \qquad (10.4)$$

The radius is however found more directly from the parallax and observed angular diameter (equation 1.18). As was seen in section 8.3.3, there are considerable uncertainties in both the observed value of the angular diameter and in the correction for limb darkening. Further discussion of the different reported measurements would be otiose. A reasonable mean is perhaps 0."024 with an uncertainty of about 15 per cent, as adopted by Mackle et al (1975). Then for a parallax of 0.092 ± 0.005:

$$R(\text{Arcturus}) = 28 \pm 6 \quad R(\text{sun}) \qquad (10.5)$$

This is very much more than the value found above from the spectrophotometry but, because of the uncertainty in the angular diameter, not inconsistent. The difference is however important in terms of the mass, determined by equation 1.8 from the surface gravity and radius.

for $23 + 2$ R(sun) : 0.56 M(sun) with lower and upper limits of 0.32 and 0.95 (10.6)

for 28 ± 6 R(sun) : 0.81 ± 0.4 M(sun) (10.7)

The value derived for a radius of 23R(sun) is of course the same as at (10.3) above because the same radius and gravity have been used.

10.2 Comparison with other measurements

The mass is determined from the gravity and radius, and its value and uncertainty reflects the values and uncertainties of those measurements. It is not therefore surprising that Mackle et al (1975) found from their gravity of 0.9 ± 0.35 a mass in the range 0.1 - 0.6 M(sun). The most probable value was 0.23. Although this value is very much less than the mass of Arcturus derived from this work, there is a further difference, in that Mackle et al used the direct measurements of angular diameter and parallax to find the radius of Arcturus as 28 R(sun). If the lower value found herein, 23R(sun), had been used the mass found would have been even less: 0.07 - 0.41 M(sun) with a modal value 0.16.

Taking account also of the difference between the masses at (10.6) and (10.7) above, the radius is clearly a source of great uncertainty. As far as the direct measurements are concerned, this arises from the uncertain angular diameter. It is therefore interesting to note that the photometric method used by Blackwell and Shallis (1977; see section 1.5 above) has given a provisional angular diameter of Arcturus as 0."0201 ± 0.0010. The radius from this measurement is 23.3 R(sun), in very good agreement with the value found here from the flux and effective temperature. Of course these two values are not wholly independent. Both use model atmospheres to provide fluxes; and both use the absolute flux measured by Blackwell et al (1975). But Blackwell and Shallis have shown that the angular diameter is not sensitive to these assumptions. As their result is not inconsistent with the direct observations, but is more precise, it is probable that the radius of Arcturus is more accurately determined as 23 R(sun) and this value is adopted for the following discussion.

The mass from this work is then very much more than the result of Mackle et al would suggest. When adjusted to the adopted radius, the difference is some 0.4 M(sun). The different surface gravities account for the discrepancy and values of the

surface gravity higher than the 1.45 dex adopted here would lead to higher masses for Arcturus. Ayres and Johnson (1977), for instance, proposed a mass of 1.1 (+0.6/-0.4) M(sun) from the gravity 1.6 $\pm$ 0.2 found from the strong CaI and II lines. But they too used the radius derived from direct angular diameters - adopting 27 R(sun). If the lower value taken here were used the mass would be 0.82 M(sun), and the range 0.52 - 1.27 M(sun).

As the surface gravity found by Ayres and Johnson is close to the value adopted herein (1.60 against 1.45) this mass is, as expected, close to the value given from this work. But like the results of Mackle et al, the gravity, and hence the mass, is sensitive to the assumed effective temperature. With this in mind, the mass from the gravity measurement which is largely independent of the temperature would appear to be more reliable; and hence the proposed value for the mass of Arcturus is 0.56 M(sun) with an uncertainty amounting to 0.32 - 0.95 M(sun).

10.3 Discussion

The large uncertainty in the mass reflects the uncertainties in the surface gravity, angular diameter and parallax. In section 1.6 the potential accuracy was assessed as 10 per cent. If the angular diameter of Blackwell and Shallis is confirmed, the required accuracy of 5 per cent in that measurement is achieved. The parallax is however less certain than the 2 per cent assumed in section 1.6. But the larger part of the uncertainty in the mass arises from the surface gravity which has been determined only to 0.15 dex (40 per cent).

This is however the accuracy set in the latter part of section 1.6 as the minimum aim for spectroscopic determinations. Bearing in mind the particular difficulties of Arcturus - its low temperature and gravity; the difficulty of determining the abundance from the no longer weak lines; the absence of precisely computed model atmospheres - the final result would appear to validate the intermediate laboratory and solar measurements. Moreover it demonstrates the principle underlying the measurement of surface gravity from the damping wings of metal lines, and the insensitivity of such results to the effective temperature and model atmosphere assumed. In contradistinction the results from methods relying on the ionisation equilibrium are, by the evidence of reported values, dependent on the accuracy of the assumed temperature.

Insofar as the aim of this work was to find a reliable measurement of surface gravity in late type stars there is no need to consider the consequential mass, radius and luminosity. But in view of the comments in chapter 1 about the use of the results it may be helpful to make the following points.

First the analysis of Arcturus has provided an example of the uncertainties in the mass, radius and luminosity which may result, even for this bright, nearby star, if any but the most precise methods are used. These uncertainties are not confined

to the surface gravity. The effective temperature, for instance, is still not finally resolved between the "high" values found by Blackwell and Shallis (1977), Blackwell and Willis (1977) and Blackwell et al (1975) and the "low" values - some 150K lower - of Mackle et al (1975) and Johnson et al (1976). In part this corresponds to the similar doubt as to the angular diameter of the star from direct and photometric measurements.

Next the results from determinations of surface gravity must be looked at critically, not just to assess the uncertainty in the measured quantities, but to see whether the underlying assumptions are valid. For example, the gravity derived from ionisation equilibria should include the effects of uncertainty in effective temperature; and the possibility of less obvious sources of error should be considered. Both the weak and strong line methods assume LTE.

Finally, there is the question of the particular results for Arcturus, and more especially the mass. The significance of the mass of Arcturus lies in the apparent anomaly between the masses derived for such red giant stars (eg Helfer and Wallerstein, 1968; Pagel and Tomkin, 1969) and the evolutionary theories which predict (eg Iben, 1972) that a star with less than solar mass could not have reached the red giant phase in the lifetime of the galaxy. The low mass found by Mackle et al (1975) for Arcturus appeared to confirm the anomaly and implied either (i) serious misunderstanding of the evolution of such stars; or (ii) substantial mass loss at some time in the star's evolution.

More extensive discussion of the implications of the low mass of Arcturus, and of the possible explanations, has been given by Mackle et al (1975). Although this is still pertinent in view of the mass found from this work, it should be recognised that the discrepancy between theory and the observed mass of Arcturus is not now so great. The upper limit on the value found above, 0.95 M(sun) would in fact be consistent with Iben's (1972)

evolutionary tracks. There may in addition be some further flexibility in the models of stellar interiors to account for a lower mass than that of the sun. And this one, preliminary value from one FeI line cannot be conclusive. But it is felt that the case for very substantial mass loss, or for serious errors in the theoretical evolution of Arcturus, no longer rests on a firm, observational basis.

11. SUMMARY AND CONCLUSIONS

It was emphasised that accurate surface gravities were necessary to determine accurate stellar abundances; and to derive from the observed surface gravity and stellar radius the mass of a star (chapter 1). Results for late type stars were considered to lack in general the desired absolute precision because they relied on the observation of weak lines from different ionisation stages to determine the ionisation equilibrium and hence the electron pressure and gravity. Although such methods were in principle sensitive to small changes in the gravity, the analysis was subject to great uncertainties because of possible non-LTE effects and errors in the oscillator strengths of the lines. Moreover the ionisation equilibrium was also very sensitive to the assumed value of the effective temperature of the stellar atmosphere (chapter 3).

Reported results for the late type giant Arcturus supported those conclusions (chapter 9). The measured values of the gravitational acceleration at the surface of the star from interpretation of the ionisation ratios of metal lines were sensitive to the effective temperatures adopted. As the effective temperature was not unambiguously determined (chapter 8) the gravity, and the mass, could not be found with reasonable accuracy. This confirmed the need for a method of determining the surface gravity of cool stars which was insensitive to the assumed effective temperature, did not assume that LTE described the ionisation and excitation in an atmosphere, and was free from errors in the oscillator strengths of the lines used. The proposed method (chapter 4) was to use the damping wing of a strong metal line which depended on the gas pressure in the atmosphere and therefore on the gravity. As the absorption in the wing depended also on the abundance of the species and on the damping constant those had to be known or measured. In order to reduce the effects of temperature and non-LTE the abundance was determined from the equivalent widths

of weak lines from the same lower level as the strong line. Damping constants were to be found from the solar spectrum as theoretical values were subject to very great uncertainties.

Oscillator strengths of lines from the a^5D and a^5F terms of FeI were measured using the large King furnace at the Department of Astrophysics, Oxford. The absorption method used largely eliminated uncertainties due to the determination of the temperature and the results were accurate to 5 per cent (0.02 dex) over a range of 6 decades. In contrast the data from other authors using emission methods appeared to show systematic errors which might be attributed to self-absorption or to errors in the source temperature. The discrepancies amounted to 0.2 dex or more for the weaker lines, which would make the results of, for instance, abundance determinations seriously wrong (chapter 5).

The precise oscillator strengths of the FeI lines were used to interpret the observed line strengths and profiles in the solar spectrum. From the weak lines abundances were derived for 5 current models of the photosphere. The spread in the derived abundances for a given model was explicable by the uncertainties in the equivalent widths and the adopted precision of the gf values, suggesting that the oscillator strengths were precisely measured. But it was necessary to adopt a solar microturbulence of about 0.8 km s^{-1}. It was not possible therefore to support the hypothesis that microturbulence was an artifact of systematic errors in the scale of oscillator strengths used in abundance determinations. The abundances determined varied from atmosphere to atmosphere but supported a value in the range 7.5 - 7.7 consistent with other high values for FeI and for FeII in the photosphere, chromosphere and corona (chapter 6).

Using the abundance for a particular model derived from the weak lines, the profiles of the stronger lines from the same

lower level were calculated and compared with the observed solar spectrum. Damping constants were determined by seeking agreement with the observed profile (for strong lines) or with the observed equivalent width (medium strength lines). The adopted values from the different atmospheres were in reasonably good agreement because the abundance was derived for that particular model and the same lower term, endorsing the proposed method. The measured damping constants were moreover close to the values predicted by simple, classical theories of the broadening of FeI lines by meutral hydrogen. This result was not unexpected in view of the relatively high iron abundance and was not an indication that the simple theories were correct. On the other hand it suggested that many of the more complex formulations of the interaction were not realistic for the low-excitation lines of FeI since they predicted very much greater damping coefficients (chapter 7).

The measured oscillator strengths and damping coefficients were then used to interpret the spectrum from Arcturus. Model atmospheres were chosen to include the effective temperature, found from the flux distribution to be 4400K (chapter 8). Abundances from the weaker lines were found for those models, and used to compute the profiles of stronger lines. Then, assuming the damping constants found from the solar analysis, the observed line profiles determined the gravity at the surface of the star (chapter 9).

The results for the abundance and microturbulence of Arcturus confirmed that the atmosphere was deficient in metals compared with the sun. The abundance was however sensitive to the assumed value of the effective temperature; and the uncertainty in the effective temperature corresponded to very great uncertainties in the measured abundance. The surface gravity derived from the strong lines was however insensitive to the adopted effective temperature and the value of 1.45 ± 0.15 took account of that factor.

The measured gravity of Arcturus confirmed that the method was capable of the desired precision and was largely independent of the temperature. Correspondingly the mass derived from the value of log g and a radius of 23 R(sun) was not sensitive to the temperature. The adopted mass, 0.56 $\pm$ 0.3 M(sun), was greater than other reported values for Arcturus and suggested i. that the lower effective temperatures proposed by other authors were incorrect; and ii. that the mass of Arcturus might not be inconsistent with theories of stellar evolution (chapter 10).

Although the gravity and mass of Arcturus were significant results, the more important aim was to test the method of determining surface gravities from the metallic line profiles. To that extent the work was qualitatively successful, even though the uncertainties amounted to more than the 10 per cent ultimately desired. The uncertainties may be traced back to the laboratory measurements of oscillator strengths, where it would be possible to measure weaker transitions which would, in the spectrum of the sun and cooler stars, allow the abundance to be found independent of all broadening factors. Following the identification of the principle source of uncertainty in the photometry of the furnace spectrum, gf values are now being measured with errors of less than 0.002 dex so that only the accuracy of the observed solar spectrum limits the precision of the abundance determination for a particular lower level and model atmosphere.

More sophisticated techniques could also be applied to the interpretation of the solar and stellar spectra. Spectrum synthesis, for instance, would permit the profiles of blended lines to be used to determine damping coefficients with greater confidence. However it is likely that the present limit on the accuracy of any derivation from the solar spectrum lies in the models of the solar atmosphere.

Turning to the gravity determination, the greatest criticism of the results for Arcturus must be that only one line, FeI 5269.5A, was used to find the adopted value. Further work should of course seek other lines which might be used to give independent values of the gravity. There are however few lines which both exhibit suitable damping wings and arise from a lower levels giving rise to weak lines which may be used to find the abundance. In the spectrum of Arcturus there are particular problems because of the very heavy blending below 5000A; and because of the low gas pressure. But in late type stars generally the more likely lines are of FeI from excited levels. These might be used but must await precise oscillator strengths which, at present, can apparently be measured only by furnace absorption methods. As indicated in chapter 5, such measurements are possible given high furnace temperatures which are precisely measured.

Finally the application of the method to the measurement of gravities of other stars would not require the quantity of observational data available for Arcturus. The equivalent widths of the weak lines used to find the abundance must be measured accurately. And the profile of the stronger line or lines must be precisely observed. But the spectral range involved might be no more than a few angstroms if a few very weak lines are used so as to be independent of the micro-turbulence. These might be observed with, for instance, an echelle grating giving high resolution over a very small region of the spectrum. This may be contrasted with the more common application of the method of ionisation equilibria where many lines are measured from a wide range of wavelengths with, it has been seen, less precise results. Similarly the use of the damping wings to determine the surface gravity has been demonstrated to be insensitive to temperature so that the effective temperature might be taken from the calibration of broad band colours, or from the photometric methods described

in chapter 1, and would not require the many observations drawn on to find the temperature of Arcturus. It is suggested however that only precise measurement and interpretation of selected lines can give surface gravities, and thereby masses, with the precision needed to test theories of stellar evolution. And that the method presented in this preliminary analysis of Arcturus could usefully be applied to other stars in preference to the more usual methods.

APPENDIX I: COMPUTATION OF LINE PROFILES

1. In chapter 2 the simple theory of line formation was summarised. It was assumed thereafter that, given a model atmosphere, the emergent flux and spectrum could be computed. In general this is true; and the computation is especially simple if LTE and pure absorption are assumed. Little attention is therefore accorded to the calculation of equivalent widths and profiles and the results are widely assumed free from errors and uncertainty.

2. The calculations are simple and straightforward. Aller (1963), for instance, showed a clear algorithm for the steps to compute equivalent widths and Baschek et al (1966) gave a general computer program for solar and stellar lines. Nevertheless there is evidence of uncertainties. These were first noticed using an earlier but not unsophisticated version of the program used in this work. It was found that the equivalent widths computed for the HSRA model (see chapter 6) varied according to the interval in optical depth at which the atmosphere was defined. Published results understandably tend not to draw attention to similar points and it is not easy to compare calculations for different models, abundances and oscillator strengths. A notable exception however was Smith and Whaling (1973) who reported iron abundances of 7.41 and 7.53 from the calculations of Ross (1972) and Evans (1972) even though the same model, equivalent width and log gf were used.

3. These small inaccuracies become important when other data, such as the gf values, are more precise. The derived abundances will clearly be uncertain. But more important are the differential effects if, for instance, the errors depend on line strength or on the excitation and wavelength of the line. As the work reported here relied on computations of both very weak and very strong lines considerable effort was devoted to eliminating errors from the FORTRAN computer program used to calculate the line profiles. The program followed, broadly

speaking, the theoretical stages outlined in chapter 2 and discussed more fully elsewhere. Nor were the computational methods exceptional and a full description would be otiose. It may be helpful however to point out the main areas for potential error.

Continuous opacity

4. Model atmospheres are conventionally defined by the temperature, gas pressure and electron pressure at values of the optical depth at a standard wavelength (usually 5000A). The continuous opacities must then be calculated to find first the optical depth scale at the wavelength of the line, and later the ratio of line to continuous opacities, from:

$$\tau_\nu = \int_0^{\tau_{std}} (\kappa_\nu/\kappa_{std}) d\tau_{std}$$

The continuum flux or intensity then follows from equation (2.14) or (2.15).

5. Continuous opacity sources are critical for constructing model atmospheres and in that connection have frequently been reviewed: eg Pecker (1965), Bode (1965), Mihalas (1967) and Gustafsson (1973). There is however uncertainty about some of the contributors. Bell (1973) for instance has found serious errors in the metal opacities used by Carbon and Gingerich (1969) and Craven (1974) pointed out an error in the hydrogen Gaunt factors used by those same authors. The question then arises whether the continuous opacity used to compute line profiles should be the best current value or the values, including errors, used to construct the model. There is of course the ideal answer, that the model should be revised. In practice however this was not possible. Fortunately there was no significant problem for the lines used in this work as the

continuous opacity is well defined in the range 4000-8000 AA; and at shorter wavelengths was in any case arbitrarily increased. It was adequate therefore to ensure that the program reproduced the opacities at visible wavelengths of published atmospheres.

6. The opacity sources included were H^-, H, He^-, H_2^-, He, H_2^+, Fe, Si and Mg. In addition Rayleigh scattering by H, H_2 and He and Thompson scattering by free electrons were included as if they were absorbers. In view of the remarks above the separate source references are not given; it is simply noted that the program reproduced the limb darkening calculations of Gingerich et al (1971) for the HSRA model to within 1% over the wavelength range above.

Concentration of absorbing atoms

7. As in the theoretical discussion, the calculation of the line absorption coefficient was divided into two broad parts: the total absorption and the profile function. The total absorption depended on the oscillator strength and abundance, which were defined externally, but the concentration of absorbing atoms (n_i in equation 2.41) had to be calculated from the ionisation and excitation in the atmosphere using the Saha-Boltzmann equation. That calculation introduced two possible sources of uncertainty.

8. First the ionisation potential of an atom is reduced by the surrounding plasma. The depression below the value in a free state is given by Debye's expression

$$\Delta\chi = 4.98 \cdot 10^{-4} \cdot \theta \cdot P_e^{\frac{1}{2}} \qquad \text{(eV)}$$

For cool, late type stars however the effect is very small.

9. There is greater uncertainty in the partition functions which enter Saha's equation. Convenient polynomial expressions

for the partition functions of many elements have been given by Bolton (1970) and by Aller and Everett (1972) which are widely used for astrophysical calculations. There are however residuals on the fitted polynomials which, though less than 1%, were felt to be unacceptable. Initially therefore the partition functions were found by interpolation in the tabulations of Drawin and Felenbok (1965). Dr Peter Craven later drew attention to the accurate calculations of partition functions described by Traving et al (1966) and kindly provided the data in a compatible form for inclusion in the program, and the results herein used those calculations.

10. Finally the Saha equation defines only the ratio of the number densities for two successive stages of ionisation, whereas the ratio required is the number of a particular ion to the total number of the element. This is readily found from the ratios of successive ionisation but the summation must include all stages which make a significant contribution. The approach adopted here was simply to sum over 4 stages, even though the higher stages were, for the sun or Arcturus, unimportant.

Profile function

11. As indicated above (eg section 6.2.2) the collisional broadening was computed assuming, purely as a convenient representation, the simple Unsold equation. Damping constants C_6 for H and for He were data; as was the natural (radiation) damping. The damping at each level of the atmosphere was then easily found from the number density of the perturber (H or He) and the mean velocity relative to the atom.

12. The Doppler width was also a straightforward calculation. The temperature and atomic weight determined the mean square velocity, assuming LTE, and this was added to the microturbulence defined for that point in the atmosphere (equation 2.45).

13. The Voigt function was less readily computed. It was necessary to evaluate the Voigt function for a number of wavelengths (defined more conveniently by their separation from line centre) at each level in the atmosphere; and for each value of the damping or microturbulence. As these many values required much computing time there was a strong practical argument for using simple approximations. Gerbiliskij (1972) for instance gave an algorithm which did not need double precision arithmetic. It was however limited to the ranges 0-1 for a and 0-4 for v. Traving (1965) provided a set of formulae over the complete range of a and v. Ibbetson (1969) found though that there were errors of the order of 0.2% generally, with as much as 4% for high values of a. Although the lines in this work were not in this uncertain region it was decided that even the small errors would be avoided by adopting the subroutine of Armstrong (1967).

Absorption line profile

14. Given the profile function for points in the line, the total line absorption, and the continuous opacity, the optical depth in the line can be found (equation 2.38) and then the intensity or flux (equations 2.39 and 2.40). Together with the intensity or flux in the continuum, this defines the line profile and equivalent width (section 2.4.2).

Numerical methods

15. Ultimately many of the calculations relied on approximations: eg the Voigt function; the partition functions; the exponential integral; and the opacities of, for instance, the metals. These were however standard and widely used expressions. Thus the exponential integral followed Kurucz (1970) in using the results of Cody and Thatcher (1968). In contrast the integration through the atmosphere to determine the optical depth scales and emergent spectrum relied on a quadrature for which there was no standard form.

16. The required integrations are needed in model atmosphere calculations also and complex quadrature formulae are often applied (see, eg, Kurucz (1970), Hummer and Rybicki (1967)). There are however general points which may be made. First, there is an important difference between the integration to find the optical depth at a given level of the model atmosphere and the indefinite integral for the flux or intensity. Hummer and Rybicki (1967) noted that the trapezoidal rule is remarkably accurate for the latter case and Craven (1972) found that with solar models sampled at 5 points per decade of optical depth the results would be within 1% of the best calculations. For the optical depth scale however a more complex formula is necessary to avoid end-point errors.

17. Secondly the quadrature formulae can be more simple, and faster in operation, if the model atmosphere is defined at equal intervals of optical depth. (Or more accurately at equal intervals of log optical depth as the integrations invariably use the logarithmic scale so that integrands vary less sharply with respect to the variable.) This does however restrict the models which may be examined without first interpolating the physical properties to an equi-interval scale. Thirdly it is recommended that whatever quadrature is adopted should be tested by the simple comparison of results when one or more levels is left out of the model.

18. Taking account of such tests the quadrature used was based on the weighted parabolic interpolation described by Kurucz (1970).

Comparison with other calculations

19. It was possible to establish broadly the accuracy of the program, eg by taking the same equivalent widths and oscillator strengths as other authors and seeing if the same abundance was derived. But invariably there were uncertain data and assumptions which might have explained the discrepancies. Few

authors specify, for instance, the precise values of the damping constants assumed or the abundances which determine the mean molecular weight of the atmosphere and hence the continuous opacity.

20. Direct comparisons were possible however as Cowley (1974) and Lambert (1974) generously arranged for the calculation of profiles for hypothetical iron lines with specified values for abundance, microturbulence, gf, natural damping and C_6. The same solar model atmosphere was used (Elste, 1967); and the equivalent widths ranged from less than 10 mA to more than 500 mA so that both the Doppler core and the damping wings were established.

21. Taking first the calculations passed on by Cowley, it was found that, except for the line centre and perhaps 10 mA on either side, the absorption depth was consistently greater than the results of the program used for this work. As the difference was a greater fraction of the absorption in the line wings, and for greater damping, it appeared to arise from differences between the damping or Voigt functions in the two programs. The magnitude of the differences amounted to as much as 0.06 in $\log(W/\lambda)$ which is significant for the precise oscillator strengths found from the Oxford furnace, though not for many applications.

22. Turning to the profiles communicated by Lambert, there was excellent agreement between the two programs for the weak lines. Throughout the profile the discrepancy was generally less than 0.5% of the absorption, so that the difference in equivalent widths was negligible. Such differences as did exist might have arisen from the different partition functions, as the polynomials of Bolton (1970) were used in the comparison program. The stronger lines on the other hand had consistent discrepancies in the damping wings, in the sense that the Lambert absorption was smaller.

23. The differential disagreement between the weak and strong lines was particularly worrying because it implied, assuming that the program used by Lambert was correct, that the damping constants could not be derived accurately from computed solar profiles of strong FeI lines; and that the derived gravity would thereby be uncertain. The differences were small - corresponding to about 0.1 dex in C_6 - but not insignificant. It was reassuring therefore to find that the results from the FORTRAN program used in this work agreed very well with calculations using an ALGOL68 program written by Dr P. G. Craven. Craven's program adopted the same broad assumptions and calculations as that used herein, but emphasised even more the need for absolute precision at each step, both in the physical constants and in the numerical methods. Thus the same opacity sources, partition functions and Voigt function were adopted. The integrations however involved more sophisticated quadratures; and the program was completely independent as far as numerical constants and detailed manipulation were concerned.

24. As an illustration of the consistency of the FORTRAN and ALGOL68 programs, calculations for the line FeI 4375.9 A were, for a range of abundances, in agreement to less than 1% in the equivalent width for values from less than 5mA to more than 1 000 mA. Furthermore the differences were not especially large in the line wings; nor were they systematic in sign. The magnitude of these differences may also be contrasted with the discrepancies with respect to the other calculations, and figure A.1 shows the residual differences with respect to the program used in this work and the profiles found by the three other authors.

Conclusions

25. Direct comparisons of the results from the Craven program and this work's with those of Lambert and Cowley are not entirely fair as the former two used the same assumptions for many of the source data: opacities, partition functions etc. Nevertheless it was not possible to explain the discrepancies solely in terms of these factors. Nor was there any evidence for the explanation

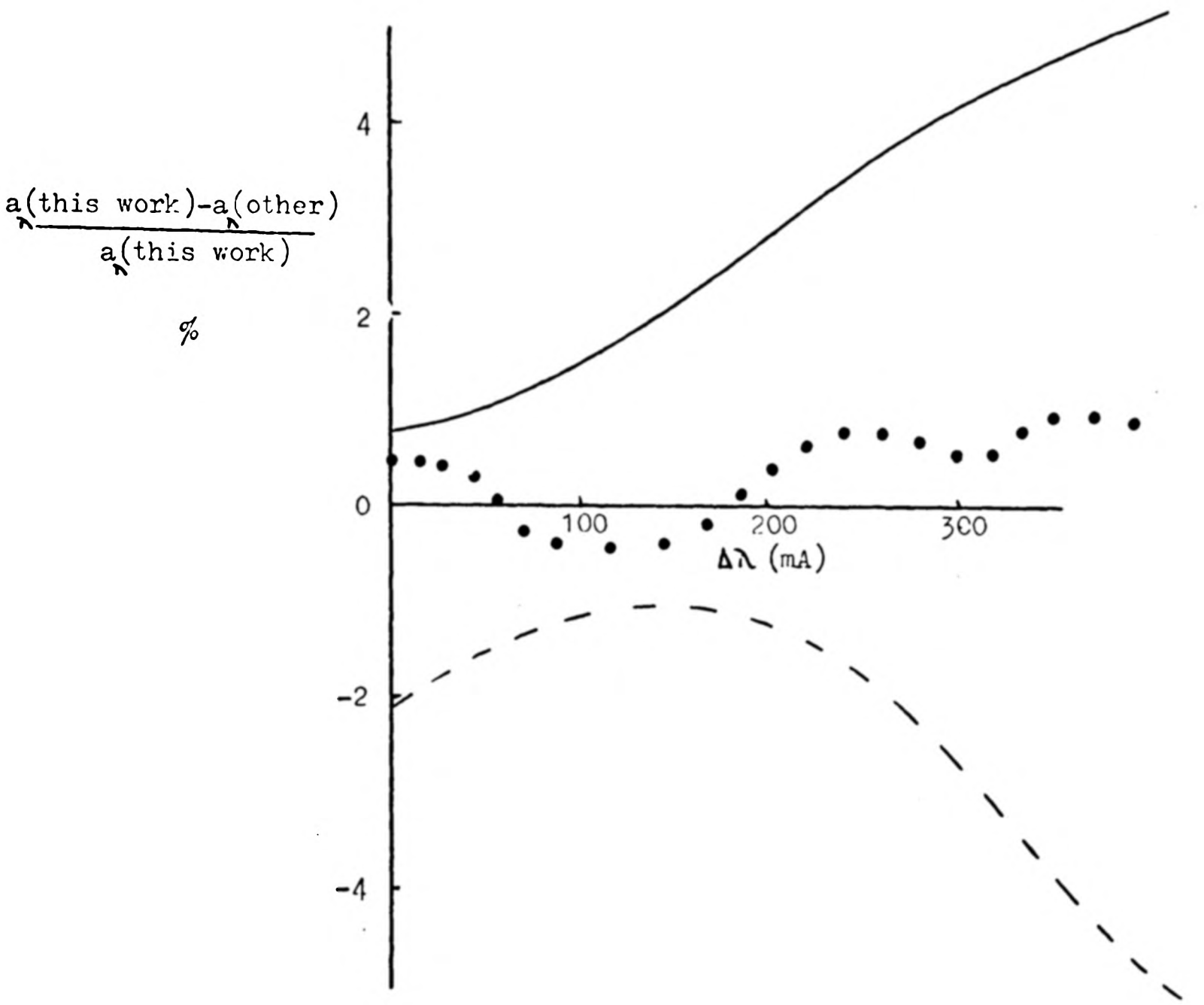
put forward by Evans (1972) for the different values reported by Smith and Whaling (1973): namely, rounding errors and truncation. This explanation would imply great carelessness in programming as most modern computers are accurate to at least 8 digits and standard techniques avoid differencing very similar quantities.

26. There was on the other hand considerable evidence of small errors in the numerical constants and coefficients which would have a significant cumulative effect when repeated and multiplied throughout the calculation. As a trivial example, it is common to use the reciprocal temperature θ and this is generally defined and calculated as 5040/T. But the figure 5040 is only a rounded value. Accordingly the calculation of ionisation equilibrium, excitation, opacities and many other physical properties may be subject to small errors simply because one figure was rounded and used without considering its underlying, precise value. Many other examples exist in the numerical formulae used to find, for example, opacities or the number of absorbing atoms.

27. It is suggested that these small details account for the major part of the discrepancies found; and that attention to those same details explains the good agreement of the results by this author and by Craven's program. Accordingly there would appear to be no reason to doubt the reliability of the computations on which the results herein were based.

Figure A•1

The differences between the theoretical profiles of the line FeI 4373.9A computed by this author and by others; the same model atmosphere, abundance, log gf, damping constants and microturbulence were used in all calculations and gave an equivalent width of about 350 mA.



profile from Cowley — — — —

• • • • • • Lambert ————————

• • • • • • Craven • • • • •

APPENDIX II: UNITS AND SYMBOLS

1. Units for astrophysical measurements are in a transitional period. There is a clear trend towards the standard (SI) units which is supported by many journals and bodies. On the other hand there are still many authors who prefer the more traditional system based, broadly speaking, on the CGS units. These more familiar units have also been used in this work although there are few important differences as a result. The main points are as follows:

a. wavelengths are generally expressed in Angstroms (A);

b. abundances of elements are usually given with respect to hydrogen, and defined by the logarithmic scale:

$$\log_{10}(N_i/N_H)$$

c. the acceleration due to gravity at the surface of a star is expressed in cm s^{-1}.

2. The mathematical and physical symbols used throughout this work are standard and are not always defined in the text. This should present no difficulties for those familiar with the subject but the more frequent and important are set out below.

a	ratio of damping to Doppler width
$\underline{a}$	vector of atomic abundances with respect to hydrogen
a_ν	line absorption depth
A	abundance relative to hydrogen
	surface area
A_{ji}	Einstein spontaneous emission probability
B_{ji}	.. stimulated .. ..
B_{ij}	.. absorption ..
$B_\nu(T)$	Planck funtion
c	velocity of light
C_p	coefficient of damping function

D	distance to star
D_B	Balmer discontinuity (in magnitudes)
e	electron charge
E_ν	energy transmitted at frequency ν
f_{ij}	oscillator strength
f_ν, F_ν	flux at frequency ν at earth and at surface of star
f, F	integrated flux . . . . .
g	acceleration due to gravity at the surface of the star
g_i	statistical weight
h	Planck's constant
$H(a,v)$	Voigt function
I_ν, I	intensity, at frequency ν and integrated
j_ν	emission coefficient at frequency ν
k	Boltzmann's constant
k_c	continuous extinction coefficient
l_ν	line absorption coefficient at frequency ν
l_0	integrated line absorption coefficient
m	electron mass
M	stellar mass
	atomic mass
n^*	effective quantum number
N	number density of atom (hydrogen)
N_i, n_i	number density of species i
P_g	gas pressure
P_e	electron pressure
r	distance from centre of star
r_ν	residual intensity in line profile
R	radius of star
S_ν	source function at frequency ν
t	time
T	temperature
T_e	effective temperature
$U_i(T)$	partition function
v	velocity
W	equivalent width
z	depth in stellar atmosphere
Z	fractional abundance of metals in the atmosphere

β	line strength of H_β
Γ	damping constant
$\Delta\nu_D$	Doppler width
θ	polar angle
	reciprocal temperature (5040/T)
	angular diameter
κ κ_ν	continuous absorption coefficient
λ	wavelength
μ	$\cos\theta$
ν	frequency
ν_0	line centre frequency
ξ	microturbulent velocity
ρ	density
σ	scattering coefficient
τ	optical depth
τ_{ij}	lifetime
$\phi(\nu)$	absorption profile
χ	ionisation potential
ω	angular frequency

REFERENCES

Chapter 1

Barnes T.G.
Evans D.S. 1976 M.N.R.A.S. 174, 489

Blackwell D.E.
Shallis M.J. 1977 M.N.R.A.S. 180, 177

Blant A.
Bonneau D.
Koechlin L.
Labeyrie A. 1977 Ap. J. Lett. 214, L79

Bonneau D.
Labeyrie A. 1973 Ap. J. Lett. 181, L1

Code A.D.
Davis J.
Bless R.C.
Hanbury Brown R. 1976 Ap. J. 203, 417

Currie D.G. 1974 Ap. J. 187, 131

De Vegt 1976 Astr. & Ap. 47, 457

Gezari D.Y.
Labeyrie A.
Stachnik R.V. 1972 Ap. J. Lett. 173, L1

Gliese W. 1975 "Space Astronomy", eds. T.D. Nguyen & B.I. Battrick, p. 109

Gray D.F. 1967 Ap. J. 149, 317

Gray D.F. 1968 Astr. J. 73, 769

Hanbury Brown R. 1974 "The Intensity Interferometer", Taylor & Francis: London

Hanbury Brown R.
Davis J.
Allen L.R. 1974 M.N.R.A.S. 167, 121

Hanbury Brown R.
Davis J.
Lake R.J.W.
Thompson R.J. 1974 M.N.R.A.S. 167, 475

Hoffleit D. 1964 "Catalogue of Bright Stars", Yale University: New Haven

Iben I. 1967 Ann. Rev. Astr. & Ap. 5. 571

Iben I. 1972 Proc. I.A.U. Colloquium No. 17

Iben I.	1974	Ann. Rev. Astr. & Ap. 12, 215
Knapp S.L. Currie D.G. Liewer K.M.	1975	Ap. J. 198, 561
Labeyrie A.	1970	Astr. & Ap. 6, 85
Lacy C.H.	1977	Ap. J. Supp. 34, 479
Lynds C.R. Worden S.P. Harvey J.W.	1976	Ap. J. 207, 174
McCalister H.	1977	Ap. J. 215, 159
Nather R.E. McCamb M.M. Evans D.S.	1970	Ap. J. Lett. 160, L181
Pease F.G.	1921	P.A.S.P. 33, 171
Pease F.G.	1931	Erg. Exact. Naturwiss. 10, 84
Van Altena W.F.	1974	Astr. J. 79, 826
Wesselink A.J.	1969	M.N.R.A.S. 144, 297
Wesselink A.J. Paranya K. Devorkin K.	1972	Astr. & Ap. Supp. 7, 257
Wooley R. Epps E.A. Penston M.J. Pocock S.B.	1970	"Catalogue of Stars within twenty-five parsec of the Sun", Roy. Obs. Ann. No. 5.
Worden S.P.	1976	P.A.S.P. 88, 69

Chapter 2

Aller L.H.	1963	"The Atmospheres of the Sun and Stars", Ronald Press: New York

Auer L.H. Mihalas D. 1969 Ap. J. 156, 157, 681

Auer L.H. Mihalas D. 1969 Ap. J. 158, 641

Auer L.H. Mihalas D. 1970 Ap. J. 160, 233

Bell R.A. Eriksson K. Gustafsson B. Nordlund A. 1976 Astr. & Ap. Supp. 23, 37

Carbon D. 1974 Ap. J. 187, 135

Carbon D. Gingerich O. 1969 "Theory and Observation of Normal Stellar Atmospheres", MIT Press: Mass. p. 377

Elste G.H.E. 1967 Ap. J. 148, 857

Kurucz R.L. 1974 Sol. Phys. 34, 17

Mihalas D. 1970 "Stellar Atmospheres", Freeman: San Francisco

Mihalas D. Auer L.H. 1970 Ap. J. 160, 1161

Van Citters D.C. Morton D.C. 1970 Ap. J. 161, 695

Unsold A. 1955 "Physik der Sternatmospharen", Springer-Verlag: Berlin

Chapter 3

Adams W.S. Joy A.H. Humason M.L. Brayton A.M. 1935 Ap. J. 81, 187

Ayres T.R. Linsky J.L. Shine R.A. 1975 Ap. J. 195, L121

Bappu B.K.V. Silvaraman K.R. 1971 Sol. Phys. 17, 316

chapter 3 (contin.)

Barbier D. Chalonge D.	1939	Ann. Ap. 2, 254
Batten A.H.	1973	"Binary Systems and Multiple Stars", Pergammon Press: Oxford
Bell R.A.	1971	M.N.R.A.S. 155, 65
Bell R.A.	1972	M.N.R.A.S. 159, 349
Berger J.	1962	Ann. Ap. 25, 1, 77
Borgman J.	1960	Bull. Astr. Neths. 15, 255
Breger M. Kuhi L.V.	1970	Ap. J. 160, 1129
Cayrel R.	1966	Ann. Ap. 29, 413
Cayrel R.	1969	"Theory and Observation of Normal Stellar Atmospheres", MIT Press: Mass.
Chalonge D. Divan L.	1953	C.R. Acad. Sci. Paris 237, 298
Crawford D.L.	1966	I.A.U. Symposium No. 24, p. 170, Academic Press: London
Crawford D.L.	1973	I.A.U. Symposium No. 54, p. 93, Reidel: Dortrect
Crawford D.L. Mander J.	1966	Astr. J. 71, 114
Crawford D.L. Stromgren B.	1966	Vistas 8, 149
Deeming J.	1960	M.N.R.A.S. 121, 52
Dickow K. Gyldenkerne K. Hansen P. Jacobsen K. Johansen P. Kjaergaard P. Olsen E.	1970	Astr. Ap. Supp. 2, 1
Edmunds F.N. Schulter H. Wells D.C.	1967	Mem. R.A.S. 71, 271
Fehrenbach C.H. Westerlund R.E.	1973	I.A.U. Symposium No. 50, Reidel: Dordrect

chapter 3 (contin.)

Furenlid I.	1971	Astr. Ap. 10, 321
Golay M.	1963	Publ. Obs. Geneve 64
Gottlieb D.M. Bell R.A.	1972	Astr. Ap. 19, 434
Gray D.F.	1967	Ap. J. 149, 317
Gray D.F	1969	Astr. J. 73, 769
Gray D.F.	1972	J.R. Can. A.S. 66, 70
Griem H.R.	1960	Ap. J. 132, 883
Griem H.R.	1967	Ap. J. 147, 1092
Griffin R.F.	1961	M.N.R.A.S. 122, 181
Griffin R.F. Redman R.O.	1960	M.N.R.A.S. 120, 287
Guinan E.F. Harrison K.A.	1975	Bull.A.A.S. 7, 234
Hansen V. Kjaergaard J.	1971	Astr. Ap. 15, 123
Hauck B. Westerlund B.E.	1973	I.A.U. Symposium No. 54, Reidel: Dordrecht
Herbison-Evans D.R. Hanbury Brown R. Davis J. Allen J.E.	1971	M.N.R.A.S. 151, 161
Hynek J.A.	1935	Ap. J. 82, 358
Johnson H.L.	1965	Comm. Lun. Planet. Lab. 3, 67
Johnson H.L. Morgan W.W.	1953	Ap. J. 117, 313
Johnson H.R. Milkey R.W. Ramsey L.W.	1973	Ap. J. 187, 147
Keenan P.C.	1958	Handbuch Phys. 50, 93
Klinglesmith D.A.	1971	N.A.S.A. Spec. Rept. 3065

chapter 3 (contin.)

Kolb A.C.	1957	Thesis, University of Michigan
Kopylov I.M.	1958	Ann. Crimean Ap. Obs. 20, 123
Lutz T.E. Furenlid I. Lutz J.H.	1973	Ap. J. 184, 787
Lutz T.E. Kelker D.H.	1975	P.A.S.P. 87, 617
McClure R.	1970	Astr. J. 75, 41
Mihalas D.	1972	Ap. J. 176, 139
Morgan W.W.	1937	Ap. J. 85, 380
Morgan W.W. Keenan P.C. Keller E.	1943	"An Atlas of Stellar Spectra", Univ. of Chicago Press: Chicago
Neff J.S.	1968	Astr. J. 73, 75
Neff J.S. Travis L.D.	1967	Astr. J. 72, 48
Newell E.B.	1971	Bull. A.A.S. 3, 381
Newell E.B.	1973	I.A.U. Symposium No. 54, Reidel: Dordrecht
Odgers G.J.	1952	Ap. J. 116, 444
Oke J.B.	1957	Ap. J. 126, 509
Olson E.C.	1968	Ap. J. 153, 187
Olson E.C.	1969	P.A.S.P. 81, 97
Olson E.C.	1971	Astr. Ap. 15, 161
Olson E.C.	1974	Astr. J. 79, 1424
Olson E.C.	1975	Ap. J. 195, 829
Pagel B.	1962	Roy. Obs. Bull. No. 55
Parsons S.B.	1970	Ap. J. 159, 951
Parsons S.B.	1971a	M.N.R.A.S. 152, 121
Parsons S.B.	1971b	Astr. J. 76, 562
Peterson P.M.	1969	Smithsonian Ap. Obs. Spec. Report No. 293

Peat D.	1969	Proc. 3rd. HSRA (ed. Gingerich O.) p. 55
Petrie R.M.	1965	Publ. Dom. Ap. Obs. 8, 253
Petrie R.M.	1966	I.A.U. Symposium No. 24, p. 304, Academic Press: London
Peytremann E.	1975	Astr. Ap. 38, 417
Popper D,M.	1967	Ann. Rev.Astr. & Ap. 5, 85
Popper D.M.	1970	I.A.U. Colloquium No. 6, p. 13, Copenhagen Univ.
Popper D.M.	1974	Ap. J. 188, 559
Price M.	1966	M.N.R.A.S. 134, 135
Redman R.O.	1966	I.A.U. Symposium No. 24, p. 155, Academic Press: London
Reimers D.	1973	Astr. Ap. 24, 79
Schmidt-Kaler T.	1965	Landolt-Bernstein Group 6, Vol.1, p. 284, Springer-Verlag: Berlin
Sharpless S.L.	1956	Ap. J. 124, 342
Smith M.A.	1974	Ap. J. 190, 481
Smith E.W. Vidal C.R. Cooper J.	1971	N.B.S. Monograph No. 120
Smith M.A. Vidal C.R. Cooper J.	1973	Ap. J. Supp. 25, 37
Spinrad H.	1962	Ap. J. 135, 715
Spinrad H. Taylor B.	1969	Ap. J. 157, 1279
Spite F.	1966	Ann. Ap. 29; 601
Stebbins J. Whitford	1964	Ap. J. 139, 424
Stebbins J. Kron G.E.	1956	Ap. J. 123, 440
Stickland D.J.	1971	M.N.R.A.S. 153, 501

chapter 3 (contin.)

Strom S.E. Peterson D.M.	1969	"Theory and Observation of Normal Stellar Atmospheres", MIT Press, p. 279
Stromgren B.	1963	"Stars and Stellar Systems", Vol. VIII, p. 123, Univ. of Chicago Press: Chicago'
Stromgren B.	1966	Ann. Rev. 4, 433
Stromgren B. Crawford D.L.	1970	
Swarmy K.S.K.	1966	Ap. J. 146, 731
Thackeray A.D.	1949	M.N.R.A.S. 109, 436
Vardya M.S. Bohm K.H.	1965	M.N.R.A.S. 131, 89
Verwoij S.	1936	Publ. Astr. Inst. Amsterdam 5
Vidal C.R. Cooper J. Smith E.W.	1973	Ap. J. Supp. 25, 37
Walraven T. Walraven J.H.	1960	Bull. Astr. Netherlands 15, 67
Whitford A.E.	1966	I.A.U. Symposium No. 24, Academic Press: London
Whitney C.A.	1969	"Theory and Observation of Normal Stellar Atmospheres", MIT Press, p. 3
Williams E.G.	1936a	Ap. J. 83, 279
Williams E.G.	1936b	Ap. J. 83, 305
Wilson O.C.	1966	Science 151, 1487
Wilson O.C. Bappu M.K.V.	1957	Ap. J. 125, 661
Wood D.	1969	Astr. J. 74, 177
Worth M.D. Heintz W.D.	1974	Ap. J. 193, 647
Young R.K. Harper W.E.	1924	Publ. Dom. Ap. Obs. 2, 3

Chapter 4

Blackwell D.E. 1974 Q.J.R.A.S. 15, 224

Blackwell D.E. 1976 Q.J.R.A.S. 16, 361

Blackwell D.E.
Calamai G.
Willis R.B. 1972a M.N.R.A.S. 160, 121

Blackwell D.E.
Kirby J.H.
Smith G. 1972b M.N.R.A.S. 160, 189

Blackwell D.E.
Ibbetson P.A.
Petford A.D. 1975 M.N.R.A.S. 171, 195

Evans J.C.
Testerman L. 1975 Sol. Phys. 45, 41

Lewis E.L.
McNamara L.F.
Michels H.H. 1971 Phys. Rev. A 3, 1939

McNamara L.F. 1971 Proc. A.S.A. 2, 40

Chapter 5

Allen C.W. 1971 M.N.R.A.S. 152, 295

Allen C.W.
Asaad A. 1957 M.N.R.A.S. 117, 36

Andersen T.
Sorensen G. 1971 Ap. Letts. 8, 39

Assousa G.E.
Smith W.H. 1972 Ap. J. 176, 259

Banfield F.P.
Huber M.C.E. 1973 Ap. J. 186, 335

Bell G.D.
Tubbs E.F. 1970 Ap. J. 159, 1093

Bell R.A.
Upson W.L. 1971 Ap. Letts. 9, 109

Biemont E. 1974a J.Q.S.R.T. 14, 959

Biemont E. 1974b Sol. Phys. 38, 15

Biemont E. 1975 Sol. Phys. 39, 305

Blackwell D.E. 1974 Q.J.R.A.S. 15, 224

Blackwell D.E. 1975 Q.J.R.A.S. 16, 356

Blackwell D.E.
Petford A.D.
Mallia E.A. 1967 M.N.R.A.S. 136, 365

Blackwell D.E.
Petford A.D.
Collins B.S.
Ibbetson P.A.
Mallia E.A.
Smith G.
Emerson D. 1971 Sol. Phys. 19, 264

Blackwell D.E.
Collins B.S. 1972 M.N.R.A.S. 157, 255

Blackwell D.E.
Ibbetson P.A.
Petford A.D. 1975 M.N.R.A.S. 171, 195

Blackwell D.E.
Ibbetson P.A.
Petford A.D.
Willis R.B. 1976 M.N.R.A.S. 176, 219

Blackwell D.E.
Ibbetson P.A.
Petford A.D.
Shallis M.J. 1978 to be submitted

Bridges J.M.
Wiese B.L. 1970 Ap. J. 161, L71

Bridges J.M.
Kornblith R.L. 1974 Ap. J. 192, 793

Byard P.L. 1967 J.Q.S.R.T. 7, 559

Collins B.S. 1970 D. Phil Thesis, University of Oxford

Collins B.S.
Blackwell D.E.
Petford A.D. 1970 Applied Optics 9, 1606

Corliss C.H.
Bozman W.R. 1962 N.B.S. (USA) Monograph No. 53

chapter 5 (contin.)

Corliss C.H. Warner B.	1964	Ap. J. Supp. 8, 395
Corliss C.H. Warner B.	1966	J. Res. N.B.S. 70A, 325
Corliss C.H. Tech J.L.	1968	N.B.S. (USA) Monograph No. 108
Corney A.	1970	Adv, Electr. Elec. Phys. 29, 115
Emerson D.	1970	D. Phil. Thesis, University of Oxford
Erman P. Lyrra M. Martinson I.	1974	Phys. Lett. 49A, 41
Fuhr J.R. Wiese W.L.	1971	N.B.S. (USA) Spec. Publ. 320 Supp. 1
Fuhr J.R. Wiese W.L.	1973	N.B.S. (USA) Spec. Publ. 320 Supp. 2
Garz T. Kock M.	1969	Astr. Ap. 2, 274
Gilbert A. Solzmann K.G.P. Penner S.S.	1974	J.Q.S.R.T. 14, 455
Glennon B.M. Wiese W.L.	1966	N.B.S. (USA) Misc. Publ. 278
Goldman A.	1969	Sci Rept. No. 5 Univeristy of Denver, Colorado
Hilborn R.C. de Zafra R.	1973	Ap. J. 183, 347
Huber M.C.E.	1971	"Modern Optical Methods in Gas Dynamics Research" (ed. D.S. Dosanijh) Plenum Press: Ney York
Huber M.C.E.	1974	Ap. J. 190, 237
Huber M.C.E. Tobey F.L.	1967	Harvard Coll. Obs. Shock Tube Spect. Lab. Sci. Rept. No. 16
Huber M.C.E. Parkinson W.H.	1972	Ap. J. 172, 229
Huber M.C.E. Tubbs E.F.	1972	Ap. J. 177, 847
King R.B. King A.S.	1935	Ap. J. 82, 377

King R.B. 1938 Ap. J. 87, 24
King A.S.

King R.B. 1942 Ap. J. 95, 78

Klose J.Z. 1971 Ap. J. 165, 637

Kock M. 1968 Zs. f. Astr. 69, 180
Richter J.

Kurucz R.L. 1973 "Blanketed Model Atmospheres for Early Type Stars",
Peytremann E. Smithsonian Institute Press: Washington
Averett E.H.

Kurucz R.L. 1974 Smithsonian Ap. Obs. Spec. Rept. No. 359

Kurucz R.L. 1975 Smithsonian Ap. Obs. Spec. Rept. No. 362
Peytremann E.

Mallia E.A. 1967 Sol. Phys. 2, 360

Martinez-Garcia M. 1971 Ap. J. 165, 213
Whaling W.
Mickey D.L.

May M. 1974 Astr. Ap. Supp. 18, 405
Richter J.
Wichelman J.

Miles B.M. 1970 N.B.S. (USA) Spec. Publ. No. 320
Wiese W.L.

Nesmayanov A.N. 1963 "Vapour Pressure of Elements", Publ. Ho. USSR
Infosearch: London

Peach J.V. 1966 D. Phil. Thesis, University of Oxford

Peach J.V. 1969 M.N.R.A.S. 144, 171

Penkin N.P. 1964 J.Q.S.R.T. 4, 41

Prokof'ev V.K. 1964 Izv. Kymshoi. Astrofiz. Obs. 31(1), 281
Nikonava E.I.
Gruzdez P.F.
Frish M.S.

Richter J. 1970 Astr. Ap. 9, 37
Wulff P.

Rogerson J.B. 1969 Ap. J. 158, 797

Ross J.E. 1973 Ap. J. 180, 599

Roth C. 1970 J. Res. N.B.S. (USA) 74A, 181

Shallis M.J. 1978 D. Phil. Thesis, University of Oxford

Smith W.H. 1970 Nucl. Instr. Methods 90, 115

Takens R.J. 1970 Astr. Ap. 5, 244

Valters A.K. 1964 Opt. Spectrosc. 17, 262
Startsev G.P.

Wagner R. 1971 Z. Phys. 220, 349
Otten E.W.

Whaling W. 1969 Ap. J. 158, 389
King R.B.
Martinez-Garcia M.

Wolnik S.J. 1970 Ap. J. 162, 1037
Berthel R.O.
Wares G.W.

Wolnik S.J. 1971 Ap. J. 166, L31
Berthel R.O.
Wares G.W.

Wolnik S.J. 1973 Ap J.. 179, 665
Berthel R.O.

Chapter 6

Altrock R.C. 1972 Sol. Phys. 26, 21
Cannon C.J.

Altrock R.C. 1973 Sol. Phys. 29, 275
Cannon C.J.

Andersen P.H. 1973 P.A.S.P. 85, 666

Athay R.G. 1969 Ap. J. 156, 695
Canfield R.C.

Athay R.G. 1972 Ap. J. 176, 809
Lites B.W.

Balfour W.J. 1970 Ap. J. 162, 1031

Baschek B. 1967 Z. Ap. 67, 143
Holweger H.

chapter 6 (contin.)

Baschek B. Garz T. Holweger H. Richter J.	1970	Astr. Ap. 4, 229
Bennet R.J.M.	1970	M.N.R.A.S. 147, 35
Biemont E. Grevesse N.	1975	Sol. Phys. 45, 59
Blackwell D.E.	1974	Q.J.R.A.S. 15, 224
Blackwell D.E. Mallia E.A. Petford A.D.	1969	M.N.R.A.S. 146, 93
Blackwell D.E. Calamai G. Willis R.B.	1972	M.N.R.A.S. 160, 121
Brault J. Testerman L.	1972	"Preliminary Editionof the Kitt Peak Solar Atlas"
Bridges J.M. Wiese W.L.	1970	Ap. J. 161, L71
Brueckner K.A.	1971	Ap. J. 169, 921
Cameron A.G.W.	1973	Space Sci. Rev. 15, 121
Canfield R.C.	1971	Sol. Phys. 20, 2 5
Chaffee F.H.	1970	Astr. Ap. 4, 291
Cowley C.R.	1970	Ap. J. Lett. 5, L149
Cowley C.R. Cowley A.P.	1964	Ap. J. 140, 713
Cowley C.R. Toney J.	1973	Astr. Ap. 22, 441
David K.	1961	Z. Ap. 53, 37
Davis S.P. Phillips J.G.	1963	"The Red System of the CN Molecule", Berkely Analysis of Molecular Spectra No. 1, University of California Press
Delbouille L. Roland G.	1969	Phil. Trans. Roy. Soc. London A264, 171
Delbouille L. Roland G. Neven L.	1973	"Photometric Atlas of the Solar Spectrum from 3 000 to 10 000 AA", Inst. d'Ap. de l'Universite de Liege, Belgium

Dunn A.R. Olson E.C.	1971	Sol. Phys. 16, 272
Edmonds F.N. Webb C.J.	1972	Sol. Phys. 25, 44
Elste G.H.E.	1967	Ap. J. 148, 857
Engvold O. Hauge O.	1974	Rept. No. 39, Inst. of Theor. Ap., Blindern, Oslo
Fichtel C.E. Bertosch D.L. Pellerin C.J. Reames D.V.	1972	Bull. A.A.S. 4, 259
Fort B. Picat J.P. Combes M. Felenbok P.	1972	Astr. Ap. 17, 55
Fosbury R.A.E.	1974	Sol. Phys. 34, 309
Foy R.	1972	Astr. Ap. 18, 26
Foy R.	1975	Astr. Ap. 39, 235
Frisch H.	1975	Astr. Ap. 40, 267
Gail H.P. Sedlmayr E.	1974	Astr. Ap. 36, 17
Gaydon A.G.	1968	"Dissociation Energies & Spectra of Diatomic Molecules", Chapman Hall: London
Garz T. Holweger H. Kock M. Richter J.	1969	Astr. Ap. 2, 446
Gingerich O. Noyes R.W. Kalkofen W. Currey Y.	1971	Sol. Phys. 18, 347
Glebocki R.	1973	Acta. Astr. 23, 135
Gonczi G. Roddier F.	1971	Astr. Ap. 11, 28
Gray D.F.	1973	Ap. J. 184, 461
Cray D.F. Evans J.C.	1973	J.R.A.S. Can. 67, 241

Grevesse N. Sauval A.J.	1973	Astr. Ap. 27, 29
Hauge O Engvold O.	1970	Rept. No. 31, Inst. of Theor. Ap., Blindern, Oslo
Hearn A.G.	1974	Astr. Ap. 31, 415
Hearnshaw J.B.	1974	Astr. Ap. 36, 191
Holweger H.	1967	Z. Ap. 65, 365
Holweger H.	1973	Sol. Phys. 30, 35
Holweger H. Muller E.A.	1974	Sol. Phys. 39, 19
Huber M.C.E. Parkinson W.H.	1972	Ap. J. 172, 229
Huber M.C.E. Tubbs E.F.	1973	Ap. J. 186, 1053
Hundt E.	1973	Astr. Ap. 29, 17
de Jager C.	1974	Sol. Ohys. 34, 91
Kovacs I.	1969	"Rotational Structure in the Spectra of Diatomic Molecules", Adam Hilger, London.
Kuli Zade D.M. Guseinov K.I.	1973	Sol System Res, 7, 145
Kurucz R.L.	1974a	Sol. Phys. 34, 17
Kurucz R.L.	1974b	Smithsonian Ap. Obs. Spec. Rept. No. 359
Kurucz R.L. Peytremann E.	1975	Smithsonian Ap. Obs. Spec. Rept. No. 362
Laborde G.	1961	Ann. Ap. 24, 69
Lites B.W.	1973	Sol. Phys. 32, 283
Lites B.W. Brault J.W.	1973	Sol. Phys. 30, 283
Lites B.W. White O.R.	1973	H.A.O. Res. Memorandum No. 185
Mallia E.A.	1968	Sol. Phys. 5, 281
May M. Richter J. Wichelmann J.	1974	Astr. Ap. Supp. 18, 405

Moore C.E. 1959 "A Multiplet Table of Astrophysical Interest", N.B.S. (USA) Tech. Note 36

Moore C.E. Minnaert M.G.J. Houtgast J. 1966 "The Solar Spectrum 2935A to 8770A", N.B.S. (USA) Mono. 61

Moore C.E. Broida H.P 1959a J. Res. N.B.S. 63A, 19

Moore C.E. Broida H.P. 1959b J. Res. N.B.S. 63A, 279

Muller E.A. Mutschlecner J.P. 1964 Ap. J. Supp. 9, 1

Nissen P.E. 1970 Astr, Ap. 6, 138

Panter S.F. Foster J.S. 1937 Proc. Roy. Soc. A162, 336

Paradijs J. van 1972 Nature 238, 37

Persi P. 1975 Sol. Phys. 43, 39

Phillips J.G. Davis S.P. 1968 "The Swan System of the C_2 Molecule", Berkely Analysis of Molecular Spectra No. 2, University of California Press.

Richter J. Wulff P. 1970 Astr. Ap. 9, 37

Rogerson J.B. 1969 Ap. J. 158, 797

Rosen B. 1970 "Spect. Data Relative to Diatomic Molecules", Pergammon Press: Oxford.

Ross J.E. 1973 Ap. J. 180, 599

Ross J.E. Aller L.H. 1972 Sol. Phys. 25, 30

Schadee A. 1964 Bull. Astr. Inst. Neths. 17, 311

Schadee A. 1971 Astr. Ap. 14, 164

Smith M. 1974 Ap. J. 190, 481

Smith P.L. Whaling W. 1973 Ap. J. 183, 313

Sotirovski P. 1971 Astr. Ap. 14, 319

Sotirovski P. 1972 Astr. Ap. Supp. 6, 85

chapter 6 (contin.)

Stenholm L.G.	1977	Astr. Ap. 54, 127
Tanaka K.	1971	P.A.S. Japan 23, 185
Turon P.	1975	Sol. Phys. 41, 271
Unsold A.	1955	"Physik der Sternatmospharen", Springer-Verlag: Berlin.
Waddell J.H.	1958	Ap. J. 127, 284
Wilson A.M. Guidry F.J.	1974	M.N.R.A.S. 166, 219
Withbroe G.L.	1967	Ap. J. 147, 1117
Withbroe G.L.	1968	Sol. Phys, 3, 146
Withbroe G.L.	1968	Harvard Coll. Obs. Shock Tube Spect. Lab. Sci. Rept. No. 30
Withbroe G.L.	1971	N.B.S. (USA) Spec. Publ. No. 353
Wolnik S.J. Berthel R.O. Wares G.W.	1970	Ap. J. 162, 1037
Wolnik S.J. Berthel R.O. Wares G.W.	1971	Ap. J. 166, L31
Worrall G.	1972	Nature 237, 49
Worrall G.	1973	Nature 241, 7
Worrall G. Wilson A.M.	1972	Nature 236, 15
Worrall G. Wilson A.M.	1973	Vistas 15, 39
Wright K.O.	1944	Ap. J. 99, 249
Yamashita Y.	1972	P.A.S. Japan 24, 49

Chapter 7

Athay R.G. 1972 Sol. Phys. 24, 18
Lites B.W.
White O.R.
Brault J.

Baranger M. 1958 Phys. Rev. 111, 494

Baranger M. 1958 Phys. Rev. 111, 855

Bates D.R. 1949 Phil. Trans. Roy. Soc. 242, 101
Damgaard A.

Bell R.A. 1973 Sol. Phys. 29, 299

Blackwell D.E. 1972a M.N.R.A.S. 160, 121
Calamai G.
Willis R.B.

Blackwell D.E. 1972b M.N.R.A.S. 160, 189
Kirby J.H.
Smith G.

Brault J. 1972 "Preliminary Edition of the Kitt Peak Solar Atlas"
Testerman L.

Bridges J.M. 1974 Ap. J. 192, 793
Kornblith R.L.

Brueckner K.A. 1971 Ap. J. 169, 921

Carbon D. 1968 Sol. Phys. 3, 55
Gingerich O.
Kurucz R.L.

Chamaraux P. 1967 Ann. Ap. 30, 67

Cooper J. 1966 Phys. Rev. Lett. 17, 991

Copley G.H. 1973 Astr. Ap. 24, 239
Camm D.M.

Corliss C.H. 1968 N.B.S. (USA) Mono. No. 108
Tech J.L.

Cowley C.R. 1969 Ap. J. 158, 1177
Elste G.H.
Allen R.H.

Cowley C.R. 1970 Ap. J. Lett. 5, L149

Delbouille L. 1973 "Photometric Atlas of the Solar Spectrum from 3000A to 10000A", Inst. d'Ap. de l'Universite de Liege, Belgium.
Roland G.
Neven L.

Deridder D. 1974 Sol. Phys. 34, 77
Rensbergen W. van

Deridder D. Rensbergen W. van	1976	Astr. Ap. Supp. 23, 147
Dreiling L.A. Bell R.A.	1975	Bull. A.A.S. 7, 248
Edmunds M.G.	1975a	Astr. Ap. 38, 137
Edmunds M.G.	1975b	Astr. Ap. 41, 119
Elste G.H.E.	1968	Sol. Phys. 3, 106
Evans J.C. Ramsey L.W. Testerman L.	1975	Astr. Ap. 42, 237
Foy R.	1972	Astr. Ap. 18, 26
Fullerton W. Cowley C.R.	1970	Ap. J. 162, 337
Fullerton W. Cowley C.R.	1971	Ap. J. 165, 643
Grasdalen G.L. Huber M.C.E. Parkinson W.H.	1969	Ap. J. 156, 1153
Griem H.R.	1964	"Plasma Spectroscopy", McGraw Hill: New York
Gurtovenko E.A.	1974	Sol. Phys. 37, 43
Gurtovenko E.A.	1975a	Sol. Phys. 42, 43
Gurtovenko E.A.	1975b	Sov. Astr. 18, 609
Hindmarsh W.R. Petford A.D. Smith G.	1967	Proc. Roy. Soc. A297, 296
Hofsass D.	1975	J.Q.S.R.T. 15, 901
Holweger H.	1970	Astr. Ap. 4,11
Holweger H.	1971a	Astr. Ap. 10, 128
Holweger H.	1971b	Astr, Ap. 12, 319
Holweger H.	1972	Sol. Phys. 25, 14
Holweger H.	1973	Sol. Phys. 36, 35
Hindmarsh W.R. DuPlessis A.A. Farr J.M.	1970	J. Phys. B3, 5
Houtgast J.	1972	Sol. Phys. 15, 273

Kolb A.C. Griem H.	1958	Phys. Rev. 111, 514
Kusch H.J.	1958	Z. Ap. 45, 1
Labs D. Neckel H.	1968	Z. Ap. 69, 1
Labs.D. Neckel H.	1972	Sol. Phys. 22, 64
Lewis E.L. McNamara L.F. Michels H.H.	1971	Phys. Rev. A3, 1939
Lewis E.L. McNamara L.F. Michels H.H.	1972	Sol. Phys. 23, 287
Lindholm E.	1945	Ark. Mat. Astr. Fys. 32A
Lites B.W.	1973	Sol. Phys. 32, 283
Lites B.W. White O.R.	1973	H.A.O. Res. Memo. No. 185
Lorentz H.A.	1915	"The Theory of Electrons", Dover: New York
Mount G.H. Linsky J.L.	1974	Sol. Phys. 35, 259
Mount G.H. Linsky J.L.	1975	Sol. Phys. 41, 17
Rensbergen W. van Doncker E. de Deridder D.	1975	Sol. Phys. 40, 303
Roueff E.	1970	Astr. Ap. 7, 4
Roueff E.	1974	J. Phys. B 7, 185
Roueff E. Regemorter H. van	1969	Astr. Ap. 1, 69
Roueff E. Regemorter H. van	1971	Astr. Ap. 12, 317
Smirnov	1967	Sov. Phys. JETP 24, 314
Smith E.W. Cooper J. Roszman L.J.	1973	J.Q.S.R.T. 13, 1523
Szudy J. Bayliss W.E.	1975	J.Q.S.R.T. 15, 641

Traving	1960	"Uber die Theorie der Druckverbreiterung von Spektrallinien", Verlag G Braun: Karlsruhe
Unsold A.	1955	"Physik der Sternatmospharen", Springer Verlag: Berlin.
Warner B.	1967	M.N.R.A.S. 136, 381
Warner B.	1968	M.N.R.A.S. 138, 229
Warner B.	1969	Observatory 89, 11
Weisskopf V.	1933	U.F.N. 13, 596
Yamashita Y.	1972	P.A.S. Japan 24, 49
Zwann C.	1974	Sol. Phys. 37, 99

Chapter 8

Ayres T.R. Johnson H.R.	1977	Ap. J. 214, 210
Bell R.A. Eriksson K. Gustafsson B. Nordlund A.	1976	Astr. Ap. Supp. 23, 37
Blackwell D.E. Ellis R.S. Ibbetson P.A. Petford A.D. Willis R.B.	1975	M.N.R.A.S. 171, 425
Blackwell D.E. Shallis M.J.	1977	M.N.R.A.S. 180, 177
Carbon D. Gingerich O.	1969	"Theory and Observation of Normal Stellar Atmospheres", MIT Press.
Conti P.S. Greenstein J.L. Spinrad H. Wallerstein G. Vardya M.S.	1967	Ap. J. 148, 165
Currie D.G. Knapp S.L. Liewer K.M.	1974	Ap. J. 187, 131
Ellis R.S.	1974	D. Phil. Thesis, University of Oxford
Gasson R.	1966	Thesis, Univeristy of Cambridge

Gehrz R.D. Woolf N.J. 1971 Ap. J. 165, 285

Gezari D.Y. Labeyrie A. Stachnik R.V. 1973 Ap. J. Lett. 173, L1

Gillett F.C. Low F.J. Stein W.A. 1968 Ap. J. 154, 677

Gillett F.C. Merrill K.M. Stein W.A. 1971 Ap. J. 164, 83

Griffin R. 1968 "A Photometric Atlas of the Spectrum of Arcturus", Cambridge Phil. Soc.: Cambridge.

Griffin R. & R. 1967 M.N.R.A.S. 137, 253

Gustafsson B. Kjaergaard P. Andersen S. 1974 Astr. Ap. 34, 99

Hanbury Brown R. Davis J. Lake R.J.W. Thompson R.J. 1974 M.N.R.A.S. 167, 475

Hayes D.S. 1970 Ap. J. 159, 165

Hoffleit D. 1964 "Catalogue of Bright Stars", Yale Univ.: New Haven

Johnson H.L. 1963 Ap. J. 136, 1135

Johnson H.L. 1965 Ap. J. 141, 940

Johnson H.L. Mitchell R.I. Iriate B. Wisniewski W.Z. 1966 Commun. Lunar Plan. Lab. 4, 99

Johnson H.L. Mitchell R.I. Latham A.B. 1967 Commun. Lunar Plan. Lab. 6, 85

Johnson H.L. Collins J.G. Krupp B. Bell R.A. 1976 Ap. J. 212, 760

Kharitonov A.V. Knyazeva L.N. 1968 Soviet A.J. 11, 598

Komarov N.S. Pozigun V.A. 1970 Soviet A.J. 14, 440

Kuiper G.P. 1938 Ap. J. 88, 429

Linsky J. 1973 Ap. J. 180, 473
Ayres T.

Mackle R. 1975 Astr. Ap. 38, 239
Holweger H.
Griffin R.
Griffin R.

Pease F.G. 1921 P.A.S.P. 33, 171

Pease F.G. 1931 Erg. Naturwiss. 10, 84

Peytremann E. 1974 (privately communicated)

Popper D.M. 1959 Ap. J. 129, 647

Simon T. 1971 P.A.S.P. 83, 607

Paradijs J. van 1974 Astr. Ap. 35, 225
Meurs E.J.A.

Paradijs J. van 1976 Astr. Ap. 49, 53

Warren P.R. 1970 Thesis, Univeristy of Cambridge

Williams P.M. 1970 Thesis, Univeristy of Cambridge

Williams P.M. 1971 M.N.R.A.S. 153, 171

Williams P.M. 1971 M.N.R.A.S. 155, 215

Willstrop R.V. 1965 Memoirs R.A.S. 69, 83

Wooley R. 1970 "Catalogue of Stars within twenty-five parsecs of
Epps E.A. the Sun", Roy. Obs. Annals No. 5
Penston M.J.
Pocock S.B.

Worden S,P. 1976 P.A.S.P. 88, 69

Chapter 9

Athay R.G. 1972 Ap. J. 176, 809
Lites B.W.

Auer L.H. 1976 Ap. J. 205, 165
Heasley J.N.

Ayres T.R. 1975 Ap. J. 200, 660
Linsky J.

Ayres T.R. 1977 Ap. J. 214, 210
Johnson H.R.

Bell R.A. Eriksson K. Gustafsson B. Nordlund A.	1976	Astr. Ap. Supp. 23, 27
Blackwell D.E. Mallia E.A. Petford A.D.	1969	M.N.R.A.S. 146, 93
Blackwell D.E. Ibbetson P.A. Petford A.D.	1975	M.N.R.A.S. 171, 195
Brault J. TestermannL.	1972	"Preliminary Edition of the Kitt Peak Solar Atlas"
Corliss C.H. Warner B.	1964	Ap. J. Supp. 8, 395
Cowley C.R. Lites B.W.	1974	Astr. Ap. 31, 361
Carbon D. Gingerich O.	1969	"Theory and Observation of Normal Stellar Atmospheres", MIT Press
Day R.W. Lambert D.L. Sneden C.	1973	Ap. J. 185, 213
Delbouille L Roland G. Neven L.	1973	"Photometric Atlas of the Solar Spectrum from 3000A to 10000A", Inst. d'Ap., Universite de Liege, Belgium
Ellis R.S.	1974	D. Phil. Thesis, University of Oxford
Griffin R.	1968	"A Photometric Atlas of the Spectrum of Arcturus", Cambridge Phil. Soc., Cambridge.
Griffin R.&R.	1967	M.N.R.A.S. 137, 253
Griffin R.&.R.	1969a	M.N.R.A.S. 143, 319
Griffin R.&R.	1969b	M.N.R.A.S. 143, 349
Griffin R.&R.	1969c	M.N.R.A.S. 143, 361
Gustafsson B. Kjaergaard P. Andersen S.	1974	Astr. Ap. 34, 99
Holweger H.	1971	Astr. Ap. 12, 319
Johnson H.R. Collins J.G. Krupp B. Bell R.A.	1976	Ap. J. 212, 760

Kurucz R.L.	1974	Smithsonian Ap. Obs. Spec. Rept. No. 359
Lites B.W.	1972	Thesis, Univeristy of Colorado
Lites B.W.	1973	Sol. Phys. 32, 283
Mackle R. Holweger H. Griffin R. Griffin R.	1975a	Astr. Ap. 38, 239
Mackle R. Holweger H. Griffin R. Griffin R.	1975b	Astr. Ap. Supp. 19, 303
Mount G.R. Ayres T.R. Linsky J.L.	1975	Ap. J. 200, 383
Paradijs J. van Meurs E.J.A.	1974	Astr. Ap. 35, 225
Peytremann E.	1974	Astr. Ap. 33, 203
Ramsey L.	1976	Ap. J. 215, 603
Sikorski J.	1976	Acta. Astr. 26, 1
Smith M.	1974a	Ap. J. 190, 481
Smith M.	1974b	Ap. J. 192, 623
Warren P.R.	1970	Thesis, University of Cambridge

Chapter 10

Ayres T.R. Johnson H.R.	1977	Ap. J. 214, 210
Blackwell D.E. Ellis R.S. Ibbetson P.A. Petford A.D. Willis R.B.	1975	M.N.R.A.S. 171, 425
Blackwell D.E. Shallis M.J.	1977	M.N.R.A.S. 180, 177
Blackwell D.E. Willis R.B.	1977	M.N.R.A.S. 180, 169
Helfer H.L. Wallerstein G.	1968	Ap. J. Supp. 16, 1

Iben I. 1972 Proc. I.A.U. Coll. No. 17

Mackle R.
Holweger H.
Griffin R.
Griffin R. 1975 Astr. Ap. 38, 239

Pagel B.E.J.
Tomkin J. 1969 Q.J.R.A.S. 10, 194

Appendix I

Aller L.H. 1963 "Atmospheres of the Sun and Stars", Ronald Press: New York.

Aller M.F.
Everett C.H.M. 1972 Ap. J. 172, 447

Armstrong B.H. 1967 J.Q.S.R.T. 7, 61

Baschek B.
Holweger H.
Traving G. 1966 "Ein Algol-Programm fur die Quantitative Analyse von Sternspektren", Abhandlungen aus der Hamburger Sternwarte, 8, 26.

Bell R.A. 1973 Sol. Phys. 29, 299

Bode G. 1965 "Die kontinuierliche Absorption von Sternatmospharen" Inst. fur Theoretische Physik und Sternwarte der Universitat Kiel.

Bolton C.T. 1970 Ap. J. 161, 1187

Carbon D.
Gingerich O. 1969 "Theory and Observation of Normal Stellar Atmospheres", MIT Press.

Cody
Thacher 1968 Math. of Comp. 22, 641

Cowley C.R. 1974 private communication

Craven P.G. 1972 private communication

Craven P.G. 1974 D. Phil. Thesis, University of Oxford.

Drawin H.R.
Felenbok P. 1965 "Data for Plasmas in Local Thermodynamic Equilibrium" Gautier-Villars, Paris.

Gerbil'skij M.R. 1972 Sol. Phys. 25, 274

Gingerich O.
Noyes R.W.
Kalkofen W.
Cuny Y. 1971 Sol. Phys. 18, 357

Gustafsson B.	1973	"A Fortran Program for calculating continuous absorption coefficients of stellar atmospheres", Uppsala Astronomika Observatoriums Annaler 5 No. 6
Hummer D.G. Rybicki G.	1967	"Methods in Computational Physics", Vol. 7 p.53 Academic Press:London.
Ibbetson P.A.	1969	D. Phil. Thesis, Oxford.
Kurucz R.L.	1970	Smithsonian Ap. Obs. Spec. Rept. No. 309
Lambert D.L.	1974	private communication
Mihalas D.	1967	"Methods in Computational Physics", Vol. 7 p. 1, Academic Press: London
Pecker J.C.	1965	Ann. Rev. 3, 143
Ross J.E.	1972	private communication to Smith & Whaling (1973)
Evans J.C.	1972	. . . . .
Smith P.L. Whaling W.	1973	Ap. J. 183, 313
Traving G.	1965	Landolt Bornstein New Series Gp. 6 Vol. 1 p. 445
Traving G. Baschek B. Holweger H.	1966	"Tabellen fur die Berechnung von Zustandssummen", Abhandlungen der Hamburger Sternwarte 8, 3

ADDENDA

Chapter 3:

Athay R.G. Lites B.W.	1972	Ap. J. 156, 695
Becker W.	1948	Z. f. Ap. 25, 145
Becker W.	1954	Z. f. Ap. 34, 1
Crawford D.L. Barnes J.V.	1970	Astr. J. 75, 946, 952, 978
Neff J.S.	1969	"Theory and Observation of Normal Stellar Atmospheres", MIT Press, p.293

Chapter 5:

Carz T.
Baschek B.
Richter J.
Holweger H. 1970 Astr. Ap. 4, 229

Smith P.L.
Whaling W.
Mickey D.I. 1970 Nucl. Instr. & Meth. 90, 47

Chapter 6:

Biemont E.
Grevesse N. 1975 Sol. Phys. 45, 59

Grevesse N.
Swings J.P 1969 Astr. Ap. 2, 28

Chapter 7:

Hindmarsh W.R.
Du Plessis A.A.
Farr J.M. 1970 J. Phys. B 3, 5

Huber M.C.E.
Tubbs E.F. 1973 Ap. J. 186, 1053

Lambert D.L.
Mallia E.A.
Petford A.D. 1971 M.N.R.A.S. 154, 265

Lites B.W. 1972 Thesis, University of Colorado

Turon P. 1975 Sol. Phys. 41, 275

Chapter 9:

Kurucz R.L.
Peytremann E. 1975 Smithsonian Ap. Obs. Spec. Rept. No. 362

Simon T. 1971 P.A.S.P. 83, 607

Stenholm L.G. 1977 Astr. Ap. 54, 127

Upson W.L. 1973 Thesis, University of Maryland

Chapter 10:

Johnson H.R.
Collins J.G.
Krupp B.
Bell K.A. 1976 Ap. J. 212, 760

ACKNOWLEDGEMENTS

The Wise Observatory of the University of Tel-Aviv and the staff at the Observatory and at the Department of Physics and Astronomy generously provided facilities for the observations of Arcturus. Computing time was provided by the Oxford University Computing Laboratory.

I acknowledge the award of a Science Research Council Studentship and a Senior Studentship at Hertford College.

Many astronomers provided helpful discussions, guidance or more tangible assistance and I wish to express my thanks to Drs. M G Adam, A D Petford, G Smith, P A Ibbetson, E A Mallia, G Wegner, P G Craven, R S Ellis and M J Shallis. Additional thanks are due to Craven for many useful suggestions concerning the calculation of line profiles; and to Petford for advice and assistance in the use of the DGC NOVA computer in the Department of Astrophysics, Oxford.

My greatest debt is to Professor D E Blackwell who supervised this work. The innumerable comments, discussions, arguments and suggestions he has offered have been of the greatest value.